Retrograde Trans-synaptic Retinal Ganglion Cell Loss following Retrogeniculate Lesions of Human Visual Pathway Identified Using Optical Coherence Tomography

By

Dr Panitha Jindahra MD, MRCP

Student number: 49030459

p.jindahra@ucl.ac.uk

A Thesis submission for PHD program

Neuro-Ophthalmology

Institute of neurology

University College London

2011

I would like to express my heartful thanks to:

Principal supervisor:

Dr Gordon T Plant, MD FRCP FRCOphth

Neuro-Ophthalmology, Institute of Neurology

The National Hospital for Neurology and Neurosurgery,

Queen square, London

Subsidiary supervisor: Prof John L Barbur

Applied Vision Research Centre, The Henry Wellcome Laboratories for Vision Sciences, City University, London

Our statistician: Ms Aviva Petrie

Biostatistic unit, UCL Eastman Dental hospital, London

Patients and friends

None of these works would have been possible without their supports and efforts. I am very grateful to Gordon who inspires me and shows me the beauty of Neuro-Ophthalmology. I also thank him for giving me this opportunity and for teaching me the art and science. Working in his team has been a wonderful experience for me.

I would like to give my special thanks to my two referees:

Prof Alan Cowey, MA, PhD, Hon DSc, FMedSci, FRS

Department of Experimental Psychology

Oxford Centre for Functional Magnetic Resonance Imaging of the Brain

Department of Clinical Neurology

Department of Physiology, Anatomy and Genetics

University of Oxford

Mr Ian Murdock, MSc MD FRCOphth

Senior lecturer and Glaucoma Specialist

Moorfields Eye Hospital

Institute of Ophthalmology

London

For my mother, father, and sisters

Declaration

'I, Panitha Jindahra, confirm that the work presented in this thesis is my own. Where information has been derived from other sources, I confirm that this has been indicated in the thesis.'

Two articles from my PHD project have been published as follows:

Panitha Jindahra, Aviva Petrie, Gordon T. Plant. Retrograde trans-synaptic retinal ganglion cell loss identified by optical coherence tomography. Brain 2009: 132; 628-634. Permission to reproduce this article has been granted by Oxford university press.

Panitha Jindahra, Thomas Hedges, Carlos Mendoza-Santiesteban, Gordon Plant. Retrograde trans-synaptic retinal ganglion cell loss following retrogeniculate lesions of human visual pathway identified using Optical Coherence Tomography. Current Opinion in Neurology 2010: 23; 16-23. Permission to reproduce this article has been granted by Wolters Kluwer Health

Abstract

Introduction

Retrograde trans-synaptic degeneration (RTSD) in the human visual pathway has not been well clarified.

Aims

1. To confirm the RTSD in human visual pathway.

2. To study the rate of RTSD.

3. To study the pupil function in the RTSD.

Methods

1. The peripapillary retinal nerve fibre layer (RNFL) thickness measured with optical coherence tomography was compared among patients with acquired and congenital retrogeniculate lesions and normal subjects. Humphrey perimetry and brain imaging were performed.

2. A relationship between the duration of the disease and the RNFL thickness measured at a single time point was evaluated. Additionally the RNFL thickness was measured in patients with homonymous hemianopia (HH) and smaller homonymous visual field defect serially following stroke.

3. Pupil responses were measured in HH patients and normal subjects, using achromatic and chromatic stimuli localised to the blind hemifield and compared with responses obtained in the sighted hemifield.

Results

1. The overall mean RNFL thickness of the patient groups was significantly less than that of the controls. The affected sectors respected the retinotopic organization.

2. There was a negative straight line relationship between the duration of disease (log years) and the mean thickness measured at a single point in time in HH patients. In the serial measurements the mean thickness had a decreasing trend over time in all HH cases in contrast to the small visual field defect group. The thinning occurred early in the first few months after the stroke.

3. In the acquired group, pupil responses from the blind hemifield were reduced in comparison with controls to all stimuli employed. However there was a greater deficit to the chromatic stimuli than to the luminance contrast stimuli.

Discussions

We showed the RTSD in patients with acquired and congenital retrogeniculate lesion by using OCT. The degeneration was correlated to the duration and occurred early after stroke. The RTSD might occur in the pupil pathway.

Acronyms

RTSD	Retrograde trans-synaptic degeneration
RGCs	Retinal ganglion cells
RNFL	Retinal nerve fibre layer
IPL	Inner plexiform layer
INL	Inner nuclear layer
OPL	Outer plexiform layer
ONL	Outer nuclear layer
L cones	Long wavelength cones
M cones	Medium wavelength cones
S cones	Short wavelength cones
M cells/layers	Magnocellular cells/layers
P cells/layers	Parvocelluar cells/layers
K cells/layers	Koniocellular cells/layers
SBCs	Small bistratified cells
ipRGCs	Intrinsically photosensitive retinal ganglion cells
LGN	Lateral geniculate nuclues
dLGN	Dorsal lateral geniculate nucleus
vLGN	Ventral lateral geniculate nucleus
TRN	Thalamic reticular nucleus
SC	Superior colliculus
OPN	Olivopretectal nucleus
OCT	Optical coherence tomography
MRI	Magnetic resonance imaging
HH	Homonymous hemianopia

HQ	Homonymous quadrantanopia
CNS	Central nervous system
PNS	Peripheral nervous system
ATP	Adenosine triphosphate
ADP	Adenosine diphosphate
AMP	Adenosine monophosphate
GABA	Gamma-aminobutyric acid
cAMP	Cyclic AMP
mTOR	Mammalian target of rapamycin complex
PTEN	Phosphate and tensin homolog
RAPD	Relative afferent pupillary defect

Contents

Figures

Tables

1 Introduction

In humans, the visual pathway consists of the neural elements connecting the retina of each eye with the occipital lobes (Walsh & Hoyt, 1969). The retina contains the following layers from the scleral area towards the vitreous: 1 pigment epithelium; 2 rods and cones; 3 external limiting membrane; 4 outer nuclear layer composed of the receptor nuclei; 5 outer plexiform layer (OPL), a synaptic layer between receptor cells and bipolar cells; 6 inner nuclear layer (INL): the bipolar cell layer; 7 inner plexiform layer (IPL), a synaptic layer between cell processes of bipolar and ganglion cells; 8 ganglion cell layer (GCL); 9 retinal nerve fibre layer (RNFL) made up of ganglion cell axons, arranging in a flat plane (Polyak, 1957); and 10 internal limiting membrane formed from the foot-plates of Muller's cells (Walsh & Hoyt, 1969). Axons forming the retinal nerve fibre layer converge at the optic disc (optic nerve head) (Walsh & Hoyt, 1969; Walsh T. J., 1996). The optic nerve arising from each eye travels within the orbit, the optic canal of the sphenoid bone, and the cranial cavity (Walsh & Hoyt, 1969; Walsh T. J., 1996). In the basal cistern 5 to 10 mm above the hypophysis, an X-shaped junction of the optic nerves or the optic chiasm is formed (Walsh & Hoyt, 1969; Walsh T. J., 1996; Polyak, 1957). The 'chiasma' is named as its appearance is similar to the Greek letter chi, x (Polyak, 1957). Sir Isaac Newton first introduced a theory of semidecussation of nerve fibres in 1704 on the basis of vision perceived by two eyes (Walsh & Hoyt, 1969). The decussation occurs within the chiasm, which is observed in both mammals and primates (Polyak, 1957). Fibres originating from the nasal retina, which is medial to the fovea, cross at the chiasm and join the opposite optic tract (Polyak, 1957). Those arising from the temporal portion of the retina in the fellow eye, which is lateral to the fovea, remain uncrossed (Polyak, 1957). The optic tracts encircle the cerebral peduncles and are covered laterally by the temporal lobes (Walsh & Hoyt, 1969; Walsh T. J., 1996). Most fibres terminate in the lateral geniculate nucleus (LGN), which is situated at the posterior lateral margin of the peduncles (Walsh & Hoyt, 1969; Walsh T. J., 1996). The remaining fibres, about 10-15%, leave the optic tract before reaching the LGN and pass medially to end in the pretectal region (Walsh T. J., 1996). From the LGN, nerve cells send axons to the optic radiation before ending at the occipital lobe (Walsh & Hoyt, 1969; Walsh T. J., 1996). For instance (Fig. 1), the upper left

quadrant of each retina is responsible for the lower right quadrant of the visual field (Walsh T. J., 1996). Axons from the nasal side of the right retina cross at the upper part of the chiasm then run in the medial part of the left optic tract to terminate at the left LGN. Fibres from the left LGN project to the upper third of the left optic radiation to terminate above the calcarine fissure in the left cuneus (Walsh T. J., 1996). The lower left quadrant of each retina is responsible for the upper right quadrant of the visual field (Walsh T. J., 1996). Axons from the nasal side of the right retina cross at the lower part of the chiasm and then pass through the lateral part of the left tract to terminate at the left LGN. Fibres from the left LGN travel along the lower third of the left optic radiation to terminate below the calcarine fissure on the left lingual gyrus (Walsh T. J., 1996).

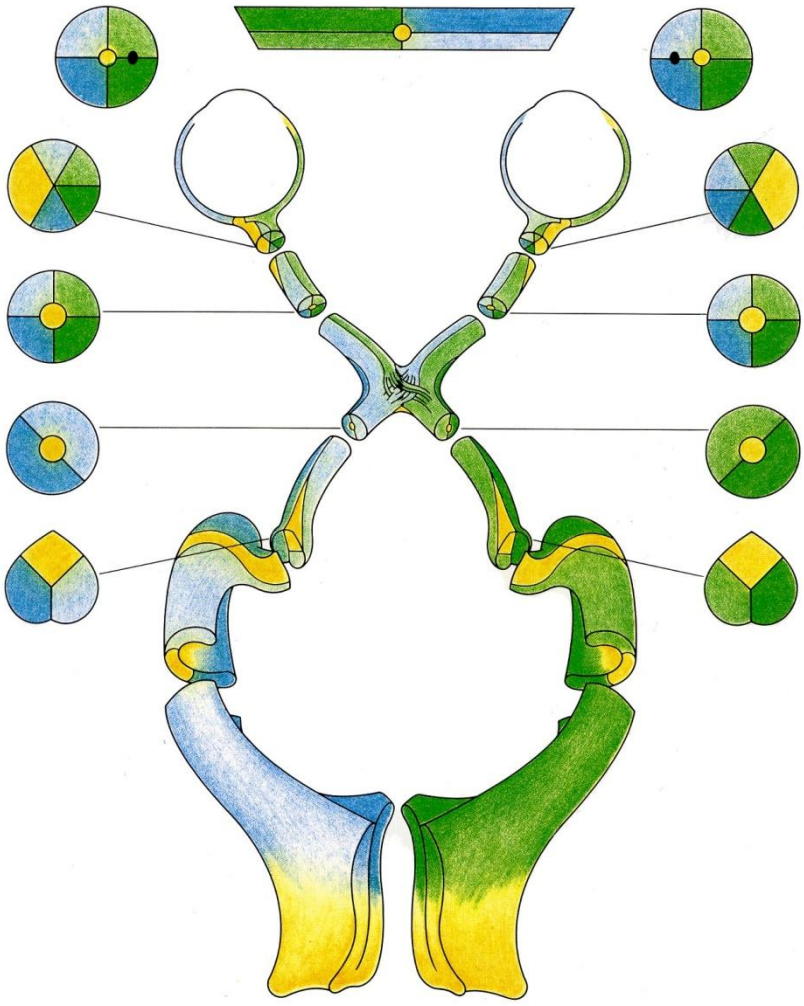

Figure 1 Visual pathway**.** A diagram shows anatomy and fibre organization in human visual pathway. Colour represents signals from each location of the visual field: yellow = central visual field, dark green = upper left visual field, light green = lower left visual field, dark blue = upper right visual field, light blue = lower right visual field. Reproduced, with permission, from Walsh, TJ, Ophthalmology Monographs: Visual Field: examination and interpretation, 2e, American Academy of Ophthalmology, 1996.

It is well established that retrograde trans-synaptic degeneration (RTSD) can occur in the human central nervous system including neuronal loss in the inferior olive after loss of purkinje cells in contralateral cerebellum (Holmes & Stewart, 1908; Sakai, Matsuda, Watanabe, Kamei, & Takashima, 1994), a chromatolytic change in Betz cells in motor cortex following limb amputation (Campbell, 1905), and in neurons of the medial mamillary body nucleus following a lesion in limbic cortex (Bleier, 1969). The RTSD in the visual pathway has been demonstrated in animals but it has remained unclear in human.

A right occipital lobectomy in an adolescent monkey was performed and brain histology was examined 2 years afterwards (Van Buren J. M., 1963). The right lateral geniculate nucleus (LGN) was grossly shrunken when compared to the left as was the optic tract on the same side. The right optic tract had 44% cross-sectional area of the left. The ganglion cell layer (GCL) of the retina on the right side of each fovea appeared symmetrically thin when compared to the left. The right GCL had less than 2 cell layers whereas the normal left side had at least 6 cell layers. This was equal to 80% RGC loss (Van Buren J. M., 1963). Van Buren proposed that the loss of ganglion cells could be accounted for by retrograde trans-synaptic degeneration or alternatively a lack of central and peripheral retinal inhibition (Van Buren J. M., 1963). RTSD in the primate visual pathway was confirmed by many investigations thereafter (Cowey, 1974; Cowey, Stoerig, & Williams, 1999; Johnson & Cowey, 2000) (Fig.2 & 3).

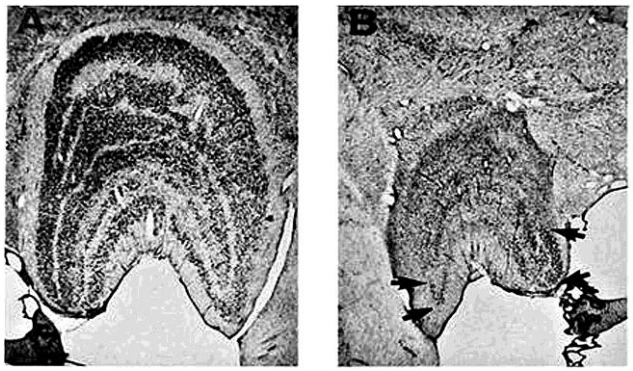

Figure 2 LGN stained with cresyl violet through the rostral third of normal (A) and degenerated (B) dLGN of a monkey with unilateral striate cortex removal. The area between the arrows was preserved. Reprinted from Vision Research, vol 39, A Cowey, P Stoerig, C Williams, Variance in transneuronal retrograde ganglion cell degeneration in monkeys after removal of striate cortex: effects of size of the cortical leisons, page 3642–52, ©1999. Permission to reproduce this figure has been granted by Elsevier.

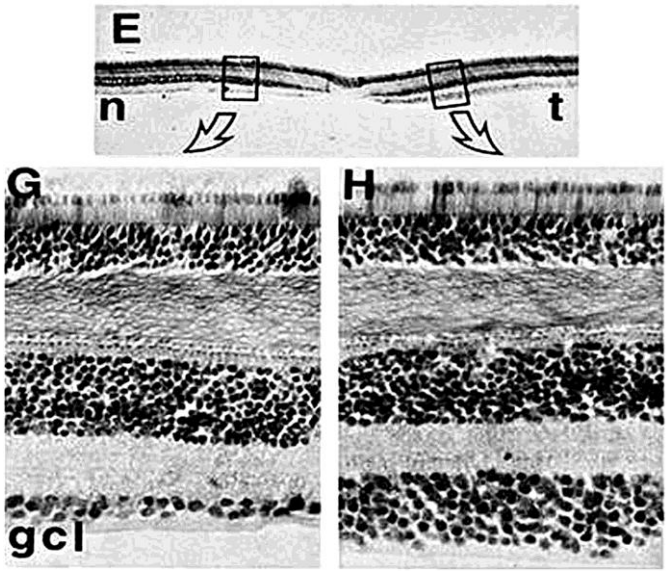

Figure 3 Low power photomicrographs of horizontal section through the fovea in a monkey (E) and high power micrographs at an eccentricity of 0.6 mm of the region outlines in E (G, H). The diagrams showed a substantial difference in the ratio of ganglion cells in the nasal (n) and temporal (t) retina. Gcl = ganglion cell layer. Reprinted from Vision Research, vol 39, A Cowey, P Stoerig, C Williams, Variance in transneuronal retrograde ganglion cell degeneration in monkeys after removal of striate cortex: effects of size of the cortical leisons, page 3642–52, ©1999. Permission to reproduce this figure has been granted by Elsevier.

Clinical observations in humans with acquired disease have been at variance with those in animals. In a case report of a patient who had suffered a cerebrovascular accident resulting in complete left homonymous hemianopia 57 years previously, the optic discs appeared healthy bilaterally (Miller & Newman, 1981), which argued against such a change in humans. However, optic disc pallor and band atrophy have been described in patients with congenital occipital lesions (Fletcher, Hoyt, & Narahara, 1988) and also in patients with unilateral periventricular leucomalacia (a type of brain injury associated with premature birth) (Ragge, Barkovich, Hoyt, & Lambert, 1991). Small optic discs and increased cup-to-disc ratio suggesting axonal loss were found in children with congenital periventricular leucomalacia associated with haemorrhage (Jacobson, Hård, Svensson, Flodmark, & Hellström, 2003). A MRI study of the brain in children with periventricular leucomalacia; bilateral occipital infarction; and neuroaxonal dystrophy showed signal hyperintensity in the LGN in T2-weighted images, indicating gliosis (Uggetti, et al., 1997). A pathological investigation revealed changes in the LGN but the retinal ganglion cells were not studied (Beatty, Sadun, Smith, Vonsattel , & Richardson Jr, 1982). Cowey showed retinal nerve fibre layer thinning in a single case of longstanding (childhood onset) hemianopia using optical coherence tomography (OCT) (Cowey, 2004). In 2005, Metha and Plant reported thinning of the peripapillary retinal nerve fibre layer in congenital occipital lesions using OCT (Mehta & Plant, 2005a; Mehta & Plant, 2005b). The thinning of the RNFL following an occipital lesion is an evidence of retrograde trans-synaptic degeneration in vivo, particularly when patterns of the axonal loss in the retina correspond with the site of the occipital damage.

Most axons (90%) of retinal ganglion cells (RGCs) synapse in the LGN, the remainder project to the pretectal region of the midbrain. The optic nerve fibres of the retinal ganglion cells in the nasal hemiretina subserve the temporal visual hemifield and cross (decussate) at the optic chiasm. The optic nerve fibres of the retinal ganglion cells in the temporal hemiretina subserve the nasal visual hemifield and do not cross at the optic chiasm. Damage to the optic chiasm or the optic tract will result in loss of retinal ganglion cells by Wallerian degeneration. It is well established from ophthalmoscopic clinical observation that loss of the crossing fibres in an eye, whether from a lesion at the optic chiasm (which will affect both eyes similarly) or at the optic tract (which affects the crossing fibres of the contralateral eye and non-

crossing fibres of the ipsilateral eye) results in a pattern of atrophy known as 'band atrophy' or 'bow-tie atrophy' (Hoyt & Kommerell, 1973). This is seen because at the nasal and temporal equatorial poles of the disc all (or almost all) fibres are lost, whereas elsewhere there is thinning only. In the eyes with the nasal hemianopic defect in cases of homonymous hemianopia due to damage of the optic tract, there is at no location around the optic disc total loss of fibres; there is thinning of all sectors with the exception of the nasal and temporal sectors to which the noncrossing fibres do not contribute (Fig. 4). The occurrence of band atrophy in the eye with temporal hemianopia in cases of optic tract lesion and also in cases of congenital post-chiasmal lesions is a common place clinical observation.

OCT (Huang, et al., 1991) is a non-invasive technique that can be used to measure the cross-sectional thickness of the retinal nerve fibre layer in vivo. We have employed this technique to look for evidence of thinning of this layer which occurs owing to the loss of retinal ganglion cell axons. In the analysis of results in the hemianopia cases, the eyes with loss of the temporal visual hemifield, whether the left or right eye, have been considered together as the 'crossing-fibre defect' eyes. As stated above in these eyes, the affected retinal ganglion cells are located in the nasal hemiretinae. The axons of these retinal ganglion cells, which decussate at the optic chiasm, are distributed in all 12 sectors studied but crossing fibres occur exclusively in the temporal and nasal sectors. The homonymous nasal field defect in the fellow 'non-crossing-fibre defect' eyes involves the axons of ganglion cells in the temporal hemiretinae which course in all sectors towards the optic disc with the exception of the temporal and nasal sectors. These axons do not decussate in the optic chiasm.

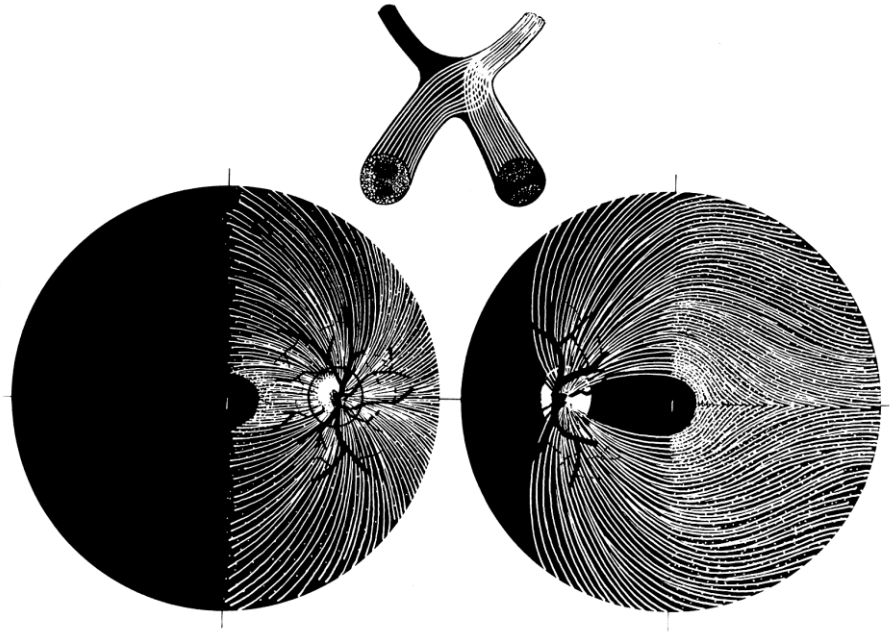

Right eye Left eye

Figure 4 The pattern of nerve fibre loss is shown diagrammatically for a case of left homonymous hemianopia secondary to a lesion of the right optic tract with total loss of affected retinal ganglion cell axons. The retinal ganglion cells subserving the unaffected hemifield (nasal retina of right eye: temporal retina of left eye) and the axons of those retinal ganglion cells are shown diagrammatically in white. In the eye with the temporal hemianopia (the crossing-fibre defect eye; on the right in the illustration) there is a total loss of fibres at the nasal and temporal equatorial poles of the optic disc (giving the appearance of band atrophy) and thinning of the remaining nerve fibre layer (the arcuate bundles). In the eye with the nasal hemianopia (the non-crossing-fibre defect eye; on the left in the illustration) there is a loss of fibres travelling to the disc in the arcuate bundles from the temporal hemiretina. Nowhere in the disc circumference of this eye is nerve fibres lost totally: there is thinning of the arcuate bundles only (Hoyt & Kommerell, 1973). In our cases, the nerve fibre loss has occurred following damage to the post-geniculate pathway (trans-synaptic degeneration) but the pattern of loss is identical to that occurring with an optic tract lesion (Wallerian degeneration). Reprinted from Klin Monbl Augenheilkd, vol 162, Hoyt, W. F., & Kommerell, G., Fundus oculi in homonymous hemianopia, 456–64 ©1973 Thieme. Permission to reproduce this figure has been granted by Thieme.

2 A map of lateral geniculate pathway and its related connections

The lateral geniculate body (LGN) is a part of the thalamus and is at the end of the course of the optic tract (Walsh & Hoyt, 1969). The LGN is a MAJor relay for conscious visual perception of form, colour, and motion (Dacey D. , 2004). It has a cap-like structure and is situated on the supero-posterior part of the thalamus and lateral to the pulvina (Walsh & Hoyt, 1969). There are alternating layers of grey and white matter (Walsh & Hoyt, 1969). The dorsal nucleus sends visual information to the striate cortex while the ventral nucleus has connections only with the midbrain (Walsh & Hoyt, 1969). The primate dLGN consists of 4 parvocellular layers in the dorsal region, 2 magnocellular layers in the ventral region, and thin bands of koniocellular layers intercalated between the two layers (White, Solomon, & Martin, 2001; Tailby, Szmajda, Buzás, Lee, & Martin, 2008; Szmajda, Buzás, Fitzgibbon, & Martin, 2006; Kaas, Huerta, Weber, & Harting, 1978; Casagrande, 1994; Usrey & Reid, 2000). There are main 6 layers, numbered from ventral to dorsal: layers 1, 4, and 6 receive inputs from contralateral (crossing) fibers of the nasal visual field whereas layers 2, 3, and 5 receive afferent fibres from the ipsilateral (uncrossing) fibers of the temporal visual field (Walsh & Hoyt, 1969). The ventral LGN was involved in light level detection and pupil control (Cowey & Stoerig, 1991). The focus of this chapter is about inputs and outputs of the dLGN (Fig.5-7). As the visual anatomy and physiology of the old world monkey, like a macaque or a baboon, are comparable to those in the human (Dacey D. , 2004), many data reviewed here are from monkey studies.

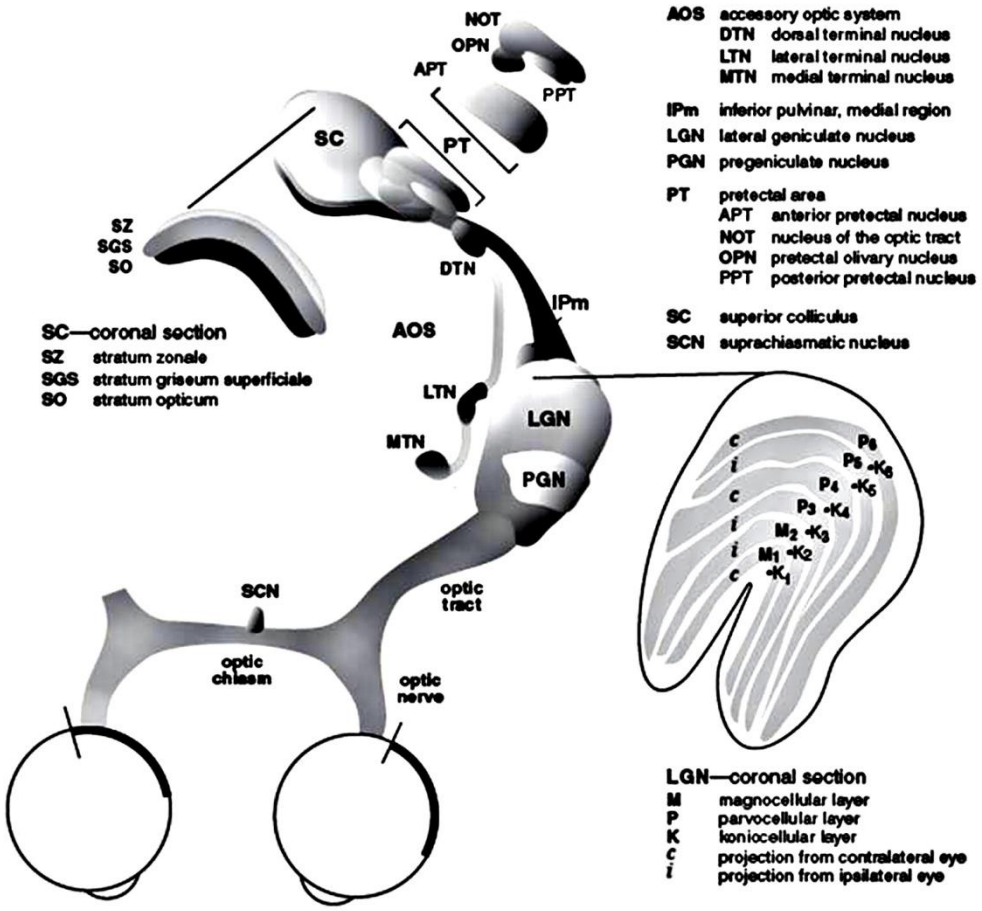

Figure 5 Inputs and outputs of dLGN. Reprinted from D Dacey, Origins of perception: retinal ganglion cell diversity and the creation of parallel visual pathways, Michael S Gazzaniga, editor, THE COGNITIVE NEUROSCIENCES III, The MIT Press, ©2004 MIT. Permission to reproduce this figure has been granted by The MIT Press.

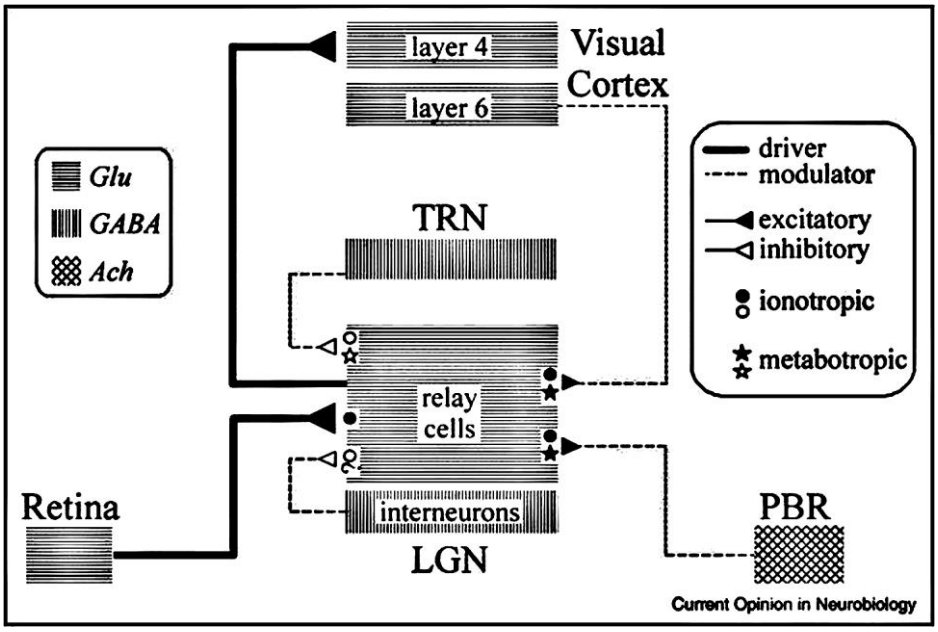

Figure 6 A diagram of circuits in the LGN shows inputs to the relay cells along with postsynaptic receptors (inotropic and metabotropic) and neurotransmitters. The LGN receives major innervations from retinal glutaminergic inputs, glutaminergic inputs from layer 6 of the cortex, local GABAergic inputs (interneurons and cells in the thanlamic reticular nucleus), and brainstem inputs. Abbreviations: *ACh,* acetylcholine; *GABA*, γ-aminobutyric acid; *Glu,* glutamate; *LGN*, lateral geniculate nucleus; *PBR,* parabrachial region; *TRN,* thalamic reticular nucleus. Reprinted from Current Opinion in Neurobioly, vol 17, SM Sherman, The thalamus is more than just a relay, page 417–22, ©2007. Permission to reproduce this figure has been granted by Elsevier.

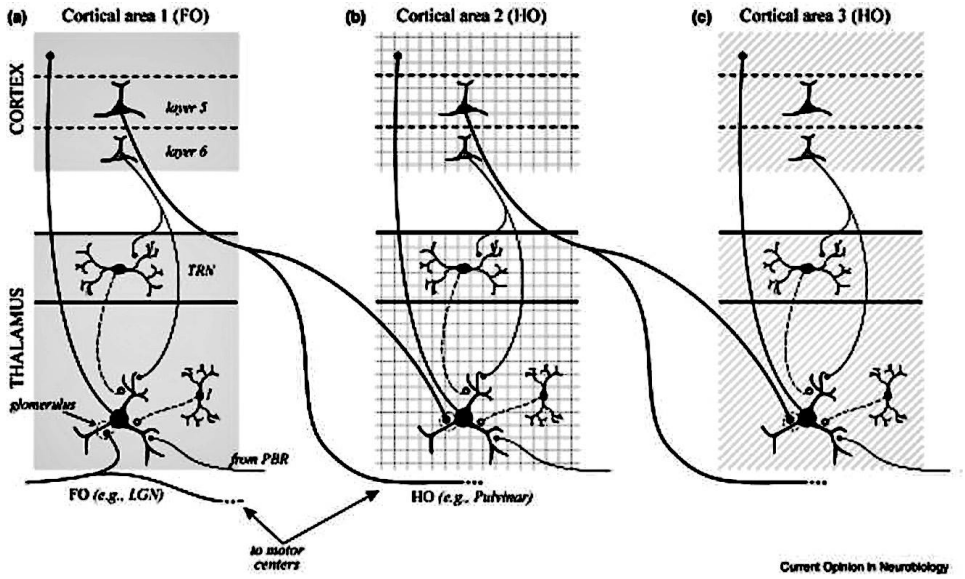

Figure 7 Diagram showing first and high order thalamic nuclei (FO, HO). A) the dLGN acts as a first order nucleus that receives signals from the retinogeniculate fibres and relays the information to the primary cortex. The dLGN also receives feedback from layer 6 of the visual cortex. B and C) the pulvinar is a higher order nucleus conveying signals from layer 5 of the primary cortex to another cortical area. TRN= thalamic reticular nucleus. Reprinted from Current Opinion in Neurobioly, vol 17, SM Sherman, The thalamus is more than just a relay, page 417–22, ©2007. Permission to reproduce this figure has been granted by Elsevier.

2.1 Dorsal LGN inputs

There are 4 main inputs to the thalamocortical (TC) relay cells of the dLGN (Sherman, 2007; Turner & Salt, 1998; Williams, Turner, Anderson, & Crunelli, 1996). 1) Glutaminergic retinal inputs. 2) Glutaminergic inputs from layer 6 of the visual cortex. 3) GABAergic inputs from the interneurones and cells of the thalamic reticular nucleus. 4) Inputs from brainstem, mostly are cholinergic input from parabrachial region. The retinal inputs activate only ionotropic receptors creating fast excitatory postsynaptic potentials (EPSPs) in the postsynaptic relay cells (Sherman, 2007). The non-retinal inputs activate metabotropic receptors (Sherman, 2007). The inputs to the relay cells of the LGN are divided into driver and modulator (Sherman, 2007). The retinogeniculate fibres are drivers that convey the main visual signal information whereas other afferents modulate the driver transmission (Sherman, 2007).

2.1.1 Retinogeniculate projections

Primate retina (Chichilnisky, 1999; Kaplan, Lee, & Shapley, 1990; Rodieck, 1988) is a sheet of brain tissue at the back of the eyes and organizes into 5 distinct layers: 3 layers of cell bodies (inner nuclear layer, outer nuclear layer, and ganglion cell layer) and 2 layers of synaptic connections (inner and outer plexiform layers). Light traverses through the mostly transparent retina and are absorbed by outer segments of photoreceptor cells (rods and cones). Enzymatic cascades in rods and cones transform light into electrical potentials. The resulting signals are transmitted to bipolar cells, to ganglion cells and to optic nerve subsequently. The signals also travel laterally via amacrine and horizontal cells (Fig 8).

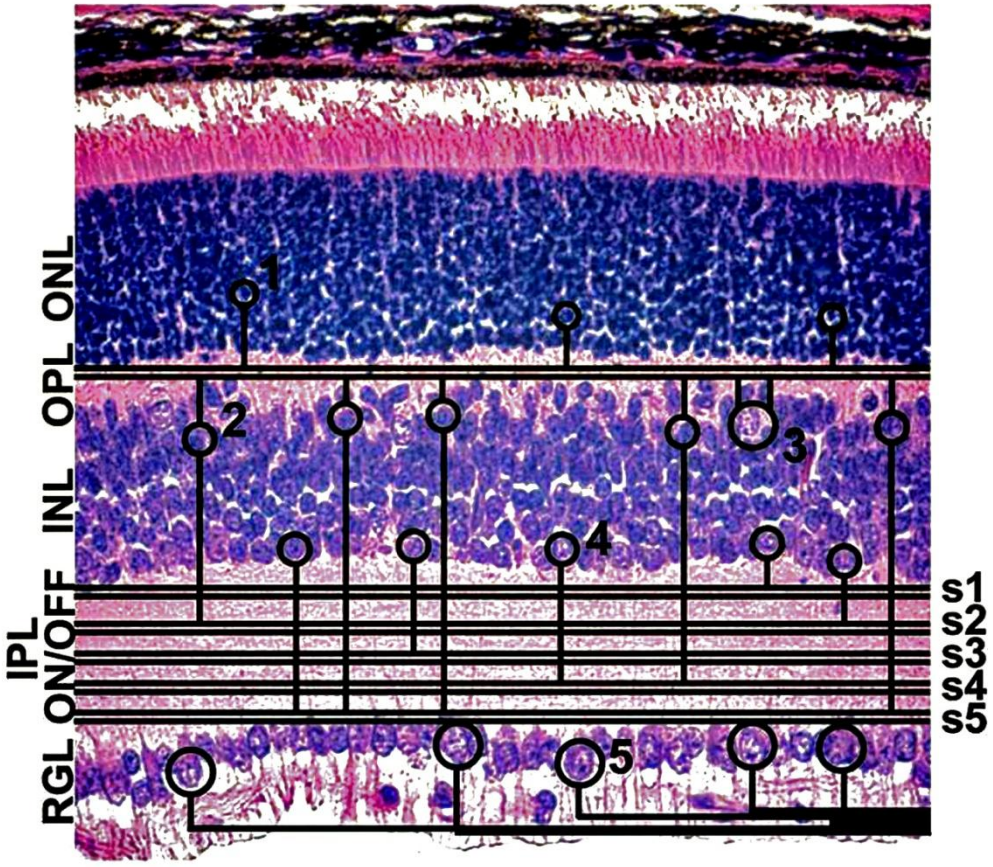

Figure 8 Retinal architecture of a mouse in a cross-section plane (6 µm) and stained with hematoxyln and Eosin. The retina is organized in three nuclear laminae and two synaptic laminae. The outer nuclear layer (ONL) comprises rod and cone photoreceptors (1). The inner nuclear layer (INL) comprises bipolar cells (2), horizontal cells (3), Müller glia and amacrine cells (4). The retinal ganglion cell layer (RGL) comprises amacrine cells and retinal ganglion cells (5). The outer plexiform layer (OPL) contains the synapses between photoreceptors and horizontal and bipolar cells. The inner plexiform layer (IPL) contains the synapses between amacrine, bipolar cells, and retinal ganglion cells. The inner plexiform layer can be broadly divided into an ON portion, proximal to the RGL, and an OFF portion, proximal to the INL, or into five synaptic bands (S1–S5). Reprinted from Current Opinion in Neurobiology, 2009, 19, 4, 389-94, PG Fuerst & RW Burgess, Adhesion molecules in establishing retinal circuitry, ©2009. Permission to reproduce this figure has been granted by Elsevier.

Rods are the most abundant photoreceptors in the retina (100 million per eye); are located at 5 mm away from the fovea or beyond 20 degree of visual angle; and are

responsible for night vision (scotopic condition). The peak wavelength sensitivity of rods is 500 nm. A visual pigment or rhodopsin in rods absorbs all photons of different wavelength and all photons give similar effects on rhodopsin. Hence the world at night appears grey to human eyes. At the fovea, which corresponds to the centre of gaze or visual field, there is no rod but only densely packed cones. Here visual acuity is greatest. Cones (5 million per eye) mediate daylight vision (photoptic condition) and are classified into 3 groups according to their wavelength sensitivity. Firstly, long wavelength (L) cones maximally absorb light at 566 nm which is normally perceived as red colour. Secondly, medium wavelength (M) cones maximally absorb light at 535 nm which is usually seen as green colour. Lastly, short wavelength (S) cones maximally absorb light at 415-420 nm which is perceived as blue colour. Yellow colour perception is a consequence of combination inputs from red and green cones. If all three cone types are stimulated, white light is perceived. Unlike the other two, S cones are absent at the centremost fovea. The L and M cones are more numerous than the S cones (10-15% of all cones) and a ratio of L: M cone is one. A ganglion cell receives inputs over a circular area of the visual field or receptive field sampled by several photoreceptors. A receptive field normally comprises two concentric zones; one in the centre and the other in the surrounding area. Less than 20 morphologically RGCs have been identified in mammals and have been classified into different ways. (Masland, 2001; Dacey D. , 2004; Field & Chichilnisky, 2007; Polyak, 1957; Perry, Oehler, & Cowey, 1984; Williams, Azzopardi, & Cowey, 1995). Three main RGC types have been categorized according to the soma size and the number of primary dendrites namely P, M, and gamma cells (Perry, Oehler, & Cowey, 1984; Williams, Azzopardi, & Cowey, 1995) (Fig. 9 & 10). Regarding dendritic stratification, RGCs that project to the dLGN have either bistratified or monostratified dendritic processes (Dacey, Peterson, Robinson, & Gamlin, 2003) (Fig. 12). Approximately 90% of RGCs including P, M, and small bistratified cells (SBCs) project to parvocellular, magnocellular, and koniocellular layers of dLGN respectively (Williams, Azzopardi, & Cowey, 1995; Dacey D. , 2004). Ratios of neurons in parvocellular to magnocellular layers of dLGN are 35:1 at the fovea and 5:1 at 15^{o}eccentricity. About 10% of all RGCs travel to the superior colliculus including gamma, Pɛ or epsilon, and a few M cells (Perry & Cowey, 1984), which, in some studies, have been classified as thorny monostratified, broad thorny

monstratified, recursive bistratified, recursive monostratified, and moderate monostratified cells (Dacey D. , 2004). Characteristic details of 4 main RGCs (P cells, M cells, SBCs, and gamma cells) have been reviewed in Table 1 and Fig. 9-11. Furthermore another important type of RGCs (Fig. 13), intrinsically photosensitive retinal ganglion cells (ipRGCs), is presented after the table 1. RGC axons form synapses with TC relay neuronal dendrites in the dLGN (Cowey & Stoerig, 1991; Turner & Salt, 1998) and activate them via NMDA receptors (Koch, 1987). Glutamate is its neurotransmitter (Turner, Leresche, Guyon, Soltesz, & Crunelli, 1994).

Table 1 A summary of main RGC types and their properties.

Properties	P cells	M cells	SBCs	Gamma cells
1 Other names	Midget Pβ β X-like cells, compared with the cat	Parosol Pα A Stratified diffuse cells X- and Y-like cells, compared with the cat	K cells	Pγ C cells
2 Morphology	Small cell body Small dendritic field size The diameter of dendritic trees increase with eccentricity except within central 10 degree where the size is stable Dendrites of ON-cells branch at the inner half of the IPL and those of OFF-cells branch in the outer half but in a different depths with M cells.	Large cell body Large dendritic field size The diameter of dendritic trees increase with eccentricity Dendrites of ON-cells branch at the inner half of the IPL and those of OFF-cells branch in the outer half. Unlike P cells, adjacent dendrites of M cells overlap.	Small cell body The diameter of dendritic trees increase with eccentricity Dendrites of the same cells stratify on two layers of the IPL, one near the inner border of the IPL and the other near the outer border.	Small-medium cell body, overlapped with the size of P cells. Sparcely-branched unistratified dendritic trees lie in a single plane of IPL. The diameter of dendritic trees increase with eccentricity. Note that Pc, have similar dendritic trees but larger cell bodies, are found with γ cells that travel to the midbrain.
3 Number	Nearly 80% of all RGCs 1.2 million cells Comprise 70% of all RGCs at the central retina Cell density is high in the fovea and decreases with increasing distance from the fovea.	10% of all RGCs 0.15 million cells At the foveal pit and peripheral retina Cell density is high in the fovea and decreases with increasing distance from the fovea.	5% of all RGCs	10% of all RGCs including γ, Pc, and rare M cells, go to the SC (~110,000 cells) Being 6% of all RGCs near the fovea; the percentage rises with eccentricity.
4 Nasal to temporal cells	1.54	1.54	No data available	1.57 not significantly difference from other types
5 Receptive fields	Small Smallest diameter 0.01° Average diameter 0.03°	Large (diameters are 2-3x and areas are 4-9x larger than those of P cells) Average diameter 0.06°	Comparable to those of M cells or larger in some studies. Larger in scotopic light and smaller in photopic light.	Similar to M cells at low eccentricity but similar to P cells at high eccentricity
6 Conduction velocity	Slow	Fast		Slow
7 Responses to grating	Linear spatial summation	Some cells: linear spatial summation Most cells: non-linear spatial summation		
8 Organization	Concentrically antagonistic centre-surround	Concentric centre-surround (broadband)	Centre-surround	Lacked well-defined centre-surround (broadband)

Properties	P cells	M cells	SBCs	Gamma cells
9 Input	P cells receive excitatory inputs from bipolar cells (glutamate) and inhibitory inputs from amacrine cells (glycine or GABA) at dyad synapses. Dyad is a synaptic site comprising presynaptic bipolar axon terminal (ribbons) & postsynpatic dendrites of P ganglion cells and amacrine cells. P cell: bipolar= 1:1 in the central retina (6-7°), 1≥2 in the periphery; bipolar cells, in turn, receive signals from long (L) & medium (M) wavelength cones (+M-L or +L-M) and mildly from S cones, combining with the other two. There are no rods in the fovea but the rods outnumber the cones in the periphery. P bipolar cells receive only cone inputs in the central but receive both cone and weak rod inputs in the periphery. Rod signals are conveyed via All amacrine and bipolar cells. ON-centre P ganglion cells receive excitatory inputs from depolarizing-ON-bipolar cells. OFF-centre P ganglion cells convey signals from hyperpolarizing-OFF bipolar cells. ON-centre P ganglion cells depolarize and produce action potentials to increment in the intensity of white light in the receptive field centres and are inhibited by that stimulus in the receptive field surrounds. OFF-centre P ganglion cells generate action potentials to decrements in light intensity. Red-ON green-OFF P ganglion cells (+L-M): their receptive field centres are excited by red light while the surrounds are excited by green light, opposing the central response. This is referred to as cone opponency. Red-ON centre cells (+L-M) receive main inputs from L cones while green-OFF centre cells (-M+L) receive main inputs from M cones. Both of them receive +L-M cone input in a dfferent magnitude. Consequently, the red-ON-centre cells respond optimally to brighter colour while the green-OFF-centre cells respond to darker colour.	M cells receive excitatory inputs from diffuse bipolar cells, which, convey signal from rods and many cones. M cells also receive inputs from amacrine cells. Unlike P cell pathway, amacrine cells rarely make contacts with bipolar cells or nearby amacrine cells but presynaptic amacrine cells receive inhibitory inputs from other amacrine cells, hence, M cells can respond to stimuli beyond their receptive fields. Some amacrine cells contact with both ON- and OFF- M ganglion cells. Dendrites of M cells make gap junctions with amacrine axons. As a consequence, M cells of the same type in the same vicinity fire synchronously. The gap junctions do not expand their receptive fields. P cells work independently as they do not possess gap junctions. M cells receive sum inputs from rods as well as L and M cones (minimally from S cones). Rod signals to M cells are stronger than to P cells. Rod inputs to M pathway are pronounced at 20 troland (td). M cells receive signals from rod-rod bipolar-All amacrine pathway at low light level (2-20 td), and from rod-cone gap junctions in bright light. In mesopic conditions, they convey signals from both rods and cones.	In photopic condtions, SBCs receive excitatory inputs from blue cone bipolar cells which, in turn, receive inputs exclusively from S cones (blue-ON yellow-OFF). They not receive rod signals as rods become saturated in this light level. Horizontal cells in the pathway convey signals to all cone types, especially S cones. SBCs receive minimal inputs from L and M cones. They also contact amacrine cells. ON-cells are excited by S cones and are inhibited by L & M cones. OFF-cells are stimulated by decrements in L or M wavelength lights. SBCs receive rod inputs particularly under low scotopic conditions via All amacrine cell rod pathway in the same polarity as ON-S-cone. There is no cone signal since the light level is below cone threshold. SBCs receive inputs from rods and cones in mesopic light levels.	

Properties	P cells	M cells	SBCs	Gamma cells
10 Project to	4 dorsal parvocellular layers of LGN do not project to midbrain	2 ventral magnocellular layers of LGN (main) superior colliculus (only a few)	Koniocellular layer 3 between magno and parvocellular layers Leading to striate, prestirate, cortex & middle temporal area	Superior colliculus (SC) (10% of all RGCs go to SC or 100,000 -150,000 cells in the monkey) Posterior olivary nucleus
11 Spectral sensitivity	Medium & long wavelength Mediate red-green colour vision	Low Mediate achromatic vision	Short wavelength (S) Mediate blue-yellow vision	Lacked colour opponency
12 Luminance contrast sensitivity (achromatic)	Lower; P cells do not respond to visual pattern under scotopic light level except in full field stimulation or stimulit of very low spatial frequency and very high contrast. There is no contrast saturation	Higher; the contrast gain of M cells are 8-10x greater than that of P cells so M cells can respond to visual pattern under scotopic conditions. Contrast is saturated when exceeding 10-15%. They are sensitive to borders between areas of different brightness. Human contrast sensitivity function is correlated with physiological responses of M cells except in 2 td (pure rod stimuli) and 200 td (pure cone stimuli).		
14 Absolute sensitivity to light	Less than M cells	Greater than P cells		
15 Motion	Not sensitive	Sensitive Lesions at magnocellular pathway do not reduce motion perception.	Sensitive	
16 Spatial resolution	In the absence of noise in the system, the resolution of P cells exceed that of M, hence, P cells suit well for high acuity. They mediate high spatial low temporal frequency. The spatial resolving power decreases in the peripheral retina because of the inverse relationship between dendritic field size and cell density. Lesions at parvocellular layers reduce visual acuity.	Given a high sufficient contrast sensitivity, M cells can respond well to fine details. M cells are sensitive to low spatial high temporal frequency.		
17 Form perception	P cells exhibited orientation selectivity regardless of colour selectivity. The process is also represented in V1.		Achromatic orientation selectivity, represented in V1	

Table 2 references for Table 1

P cells

De Monasterio & Gouras, 1975; Shapley & Perry, 1986; Lee, Smith, Pokorny, & Kremers, 1997; Merigan & Eskin, 1986; Thorell, De Valois, & Albrecht, 1984; Johnson, Hawken, & Shapley, 2001; Heimel, Van Hooser, & Nelson, 2005; Johnson, Van Hooser, & Fitzpatrick, 2010

M cells

Shapley & Perry, 1986; De Monasterio & Gouras, 1975; Lee, Smith, Pokorny, & Kremers, 1997; Cao, Lee, & Sun, 2010; Merigan & Eskin, 1986; Davis & McKinnon, 1982; Cowey & Stoerig, 1991; Perry, Oehler, & Cowey, 1984; Perry & Cowey, 1984; Schiller & Malpeli, 1977

SBCs

Dacey D. , 2004; Szmajda, Grunert, & Martin, 2008; Dacey & Lee, 1994; Tailby, Szmajda, Buzás, Lee, & Martin, 2008; Field, et al., 2009; Martin, White, Goodchild, Wilder, & Sefton, 1997; Johnson, Van Hooser, & Fitzpatrick, 2010; Szmajda, Buzás, Fitzgibbon, & Martin, 2006; White, Solomon, & Martin, 2001

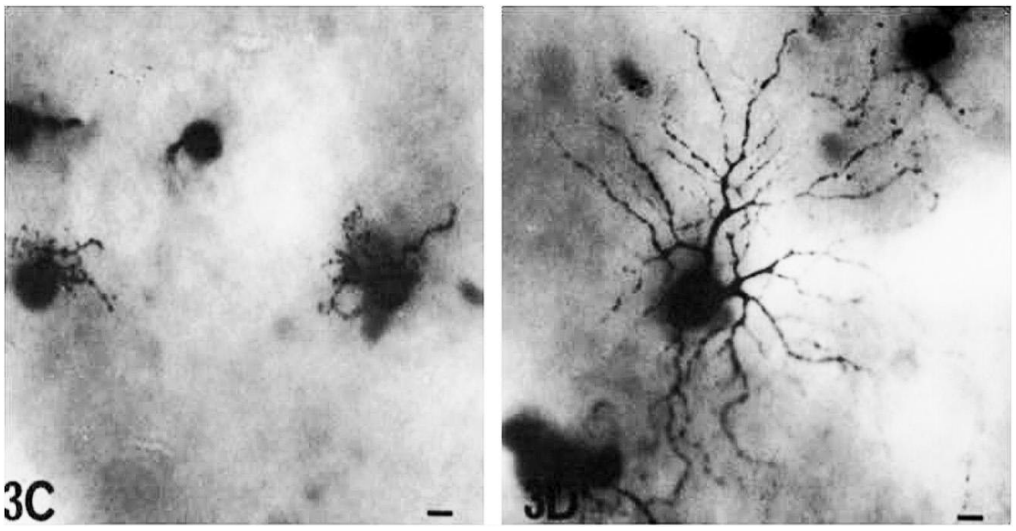

Figure 9 By injecting horseradish peroxidase to the optic nerve to retrogradely label RGCs, P cells (left) 5.2 mm nasal to the fovea and M cells (right) 5 mm nasal to the fovea were demonstrated. Scale bars = 10 microns. Reprinted from Neuroscience, vol 12, VH Perry, R Oehler, & A Cowey, Retinal ganglion cells that project to the dorsal lateral geniculate nucleus in the macaque monkey, page 1101-23, ©1984. Permission to reproduce this figure has been granted by Elsevier.

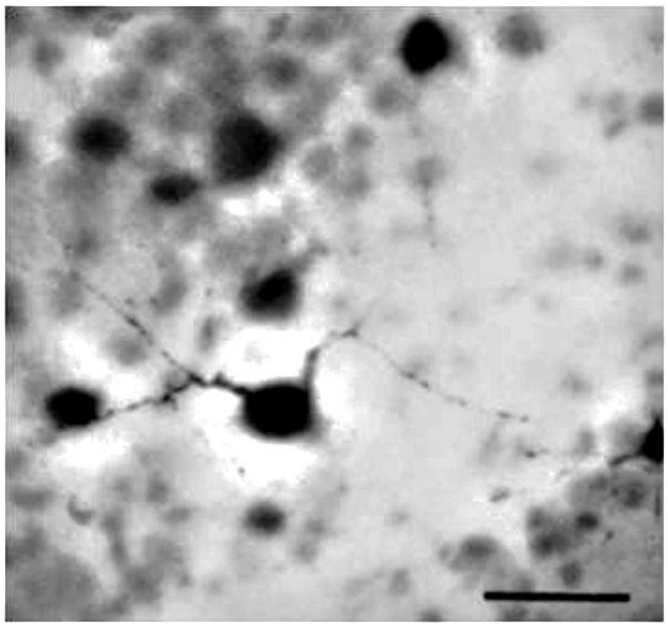

Figure 10 Gamma cell 5.7 mm temporal to the fovea retrogradely labelled with HRP from the superior colliculus**.** Scale bar = 50 microns. Reprinted from Neuroscience, vol 12, VH Perry & A Cowey, Retinal ganglion cells that project to the superior colliculus and pretectum in the macaque monkey, page 1125-37, ©1984. Permission to reproduce this figure has been granted by Elsevier.

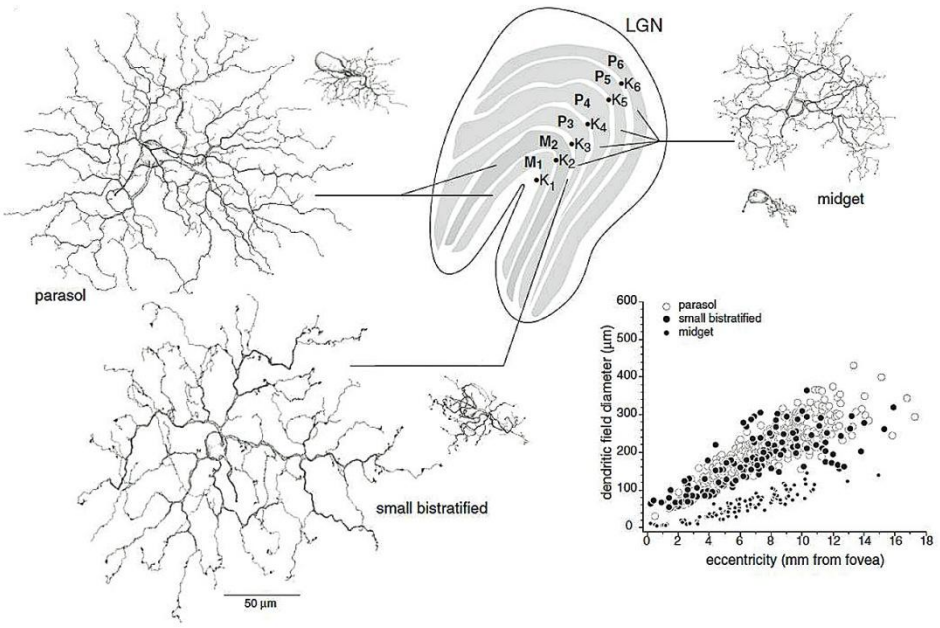

Figure 11 A diagram shows RGCs and LGN. M or parosol cells project to magnocellular layers of the LGN (M_1 and M_2). P or midget cells project to parvocellular layers of the LGN (P_{3-6}). Small bistratified cells project to koniocellular layer 3 of the LGN (K_3). Reprinted from D Dacey, Origins of perception: retinal ganglion cell diversity and the creation of parallel visual pathways, Michael S Gazzaniga, editor, THE COGNITIVE NEUROSCIENCES III, The MIT Press, ©2004 MIT. Permission to reproduce this figure has been granted by The MIT Press.

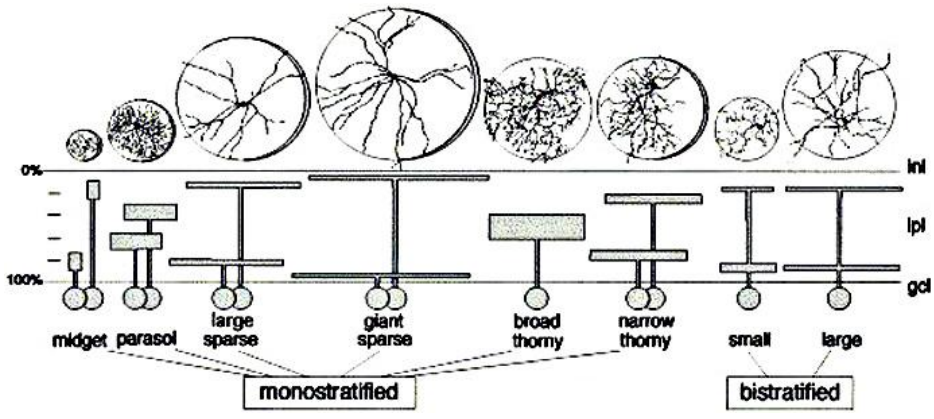

Figure 12 By employing photodynamic techniques, 13 types of RGC that project to the LGN have been demonstrated. Abbreviations: inl= inner nuclear layer, ipl= inner plexiform layer, gcl= ganglion cell layer. Reprinted from Neuron, vol 37, D Dacey, BB Peterson, FR Robinson, & PD Gamlin, Fireworks in the primate retina: in vitro photodynamics reveals diverse LGN-projecting ganglion cell types, page 15-27, ©2003. Permission to reproduce this figure has been granted by Elsevier.

ipRGCs

Intrinsically photosensitive retinal ganglion cells (ipRGCs), another type of the RGCs, contain the photopigment melanopsin (Ecker, et al., 2010). They respond directly to light to drive the circadian clock and pupil light reaction (Ecker, et al., 2010). The ipRGCs are diverse and divided into 5 subclasses (Ecker, et al., 2010). 1) Type I or M1 ipRGCs have sparsely branching monostratified dendritic ramification in the outermost of the inner plexiform layer (IPL) (Ecker, et al., 2010; Berson, Dunn, & Takao , 2002). This type is also known as giant monostratified cells (Marshak, 2009; Dacey D. , 2004). There are around 3000 cells or 1% of all RGCs with highest density at the fovea (Dacey D. , 2004). Driven by cones, they have OFF response to short wavelength light but ON responses to medium and long wavelengths in bright stimuli (S-OFF color opponency). They also respond to dim light with strong rod inputs. However they can respond to light without any inputs to rods and cones (Dacey D. , 2004). Mice lacking functional rods and cones rely on the ipRGCs to discriminate high contrast and grating grey stimuli but not to optokinetically track gratings (Ecker, et al., 2010). They generate slow sustained discharge driven by rod and cones over the full scotopic-photopic range, enabling them to transmit information about absolute light intensity to the brain especially pretectal olivary nucleus (pupillomotor control area in the pretectum) (Gamlin, Peterson, & Dacey, 2001). Thus, they control pupil size (Güler, et al., 2008). They evoke the greatest light responses and contained a higher level of the melanopin than other types (Ecker, et al., 2010). 2) Type II or M2 ipRGCs have a large dendritic arborization in the ON sublayer of the IPL (Ecker, et al., 2010). The dendritic processes of M2 are sparser and slightly smaller than those of M4 (Ecker, et al., 2010). M2 cells contain the melanopsin and exhibit light responses. 3) Type III or M3 ipRGCs: some cells have cell bodies displaced into the inner nuclear layer and some cells have bistratified dendritic arbor (Ecker, et al., 2010; Schmidt & Kofuji, 2009). 4) By using Cre mediated recombination technique in place of the melanopsin gene (opn4) in mice and enhanced green fluorescent proteins are expressed, two more ipRGCs subtypes have been identified that are M4 and M5 ipRGCs (Ecker, et al., 2010). M4 ipRGCs resemble the ON alpha ganglion cells with large soma and dendritic field size monostratifying in the ON sublayer of the IPL. They exhibit weak light responses and express low level of the melanopsin. 5) M5 ipRGCs have a smaller bushy highly-

branched dendritic arborization stratifying in the ON sublayer of the IPL (Ecker, et al., 2010). They express the melanopsin in low levels as reflected in negative melanopsin immunoreactivity. Like M2 and M4 ipRGCs, the light responses of the M5 are much weaker than those of M1. All ipRGCs receive synaptically excitatory influences from rods and cones. They send their axons to the optic nerve, the chiasm, the optic tract, and central visual nuclei (retinofugal trajectory) (Ecker, et al., 2010). M1 and non-M1 ipRGCs project to the suprachiasmatic nucleus (SCN), the intergeniculate leaflet (IGL), the dLGN, the vLGN but only M1 cells project to the olivopretectal nucleus (OPN) shell and the habenular region (Ecker, et al., 2010). The OPN shell is involved in pupil light responses by acting as a link between the retina and the pupillomotor output (Baver, Pickard, Sollars, & Pickard, 2008; Prichard, Stoffel , Quimby, Obermeyer, Benca, & Behan, 2002). Non-M1 axons outnumber M1 fibres in the dLGN, the core of the OPN, the posterior pretectal nucleus and the superior colliculus (Ecker, et al., 2010) (Fig.7). The extensive terminations of the ipRGCs within the dLGN and the superior colliculus are associated with spatial perception (Ecker, et al., 2010).

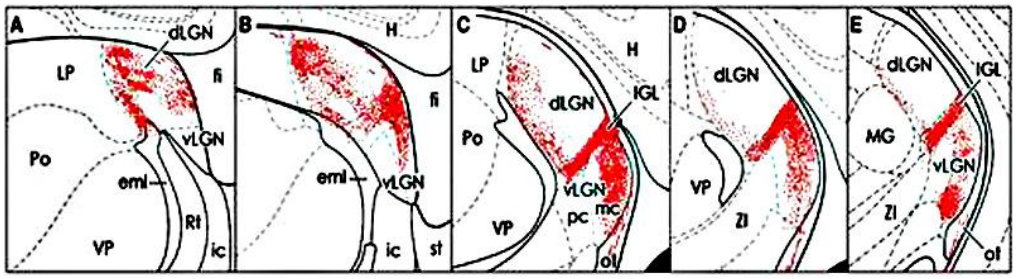

Figure 13 Diagrams showing alkaline-phosphatase stained retinal fibres in the LGN of the mouse in five coronal sections from the rostral (A) to the caudal parts (E) There are substantial inputs from the ipRGCs to the dLGN (Ecker, et al., 2010). Eml= external medullary laminar, fi=fimbria, h=hippocampus, ic=internal capsule, IGL=intergeniculate leaflet, lp= lateral posterior nucleus, MG= medial geniculate nucleus, ot= optic tract, po= posterior nuclei, rt= thalamic reticular nucleus, st=stria terminals, vLGN= ventral lateral geniculate nucleus. Reprinted from Neuron, vol 67, JL Ecker et al, Melanopsin-Expressing Retinal Ganglion-Cell Photoreceptors: Cellular Diversity and Role in Pattern Vision, page 49-60, ©2010. Permission to reproduce this figure has been granted by Elsevier.

In contrast to the findings in the old world monkey, RGC trajectory in rats and rabbits is different in that all of their axons terminate in the superior colliculus while only 10% of RGCs in monkeys terminate there (Perry, Oehler and Cowey 1984; Table 3). It is fundamental evidence that might explain why retrograde transynaptic degeneration is absent in the rat and rabbit visual pathway but present in the monkey and man. This topic will be discussed with sustaining collateral theory later.

RGcs project to	Dorsal LGN	Superior colliculus
Monkeys	More axons	10% of all RGCs
Rats	Less axons	All RGCs
Rabbits	Less axons	All RGCs

Table 3 A comparison of RGC projection between monkey, rat and rabbit (Perry, Oehler and Cowey 1984).

2.1.2 Cortico-geniculate or cortico-fugal projections

Neurons arising from layer 6 of the visual cortex project to the dLGN (Shatz, 1992; Sherman, 2007). In cats, striate cortex lesions produce significant anterograde degeneration in the dLGN within seven days as a result of corticofugal fibers degeneration (Hollander, 1972). By using a radioaudiographic technique, the transport of physiologic proteins from the cell body towards the axonal terminals was demonstrated and any retrograde changes could be excluded (Hollander, 1972). The projections from the visual cortex to the dLGN have also been confirmed by many studies using other staining methods (Garey, Jones, & Powell, 1968; Gosavi & Dubey, 1972; Guillery, 1967). Axons from the visual cortex form synapses with the relay neuronal dendrites in the dLGN (Turner & Salt, 1998). The geniculo-cortical and cortico-geniculate pathways are situated in different layers along their courses in the white matter of rats (Woodward & Coull, 1984). The geniculo-cortical fibres are running in the external sagittal stratum while the corticofugal fibres, arranged in fibre bundles, are in the internal sagittal stratum of the white matter (Woodward & Coull, 1984). Cortico-geniculate or cortico-thalamic fibres inhibit or enhance the relay cells (Crunelli & Leresche, 1991; von Krosigk, Monckton, Reiner, & McCormick, 1999). Stimulations of the cortico-thalamic fibers generate excitatory postsynaptic potentials (EPSPs) via N-methyl-D-aspartate (NMDA) and non-N-methyl-D-aspartate

glutamate receptors (non-NMDA) receptors (Crunelli & Leresche, 1991; von Krosigk, Monckton, Reiner, & McCormick, 1999; Koch, 1987). A brief train of stimulation delivers a slow EPSP (von Krosigk, Monckton, Reiner, & McCormick, 1999). A repetitive activation of the optic radiation evokes inhibitory postsynaptic potentials (IPSPs) via GABA receptors (Crunelli & Leresche, 1991; von Krosigk, Monckton, Reiner, & McCormick, 1999). GABAb receptor-mediated IPSP has two roles that are a relatively weak inhibitory neurotransmitter and a neuromodulator with a prime role in preparing the TC relay cells for burst firing by activating low-threshold calcium potentials (Crunelli & Leresche, 1991).

2.1.3 Interneuron projections to the thalamocortical relay neurones in the dLGN

EPSP, IPSP, or both of interneurons in rat dLGN, evoked by optic tract stimulation, is mediated by activation of non-NMDA and NMDA receptors (Williams, Turner, Anderson, & Crunelli, 1996). In rat dLGN, the interneurones and thalamocortical relay neurons have different properties. The interneurons fire a single action potential with a maximum frequency of < 130 Hz, whereas thalamocortical neurones fire a greater frequency of > 250 Hz (Williams, Turner, Anderson, & Crunelli, 1996).

2.1.4 Superior colliculus-dLGN projections

A study in cats found a tecto-geniculate projection from the superior colliculus

to the C3 layer of the dLGN which receives no retinal input (Torrealba, Partlow, & Guillery, 1981). The projection is retinotopically arranged and consists of a complete representation of the contralateral hemifield (Torrealba, Partlow, & Guillery, 1981). Although it is small, it joins the tecto-thalamo-cortical pathway and the retino-geniculo-cortical pathway together (Torrealba, Partlow, & Guillery, 1981).

2.2 Dorsal LGN outputs

2.2.1 Geniculo-striate cortex projections

The input from the dLGN terminates mainly in layer 4 of the striate cortex (Shatz, 1992; Fitzpatrick, Itoh, & Diamond, 1983). A study in squirrel monkey using horseradish peroxidase confirmed the projections of both magnocellular and parvocellular layers in the dLGN to separate sublaminae of layer 4 in the striate cortex (Fitzpatrick, Itoh, & Diamond, 1983). In developing brains, axons from the LGN gather underneath the cortical plate, waiting in a zone called subplate for

several weeks (cats) to months (primates) before extending into the visual cortex, when layer 4 develops (Shatz, 1992).

A study in macaque monkeys recorded responses in the superficial layers of V1 while selectively inactivating either parvocellular or magnocellular layers of the dLGN (Nealey & Maunsell, 1994). It had been revealed that the inactivation of either layer produced a decline of V1 neuronal responses, indicating that V1 received afferent fibres from both pathways (Nealey & Maunsell, 1994). The signals derived from parvocellular and magnocellular layers are segregated in their passage to the striate cortex in some studies but not segregated in some others. Cells responded to the magnocellular signals are not restricted to the cytochrome oxidase blobs or interblobs (Nealey & Maunsell, 1994). A study used achromatic grating stimuli visually presented to monkeys with 14C-2-deoxy-d-glucose (DG) infusion to measure contrast sensitivity in the primary visual cortex (Tootell, Hamilton, & Switkes, 1988) It had been found that the magnocellular input was dominant in layer 4B, 4Ca, and 6 and moderate into blobs of layer 2/3 and blob-aligned portions of layer 4A (Tootell, Hamilton, & Switkes, 1988). Parvocellular input was dominant in blob and interblob portions of layers 2/3,4A, 4Cb, and 5 (Tootell, Hamilton, & Switkes, 1988). The colour neurons in the striate cortex are clustered within the cytochrome oxidase blobs, which project to the cytochrome oxidase thin stripe in V2, then to globs in the posterior inferior temporal cortex and finally to the inferotemporal cortex (Conway, 2009). However a study revealed that the degree of selectivity was diverse among cells in the layer 2/3 of V1 and there was no discrete region that was selective only to orientation and direction but not colour and vice versa (Leventhal, Thompson, Liu, Zhou, & Ault, 1995). A study of chromatic and temporal responses using functional magnetic resonance imaging revealed that temporal responses from luminance and red-green were constant up to 10 Hz but temporal responses from yellow decreased (Liu & Wandell, 2005). The ventral occipital cortex showed strong responses to all chromatic stimuli (Liu & Wandell, 2005). For each colour, the responses to low temporal frequency were better than the high frequency in the ventral occipital cortex (Liu & Wandell, 2005). The motion selective cortex showed weak responses to yellow stimuli and strong responses to luminance and red-green high temporal frequency modulations (Liu & Wandell, 2005).

The parvocellular and koniocellular pathways are segregated while travelling in the white matter from the dLGN to the striate cortex (Callaway & Chatterjee, 2003). The koniocellular pathway projects to the striate, prestriate cortex, and middle temporal area (Szmajda, Buzás, Fitzgibbon, & Martin, 2006; Martin, White, Goodchild, Wilder, & Sefton, 1997; Johnson, Van Hooser, & Fitzpatrick, 2010). Cortical cells responding to s-cone stimuli are 40% of total cells in layer 2/3 of V1 in tree shrews, which outnumber the ganglion cell inputs in the retina (Johnson, Van Hooser, & Fitzpatrick, 2010). The s cone signals might have been amplified in the visual cortex (Sumner, Anderson, Sylvester, Haynes, & Rees, 2008; Liu & Wandell, 2005). It has also been observed in tree shrew that S/ML chromatic responses in the striate cortex are varied in layer 2/3 (Johnson, Van Hooser, & Fitzpatrick, 2010). The responses of some cortical neurons are the consequence of a summation of S- and ML- cone signals and might be selective for achromatic stimuli; a few neurons responses are predominantly from s-cone signals; many cells respond exclusively from the ML-cone signals; and lastly many neurons respond to all colour stimuli (Johnson, Van Hooser, & Fitzpatrick, 2010). For achromatic stimuli, S-cone responded cortical neurons are well tuned for orientation and have different spatiotemporal tuning property from the ML-cone responded neurons (Johnson, Van Hooser, & Fitzpatrick, 2010). P, M, and SBCs have contrast-dependent spatial properties and responses to high spatial frequency from SBCs are the weakest (White, Solomon, & Martin, 2001). (Field, et al., 2009).

In cats, fibres in layer 4ab, and 4c, and upper part of layer 6 that receive inputs from the dLGN contain NMDA and kainate receptors with glutamate and aspartate as their neurotransmitters (Tsumoto, Masui, & Sato, 1986). The output of the TC relay cells comprises two modes namely tonic and burst firings (Turner, Leresche, Guyon, Soltesz, & Crunelli, 1994). The action potential of the tonic mode is single and is elicited by depolarization from the membrane potentials positive to -60 mv. The burst firing mode of more than 150 Hz of action potentials is evoked by depolarization from the membrane potentials negative to -65 mv and is dependent on low threshold calcium current. The NMDA receptors and non-NMDA receptors are responsible for the burst firing mode. The TC relay cells in the dLGN have oscillation potentials (Turner, Leresche, Guyon, Soltesz, & Crunelli, 1994).

2.2.2 Geniculo-extrastriate cortex projections

A few thousand neurones from the dLGN project directly to the extrastriate cortex (Cowey & Stoerig, 1991; Yukie & Iwai, 1981; Bullier & Kennedy, 1983; Fries, 1981). It is these neurons that survive after striate cortex damage and perhaps contribute to residual visual functions (Cowey & Stoerig, 1991; Cowey & Stoerig, 1989) (Fig.14).

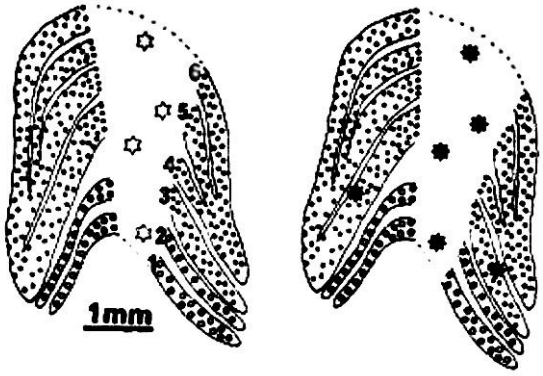

Figure 14 Diagram showing degenerated dLGN after a long-standing striate cortex lesion, which is represented by striped regions in the centre. The degenerated zone is involved in both parvocellular and magnocellular layers. When placing horseradish peroxidase (HRP) into the striate cortex adjacent to the lesion, no label is detected in the degenerated zone as indicated by stars in the left picture. When placing HRP into V4, scattered surviving neurones are labelled throughout the nucleus, as shown in black stars. Repritned from Trends Neurosci, vol 14, A Cowey & P Stoerig, The neurobiology of blindsight, page 140-5, ©1991; and from Exp Brain Res, vol 75, A Cowey & P Stoerig, Projection patterns of surviving neurones in the dorsal lateral geniculate nucleus following discrete lesions of striate cortex: Implications for residual vision, page 631–8, ©1989. Permission to reproduce this figure has been granted by Elsevier and Springer.

Cells in the interlaminar zones of the dLGN project to layer 5 of the area 19 and the anterior part of the area 18 or prestriate cortex in macaque monkeys (Benevento & Yoshida, 1981). It is sparse compared to its projections to the striate cortex and topographically organized (Benevento & Yoshida, 1981). The medial and lateral parts of dLGN projected to the dorsal, between lunate and superior temporal sulci, and ventral, between inferior occipital and occipital-temporal sulci, parts of prestriate respectively (Benevento & Yoshida, 1981). The projections are prominent in the occipito-temporal sulcus (Benevento & Yoshida, 1981). It has been suggested that the LGN-extrastriate cells might not receive inputs from the retina but receive inputs

from the midbrain (Benevento & Yoshida, 1981). The distribution of the terminals from the superior colliculus overlaps with the LGN-extrastriate cell bodies in the dLGN (Benevento & Yoshida, 1981).

2.3 Centrifugal projections

Fibres from brain to retina or centrifugal projections have been identified histologically in human retina following central retinal artery occlusion (Wolter, 1965). They have cell bodies in the brain and their axons are situated next to or on the optic disc in the retina, branching dichotomously in the direction away from the disc (Wolter, 1965). There are different types of centrifugal fibres morphologically (Wolter, 1965). Two types of centrifugal fibres have been shown in a patient with a history of 50 year bilateral enucleation (Wolter, 1965). The first type runs along the optic tract by way of the chiasm towards the optic nerve (Wolter, 1965). The second type originates from the pituitary stalk and travelled into the chiasm (Wolter, 1965). A centrifugal trajectory has been observed in mammals (Perry, Oehler, & Cowey, 1984). They enter the retina from the margin of the optic nerve head and terminate close to the inner border of the inner nuclear layer (Perry, Oehler, & Cowey, 1984). Following HRP injection to the central part of the optic nerve in old world monkeys, bilateral contralaterally biased labelled neurons in many brain areas were found to project to the retina (Labandeira-Garcia, Guerra-Seijas, Gonzalez, Perez, & Acuña, 1990). These areas included the hypothalamus, the premamillary area, nucleus of the stria terminalis, nucleus of the anterior commissure, the dorsal raphe neurons (DRN), the mesencephalic tectal reticular formation, between the substantia nigra and the red nucleus, the tegmental area just dorsal to the tegmental nucleus (Labandeira-Garcia, Guerra-Seijas, Gonzalez, Perez, & Acuña, 1990). Another primate study demonstrated projections from bilateral suprachiasmatic nucleus and anterior arcuate nucleus to the retina (Bons & Petter, 1986). Physiology studies found that stimulations on the optic tract in rabbits produced small retinal spikes of late appearance and these activations could be carried along the centrifugal fibres to the retina (Dodt, 1956). Likewise stimulations of the mesencephalic reticular substance in cats created a decrease in the frequency of discharges from the RGCs to a light stimulus. When the central stimulation was stopped, the firing from the RGCs to the light stimulus increased subsequently (Granit, 1955b; Granit, 1955a).

2.4 Striate cortex outputs

Fibres in layer 5 of rat primary cortex project to the superior colliculus, the pons, the lateral posterior nucleus, and the contralateral hemisphere through corpus callosum (Hübener & Bolz, 1988). Several corticotectal neurons extend collaterals to the pons and the lateral posterior nucleus (Hübener & Bolz, 1988). Neurons from layer 6 of area 17 travel to the dLGN and the claustrum (Hübener & Bolz, 1988). These pyramidal neurons in the visual cortex have different dendritic and axonal morphology (Hübener & Bolz, 1988). Interhemispheric connections for area 17 and area 18 in rats have been identified through the callosal trajectory (Berry, Nowicky, & Teyler , 1990). Stimulations of the white matter on the contralateral hemisphere yield visual cortical field potentials (Berry, Nowicky, & Teyler , 1990). Cells in all layers except layer 6 produced EPSPs in response to callosal stimulations (Berry, Nowicky, & Teyler , 1990).

2.5 Summary

Following this review, one might expect a retrograde trans-synaptic degeneration to develop from the geniculo-cortical fibres by way of the dLGN to the retina after occipital lobe damage. Additionally there would be anterograde degeneration from the cortico-geniculate fibres towards the dLGN.

3 Retinotopic organization and retinal nerve fibres

In this chapter, retinal nerve fibre distribution and ganglion cell number in have been reviewed. The topics include nasal-temporal retinal nerve fibre, dorsal-ventral retinal nerve fibre, periphero-central fibre organization, fibre distribution within the nerve fibre layer, retinal ganglion cell number and density. The projection of the axons within the optic nerve and chiasm is also reviewed.

3.1 Retinotopic organization in the retina and optic disc

There is evidence of retinotopic organization in several studies (Naito, 1989; Ogden, 1983). It is defined as a definite and stable arrangement of retinal nerve fibres throughout their course (Walsh & Hoyt, 1969). However it was not completely homogeneous in a macaque study which revealed slightly scattered stained ganglion cells outside labeled fibre bundles (Ogden, 1983). Only a few studies had a view against the retinotopic organization (Horton, Greenwood, & Hubel, 1979; Hubel & Wiesel, 1960). Retinotopic mapping had a great advance in the 19th century as microscopy and histologic techniques markedly developed (Walsh & Hoyt, 1969). The retinotopic organization is different between primates and other species. In nonmamalian vertebrates, new ganglion cells are added as concentric rings to the retinal periphery throughout life (Walsh & Polley, 1985; Hollyfield, 1972; Bunt, 1982). This addition is a specialization of frogs and fishes, and different from mammals (Walsh & Polley, 1985).

Fishes: Goldfish is a surface feeder and is presumed to use vision to obtain food (Bruesch & Arey, 1942). In goldfish, fibres from the peripheral retina move toward the blood vessel in the optic nerve head, and follow the vessel behind the eye until it leaves the optic nerve. The youngest fibres from peripheral retina are situated on one side of the optic nerve, whereas the oldest fibres from the central retina are on the other (Bunt, 1982). The optic nerve fibres decussate completely and intermingle before they reach the optic tracts (Bunt, 1982; Roth, 1979).

Amphibians: Frogs catch prey on land using vision (Olmsted, 2006). Frogs are insensitive to the stationary part of the environment and can hunt only moving targets (Olmsted, 2006). They escape enemies by leaping into a darker area (Olmsted, 2006). There is neither fovea nor area centralis in the retina but there are

rods, cones, bipolar cells, and ganglion cells (Olmsted, 2006). In the frog, *Xenopus laevis*, a zone of reorganization at the optic nerve head has been observed (Taylor, 1987). The retinal nerve fibres are arranged in a circumferential organization (Taylor, 1987). The fibres relocate their positions at the optic nerve head and the circumferential organization of the fibres is lost subsequently (Taylor, 1987). In the optic nerve, the axons lie in an annular organization, that is, the peripheral retinal nerve fibres are in the outer portion of the optic nerve, whilst the central retinal nerve fibres lie in the core (Taylor, 1987). Toads can eat moving targets as well as white grubs crawling on the ground and vision is more developed than the vision of the frog (Olmsted, 2006). The horned toad, *Phrynosoma cornutum*, diurnal in its visual habits, has a pure cone retina and develops considerably a fovea (Bruesch & Arey, 1942).

Birds: Vision plays a very important part in their life such as finding food, normal flight, and nesting (Bruesch & Arey, 1942). In the chick, circumferential fibres were observed at the peripheral retina without any evidence of macular or fovea in one study (Goldberg & Coulombre, 1972). The fovea of domestic birds such as duck, chicken, and canary tend to be quite shallow (Bruesch & Arey, 1942). A well-developed fovea and area centralis are found in pigeons (Polyak, 1957).

Mammals: The fovea centralis and visual streak of primates are different from other mammals (Stone & Johnston, 1981; Provis, 1979). In rabbits, for instance, the visual streak is more distinct than the area centralis (Provis, 1979). In primates, including bushbaby, new- and old- world monkey, and man, the foveal development is the most prominent feature of the retinal topography (Stone & Johnston, 1981). The visual streak appears less developed in primates than in cats (Stone & Johnston, 1981). In cat retina, ganglion cells develop in a rough spiral pattern around the area centralis and the development is completed within the first 2 weeks of life (Walsh & Polley, 1985). The oldest cells lie superior and nasal to the area centralis (Walsh & Polley, 1985). There is evidence of gradient density of the ganglion cells (Wässle & Illing, 1980). The density is highest at the centre and becomes lesser in the increasing periphery (Wässle & Illing, 1980). Cat optic nerve has 2 distinct bends (Naito, 1986). The anterior bend is 2 mm behind the globe and ventrally flexing, while the posterior bend is about 6 mm behind the globe and dorsally flexing (Naito, 1986). This has created a macroscopic twisted appearance of the optic nerve as well

as a partial helical twist of the nerve fibre bundles (Naito, 1986). The nerve fibres also intermingle markedly within the optic nerve (Naito, 1986). Near the chiasm, nerve fibres scatter in a great degree, having a partial dorsoventral inversion with substantial overlapping (Naito, 1986). Fibres arising from the nasal retina cross to the contralateral optic tract (Torrealba, Guillery, Eysel, Polley, & Mason, 1982). In addition, there is a projection from the retina to the superior colliculus (Wässle & Illing, 1980). Retinal ganglion cells in both nasal and temporal portions of the retina send crossing projections to the contralateral superior collicullus, while fibres from the nasal retina of the ipsilateral eye do not cross (Wässle & Illing, 1980). Polyak suggested that the retina, the optic nerve, and the intrinsic chiasmal fibres of humans and non-human primates are similar (Polyak, 1957). However, the extrinsic anatomy of the chiasm differs substantially (Polyak, 1957). The primate chiasm is partially encased in the bone and the intracranial portion of the optic nerve is very short (Polyak, 1957). The human chiasm in sagittal and frontal section tends to be more flattened than that of the other primates (Polyak, 1957). A summary of retinotopic organization in the anterior visual pathway is presented in Fig. 15 and the arrangement in the optic disc in primates is reviewed below.

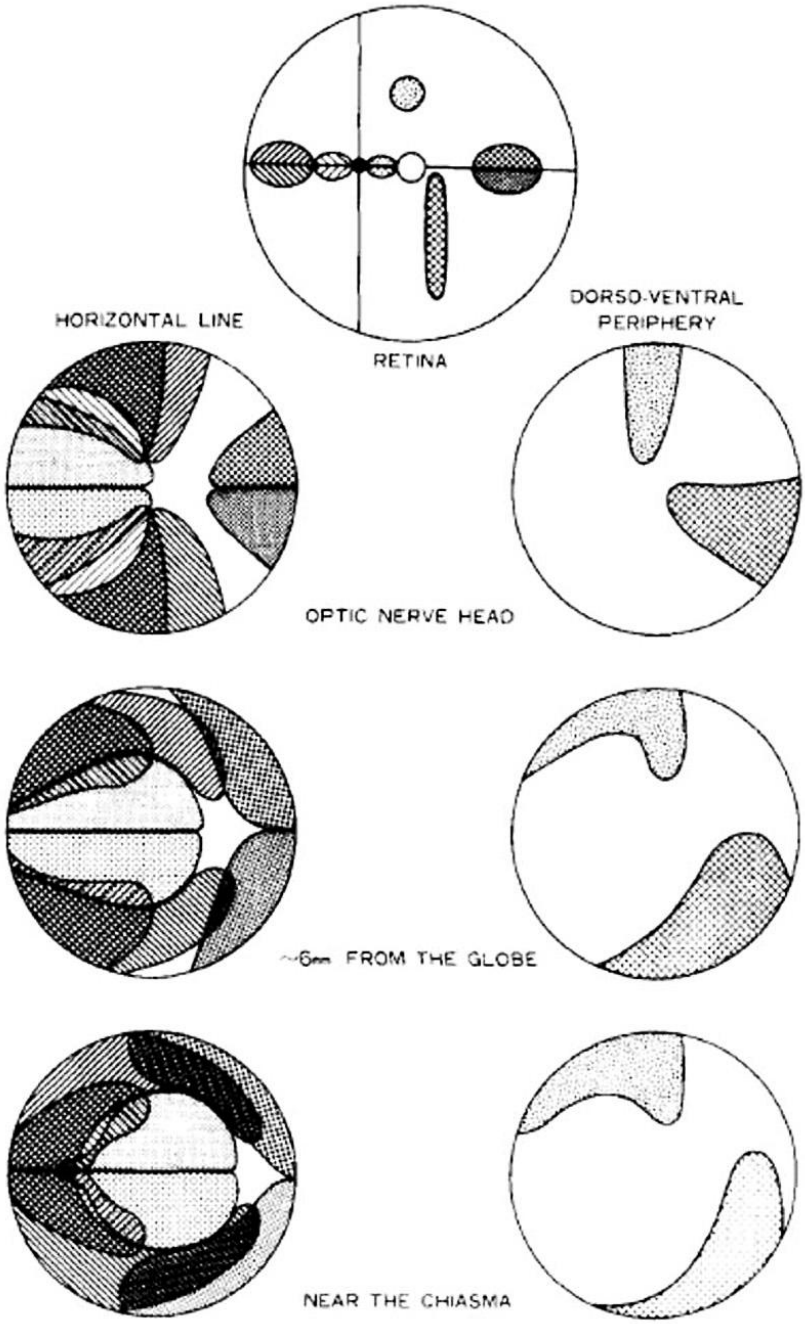

Figure 15 A summary of retinotopic organization in the anterior visual pathway in monkey optic nerve. Fibres from dorsal and ventral retinae are separated from each other. Fibres from nasal central retina are isolated from fibres of other areas. Fibres from other areas overlapped. Reprinted from J Comp Neurol, vol 284, J Naito, Retinogeniculate projection fibers in the monkey optic nerve: a demonstration of the fiber pathways by retrograde axonal transport of WGA-HRP, page 174–86, ©1989. Permission to reproduce this figure has been granted by John Wiley and Sons.

3.1.1 Nasal-temporal retinal nerve fibres

Fibres from the nasal central retina: The central area of retina is called fovea-perifovea or macular. The projection of central retina to the optic disc is often referred to as the papillomacular bundle. Plant and Perry have pointed out that the concept of the 'papillomacular bundle' has no counterpart in the normal anatomy and is applied inconsistently in the literature (Plant & Perry, 1990). They suggested the term 'centro-caecal projection' originating from the entire fovea and the area between the fovea and optic disc on to the temporal optic nerve (Plant & Perry, 1990). The macular and foveal projections can be divided into nasal and temporal hemi-projections. Retinal ganglion cells originating from the nasal part of this area form the nasal hemi-foveal projection, which projects towards the optic disc (Naito, 1989). In 1989 Naito studied the courses of the retinal ganglion cell axons in primate (Naito, 1989). Optic nerve fibres and retinal ganglion cells were retrogradely labelled by iontophoretic injections of wheat germ agglutinin conjugated to horseradish peroxidase (WGA-HRP) into the lateral geniculate nucleus. He observed that the nasal hemi-foveal fibres approach the temporal sector of the optic nerve head directly (Naito, 1989). They take a straight horizontal course and separate well from the temporal central and temporal peripheral retinal fibres (Naito, 1989). On the optic disc, the centro-caecal projection has a wedge shape with a base on the outer periphery (Dean & Usher, 1903; Fitzgibbon & Taylor, 1996) or a shape like a small bar at the temporal-superior sector (Naito, 1989). In the optic nerve, the fibres lie in the centre (Naito, 1989). Other monkey and human studies agreed with these findings (Brouwer & C Zeeman, 1926; Dean & Usher, 1903; Polyak, 1957; Fitzgibbon & Taylor, 1996; Parsons, 1902; Nettleship, 1896; Duke-Elder, 1932). The proportion of these macular fibres in the optic disc varied among studies as the techniques have been changed over time. They were found to occupy 1 to 3.6 in 12 sectors of the overall cross-sectional area of the optic disc (Fitzgibbon & Taylor, 1996)(Dean & Usher, 1903). There were several small blood vessels encircling the central retinal area (Polyak, 1957). They were arranged in a way to prevent an optical obstruction from the vessels (Polyak, 1957).

Fibres from the temporal central retina: retinal ganglion axons located at the temporal side of the macular are divided sharply by the horizontal raphe (Dean & Usher, 1903; Naito, 1989; Fitzgibbon & Taylor, 1996). The raphe extends from the fovea to the ora serrata along the horizontal meridian (Polyak, 1957). It is a line,

which separates bundles of nerve fibres arising in the upper temporal quadrant from those arising in the lower temporal quadrant (Polyak, 1957). This anatomical cleavage persists throughout the visual pathway as far as the occipital lobe (Polyak, 1957). It may be an anatomical basis of homonymous quadrantanopia of central origin (Polyak, 1957) although others have disagreed (Horton & Hoyt, 1991). Upper temporal retinal fibres converge upon the optic disc at the superior-temporal area and the lower temporal retinal fibres reach the inferior-temporal area of the disc (Naito, 1989; Fitzgibbon & Taylor, 1996). While approaching the chiasm, they move toward each other to the lateral temporal peripheral part of the optic nerve, surrounding the nasal hemi-foveal projection fibres with minimal overlap (Naito, 1989).

Fibres from the temporal peripheral retina: These fibres reach the optic disc either at the superior or the inferior region (Naito, 1989; Fitzgibbon & Taylor, 1996) and intermingle with the temporal central retinal fibres at this level (Naito, 1989). Passing posteriorly, they rearrange their location laterally and medially along the peripheral region of the temporal half of the optic nerve (Naito, 1989). These fibres clearly separate from the centro-caecal projection fibres (Brouwer & C Zeeman, 1926).

Fibres from the nasal peripheral retinas: The nasal peripheral fibres approach the disc directly in straight lines, like spokes of a wheel (Naito, 1989; Polyak, 1957; Fitzgibbon & Taylor, 1996). The horizontal raphe is also found nasal to the optic disc, dividing the area into upper and lower portions (Naito, 1989; Fitzgibbon & Taylor, 1996). At the optic nerve head, the upper retinal nerve fibres attain the nasal-superior part, while the lower retinal fibres reach the inferior-nasal part (Naito, 1989; Dean & Usher, 1903; Fitzgibbon & Taylor, 1996; Parsons, 1902). Retinal nerve fibres near the horizontal meridian reach the optic disc at 3 or 9 o'clock position in the right or left eye respectively (Naito, 1989; Fitzgibbon & Taylor, 1996). The fibres appear as a wedge shape on the disc with an apex pointing towards the centre. The location is relatively unchanged as the fibres proceed posteriorly (Naito, 1989; Dean & Usher, 1903; Parsons, 1902). At the posterior part of the chiasm, these fibres entirely cross to the opposite side (Brouwer & C Zeeman, 1926; Dean & Usher, 1903; Parsons, 1902).

3.1.2 Crossing and uncrossing fibres

The retinal fibres nasal to a line drawn vertically through the fovea cross whilst the fibres temporal to the line do not cross (Ogden, 1983; Brouwer & C Zeeman, 1926; Polyak, 1957; Walsh & Hoyt, 1969). This is the anatomical basis for homonymous hemianopia. The nasal region of the optic disc contains only the crossing fibres (Brouwer & C Zeeman, 1926; Dean & Usher, 1903; Walsh & Hoyt, 1969; Parsons, 1902). The crossing fibres in the temporal half of the disc have a small sector at about 9 or 3 o'clock on the disc of the right or left eye respectively (Ogden, 1983; Polyak, 1957; Walsh & Hoyt, 1969). Uncrossing fibres are found in the remaining areas of the disc (Walsh & Hoyt, 1969). Moreover, it has been proposed that fibres from the nasal hemiretina, which carries the crossing fibres, also contribute to the upper and lower parts of the disc (Kanamori, et al., 2004; Mehta & Plant, 2005a). At the termination of the optic nerve and the very beginning of the optic chiasm, there is a pial septum, extending from the dorsal surface to the ventral-medial part (Walsh & Hoyt, 1969). The septum may segregate the crossing from uncrossing fibres (Walsh & Hoyt, 1969). However binocular stereopsis in the midsagittal plane would not be possible if the crossing and non-crossing fibres separate completely in the vertical meridian passing through the fovea (Blakemore, 1969). It has been shown in monkeys that there is a thin strip of nasotemporal overlap in the central retina where crossing and non-crossing fibres intermingle (Fukuda, Sawai, Watanabe, Wakakuwa, & Morigiwa, 1989). Crossing fibres in the temporal part of the overlap are mainly from large and small cells presumably M and gamma cells (Fukuda, Sawai, Watanabe, Wakakuwa, & Morigiwa, 1989). Uncrossing fibres in the nasal part of the overlap originate from P cells (Fukuda, Sawai, Watanabe, Wakakuwa, & Morigiwa, 1989).

3.1.3 Dorsal and ventral retinal nerve fibres

Human fibres from all retinal areas segregate dorsoventrally by the horizontal raphe and that fibres from ventral or dorsal retinal area do not cross to the opposite side (Naito, 1989; Fitzgibbon & Taylor, 1996; Walsh & Hoyt, 1969; Dean & Usher, 1903; Parsons, 1902). All bundles above and below the horizontal raphe except for the centro-caecal projection radiate as arches along the fibre courses (Polyak, 1957). The arches curve above and below the fovea to the disc and closely followed the large arteries and veins (Polyak, 1957). Upper retinal fibres reach the superior region of the optic disc and the lower retinal fibres project to the inferior area of the

disc (Naito, 1989; Fitzgibbon & Taylor, 1996; Walsh & Hoyt, 1969). They have a wedge shape upon the disc with an apex pointing towards the centre (Naito, 1989; Fitzgibbon & Taylor, 1996). Within the optic nerve, the fibres from the 2 groups radiate more temporally and move towards each other as they are approaching the optic chiasm (Naito, 1989). Upper and lower retinal fibres relatively retain their positions throughout the visual pathway except in the optic tract and lateral geniculate body (Walsh & Hoyt, 1969).

3.1.4 Periphero-central fibre organization

It is controversial whether the peripheral retinal fibres are located at the periphery of the optic disc whilst the central retinal fibres are at the centre of the disc (Walsh & Hoyt, 1969). It has been demonstrated that human retinal nerve fibres beyond the arcuate bundles and the fovea occupy the optic nerve from the edge to the middle part (Fitzgibbon & Taylor, 1996). There is no evidence of periphero-central distribution at the optic nerve head or the proximal optic nerve as the peripheral retinal nerve fibres (10-15 mm from the optic disc) and the central retinal nerve fibres (5 mm from the optic disc) overlap and that the centre of the optic nerve head is poorly mapped (Fitzgibbon & Taylor, 1996).

3.1.5 Fibre distributions within the retinal nerve fibre layer

A study revealed that most retinal nerve fibres are arranged in parallel within a fascicle as they approach the optic disc but some fibres cross between various fascicles (Fitzgibbon & Taylor, 1996). The axons in the superior, inferior, and nasal periphery retinae are scattered throughout the retinal nerve fibre layer (RNFL) thickness from the vitreal to scleral surfaces whereas fibres temporal to the fovea and in the arcuate bundles lie within the scleral region of the RNFL. The arcuate fibres approach the peripheral part of optic discs and do not enter the centre; in some cases they take a straight path along the vitreal half of the RNFL to the disc. In the centro-caecal projection, the fibres are scattered evenly throughout the thickness of the RNFL. There is no zone of reorganization in human retina like in non-mammalian species (Taylor, 1987). Retinal fibres in the vitreal part process to the optic disc centre while the fibres in the scleral part process to the optic disc periphery (Fitzgibbon & Taylor, 1996). Another study has come out with another conclusion (Ogden, 1983). Peripheral long fibres of less than 3 mm from the optic disc are mainly in the vitreal half of the RNFL but spread widely as they cross the disc

margin. Axons of intermediate ganglion cells, 1-3 mm from the optic disc, are located at the scleral part of the RNFL. At the peripapillary area and the prelaminar part of the disc, short fibres of less than 1 mm from the optic disc join the long fibres. This greatly increases the thickness of the RNFL in these areas.

3.2 RGC and optic nerve fibre number and density

The total number of the fibres in the optic nerve varies among species: 53,000 in goldfish, 113,000 in dogfish shark, 362 in necturus, 105,000 in turtle, 105,000 in alligator, 129,000 in horned toad, 408,000 in duckling, 414,000 in chick, 988,000 in pigeon, 82,100 in opossum, 119,000 in cat, 154,000 in dog, 80,100 in Norway rat, 74,800 in albino rat, 681,000 in pig, 1,210,000 to 1,304,816 in monkey, and 1,010,000 in man (Bruesch & Arey, 1942; Harwerth, Carter-Dawson, Shen, Smith 3rd, & Crawford, 1999) (Table 4).

Author	Year	Mean	Minimum	Maximum
Bruesch and Arey	1942	1,010,000	871,000	1,200,000
Kupfer	1967	1,100,000		
Potts	1972		1,163,000	1,274,000
Quigley	1982	963,932		
Balazsi	1984	1,244,005		
Johnson	1987		759,000	1,685,000
Repka and Quigley	1989	693,316		
Jonas	1990	1,159,000	816,000	1,502,000
Jonas	1992	1,158,000	777,000	1,679,000

Table 4 Human optic nerve fibre counts

(Jonas, Müller-Bergh, Schlötzer-Schrehardt, & Naumann, 1990; Jonas, Schmidt, Müller-Bergh, Schlötzer-Schrehard, & Naumann, 1992; Repka & Quigley, 1989; Johnson, Miao, & Sadun, 1987; Balazsi, Rootman , Drance , Schulzer, & Douglas, 1984; Quigley, Addicks, & Green, 1982; Potts, Hodges, Shelman , Fritz , Levy, & Mangnall , 1972; Kupfer, 1963)

The total human neuron number in the retinal ganglion cell layer also varies among individuals and research studies. The data are as follows: between 0.7 and 1.5

millions (Curcio & Allen, 1990; Stone & Johnston, 1981), with a mean of 1.07 and SD of 0.4 millions in 27-37 year-old individuals (Curcio & Allen, 1990); between 1.27 and 2.8 millions in 16-77 year-old individuals (Harman, Abrahams, Moore, & Hoskins, 2000). The optic nerve fibre count is not significantly different between age-matched females and males but there is a tendency to have a smaller count in females (Jonas, Müller-Bergh, Schlötzer-Schrehardt, & Naumann, 1990). No statistical differences between left and right eyes are detected (Jonas, Müller-Bergh, Schlötzer-Schrehardt, & Naumann, 1990; Jonas, Schmidt, Müller-Bergh, Schlötzer-Schrehard, & Naumann, 1992).

The area of the retina is 833 mm^2 in human, followed by cat (542 mm^2), macaque (527 mm^2), squirrel monkey (345 mm^2), and bushbaby (319 mm^2) (Bruesch & Arey, 1942). The human retinal area differs slightly among studies. It ranges from 975.7 to 1,104.5 mm^2, with a median of 1,011 and a standard deviation (SD) of 68.1 mm^2 in one study (Curcio & Allen, 1990), and ranges from 885 to 1174 mm^2 in another study (Harman, Abrahams, Moore, & Hoskins, 2000). The retinal area is increasing throughout life (Harman, Abrahams, Moore, & Hoskins, 2000). The distance from the foveal centre to the temporal edge of the optic disc is between 3.16 and 3.91 mm, with a median of 3.44 and SD of 0.28 mm (Curcio & Allen, 1990). The proportions of the temporal and nasal parts of the retina may be associated with the frontalization of the eyes and a partial binocular overlap of the visual field (Brouwer & C Zeeman, 1926; Stone & Johnston, 1981). Both humans and non-human primates have frontally placed eyes (Polyak, 1957), while rabbit eyes are far apart on the lateral side of the head (Brouwer & C Zeeman, 1926). The binocular field is larger in monkeys than cats, and it is also greater in cats than rabbits (Brouwer & C Zeeman, 1926). Hence, the number of uncrossed fibres at the chiasm is the smallest in the rabbit, followed by the cat, and monkey, respectively (Brouwer & C Zeeman, 1926). It has been estimated that the area of the temporal retina is 41% in human, 43% in macaque, 39% in squirrel monkey, 32% in bushbaby, and 34% in cat (Brouwer & C Zeeman, 1926). In one study, the human retinal ganglion axons at the macular contribute to 2% of the total retinal area (Fitzgibbon & Taylor, 1996).

Optic disc area of fixed eyes in human ranges from 1.94 to 2.65 mm^2 with a mean of 2.31 ± 0.28 mm^2 in one study (Jonas, Müller-Bergh, Schlötzer-Schrehardt, & Naumann, 1990), and from 0.80 to 5.54 mm^2 with a mean of 2.69 ± 0.70 mm^2 in

another study (Jonas, Gusek, & Naumann, 1988). It is estimated that the optic disc area in the fixed eye is smaller that in the unfixed eyes with a shrinkage area factor of 10.8% (Jonas, Müller-Bergh, Schlötzer-Schrehardt, & Naumann, 1990). The optic disc appears oval in shape with a mean diameter in a horizontal orientation of 1.76 ± 0.31 mm (0.91-2.61 mm), and a mean diameter in a vertical orientation of 1.92 ± 0.29 mm (0.96-2.91 mm) (Jonas, Gusek, & Naumann, 1988). Mean horizontal cup diameter is 0.83 ± 0.58 mm (0.00-2.08 mm) and mean vertical diameter is 0.77 ± 0.55mm (0.00-2.13 mm) (Jonas, Gusek, & Naumann, 1988). Cup/disc ratio horizontally (mean 0.39 ± 0.28, minimum 0.00, maximum 0.87) is larger than the vertical one (mean 0.34 ± 0.25, minimum 0.00, maximum 0.85) (Jonas, Gusek, & Naumann, 1988). No significant correlation is found between these morphometric optic disc data and refraction, age, sex or side (Jonas, Gusek, & Naumann, 1988).

The density of the optic nerve fibres as a ratio of number of nerve fibres to optic disc area is significantly correlated with the optic disc area (Jonas, Schmidt, Müller-Bergh, Schlötzer-Schrehard, & Naumann, 1992). The density of small optic discs is significantly greater than that of large optic discs (Jonas, Schmidt, Müller-Bergh, Schlötzer-Schrehard, & Naumann, 1992). Furthermore, the number of the optic nerve fibres increases significantly with enlarging optic disc size (Jonas, Schmidt, Müller-Bergh, Schlötzer-Schrehard, & Naumann, 1992; Quigley, Coleman, & Dorman-Pease, 1991). This creates crowded nerve fibres within the small optic discs (Jonas, Schmidt, Müller-Bergh, Schlötzer-Schrehard, & Naumann, 1992). Blacks have larger discs than whites (Chi, Ritch , Stickler , Pitman, Tsai, & Hsieh , 1989). Moreover, the large discs have a higher anatomic reserve capacity than the small ones, and the disc area can contribute to a prognostic value on optic neuropathy (Jonas, Schmidt, Müller-Bergh, Schlötzer-Schrehard, & Naumann, 1992). The neuroretinal rim from an ophthalmoscopic view is equivalent to the nerve fibres of the optic nerve head (Jonas, Müller-Bergh, Schlötzer-Schrehardt, & Naumann, 1990). The normal rim area is between 0.80 and 4.66 mm^2 with a mean of 1.97 ± 0.50 mm^2 (Jonas, Gusek, & Naumann, 1988). It is widest in the inferior optic disc section, followed by the superior, nasal and temporal sections (Jonas, Gusek, & Naumann, 1988). It increases significantly with disc size (Jonas, Müller-Bergh, Schlötzer-Schrehardt, & Naumann, 1990; Jonas, Gusek, & Naumann, 1988). The regression line of the correlation between optic nerve fibre count and the disc area has a slope

of 175,000 fibres/mm^2 optic disc area. (Jonas, Schmidt, Müller-Bergh, Schlötzer-Schrehard, & Naumann, 1992). The regression line of the correlation between the neuroretinal rim area and the disc size in normal eyes with circular steep optic disc cupping has a slope of 0.30 mm^2 of rim area / mm^2 optic disc area (Jonas, Gusek, & Naumann, 1988). It has been estimated that an increase of 0.30 mm^2 of the rim corresponds to an increase of 175,000 fibres in normal eyes with circular steep cupping (Jonas, Schmidt, Müller-Bergh, Schlötzer-Schrehard, & Naumann, 1992). This interpretation can be used only in a certain age group (Jonas, Schmidt, Müller-Bergh, Schlötzer-Schrehard, & Naumann, 1992) because the neuroretinal rim does not change in size with increasing age (Jonas, Gusek, & Naumann, 1988) whilst the fibre count is declining (Jonas, Schmidt, Müller-Bergh, Schlötzer-Schrehard, & Naumann, 1992). The rim in medium-sized optic discs with physiologic cupping is significantly larger than in small optic discs with no cupping (Jonas, Gusek, & Naumann, 1988). In non-glaucomatous optic nerve damage, the size of the rim has remained stable (Jonas, Nguyen, & Naumann, Optic disc morphometry in simple optic nerve atrophy, 1989). However, in glaucomatous eye, both the neuroretinal rim and number of optic nerve fibres have dropped (Airaksinen, Drance, & Schulzer, 1985; Oppel, 1963).

The mean area of the inner aperture of the optic nerve scleral canal in fixed specimens is 2.30 ± 0.42 mm^2, with an area shrinkage factor of 13% or 2.59/2.30 mm^2 (Jonas, Schmidt, Müller-Bergh, Schlötzer-Schrehard, & Naumann, 1992). It is significantly correlated with the nerve fibre count (Jonas, Schmidt, Müller-Bergh, Schlötzer-Schrehard, & Naumann, 1992). It also correlated with the optic nerve cross sectional area but did not reach a significant level (Jonas, Schmidt, Müller-Bergh, Schlötzer-Schrehard, & Naumann, 1992). It does not vary with age (Jonas, Schmidt, Müller-Bergh, Schlötzer-Schrehard, & Naumann, 1992).

A mean of the cross-section area of the human retrobulbar optic nerve, excluding the leptomeninges, is 8.09 ± 1.38 mm^2 with a minimum of 5.50 mm^2 and a maximum of 10.89 mm^2 in one study (Jonas, Müller-Bergh, Schlötzer-Schrehardt, & Naumann, 1990) and 8.22 ± 1.60 mm^2 in another study (Jonas, Schmidt, Müller-Bergh, Schlötzer-Schrehard, & Naumann, 1992). The optic nerve cross-sectional area is related to the optic disc size (Jonas, Schmidt, Müller-Bergh, Schlötzer-Schrehard, & Naumann, 1992). It is also positively correlated with the nerve fibre count (Jonas,

Schmidt, Müller-Bergh, Schlötzer-Schrehard, & Naumann, 1992; Jonas, Müller-Bergh, Schlötzer-Schrehardt, & Naumann, 1990). It can therefore be an indicator of the nerve fibre number (Jonas, Schmidt, Müller-Bergh, Schlötzer-Schrehard, & Naumann, 1992; Jonas, Müller-Bergh, Schlötzer-Schrehardt, & Naumann, 1990). It is essential that the optic nerve thickness can be measured by accurate diagnostic procedures such as MRI to estimate the nerve fibre number indirectly (Jonas, Müller-Bergh, Schlötzer-Schrehardt, & Naumann, 1990). A thin retrobulbar optic nerve, for instance, represents optic nerve atrophy (Jonas, Schmidt, Müller-Bergh, Schlötzer-Schrehard, & Naumann, 1992). Nerve fibre count per area in the optic nerve at a distance of 2 to 5 mm behind the globe is significantly higher in the temporal and inner parts of the optic nerve than in the nasal and outer parts, respectively (Jonas, Müller-Bergh, Schlötzer-Schrehardt, & Naumann, 1990). No significant difference between the superior and inferior regions of the optic nerve is demonstrated (Jonas, Müller-Bergh, Schlötzer-Schrehardt, & Naumann, 1990).

The retinal nerve fibre layer thickness increases from the fundus periphery to the optic nerve head with regional differences. It is thickest at the vertical optic disc poles and thinner at the temporal and nasal optic disc borders (Quigley & Addicks, 1982). There is no nerve fibre layer at the fovea (Quigley & Addicks, 1982).

A map of the retinal ganglion cell density (cells/mm^2) has been proposed (Harman, Abrahams, Moore, & Hoskins, 2000; Curcio & Allen, 1990; Stone & Johnston, 1981). Isodensity lines have arranged circumferentially and are elongated horizontally in human and primates, suggesting remnants of visual streaks in primates (Stone & Johnston, 1981)(Curcio & Allen, 1990). The ganglion cell density becomes less in the periphery (Stone & Johnston, 1981; Harman, Abrahams, Moore, & Hoskins, 2000). The streaks are not close to the watershed area of blood vessels (Stone & Johnston, 1981). In human, isodensity lines from the centre to the periphery are 3000, 2000, 1000, to 500 cell / mm^2 (Stone & Johnston, 1981). The nasal retina has more cells than other meridians in every eccentricity beyond the disc (Curcio & Allen, 1990). The peak ganglion cell density in the central retina ranges from 31,900 to 37,800 cells/mm^2, with a median of 35,100. The ganglion cell density in the central retina decreases more rapidly along the vertical meridian than along the horizontal meridian as the eccentricity becomes greater (Curcio & Allen, 1990). The margin of the fovea varies since ganglion cells are found between 63 microns and 234 microns

from the fovea centre in different orientation and in different eyes (Curcio & Allen, 1990). Several factors have been proposed to account for the formation of the cell density gradient in the centro-peripheral distribution during the developmental period (Provis, 1987; Mastronarde, Thibeault, & Dubin, 1984; Beazley & Dunlop, 1983). These included retinal loss of ganglion cells (Provis, 1987), differential growth rates in the retina (Mastronarde, Thibeault, & Dubin, 1984), migration of cells towards the regions of central specialisation (Beazley & Dunlop, 1983), and transformation of cells (Hinds & Hinds, 1978). Natural ganglion cell death in human fetal retina was studied by Provis in 1987 (Provis, 1987). Pyknotic figures, which appear as round, darkly stained bodies, and fragments, and viable cells in the ganglion cell layer were counted in number and assessed in density. The cell loss or pyknotic figures are highest between the 16th and 21st week of gestation, whereas the loss is relatively low prior to the 16th week and after the 30th week of gestation. It is suggested that the cell death within ganglion cell layer comes to an end at the 30th week of gestation. The pattern of the peripheral retinal cell loss persists and creates the centroperipheral gradient of cell density in the retina in the subsequent development. By the 23rd week of gestation, cell density in the ganglion cell layer is significantly elevated at developing fovea, while that in the peripheral retina declines. The period of cell loss in the ganglion cell layer observed in this study coincides with the axonal loss in the developing optic nerve (Provis, 1987; Provis, Driel, Bilson, & Russell, 1985). In another study of human fetus, a maximum number of 3.7 million axons were observed in the optic nerve at 15 weeks of gestation (Provis, Driel, Bilson, & Russell, 1985). Around 2.5 million axons are eliminated during subsequent development, (Provis, Driel, Bilson, & Russell, 1985).

The total number and density of human retinal ganglion cells as well as optic nerve axons decrease significantly with increasing age (Jonas, Müller-Bergh, Schlötzer-Schrehardt, & Naumann, 1990; Jonas, Schmidt, Müller-Bergh, Schlötzer-Schrehard, & Naumann, 1992; Harman, Abrahams, Moore, & Hoskins, 2000; Balazsi, Rootman , Drance , Schulzer, & Douglas, 1984) but macular neurons are lost minimally (Harman, Abrahams, Moore, & Hoskins, 2000). Mean annual losses of 4,000, 5,436, and 5637 optic nerve fibres were observed in 3 studies (Jonas, Müller-Bergh, Schlötzer-Schrehardt, & Naumann, 1990; Jonas, Schmidt, Müller-Bergh, Schlötzer-Schrehard, & Naumann, 1992; Balazsi, Rootman , Drance , Schulzer, & Douglas,

1984). Dorsal and nasal retinal regions have the strongest correlations between cell density and age (Harman, Abrahams, Moore, & Hoskins, 2000). No significant correlation between density and age in the temporal region has been demonstrated (Harman, Abrahams, Moore, & Hoskins, 2000). The age-dependent nerve fibre loss is one of several reasons that explain the decreased visual function and increased differential light threshold in the elderly (Jonas, Müller-Bergh, Schlötzer-Schrehardt, & Naumann, 1990).

3.3 Retinotoopic organization in striate cortex

The first map of primary visual cortex was presented by an opthalmologist, Tatsuji Inouye in 1909 (Ionuye, 1909). Polar angle is arranged in horizontal lines and eccentricity is arranged in vertical lines. It has been criticised since the fovea is elongated as a single line, which is not possible (Adams & Horton, 2003). In 1941, Talbot and Marshall proposed a new map, having a fovea point instead of a line (Talbot & Marshall, 1941). Adams and Horton have introduced a map of primate striate cortex based on the representation of angioscotomas (Adams & Horton, 2003). Retinal landmarks were presented on a tangent screen to locate the visual field position. Flat-mounted of the contralateral cortex was stained for cytochrome oxidase (CO) and demonstrated ocular dominance columns (Fig. 16). Then the retina was superimposed on the striate cortex with some distortions to match the retinal vessel to its cortical representation. Furthermore, a retinal ganglion cell (RGC) density was measured from a range of eccentricities. Corrections for displaced amacrine cells and centripetal displacement of retinal ganglion cell from central photoreceptors were performed. The CO patches in the cortex were projected onto the visual field to evaluate their density along the different eccentricities. Next, CO patches density of V1 and RGC density were compared at each eccentricity. It was found that more cortical tissues are allocated per RGC from the macula when compared with the peripheral retina, so called cortical magnification (Fig. 17). From the map, cortical magnification equation is derived: $M = a (b + E)^{C}$ E = eccentricity; M = magnification factor; a, b, and c = constants.

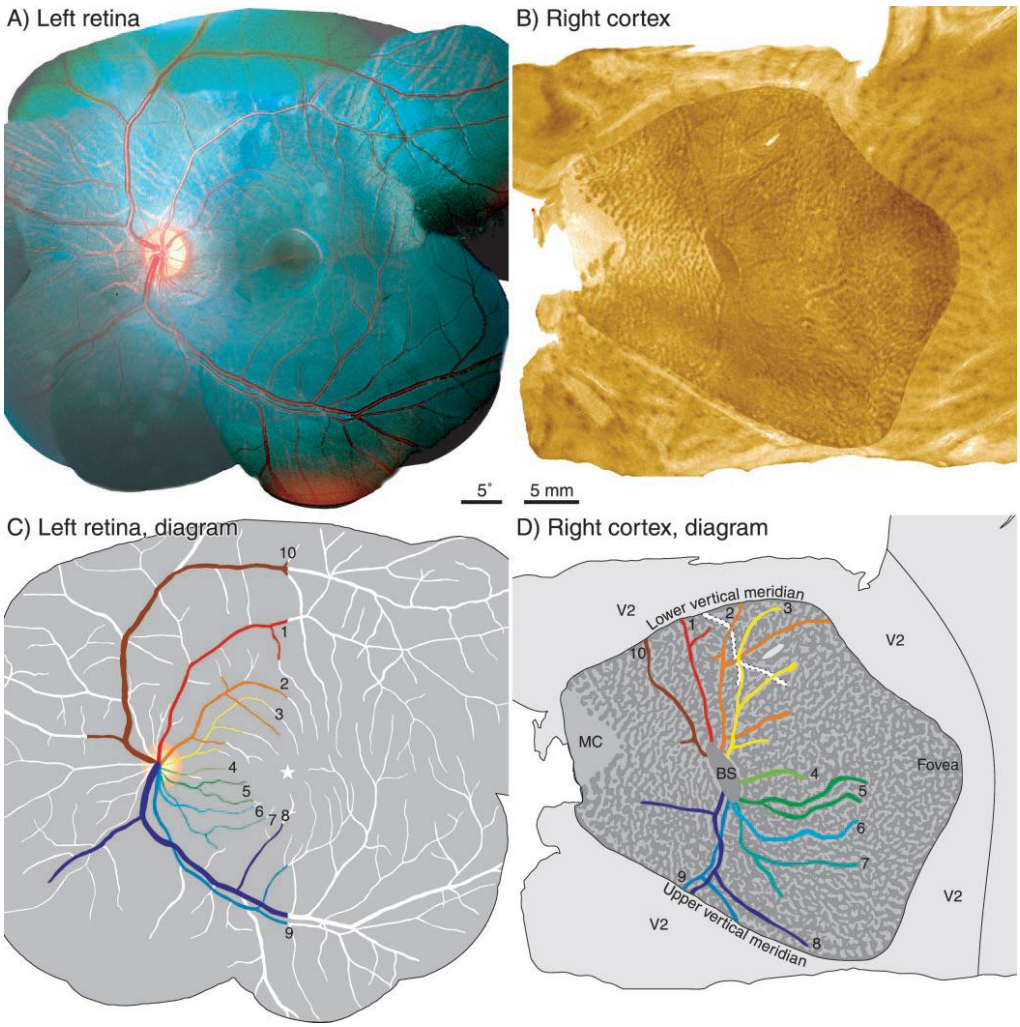

Figure 16 Diagrams show retinal photograph of the left eye (A) and right occipital cortex (B) in a monkey. The cortex, stained for cytochrome oxidase (CO), revealed ocular dominance columns in V1 and the dark lines emerging from the blind spot correspond to cortical representation of retinal blood vessels. The CO pattern of pale-thin-pale-thick stripes in the surrounding area is V2. V1/V2 border corresponds to vertical meridian of the visual field. D and E) Drawings of angiosotoma representation observed in the visual cortex. Reprinted from The Journal of Neuroscience, vol 23, DL Adams & JC Horton, A precise retinotopic map of primate striate cortex generated from the representation of angioscotomas, page 3771-89. Permission to reproduce this figure has been granted by Prof Jonathan C Horton, Prof Daniel L Adams, and The Journal of Neuroscience.

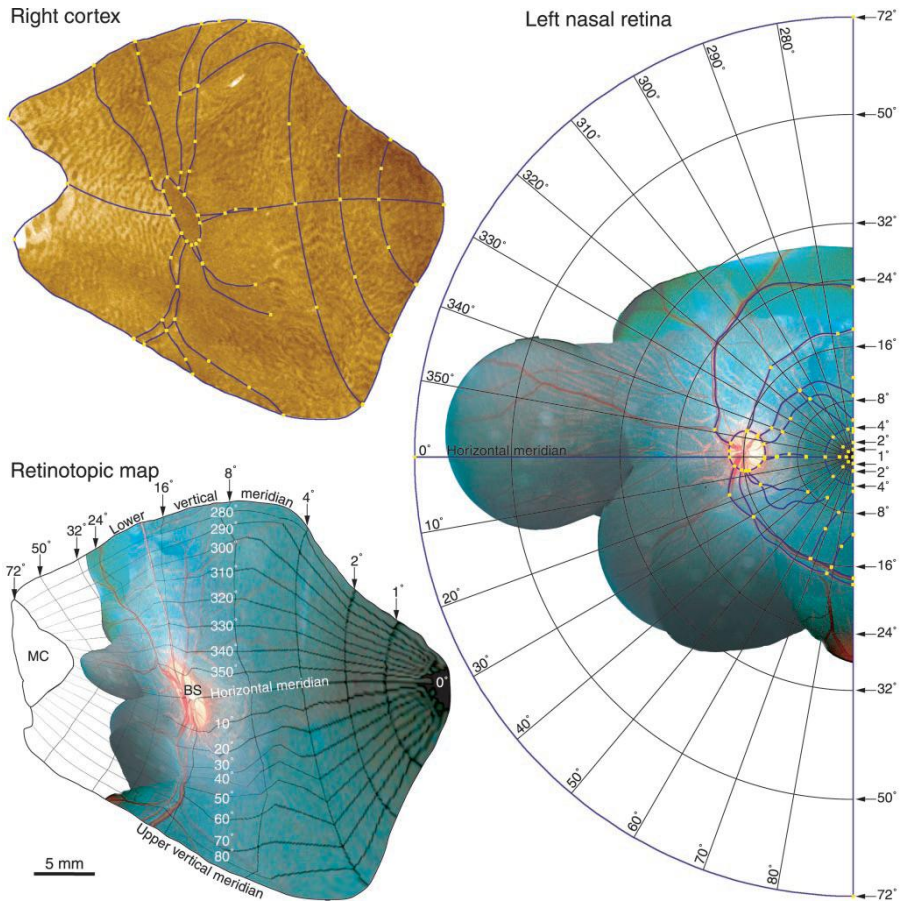

Figure 17 To generate a retinotopic map in the occipital cortex (area 17 or V1), the authors superimposed a ring and ray pattern on the left nasal retina. Correspondence points, marked with yellow squares, were placed at locations that could be identified unambiguously in the cortex and the retina. In this example 64 correspondence points and their intercalated segments were warped from the retina onto the cortex to prepare the retinotopic map. MC = macular cresent. Reprinted from The Journal of Neuroscience, vol 23, DL Adams & JC Horton, A precise retinotopic map of primate striate cortex generated from the representation of angioscotomas, page 3771-89, ©2003. Permission to reproduce this figure has been granted by Prof Jonathan C Horton, Prof Daniel L Adams, and The Journal of Neuroscience.

4 Optical coherence tomography

Optical coherence tomography (OCT) permits non-invasive cross-sectional imagings of internal structures in biological tissues by measuring optical reflections (Huang, et al., 1991; Fugimoto, et al., 1995). It works like ultrasound but light is used instead of sound. The light is transmitted through and reflected from biological tissues. The coherence property of light reflecting from the tissues contains information of time-of-flight-delay. The delay information is then used to evaluate the depth of the tissue samples. The core system of OCT is a fibre optic Michelson interferometer (Industrial Fiber Optics, Tempe, Arizona, USA) (Huang, et al., 1991; Fugimoto, et al., 1995). A beam of light is generated from a superluminescent diode (SLD) which has a wide range of constituent wavelengths (low coherence) and is near infrared, 800–1400 nm. It travels through a 50/50 coupler, which separates the output into two arms. One interferometer arm leads to the tissue sample, whereas the other leads to the reference mirror (Fig. 18). The mirror is moved by an examiner to receive a clear image. Then the light is scanned across the tissue sample. The reflections from the two arms are then combined at the 50/50 coupler, and an interference signal is produced. The interference signal is detected by a photodetector when the reflections from the sample and reference arm are nearly matched or coherent. The path length of the sample arm is calculated from the known path length of the reference mirror. OCT can measure the reflected signals with high detection sensitivity. The measurements of the amplitude of the reflection on a decibel scale as a function of the depth in microns form an axial scan (A-scan) of the retina (Fig. 19) (Costa, et al., 2006). Multiple longitudinal A-scans at a series of lateral locations were performed to create two-dimensional or cross-sectional images of the tissue samples or B-scan (Fig. 20). Two OCT methodologies are available commercially. The first type to be developed uses time-domain imaging. For example, the current available Stratus OCT system (Carl Zeiss Meditec, Inc., Dublin, California, USA) creates a single B scan from 512 A-scans in 1.3 seconds. The fast 3.4 mm circular protocol comprising three circles sequentially in one scan have 256 A-scans per image with 1.92 seconds scanning time. Reproducibility of peripapillary retinal nerve fibre layer (RNFL) measurements using the Stratus OCT in standard and fast scan protocols is great with comparable measurements (Budenz, Chang, Huang,

Knighton, & Tielsch, 2005). There is a good intra- and inter-observer agreement (Krist, Hoffmann, & Schwenn, 2005). Scans with signal strength of at least 7 have higher reproducibility than those of <7, therefore, it is important to aim for signal strength of at least 7 (Wu, Huang, Dustin, & Sadda, 2009). Fast RNFL thickness scan protocol with a fixed 3.4 mm diameter scan circle around the optic disc is commonly utilized in glaucoma and neurology clinics. The measurement is slightly beyond the margin of the optic disc. Since the size of optic disc varied among individuals, this scan protocol measured the RNFL thickness close to the disc margin in larger discs and further away in smaller discs. It is not yet clear whether the large optic discs show thicker peripapillary RNFL. A study employing fixed 3.4-mm-circular protocol revealed that the peripapillary RNFL thickness increased with an increase in the optic disc size (Savini, Zanini, Carelli, Sadun, Ross-Cisneros, & Barboni, 2005) while another study showed no effect of the optic disc size on the peripapillary RNFL thickness in healthy subjects (Kaushik, Pandav, Ichhpujani, & Gupta, 2009).

The alternative OCT type employs Fourier domain (Van Velthoven, Faber, Verbraak, van Leeuwen, & de Smet, 2007). The heart of the system is still the Michelson interferometer. However, the reference mirror is stationary and the backscattered signals are analyzed as a function of wavelength frequency instead of as a function of time. This provides faster A-scans and higher resolution compared with the time-domain type. The technique to date has been used mainly in ophthalmic disorders but, in the last decade, OCT has been applied in several areas in neurology. In this chapter peripapillary RNFL thickness in optic neuritis, multiple sclerosis, Alzheimer's disease, and Parkinson disease were reviewed.

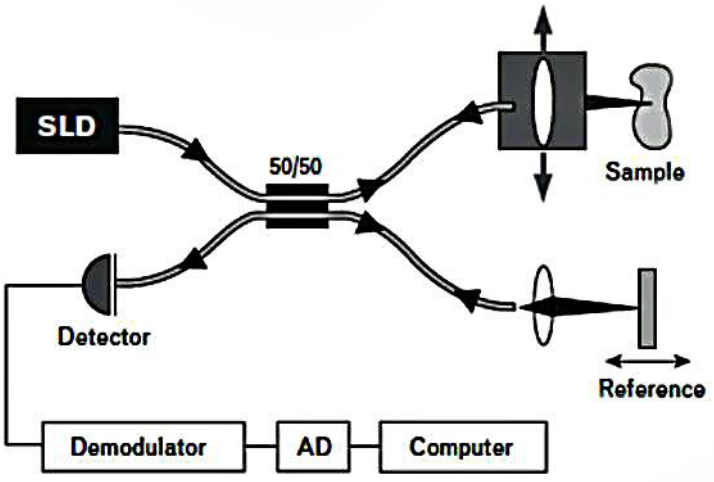

Figure 18 Schemetic representation of optical coherence tomography technology (Huang, et al., 1991). SLD = superluminescent diode. Reprinted from Science, vol 254, D Huang, EA Swanson, CP Lin, JS Schuman, WG Stinson, W Chang et al, Optical coherence tomography, page 1178–81, ©1991. Permission to reproduce this figure has been granted by The American Association for the Advancement of Science.

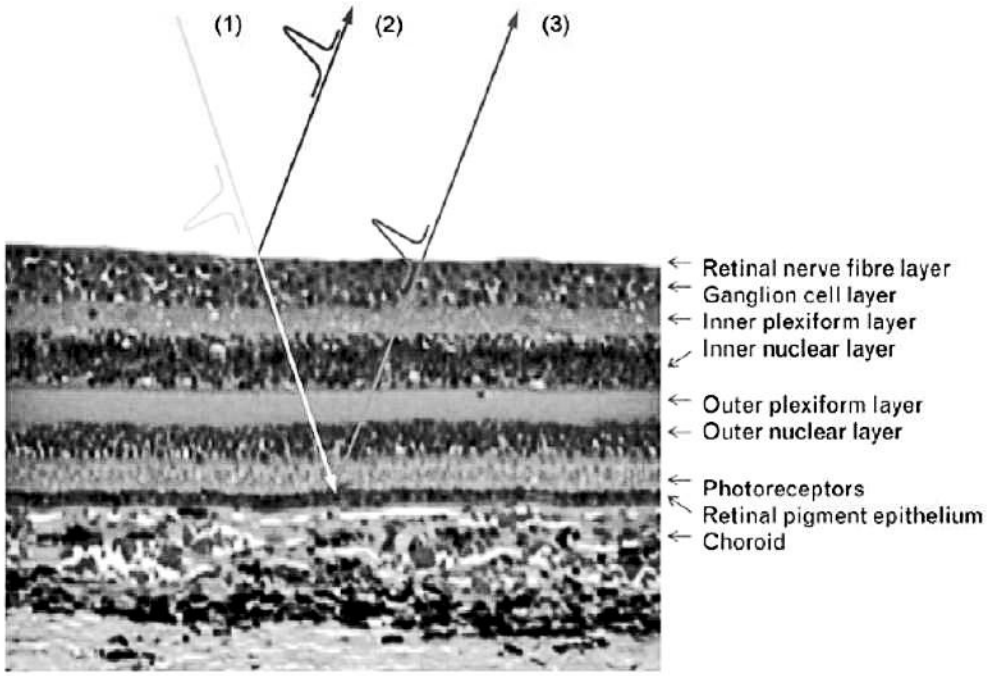

Figure 19 Illustrations of an A scan of OCT. The reflection of incident light (1) has a shorter delay of superficial (2) than if reflected from deeper retinal layers (3). Reprinted from Prog Retin Eye Res, vol 25, RA Costa et al, Retinal assessment using optical coherence tomography, page 325–53, ©2006. Permission to reproduce this figure has been granted by Elsevier.

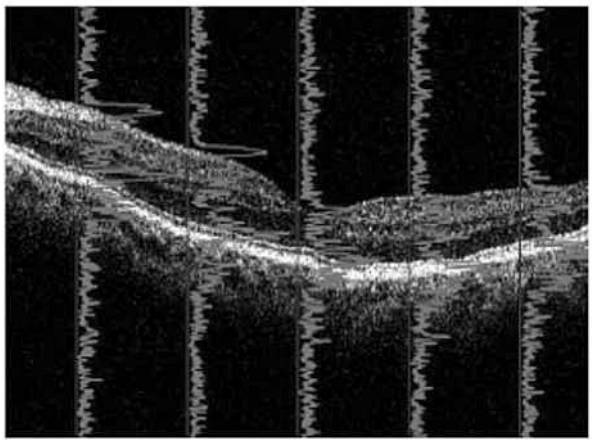

Figure 20 A cross-sectional optical coherence tomography, built up from many A scans. Reprinted from Prog Retin Eye Res, vol 25, RA Costa et al, Retinal assessment using optical coherence tomography, page 325–53, ©2006. Permission to reproduce this figure has been granted by Elsevier.

4.1 Optic neuritis and multiple sclerosis

MS is characterized by both demyelination and axonal degeneration (Compston & Coles, 2008; McDonald, 1984; Plant, Optic neuritis and multiple sclerosis., 2008). Pathologically, axonal transection has been demonstrated in active MS lesions with disease duration between 2 weeks and 27 years (Trapp, Peterson, Ransohoff, Rudick, Mörk, & Bö, 1998). As the injury starts early in the course of the condition as well as during relapses, early intervention and aggressive treatment may be advantageous (Van Velthoven, Faber, Verbraak, van Leeuwen, & de Smet, 2007). In vivo there are several ways to detect axonal loss. The RNFL has the advantage that the axons are unmyelinated and any change is not confounded by demyelination as is the case for the optic nerve itself. Techniques such as OCT and scanning laser polarimetry with variable corneal compensation (GDx; Carl Zeiss Meditec) are used to measure RNFL thickness (Zaveri, et al., 2008; Pueyo, et al., 2010). Measurements obtained using time-domain OCT and GDx methodology show good agreement (Zaveri, et al., 2008; Pueyo, et al., 2010; Pueyo, et al., 2008). Scanning laser polarimetry (GDx) measures the RNFL thickness by measuring the amount of 'retardation' created by polarized laser light as it passes through the nerve fibres (Knighton, Huang, & Greenfield, 2002). The first quantitative study of RNFL thickness in MS was by Parisi et al. in 1999 (Parisi, et al., 1999). Since then there has been rapidly developing interest in various applications of OCT in the diagnosis and management of patients with MS with optic neuritis (MSON) and MS without optic neuritis (MS-non-optic neuritis).

Findings in recovered optic neuritis: Mean overall peripapillary RNFL thickness, measured by OCT in MSON (vision recovered completely or incompletely) has been shown to be significantly less than in healthy individuals (Parisi, et al., 1999; Trip, et al., 2005; Pulicken, Gordon-Lipkin, Balcer, Frohman, Cutter, & Calabresi, 2007; Fisher, et al., 2006). Macular volume measured after an episode of optic neuritis declines significantly in MSON (Trip, et al., 2005; Pulicken, Gordon-Lipkin, Balcer, Frohman, Cutter, & Calabresi, 2007)

Findings in asymptomatic eyes: Mean overall peripapillary RNFL thickness, measured by OCT, in MS-non-optic neuritis eyes of patients has been shown to be less than controls (Fisher, et al., 2006; Parisi, et al., 1999; Pueyo, et al., 2008) indicating that there is subclinical axonal damage in the anterior visual pathway in MS patients without clinical episodes of optic neuritis (Fisher, et al., 2006). However, a non-significant reduction in unaffected eyes was found in a study of patients with clinically isolated optic neuritis as well as in a relapsing remitting MS (RRMS) study (Trip, et al., 2005; Siger, et al., 2008). As might be expected, mean overall peripapillary RNFL thickness in MSON eyes was less compared with MS non-optic neuritis eyes (Siger, et al., 2008; Trip, et al., 2005). However, in another study, Sepulcre et al. found no significant difference in thickness between MSON and MS-non-optic neuritis, probably due to a small number of cases with severe visual loss (Sepulcre, Murie-Fernandez, Salinas-Alaman, García-Layana, Bejarano, & Villoslada, 2007). The RNFL thickness was also correlated with visual acuity, visual field, colour vision, and visual evoked potential amplitude (Trip, et al., 2005). This indicates that axonal loss has an influence on visual recovery after optic neuritis (Trip, et al., 2005). There was a decreasing trend in macular volume of MS-non-optic neuritis eyes but the value was not significantly different from controls (Trip, et al., 2005; Pulicken, Gordon-Lipkin, Balcer, Frohman, Cutter, & Calabresi, 2007)

Findings in acute optic neuritis: The earliest evidence of RNFL thinning by OCT has been observed to occur within 3–6 months following the onset of optic neuritis in a group of patients mostly showing good recovery (Fisher, et al., 2006). The temporal sector appears to be the earliest sector to be involved after acute optic neuritis (Costello, Hodge, Pan, Eggenberger, Coupland, & Kardon, 2008). The thickness stabilized from 7–12 months after the onset (Costello, Hodge, Pan, Eggenberger, Coupland, & Kardon, 2008; Costello, Hodge, Pan, Eggenberger, Coupland, & Kardon, 2008). Patients with marked loss of RNFL and poor visual recovery at 3–6 months did not show subsequent visual improvement (Trip, et al., 2005). It has been proposed that a period of 3–6 months is the best time to predict the visual outcome following optic neuritis and that any treatment should be given within 6 months after the onset (Fisher, et al., 2006). In addition, a threshold of RNFL thickness taken at 75m can be used to best predict visual outcome (Fisher, et al., 2006; Costello, Hodge, Pan, Eggenberger, Coupland, & Kardon, 2008).

Findings in multiple sclerosis; expanded Disability Status Scale versus retinal nerve fibre layer: The RNFL thickness from OCT in MS patients correlates well with low contrast letter acuity (Sloan chart 1.25 and 2.5%) and contrast sensitivity (Pelli-Robson chart) (Fisher, et al., 2006). RNFL atrophy has a high correlation with physical disability as measured by the Expanded Disability Status Scale (EDSS) and longer disease duration (Sepulcre, Murie-Fernandez, Salinas-Alaman, García-Layana, Bejarano, & Villoslada, 2007). However, one study showed no correlation between the RNFL thickness and EDSS (Parisi, et al., 1999). The temporal quadrant of the peripapillary RNFL shows greater thinning than the other three quadrants (Sepulcre, Murie-Fernandez, Salinas-Alaman, García-Layana, Bejarano, & Villoslada, 2007). It declines in MS patients with an increase in EDSS and new relapses (Sepulcre, Murie-Fernandez, Salinas-Alaman, García-Layana, Bejarano, & Villoslada, 2007). As in primary progressive MS (PPMS) and secondary progressive MS (SPMS) the temporal quadrant is thin in clinically isolated syndromes (CIS), compared with healthy controls (Sepulcre, Murie-Fernandez, Salinas-Alaman, García-Layana, Bejarano, & Villoslada, 2007). This result suggests that axonal damage occurs early in the course of the disease (Sepulcre, Murie-Fernandez, Salinas-Alaman, García-Layana, Bejarano, & Villoslada, 2007). It has been found that RNFL measurement provides good specificity but low sensitivity to identify patients who will have increased EDSS (Sepulcre, Murie-Fernandez, Salinas-Alaman, García-Layana, Bejarano, & Villoslada, 2007). The best result can be achieved by using 5^{th} percentile cutoff of the normal database from the OCT 4.0 software (Carl Zeiss Meditec) (Sepulcre, Murie-Fernandez, Salinas-Alaman, García-Layana, Bejarano, & Villoslada, 2007). The average overall and temporal RNFL thickness shows a smaller decrease in patients treated with immunomodulatory drugs from 0–24 months (Sepulcre, Murie-Fernandez, Salinas-Alaman, García-Layana, Bejarano, & Villoslada, 2007).

Findings in multiple sclerosis: MRI versus retinal nerve fibre layer: Findings varied among studies as patients were different. Sepulcre et al. recruited RRMS, SPMS, and PPMS patients with less than 10-year-disease duration. They found that the average RNFL thickness correlates only moderately with white and grey matter volume using 1.5T MRI. This may have been due to inherent limitations from local measurement of RNFL by OCT as only a part of the myelinated system of the brain (Sepulcre, Murie-Fernandez, Salinas-Alaman, García-Layana, Bejarano, & Villoslada, 2007).

There was no significant correlation with the volume of T1-weighted and T2-weighted nor of gadolinium- enhancing lesions (Sepulcre, Murie-Fernandez, Salinas-Alaman, García-Layana, Bejarano, & Villoslada, 2007). Grazioli et al. recruited only RRMS patients who had > or < 10-year-disease duration. They found a strong association between the average RNFL thickness and brain atrophy. The measurement was based on normalized brain volume from 1.5T MRI (Grazioli, et al., 2008). The T2 lesion volume and normalized white matter volume correlated well with the RNFL thickness (Grazioli, et al., 2008). However, the association with T1 lesion volume and normalized grey matter volume did not achieve a statistically significant level (Grazioli, et al., 2008). Siger et al. performed 1.5T MRI in RRMS patients and found a good correlation between the average RNFL thickness and both T1 and T2 lesion volumes in the brain in MS-non-optic neuritis cases (Siger, et al., 2008). The RNFL thickness in MS-non-optic neuritis patients was also associated with a reduction of brain parenchyma fraction and percentage grey matter. They could not find the same correlation in MSON patients. The authors pointed out that axonal loss after optic neuritis occurred independently of brain atrophy whereas in nonoptic neuritis cases, RNFL degeneration was associated with the degenerative process in the brain.

Gordon-Lipkin et al. showed a good association between the RNFL thickness and global brain atrophy. They employed brain parenchymal fraction (BPF) and cerebrospinal fluid (CSF) volume in high resolution anatomic MRI (Gordon-Lipkin, et al., 2007). The BPF is defined as (greyþwhite white volume)/(greyþwhite volumeþCSF volume). The BPF, CSF volume, and EDSS correlate well with the RNFL thickness in MS patients. The RNFL thickness was not associated with white and grey matter volume. The authors suggested that the results were partly due to localization of the disorder in the brain primarily to white matter. To definitively separate the effect of the ageing process, a longitudinal study should be pursued. In their subgroup analysis, the correlation was high in RRMS but not in SPMS and this may be because most SPMS patients had more spinal cord lesions than brain lesions.

Findings in multiple sclerosis: retinal nerve fibre layer in multiple sclerosis subtypes: Costello et al. measured RNFL thickness by OCT over 2 years in patients with optic neuritis as a CIS, in RRMS, and in SPMS. RNFL thickness in MS-non-optic neuritis eyes yielded greater differences between MS subtypes than MSON (Costello, Hodge, Pan,

Freedman, & DeMeulemeester, 2009). Overall RNFL values in MSON and MS-non-optic neuritis eyes were significantly reduced in SPMS, compared with CIS and RRMS patients. Temporal quadrant degeneration was greater in RRMS eyes as compared with CIS eyes. RNFL thickness values did not change significantly for any MS subtype during the 2-year duration of the study (Costello, Hodge, Pan, Freedman, & DeMeulemeester, 2009). Pulicken et al. showed that patients with PPMS,SPMS, and RRMS (after adjusting for age and duration of the disease) have decreased RNFL thickness compared with controls (Pulicken, Gordon-Lipkin, Balcer, Frohman, Cutter, & Calabresi, 2007). RNFL thickness of PPMS and SPMS showed greater reduction compared with RRMS but the differences did not reach statistical significance. Also, the PPMS and RRMS groups did not show a significant decrease in the macular volume. Macular volume in SPMS was lower than in controls but patients in this subgroup also had the longest disease duration. Macular volume correlated well with RNFL thickness in controls and all MS subgroups. The authors concluded that retinal axonal damage can occur without clinical optic neuritis as a part of MS progression, and OCT can be used as a potential biomarker in MS (Pulicken, Gordon-Lipkin, Balcer, Frohman, Cutter, & Calabresi, 2007). In contrast, Henderson et al. showed reduced average RNFL thickness and macular volume in SPMS but not in PPMS compared with a control group (Henderson, et al., 2008).

Findings in multiple sclerosis; visually evoked potential versus retinal nerve fibre layer: The latency of the visually evoked potential (VEP) was shown by Naismith et al. to have higher sensitivity in detecting evidence of optic nerve damage than did RNFL (Naismith, et al., 2009b). Klistorner et al.compared RNFL thickness using OCT and multifocal VEP (mfVEP) in post acute optic neuritis (Klistorner, et al., 2008). A significant reduction of RNFL thickness of the optic neuritis eyes was shown, but there was a greater decline in the amplitude of the mfVEPs. Latency of the mfVEPs was also significantly delayed in optic neuritis eyes. In fellow eyes, the amplitude of mfVEPs was significantly reduced and the latency prolonged, but RNFL thickness remained unaltered. RNFL thickness was correlated highly with the mfVEP amplitude. There was also strong correlation between OCT measure of axonal loss and mfVEP latency. This is in contrast to Trip et al. (Trip, et al., 2005) who showed a correlation between RNFL thickness and VEP amplitude but not latency.

Findings in children: In a study performed in children, the results were more or less similar to the adult studies. Four groups were evaluated, namely, control, MSON, acute disseminated encephalomyelitis/ transverse myelitis (ADEM/TM), CIS/ optic neuritis, and chronic relapsing inflammatory optic neuropathy (CRION). All groups with a history of optic neuritis had lower average RNFL thickness than controls. The average of RNFL thickness in MSON and MSnon-optic neuritis was significantly lower than controls. The average of RNFL thickness decreased as the episodes of optic neuritis increased. The average of RNFL thickness of ADEM/TM was lower than controls but it did not reach a statistical significance. There was no association between the average of RNFL thickness of both eyes and EDSS (Yeh, et al., 2009). ADEM/TM and CRION had greater macular volume loss than other groups, which was may indicate more widespread disease perhaps affecting the retina as well. These results suggest that axonal loss within the retinal nerve fibre measured by OCT may reflect degenerative changes in the brain and may occur early in the course of MS. There is a high correlation between other visual parameters and the RNFL thickness. Hence RNFL thickness can be used as a biological marker of MS to monitor disease progression even without attacks of optic neuritis. Also, it may be a useful measurement in cases of acute optic neuritis with regard to prognosis and management.

4.2 Neuromyelitis optica

Findings could vary among studies as patient characteristics in each study group were not similar. In one study the mean RNFL thickness measured by OCT in affected eyes (in remission) of patients suffering from NMO was thinner than in MSON (Merle, Olindo, Donnio, Richer, Smadja, & Cabre, 2008). The thickness was less in all quadrants of the same magnitude, but the difference was not significant in the superior quadrants nor in the nasal quadrants. Visual outcome was less favourable in the NMO group. In unaffected eyes, RNFL thicknesses in both NMO and MS patients were less than controls (Merle, Olindo, Donnio, Richer, Smadja, & Cabre, 2008). An overall thickness of 52 µm was associated with visual acuity of less than 20/200. Micron thickness less than 52 had a sensitivity of 50% and specificity of 94% with NMO. Visual acuity 20/200 or less had a sensitivity of 53% and specificity of 79% with NMO. The average thickness of the peripapillary RNFL correlated with visual acuity, scores of contrast sensitivity and the number of

episodes per patient. In another report the average RNFL thickness in NMO cases was significantly lower than in the controls. The thinning was found in all four quadrants. The severity of RNFL degeneration in NMO was higher than that found in MS in the previous studies. In isolated myelitis cases (mean disease duration of 1.7 years, SD 0.7), no reduction of the RNFL thickness was found. The OCT results showed a good correlation with Humphrey perimetry, visual acuity, VEP, and EDSS (excluding visual data) (De Seze, et al., 2008). There are other studies indicating that OCT may help to distinguish MS and NMO (Merle, Olindo, Donnio, Richer, Smadja, & Cabre, 2008). Ratchford et al. studied four groups; NMO with optic neuritis, NMO with isolated longitudinal extensive transverse myelitis (LETM), RRMS, and controls.NMO optic neuritis eyes had lower RNFL thickness and macular volume than control eyes and RRMS optic neuritis eyes (Ratchford, et al., 2009). Note that this difference could result from either a greater severity or a greater number of optic neuritis episodes in patients with NMO compared with patients with RRMS. Optic neuritis was also associated with more severe visual impairment in NMO spectrum patients than in RRMS patients. Using a multivariate linear regression analysis to control for age and disease duration, a single episode of optic neuritis was estimated to cause 24 μm more RNFL loss in NMO than in RRMS. The difference in RNFL thickness between optic neuritis and non-optic neuritis eyes is much greater in NMO spectrum patients than in RRMS. In eyes without a history of optic neuritis, the RNFL was mildly thinner in all groups relative to controls. This difference was only significant for RRMS eyes. Eyes in the longitudinal transverse myelitis (LETM group) and unaffected NMO eyes were not significantly different from controls (Ratchford, et al., 2009). In NMO optic neuritis eyes, there was a threshold RNFL thickness of approximately 60 m, below which the Early Treatment Diabetic Retinopathy study (EDTRS) eye test visual acuity was poor (Ratchford, et al., 2009). These data suggest that optic neuritis in NMO is a more destructive process with greater potential for causing visual disability than in MS. The authors found that in patients with prior unilateral optic neuritis, a 15 μm difference in RNFL thickness between the two eyes was more likely to occur in NMO (75%) than in RRMS (Ratchford, et al., 2009). Following a remote episode of optic neuritis, NMO had a thinner RNFL thickness than MS, when comparing patients with similar visual acuity and contrast sensitivity. This indicates that there is greater axonal loss after optic neuritis in NMO than in MS. The superior and inferior quadrants were affected to a

greater magnitude in NMO than MS, whereas the temporal quadrants were not demonstrably different (Naismith, et al., 2009a). RNFL thickness of MS non-optic neuritis was low, compatible with the previous publication. The mean RNFL thickness for the unaffected NMO eyes was greater than the unaffected MS eyes. In both the MS and NMO groups, having a RNFL thickness of 50 µm or less conferred 50% odds of having vision 20/100 or less (Naismith, et al., 2009a). Severe optic neuritis (visual acuity <20/100) in NMO was associated with vascular changes and more axonal losses compared with MS (Green & Cree, 2009). The thinning of RNFL of NMO optic neuritis cases was in a diffuse pattern whereas MSON had mainly temporal quadrant involvement (Green & Cree, 2009). Attenuation of the peripapillary vascular tree, focal arteriolar narrowing, sometimes with lumen obstruction were observed (Green & Cree, 2009). Further studies are needed. Optic neuritis in NMO cases seems to be more destructive and has poorer visual outcome than MSON. In unaffected eyes, NMO cases have thicker RNFL on OCT than eyes from patients with MS. It seems that there is a role for OCT to distinguish NMO optic neuritis from MSON. However, further studies need to be done to clarify this, for instance a longitudinal study following optic neuritis in NMO cases to see the nature of the disease over a period of time, to see whether OCT can predict the next relapse and help decide when to initiate immunosuppressive medication. Studies of relationships between aquaporin-4 antibody titres and RNFL thickness, between MRI brain and RNFL, between patterns of optic nerve enhancement in MRI scans and RNFL, and between CSF findings and RNFL, would be beneficial. The greater magnitude of optic nerve damage in NMO raises other questions. Is the whole retina involved? Would a study of the whole thickness of the retina along with electrophysiological testing be interesting? What happens at the molecular level such as lactate and oxygen levels during the acute and chronic episodes? Is the molecular change in NMO different from other causes of optic disc swelling? Is the molecular change related to the RNFL thickness? As aquaporin-4 channels are present in kidneys (inner medullary collecting ducts in rats (Terris, Ecelbarger, Marples, Knepper, & Nielsen, 1995)) and in the brain, urine examination would be of great interest. We can look for the antibody in the urine, and other profiles, for example electrolyte, specific gravity, protein, sugar, white blood cells (WBC), red blood cells (RBC), etc., during the acute episode of optic neuritis and measure the RNFL at the same time. Our hypothesis is that urine specific gravity during acute

optic neuritis and swollen RNFL would be abnormal. Then it may recover when the disease activity settles down but the RNFL becomes thinner.

4.3 Alzheimer disease

Pathological and clinical studies in Alzheimer disease indicate that there is loss of retinal ganglion cells in Alzheimer patients when compared with controls (Hinton, Sadun, Blanks, & Miller, 1986; Blanks, Hinton, Sadun, & Miller, 1989). However, the findings are still controversial (Curcio & Drucker, 1993). A reduction of RNFL thickness has also been observed in a study used scanning laser ophthalmoscopy (Danesh-Meyer, Birch, Ku, Carroll, & Gamble, 2006). Several studies using OCT revealed mean peripapillary RNFL thickness of Alzheimer disease (Danesh-Meyer, Birch, Ku, Carroll, & Gamble, 2006; Iseri, Altinas, Tokay, & Yüksel, 2006) and mild cognitive impairment patients (Paquet, Boissonnot, Roger, Dighiero, Gil, & Hugon, 2007) to be significantly less than controls. Total macular volume was reduced and related to the mini-mental state examination in another report (Iseri, Altinas, Tokay, & Yüksel, 2006). Also, the loss of RNFL was found to be correlated with pattern electroretinogram (Parisi, 2003). In another study, patients with early Alzheimer disease showed a significant narrowing of the venous blood column diameter, a significantly reduced venous blood flow rate, and a thin superior peripapillary RNFL, compared with age matched healthy individuals (Berisha, Feke, Trempe, McMeel, & Schepens, 2007).

4.4 Parkinson disease

There is evidence of visual dysfunction in patients with Parkinson disease. Dopamine is an essential neurotransmitter in the retina (Djamgoz, Hankins, Hirano, & Archer, 1997), and retinal dopamine at postmortem is decreased in Parkinson disease patients (Harnois & Di Paolo, 1990). Recently, investigators have evaluated peripapillary RNFL thickness. Inzelberg first showed that the thickness was reduced in the inferotemporal area (Inzelberg, Ramirez, Nisipeanu, & Ophir, 2004). Their visual field sensitivity was also reduced in accord with RNFL degeneration (Inzelberg, Ramirez, Nisipeanu, & Ophir, 2004). A few other studies have shown more or less the same results whereby mean peripapillary RNFL and mean total macular volume of Parkinson disease patients were reduced (Altintas, Iseri, Ozkan, & Cağlar, 2008).

Another study showed inner retinal layer of Parkinson disease patients to be thinner than controls (Hajee, et al., 2009).

4.5 Conclusion

The RNFL thickness in Alzheimer disease and Parkinson disease becomes thin, and as with MS and NMO, OCT may allow for this biological marker to assist in monitoring disease progression. Also, OCT may be useful in identifying these conditions early in their course so that early treatment can be initiated.

5 A retrograde trans-synaptic degeneration study in patients with homonymous hemianopia from retrogeniculate lesions identified by OCT

5.1 Aims

We would like to study the retrograde trans-synaptic degeneration in the human visual pathway and particularly to prove that the degeneration developed in adulthood.

5.2 Methods

Forty-eight cases were recruited to the present study. There were three groups. The first pathological group, comprising 19 cases, had acquired homonymous hemianopia (Fig.21); the median duration of disease was 3.5 years (range 0.3–67 years) and the median age was 65 years (range 30–83 years). In this group, there were fifteen patients with cerebral infarct, one patient with occipital meningioma removal, one with haemorrhagic infarct, one with skull fracture, and one with demyelination. The second pathological group, comprising seven cases, had congenital homonymous hemianopia; the median age was 31 years (range 17–59 years). In this group, there were two patients with cerebral infarct, one patient with porencephalic cyst, one patient with arachnoid cyst, one with cortical dysplasia, one with birth trauma, and the last one with congenital cerebral hemisphere injury. The control group consisted of 22 volunteers with normal vision and no ophthalmic disorder (Fig.22). The median age of this group was 45 years (range 23–61 years). Visual field analysis was carried out using the Humphrey visual field analyser. Patients were recruited if there was substantial visual loss in either the left or right homonymous hemifields using the 24-2 protocol. The deficit ranged from a mean deviation loss of -11 dB to a loss of -19.1 dB for all cases. Hence a wide range of visual deficit was represented ranging from a total failure to detect any stimuli within the affected hemifield to incomplete loss. Thirty-three percent of patients had macular sparing. The StratusTM Optical Coherence Tomography version 4 (Carl Zeiss Meditec, Inc.) was used to measure the cross-sectional retinal nerve fibre layer thickness (RNFL) in every case. The aim was to investigate the possibility of loss of

axons corresponding to the fibre trajectories of ganglion cells located in the right and left hemiretinae. Fast RNFL thickness scan protocol was utilized with a fixed 3.4 mm diameter scan circle around the optic disc. The measurements are given in microns, according to the calibration provided by the manufacturers. The peripapillary RNFL thickness was measured in each eye and in each of 12 sectors around the optic nerve head (Fig.23). The overall mean RNFL of each eye was also evaluated. The study was approved by the local Ethics Committee and informed consent was obtained from all subjects who participated in the study.

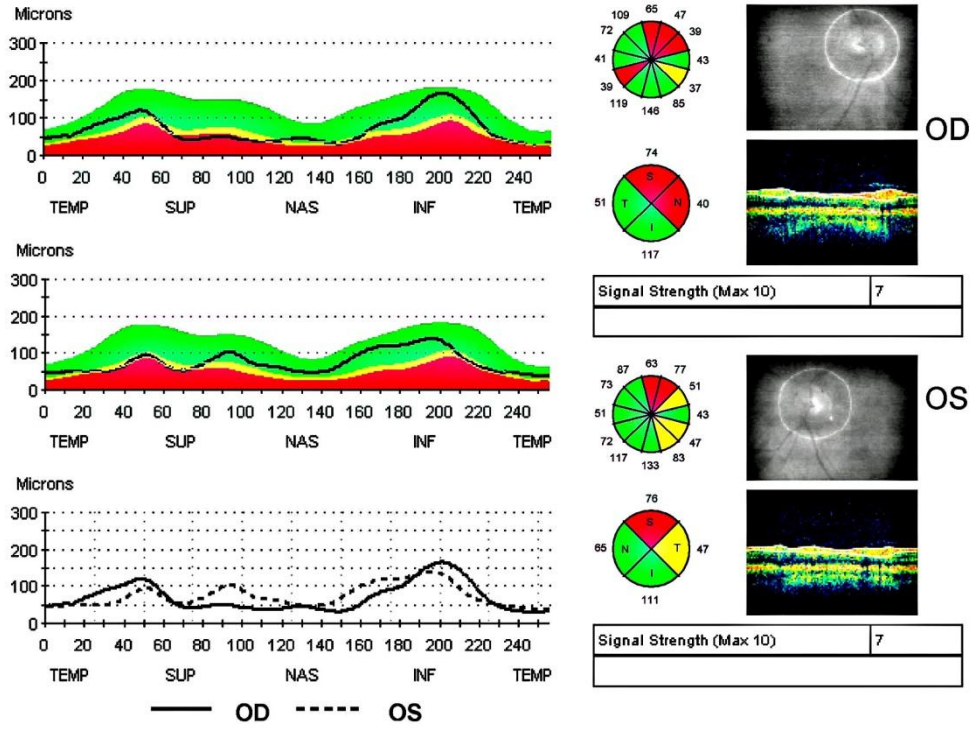

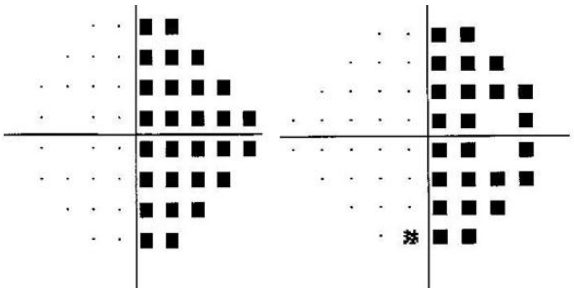

Left visual field Right visual field

Figure 21 GY: A case with longstanding right homonymous hemianopia: MRI scan in the bottom left revealed a lesion in the left occipital area. Note that the left side of the brain was presented on the left side of the picture only in this MRI scan. Humphrey perimetry 24-2 (pattern deviation) on the bottom right demonstrated dense right homonymous hemianopia. The RNFL thickness of both eyes was presented on the top. It revealed that the RNFL over the nasal quadrant of the right eye (OD) was thin when compared to the left; whereas the RNFL of the left eye (OS) over the inferior and superior quadrants were thinner than the right. This corresponded to the retinotopic organization and hence the retrograde trans-synaptic degeneration was identified. Reprinted GY's MRI scan from Vision Research, vol 38, J.L Barbur et al, Residual processing of chromatic signals in the absence of a geniculostriate projection, page 3447-53, ©1998. Permission to reproduce the MRI scan has been granted by Elsevier.

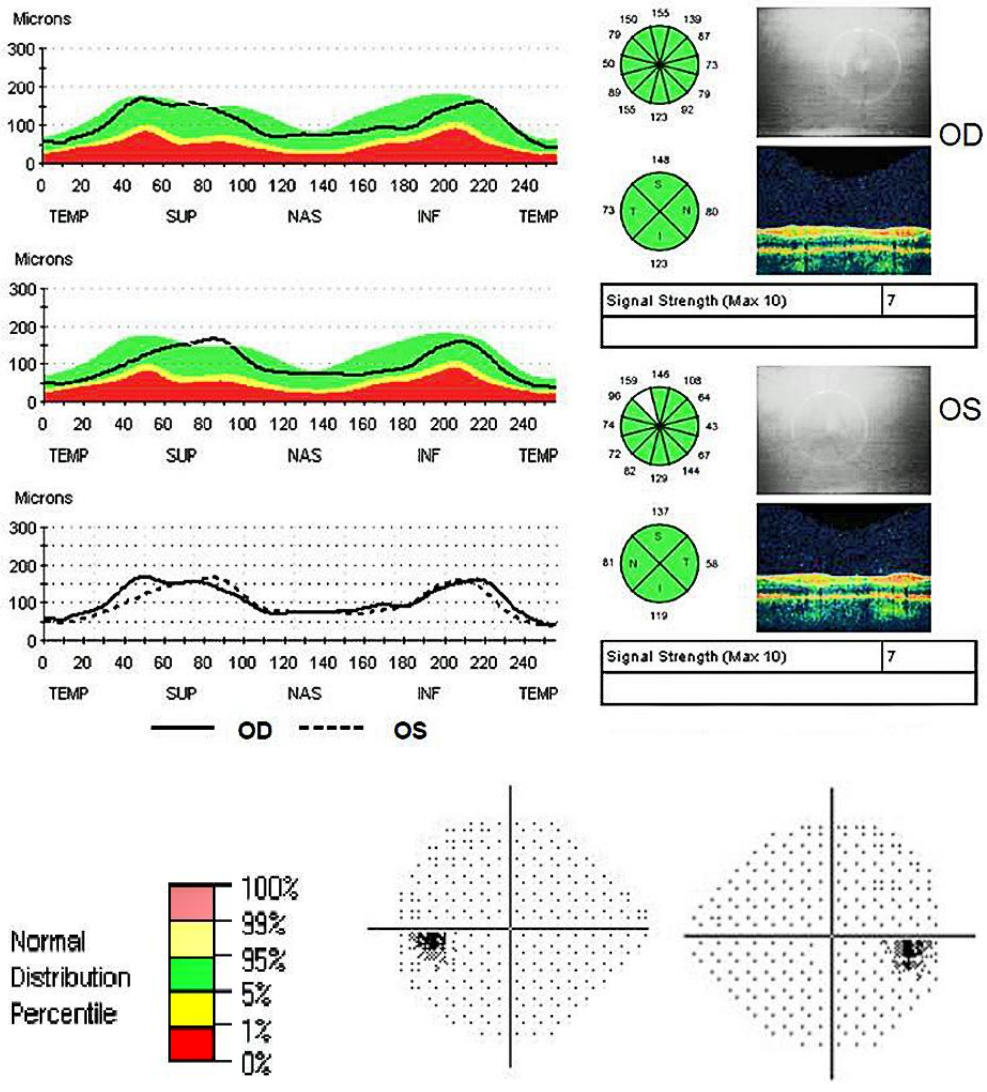

Figure 22 Control: A healthy subject has normal Humphrey perimetry 24-2 and peripapillary RNFL thickness of both eyes. The RNFL thickness: green = normal (5th - 95th percentile), yellow = thin or less than 5% of age matched control (1st-5th percentile), red = very thin or less than 1% of age matched control (1 percentile). The RNFL thickness from both eyes was almost the same.

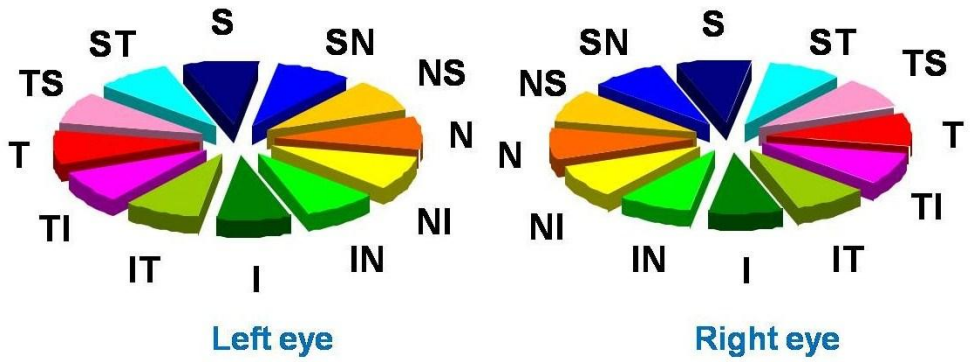

Figure 23 For each eye of each subject the RNFL was measured in a circular cross-section centred on the disc. The circle had 12 equal sectors. T= temporal, N= nasal, I= inferior, S=superior. The labeling is mirror symmetric in both eyes. Reprinted from Brain, 132, 628-634, P Jindahra, A Petrie, & GT Plant, Retrograde trans-synaptic retinal ganglion cell loss identified by optical coherence tomography, ©2009. Permission to reproduce this figure has been granted by Oxford University Press.

5.3 Statistical analysis

We report the estimated overall mean RNFL in each eye and the ratio of the two measurements with confidence intervals for every group. The difference in the group means among the three groups, i.e. between the control and acquired, between the control and congenital and between the acquired and congenital, are shown together with 95% CI and P-values. We performed hierarchical repeated measures ANOVA (analysis of variance) separately for each variable, with cases nested in groups and sectors representing the repeated measures. Bonferroni post hoc comparisons were made if the group means were significantly different in the ANOVA. If there was a significant interaction between groups and sections in the ANOVA, a one-way ANOVA to compare the group means was performed separately for each sector. The assumptions underlying every analysis were checked by a study of the residuals and were verified for the non-crossing-fibre defect eyes and the ratio of crossing- to non-crossing-fibre defect eyes. In order for the constant

variance assumption to be satisfied for the crossing-fibre defect eyes, the ANOVA was performed on the logarithm of the RNFL. A significance level of 0.025 was used rather than the conventional level of 0.05 as an additional safe guard against spurious results arising from multiple testing. Correlations were also calculated between the mean magnitude of the RNFL and the loss of visual sensitivity (as measured by automated perimetry).

5.4 Results

Results are presented as the mean together with the 95% confidence interval (CI) of each measurement. In non-crossing-fibre eyes the estimated mean RNFL was 83 microns (CI 79–87 microns) in the acquired group; 73.4 microns (CI 67.7–79 microns) in the congenital group; and 101.4 microns (CI 97–105.8 microns) in the left eyes of the control group. The overall ANOVA indicated that there were significant differences in RNFL between the group means and the sector means and a significant interaction between groups and sectors. Post hoc comparisons indicated that there were significant differences in all three group means as follows: (control–acquired) difference in means = 18.4 microns, (CI 14.3–22.4 microns, $p< 0.001$); (control–congenital) difference in means = 28 microns, (CI 22.2–33.5 microns, $P< 0.001$); and (acquired–congenital) difference in means = 9.7 microns, (CI 4–15.3 microns, $p< 0.001$). One-way ANOVA comparing the groups in each sector, followed by post hoc comparisons, demonstrated significant differences in the group means in Sectors S, I, IT, TI, TS and ST between the congenital and control groups and in Sectors S, SN, IT, TI, TS, and ST between the acquired and control groups. There were no statistically significant differences in the group means in sectors NS, N, NI nor T. A significant difference in the group means was detected only in Sector I between the acquired and congenital groups. The group means for all sectors are plotted in Fig. 24.

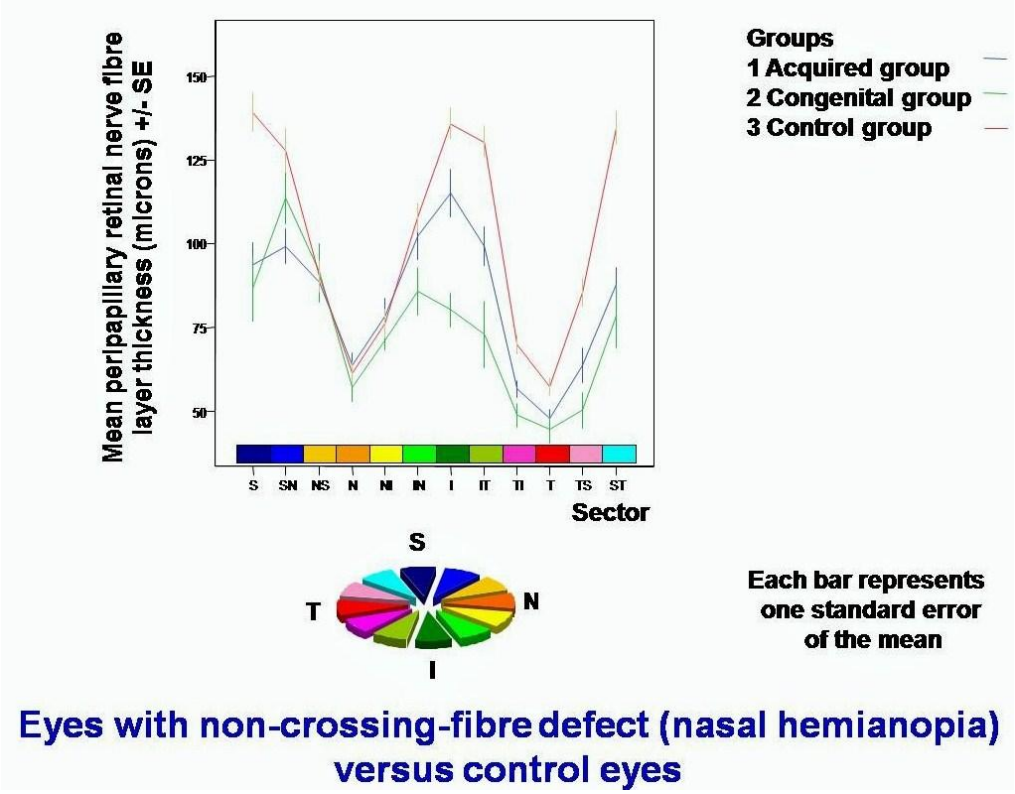

Figure 24 Mean RNFL thickness for each sector of the non-crossing fibre defect eye. In both homonymous hemianopia groups, there was no significant thinning of the RNFL in Sectors NS, N, NI, and T compared with controls. Reprinted from Brain, 132, 628-634, P Jindahra, A Petrie, & GT Plant, Retrograde trans-synaptic retinal ganglion cell loss identified by optical coherence tomography, ©2009. Permission to reproduce this figure has been granted by Oxford University Press.

Results in the crossing-fibre eyes were as follows: the mean values for RNFL were 79.8 microns (CI 75–84.5 microns) in the acquired group; 72.7 microns (CI 65.5–79.9 microns) in the congenital group; and 100.8 microns (CI 96.6- 105.1 microns) in the right eyes of the control group. The overall ANOVA on the log values indicated that there were significant differences in RNFL between the group means and between the sector means but that there was no significant interaction between the groups and sectors. Post hoc comparisons indicated that there was a significant difference between the acquired and control group means and between the congenital and control group means: there was no significant difference between the acquired and congenital group means. To conform with the presentation of the results for the non-crossing-fibre defect eyes, the difference in the means of the raw data are presented: (control–acquired) difference in means = 21 microns, (CI 16.9–25.2 microns, P< 0.001); (control–congenital) difference in means = 28 microns, (CI 22.5–33.8 microns, P< 0.001); and (acquired–congenital) difference in means = 7 microns, (CI 1.3–12.9 microns, P = 0.011). Using the log data, one-way ANOVA comparing the groups means in each sector, followed by post hoc comparisons, demonstrated significant differences in the group means in all sectors except ST, I and IT between the congenital and control groups; and in all sectors except NI, IN, I and IT between the acquired and control groups. A significant difference in the group means were detected in any sector when the acquired and congenital groups were compared. The group means (raw data) for all sectors are plotted in Fig. 25.

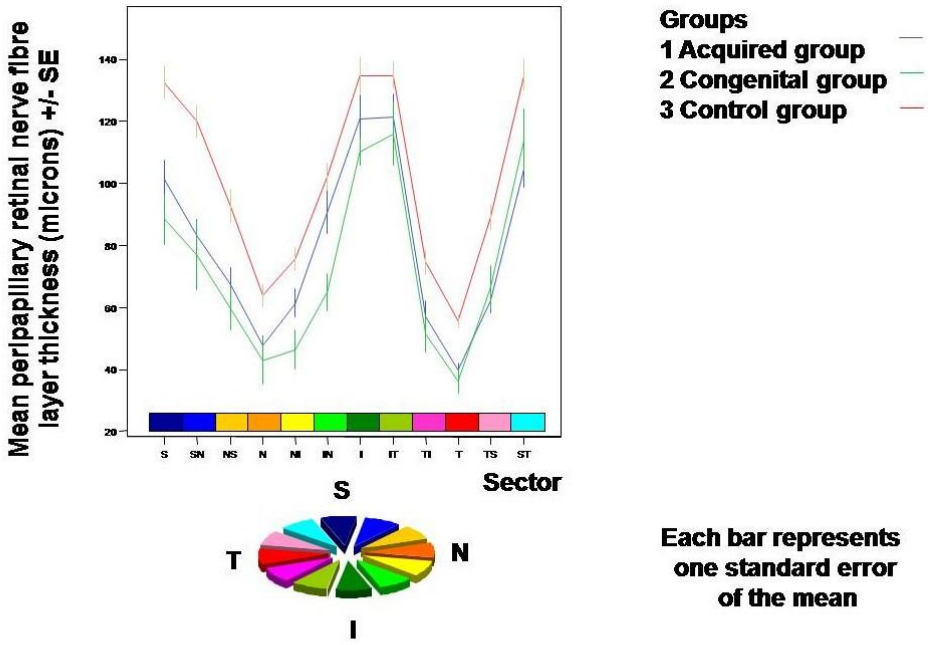

Eyes with crossing-fibre defect (temporal hemianopia) versus control eyes

Figure 25 Mean RNFL thickness for each sector in crossing fibre defect eyes. The differences between the homonymous hemianopia and control group means did not achieve statistical significance in Sectors I, IT, ST for the congenital group nor in Sectors NI, IN, I, IT for the acquired group. Reprinted from Brain, 132, 628-634, P Jindahra, A Petrie, & GT Plant, Retrograde trans-synaptic retinal ganglion cell loss identified by optical coherence tomography, ©2009. Permission to reproduce this figure has been granted by Oxford University Press.

In order to better illustrate the different pattern of retinal nerve fibre layer thinning between the crossing- and non-crossing-fibre defect eyes, the same data employed to generate the results shown in Figs 24 and 25 were analysed as the ratio of the group means. In Fig. 26 the ratio crossing-fibre eye: non-crossing-fibre eye is plotted for the congenital and acquired groups and the ratio right eye: left eye for the control group. The results indicate a broad area on the nasal side of the disc where there is predominantly a loss of crossing fibres (sectors SN, NS, N, NI and IN) but only a solitary sector temporally (T). This pattern is identical for both the congenital and the acquired groups. There was no significant linear correlation between the mean magnitude of the RNFL and the magnitude of the loss of visual sensitivity (as measured by automated perimetry). This was the case for all sectors and for both eyes of both the congenital and the acquired groups.

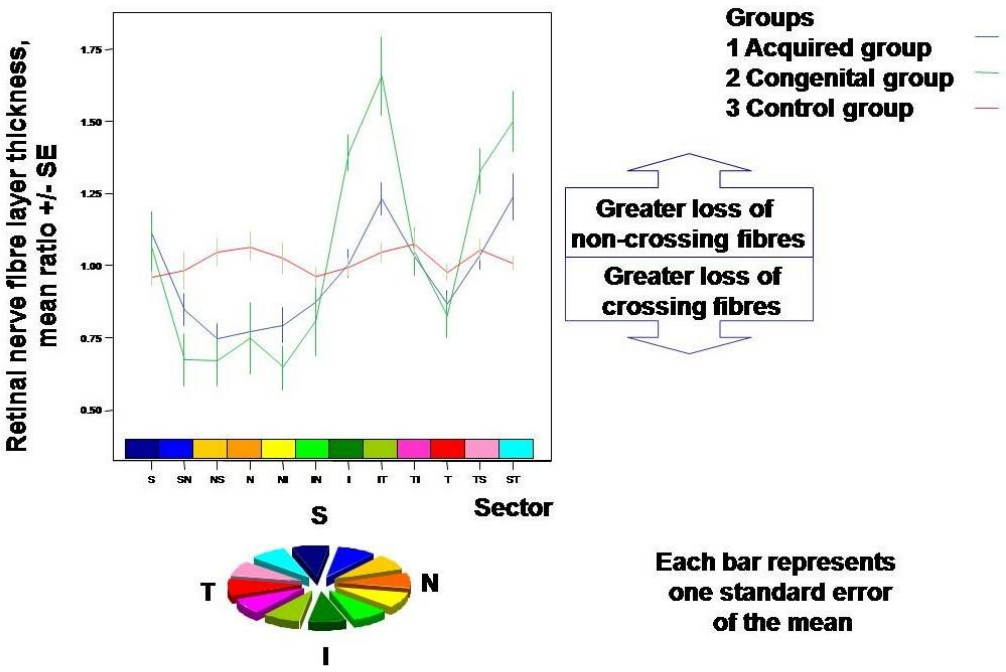

Figure 26 Mean ratio of right/left eye RNFL was plotted for each sector in the control group, represented by the red line. The ratio was close to unity indicating no inter-ocular difference. Mean ratio of crossing/ non-crossing fibre defect eye RNFL was plotted for each sector in the other two groups. The blue line represented the acquired group and the green line represented the congenital group. For instance, crossing fibre defect eye in a patient with right homonymous hemianopia is the right eye, thus, the ratio would be derived from the RNFL thickness in the right eye divided by that in the left eye. The ratio was calculated for each sector separately. Values below unity indicated a greater loss of crossing than non-crossing fibres, and vice versa for values above unity. Reprinted from Brain, 132, 628-634, P Jindahra, A Petrie, & GT Plant, Retrograde trans-synaptic retinal ganglion cell loss identified by optical coherence tomography, ©2009. Permission to reproduce this figure has been granted by Oxford University Press.

5.5 Discussion

The retrograde trans-synaptic degeneration has been proved in acquired retrogeniculate lesions in human by using OCT measurement in the presented studies. Our study is comparable to the results in primate studies. The overall mean RNFL thickness of both acquired and congenital homonymous hemianopia groups are less than the normal subjects. In particular, the thinning of the nerve fibre layer of the 12 sectors corresponds to the retinotopic organization. We expect the cell loss in the nasal and temporal areas in the crossing fibre defect eyes or the eyes with temporal hemianopia, while the loss in other areas would be anticipated in the other eye or the eye with nasal hemianopia. Figure 26 is a diagram showing the ratio of the RNFL thickness of the crossing/ non-crossing fibre defect eyes. As expected, the ratios in both patient groups are less than one in the nasal and temporal areas, indicating the degeneration was greater in the crossing fibre defect eyes in these regions. The ratios in both patient groups are higher than one in the remaining areas, indicating the thinning in these parts was greater in the non-crossing fibre defect eyes. The projection of crossing fibres from nasal retina makes up exclusively a larger sector on the nasal than on the temporal equatorial pole of the disc (Naito, 1989). This finding is in accord with the results shown in Fig. 26 where the predominantly crossing fibre loss extends over 4–5 sectors nasally but only one sector temporally. Thus, there is considerably greater intermingling of crossing and non-crossing fibres on the temporal than on the nasal side of the disc. It appears that the OCT is more sensitive in detecting such degeneration in the retina than the clinical observation. Hence the lack of clinical nerve fibre layer thinning in the acquired occipital lesion can be explained because of the OCT greater sensitivity. If this were the entire explanation, it would be expected that the changes in the acquired would be less than in congenital cases where the data reported here, the retinal changes were similar. In mammals the immature central nervous system preserves greater capacity to withstand injury or recover from damage than does the adult nervous system (Rosner, 1974). It has been suggested the age of monkey at the operation affects the magnitude of the retrograde trans-synaptic degeneration (Weller & Kaas, 1989; Cowey, Stoerig, & Williams, 1999; Dineen & Hendrickson, 1981). A remaining question relates to the lack of clinical evidence for nerve fibre loss in acquired as opposed to congenital hemianopia. This suggests that the process does not lead to the same visible changes at the optic disc

and the explanation of this will be the subject of future investigation. Apart from age, other factors that influenced the retrograde trans-synaptic degeneration in monkeys were the species of monkey (Weller & Kaas, 1989), postoperative survival time (Weller & Kaas, 1989; Cowey, Stoerig, & Williams, 1999; Dineen & Hendrickson, 1981), and the retinal eccentricity (Cowey, 1974; Cowey & Stoerig, 1989). Size of the cortical lesion was still controversial.

Age

The magnitude of RTSD in monkeys was inversely correlated with age at the time of the striate cortex operation if their survival times were similar (Herbin, Boire, Théoret, & Ptito, 1999; Dineen & Hendrickson, 1981). The rate of RGC loss in the infant operated monkeys was faster than that of the adults (Weller & Kaas, 1989). Adult operated macaque monkeys with 8-year survival time had 80% loss of the total RGCs (Cowey, 1974; Van Buren J. M., 1963; Dineen, Hendrickson, & Keating, 1982). One-year-old operated monkeys with one-year survival time had 80% RGC loss (Dineen & Hendrickson, 1981). Infant-operated (1-9 month old) monkeys with ½ to one year survival time had 70-72.5% RGC loss (Weller & Kaas, 1989). The RGC loss was around 80% when the infant operated monkeys were followed up to 8 years. The findings indicated that the RGCs of monkeys lesioned soon after birth were more vulnerable to degenerate than monkeys lesioned in adulthood. There might be some protective factors for RGCs after the decortication in adults (Weller & Kaas, 1989). In an investigation, six monkeys were hemispherectomized on the left side of the brain at different age i.e., 4, 6, 8, 9 months old and adult (Herbin, Boire, Théoret, & Ptito, 1999). All of them had 4 year survival time. The RGC degeneration obviously developed on the temporal side of the left central retina and on the nasal side of the right central retina in every subject (Herbin, Boire, Théoret, & Ptito, 1999). The primarily affected RGCs were P cells which were mainly in the central retina; this could explain why the peripheral retinae were relatively spared in all subjects. The RGC loss in the central retina (7.5-15 degree eccentricity from fovea) of a monkey operated at age 4 months was the most pronounced approximately 70% of all RGCs, followed by the loss in monkeys operated at age 6, and 8 months respectively. In monkeys operated at age 9 months and in adulthood, the observation was not different from normal eyes (Herbin, Boire, Théoret, & Ptito, 1999). No age effect was seen when the age at operation was more than 17 month

old (Cowey, Stoerig, & Williams, 1999). In a study (Dineen & Hendrickson, 1981), a unilateral striate cortex removal was performed in 2 month old infant monkey and 5+ year old monkeys. Two sequential operations were also carried out in an adolescent monkey at 12 month old in one cortex and 15 month old in the other. All cases had 10 to 13 month survival times. The RGC loss in the affected hemiretinae was 70% in the infant operated and 15% in the adult operated. The RGC loss in the serial operation in the adolescent case was 80% in the areas corresponded to the operation at age 12 months and 65% in the areas corresponded to the operation at age 15 months. Interestingly there appeared not much different when the operation was performed at 2 or 12 months of age. (Dineen & Hendrickson, 1981). In an investigation, left striate cortices of infant (1-9 months), adolescent and adult macaque monkeys were removed and pathological studies were performed in 3.5 weeks to 8 years after the operation (Weller & Kaas, 1989). The cortical lesions corresponded to 5-10^{o} of the central visual field. In the infant operated monkeys, the parvocellular and magnocellular layers of the dLGN degenerated rapidly even in the 3.5 week duration. Cells in the degenerative zone of the dLGN were almost completely gone. Despite the similar findings of the dLGN in all cases, the retinal changes differed. The terminations of retinogeniculate fibres were reduced at the degenerated parvocellular layer but not other degenerated layers. The findings indicated that the P cells rather than other RGCs were affected by the RTSD. The reduction of the retinal fibre terminations to the parvocellular layer was the greatest in the adult operated monkeys with 6-8 years survival time, followed by infant operated monkeys with 3.5 week to 1 year survival time, adolescent operated monkeys with 14, and 12 month survival time respectively. No alteration was observed in the adolescent operated monkeys with 6 month survival time. The RGC loss paralleled the loss of retinal termination at the parvocellular layer in the LGN. Many behavioural studies in cats provided controversial results. In cats after bilateral ablation of visual cortical areas 17, 18, and 19, some studies revealed postoperative relearning of pattern discrimination (Spear, 1969) but some studies revealed none (Doty, 1971; Meyer, 1963; Wetzel, Thompson, Horel, & Meyer, 1965). The recovery of the visual function after bilateral decortication of area 17 and/or 18, 19 in neonatal cats was related to the extent of the lesion (Cornwell, Overman, & Ross, 1978). A study revealed that after bilateral removal of the visual cortex in infant cats, their pattern discrimination was not different from normal cats (Dotty,

1961). The dLGN was not completely destroyed (Dotty, 1961). In another study, after bilateral ablation of area 17, 18, and 19, the relearning pattern discrimination of infant operated cat was better than that of the adult operated cats and not different from the normal cats (Murphy, Mize, & Schechter, 1975). However, the lesions were more extensive in the adult operated cats (Murphy, Mize, & Schechter, 1975). Two out of three adult operated cats failed to relearn the task. Only one adult operated cat was able to relearn the task. This cat had the largest lesion with the most destructive lesion in area 17, 18, and 19 and shortest postoperative recovery time. The authors pointed out that it might be due to a preoperative training and using visual cues (Murphy, Mize, & Schechter, 1975).

Species

Macaque monkeys, old world monkeys, had higher susceptibility to the retrograde trans-synaptic degeneration than squirrel and owl monkeys, new world monkeys, but had similar susceptibility to humans (Weller & Kaas, 1989). The rate of the retinal ganglion cell loss in infant operated squirrel monkey was as same as that of older macaque monkeys whereas adult operated squirrel monkeys were not vulnerable to the degeneration (Weller & Kaas, 1989). Unlike other mammals, no significant retinal ganglion cell loss was found in infant and adult rats with unilateral striate cortex ablation (Perry & Cowey, 1979a). However, small aberrant innervations were found in the infant but not in the adult rats (Perry & Cowey, 1979b). Following the striate cortex ablation, infantile damaged retinal fibres were rearranged to innervate the dLGN and partly to the tectum because many axons in infants did not reach their synaptic targets at the time of the injury. It was only these fibres that continue to grow to new targets (Perry & Cowey, 1979b).

Retinal eccentricity

In normal retina, the density of P cells was the greatest in the central area and became less in the periphery whereas the density of M cells was in a reverse fashion (Glovinsky, Quigley, & Dunkelberger, 1991). The central retina was affected more than the periphery in monkey (Cowey, 1974; Herbin, Boire, Théoret, & Ptito, 1999). At eccentricity 0-2 mm or 0-10 degree from the fovea, the ganglion cell loss was 80% of all RGCs whereas the ganglion cell density was normal beyond 2 mm from the fovea in destriated monkeys. These findings were consistent with behavioural studies (Humphrey, 1974; Weiskrantz, 1972). The retrograde trans-synaptic

degeneration in the cat were more prominent in the peripheral retina than the centre (Pearson 1981), in contrast to that observed in monkeys (Van Buren J. M., 1963; Cowey, 1974; Weller, Kaas, & Wetzel, 1979). This might be due to the maturation process in the peripheral retina occurred before the central area in primates (Abramov, Gordon, Hendrickson, Hainline, Dobson, & LaBossiere, 1982). In the cat, cells in the central retina developed before the periphery (Rapaport & Stone, 1982; Walsh, Polley, Hickey, & Guillery, 1983). The retinal ganglion cells that developed early in life might show greater resistance to the retrograde trans-synaptic degeneration (Payne, Pearson, & Cornwell, 1984).

Cell types

Despite a long survival time up to 4 years in unilaterally hemispherectomized monkeys, only 70% of RGCs in the central retina disappeared and no degeneration was found in the peripheral retina (Herbin, Boire, Théoret, & Ptito, 1999). These implied that not all types of retinal ganglion cells were affected and certain types of the RGCs were more vulnerable to the retrograde trans-synaptic degeneration than other types. In functional studies, it had been shown that de-striated monkeys could see well in the ambient light but their focus abilities were impaired. It was like having normal peripheral vision over its whole visual field (Humphrey, 1974; Weiskrantz, 1972). The night vision of monkeys with bilateral striate cortex removal was better than the vision in the bright light. If the de-striated monkeys had only scotopic vision, their colour perception might have been impaired (Malmo, 1966). However results from a behavioural study in patients with postgeniculate lesion disagreed (Stoerig, 1987). Achromatic and chromatic stimuli with the peak of wavelength of green targets at 505 nm and the wavelength of red targets between 660 and 620 nm were presented on a screen. Patients concentrated on a fixation target on the screen and were asked if they could perceive the stimuli or not. The patients were able to discriminate the green and red targets but not able to detect achromatic targets that were presented on the same retinal region. The results indicated that vision in homonymous hemianopia patients was not scotopic and that cones still functioned. It was found histologically that P cells were selectively lost in the retrograde trans-synaptic degeneration in macaque monkeys (Cowey, Stoerig, & Perry, 1989). In the retina of striated-ablated cats, P cells were reduced by 90% in the peripheral retina whereas other cell types did not degenerate (Payne, Pearson,

& Cornwell, 1984). In this study, cells lamina A and A1 of the dLGN, which were the main targets of P cells but not the others, markedly degenerated after the cortical removal (Payne, Pearson, & Cornwell, 1984). M and gamma ganglion cells were relatively spared (Cowey, Stoerig, & Perry, 1989; Payne, Pearson, & Cornwell, 1984). Nonetheless their morphologies changed. Cell hypertrophy might be due to the increase in the target availability and cell atrophy might proceed through target losses (Cunningham, 1982). Gamma cells appeared hypertrophied as a result of an in increase in projections towards the pulvinar (Labar, Berman, & Murphy, 1981), the superior colliculus and the c complex of the LGN (Payne, Pearson, & Cornwell, 1984). It had been suggested that these areas were previous targets of the cortical neurons and the partial deafferentiation after cortical removal created available targets for the retinal fibres (Updyke, 1977). In addition, gamma cells received more afferent inputs from the inner retina that usually connected to the degenerated P cells (Payne, Pearson, & Cornwell, 1984). M cells became atrophied as a result of loss of their targets in the laminae A, A1, and c of the dLGN without sufficient collateral sprouting to other target areas (Payne, Pearson, & Cornwell, 1984). The preservation of M and gamma cells could be account for the spared peripheral retina in retrograde trans-synaptic degeneration.

Our findings were in good agreement with a MRI study, showing damage to the optic tract and the LGN in patients with longstanding retrogeniculate lesions (Fig. 27 & 28) but not in a patient with recent onset (Fig. 29) (Bridge, Jindahra, Barbur, & Plant, 2011). In primate study, the retinal degeneration was significantly related to the volume of the degenerated dLGN (Cowey, Stoerig, & Williams, 1999).

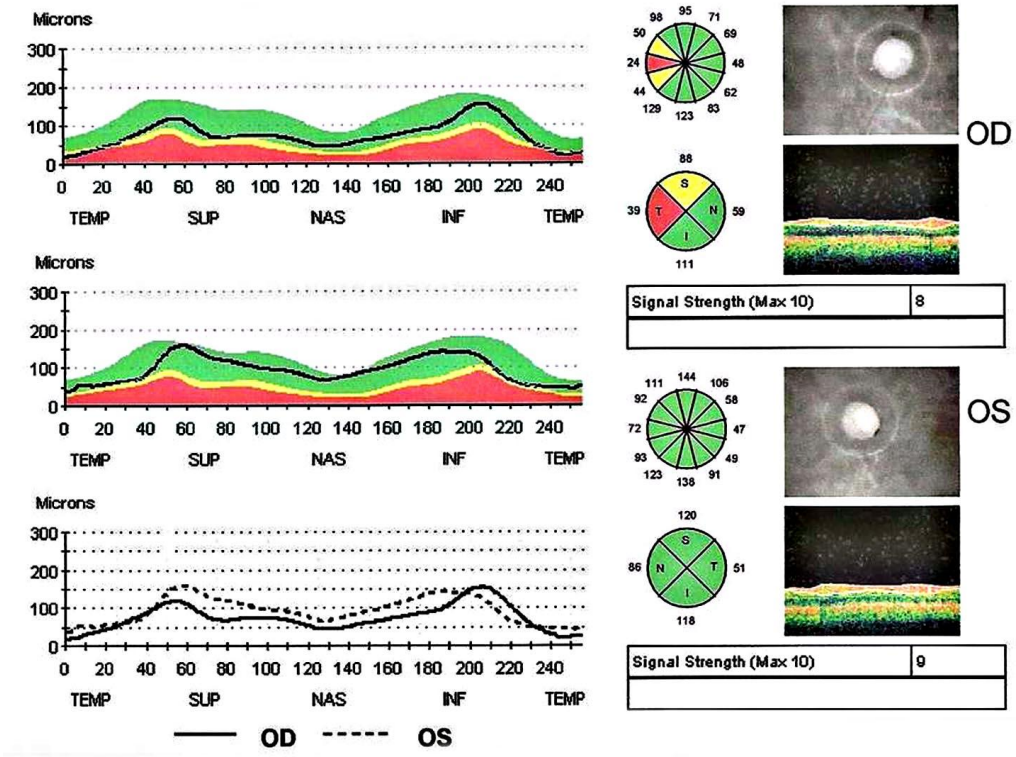
Microns
300
200
100
0
0 20 40 60 80 100 120 140 160 180 200 220 240
TEMP SUP NAS INF TEMP
Microns
300
200
100
0
0 20 40 60 80 100 120 140 160 180 200 220 240
TEMP SUP NAS INF TEMP
Microns
300
200
100
0
0 20 40 60 80 100 120 140 160 180 200 220 240
TEMP SUP NAS INF TEMP
OD ----- OS
98 95 71 50 69 24 48 44 62 129 123 83
88 S 39 T N 59 I 111
OD
Signal Strength (Max 10) 8
111 144 106 92 58 72 47 93 49 123 138 91
120 S 86 N T 51 I 118
OS
Signal Strength (Max 10) 9

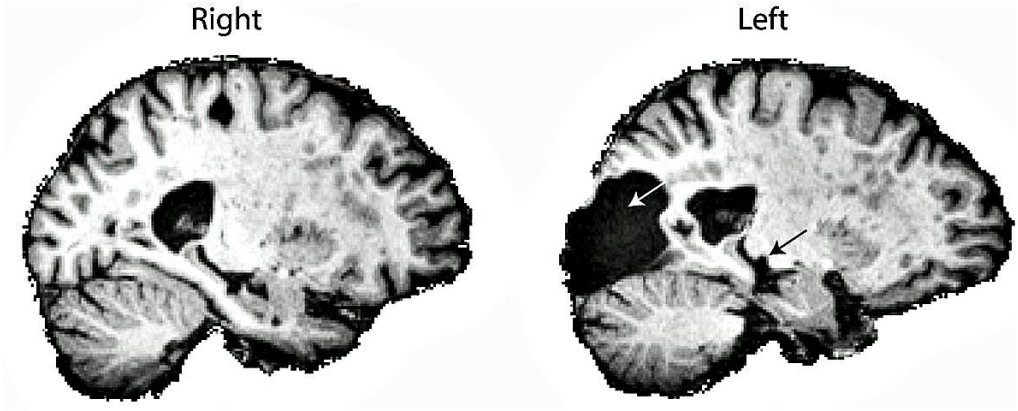
Right
Left

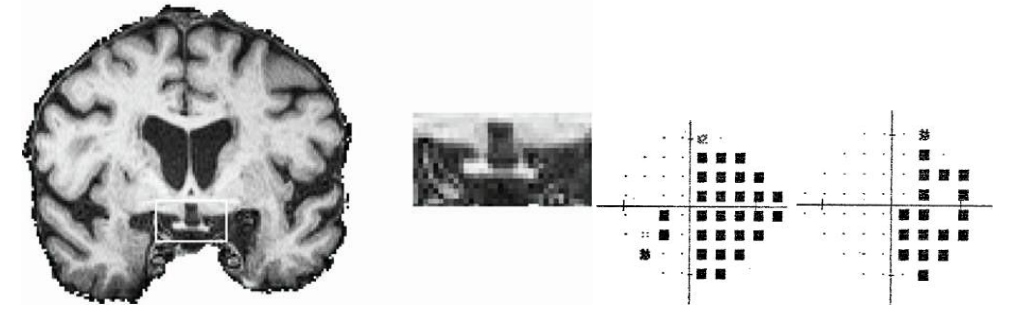

Figure 27 POV: Diagram showed data from a patient with right homonymous hemianopia caused by left occipital meningioma removal 18 years ago (white arrow). The RNFL thickness was presented on the top showing the pattern of RTSD. MRI T1 images revealed that the left optic tract (inset) was smaller than the right and the left LGN degenerated (black arrow). The right optic tract and the right LGN were intact. Reprinted MRI scans from Invest Ophthalmol Vis Sci, vol 52, H Bridge, P Jindahra, J Barbur, & GT Plant, page 382-8, ©2011. Permission to reproduce MRI scans has been granted by Investigative ophthalmology and visual science.

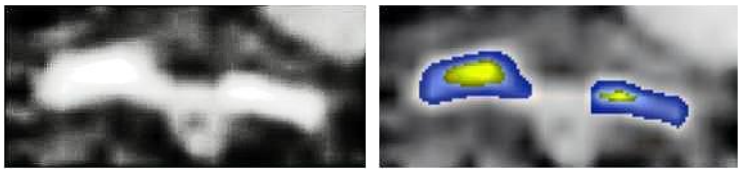

Optic tract

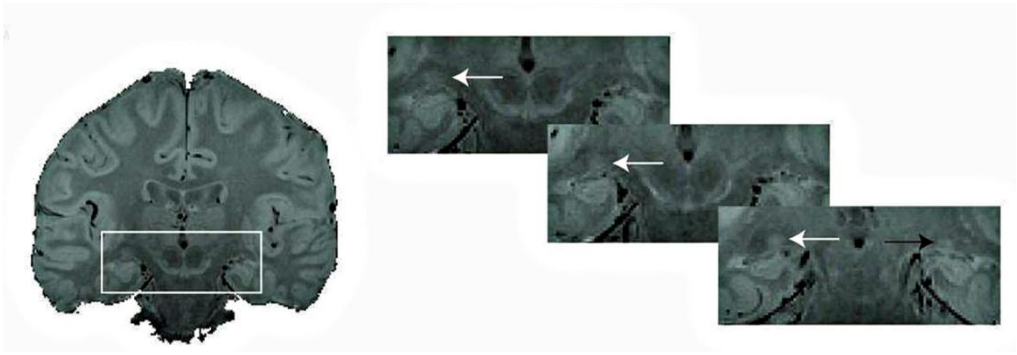

LGN

Figure 28 GY: Diagram showed MRI scans of the patient with right homonymous hemianopia for 45 years. His data was previously presented in Fig. 21. The MRI on the top panel showed slender left optic tract but relatively intact right tract. His LGN was not as atrophic as that found in POV in Fig. 27 but proton density in the middle panel revealed smaller left LGN, black arrow, as compared to the right, white arrows. Three sagittal T1 images in the bottom panel were arranged from the lateral to the medial part (from left to right). The lesion appeared quite extensive in the left medial occipital area and extended to the optic radiation. Permission to

reproduce the optic tract and LGN figures has been granted by Investigative ophthalmology and visual science. Reprinted MRI scans of optic tracts and LGN from Invest Ophthalmol Vis Sci, vol 52, H Bridge, P Jindahra, J Barbur, & GT Plant, page 382-8, ©2011. Permission to reproduce the MRI scans has been granted by Investigative ophthalmology and visual science. Reprinted the MRI scans on the bottom panel from Brain, vol 116, JL Barbur, JD Watson, RS Frackowiak, & S Zeki, Conscious visual perception without V1, page 1293-302, ©1993. Permission to reproduce the MRI scans has been granted by Oxford University Press.

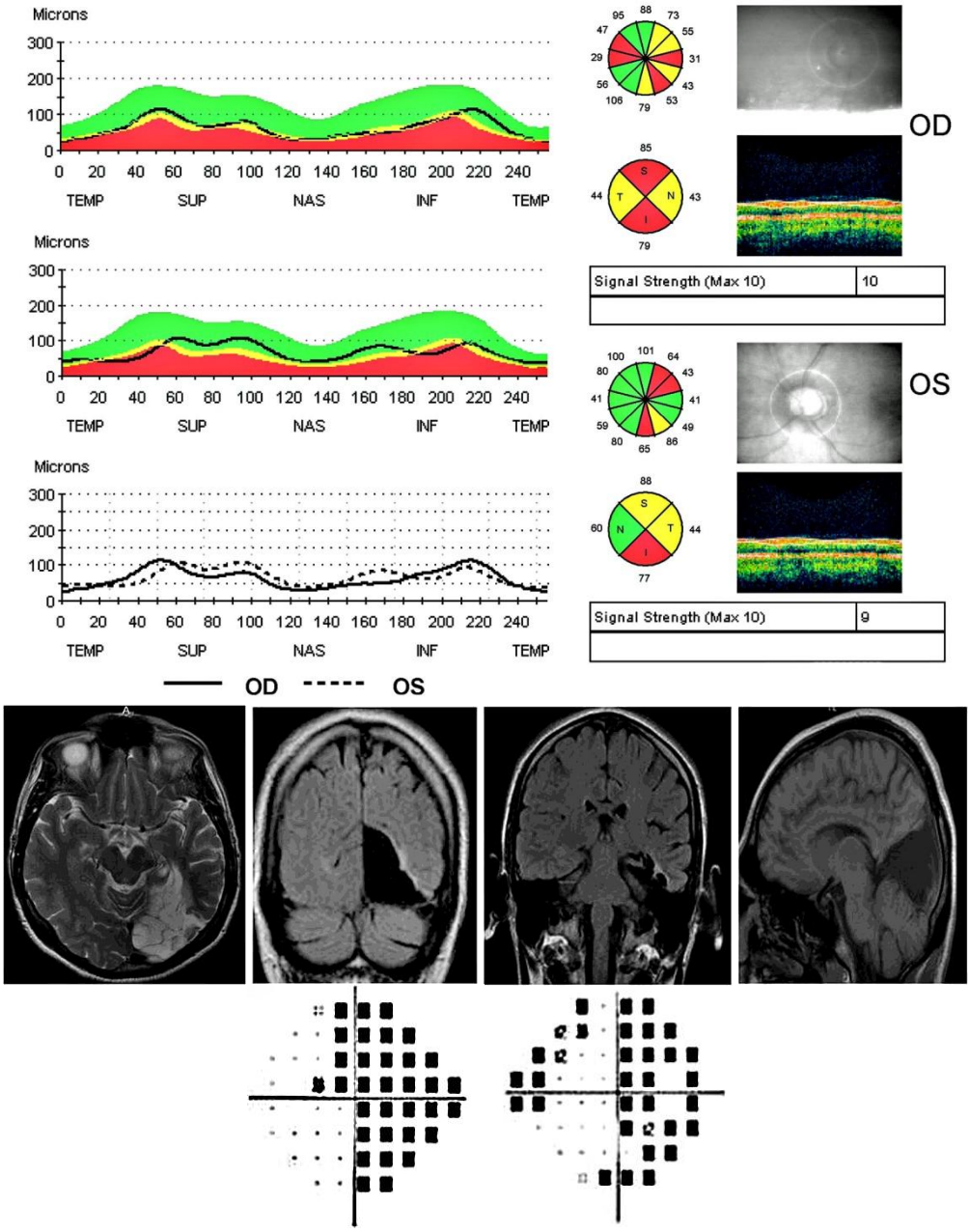

Figure 29 MAJ: Diagram showed results from Humphrey perimetry 24-2 on the bottom and OCT on the top in a patient with 5-year-history of right homonymous hemianopia. MRI scans in the middle panel revealed an extensive infarction in the left occipital lobe and optic radiation.

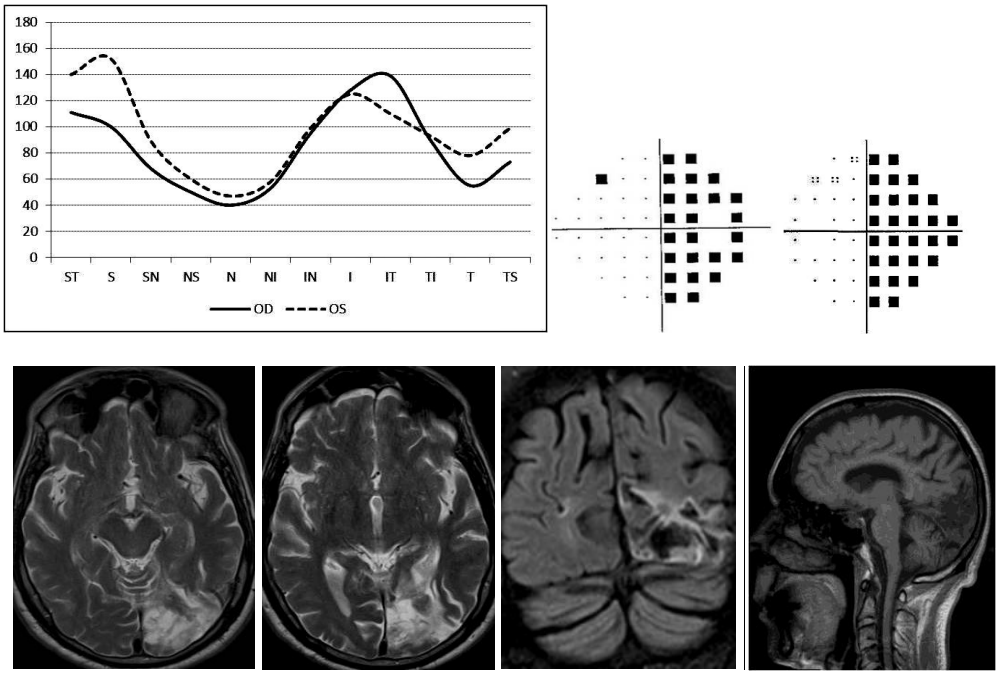

Figure 30 JAS: Diagram showed results from Humphrey perimetry 24-2 on the top right and OCT on the top left in a patient with an 18-month history of right dense homonymous hemianopia. MRI scans in the bottom panel revealed left occipital and optic radiation infarct. There was no significant difference in the ipsilateral optic tract cross-sectional area and volume compared to the optic tract of age-matched control or compared to his contralateral tract (Bridge, Jindahra, Barbur, & Plant, 2011).

	POV	GY	MAJ	JAS
Age at examination	72	53	46	65
Age at onset	54	8	41	63
Duration (year)	18	45	5	1.5
Cause	Surgery	Head injury	Infarction	Infarction
Lesion at	Occipital lobe	Occipital lobe & optic radiation	Occipital lobe & optic radiation	Occipital lobe & optic radiation
Size of the occipital lesion	Large complete	Large incomplete	Large complete	Large incomplete
Ipsilateral LGN	Totally lost	Small	Small	No change
Ipsilateral tract	Thin	Thin	Thin	No change
RNFL (microns)	84.1	72.4	65.1	89.7
MD (dB)	-13.87	-18	-16.8	-17

Table 5 Data comparison between four acquired dense unilateral homonymous hemianopia cases (POV, GY, MAJ, and JAS). RNFL = mean RNFL thickness of both eyes; MD= mean of median deviation in both eyes in Humphrey perimetry 24-2; dB= decibel. Among the long-standing cases namely, POV, GY, and MAJ; POV had the best visual outcome evaluated by RNFL and MD. The outcome of the other two patients was not much different from each other. What factors make POV unlike the others? Apart from the age of onset, POV had the least extent of the lesion that was only in the occipital lobe and very atrophic ipsilateral LGN. The age of onset and the duration were in an opposite direction between GY and MAJ so we are not going to consider these two factors in this discussion. Both GY and MAJ had lesions in the occipital lobe and the optic radiation; and a slight change in the ipsilateral LGN. Perhaps POV's ipsilateral optic radiation gave off small aberrant collaterals that sustained the retinal ganglion cells; hence, he had a slightly better visual outcome. Alternatively, the collaterals from the optic radiation might already be there since birth. They were just spared in POV but were destroyed in the others. What would happen if a patient had a discrete lesion only at the optic radiation? A patient (GIH) had a lesion in the optic radiation (Fig. 31). The mean RNFL thickness of both eyes was 115.8 microns at 0.3 year and 103.3 microns at 1.7 years after the stroke. Three years after the stroke, his vision did not recover and he was left with dense homonymous hemianopia. His visual outcome was poor regarding the visual field analysis. The RNFL thickness appeared thicker than JAS whose duration of the

homonymous hemianopia was similar to that of GIH. It was difficult to compare the change of RNFL thickness between the two patients as JAS data was recorded only once. It has been well known that young age or African in origin tends to have high RNFL thickness. No evidence of ipsilateral LGN and optic tract degeneration in the MRI scans was found. POV, who had only occipital lesion, showed a slightly better visual prognosis than GIH, who had only lesion at the optic radiation. More data are required to determine whether a lesion at the optic radiation produced more retrograde trans-synaptic degeneration than a lesion at the striate cortex. However the difference in RNFL and MD in these patients was not great and the clinically visual outcome appeared almost the same. Among the patients with extensive lesions that were a combination of the occipital lobe and the optic radiation (GY, MAJ, and JAS), the patient with the shortest duration (JAS) had the greatest RNFL thickness, the least degenerated LGN, and optic tract.

All of them had similar degree of hemianopia. If we repeat the measurement in five or ten years' time, JAS's results might catch up with the other two. Duration of the cortical injury might determine the degree of the retrograde trans-synaptic degeneration. A relationship between the duration and the RNFL thickness will be presented in following chapters.

These findings have significant implications also for proposed rehabilitation strategies in patients with homonymous hemianopia (Sabel, Kenkel, & Kasten, 2005; Sahraie, Trevethan, MacLeod, Murray, Olson, & Weiskrantz, 2006) as retinal ganglion cell loss might be expected to reduce the potential for recovery. The potential impact of retinal ganglion cell loss should be taken into account in such studies.

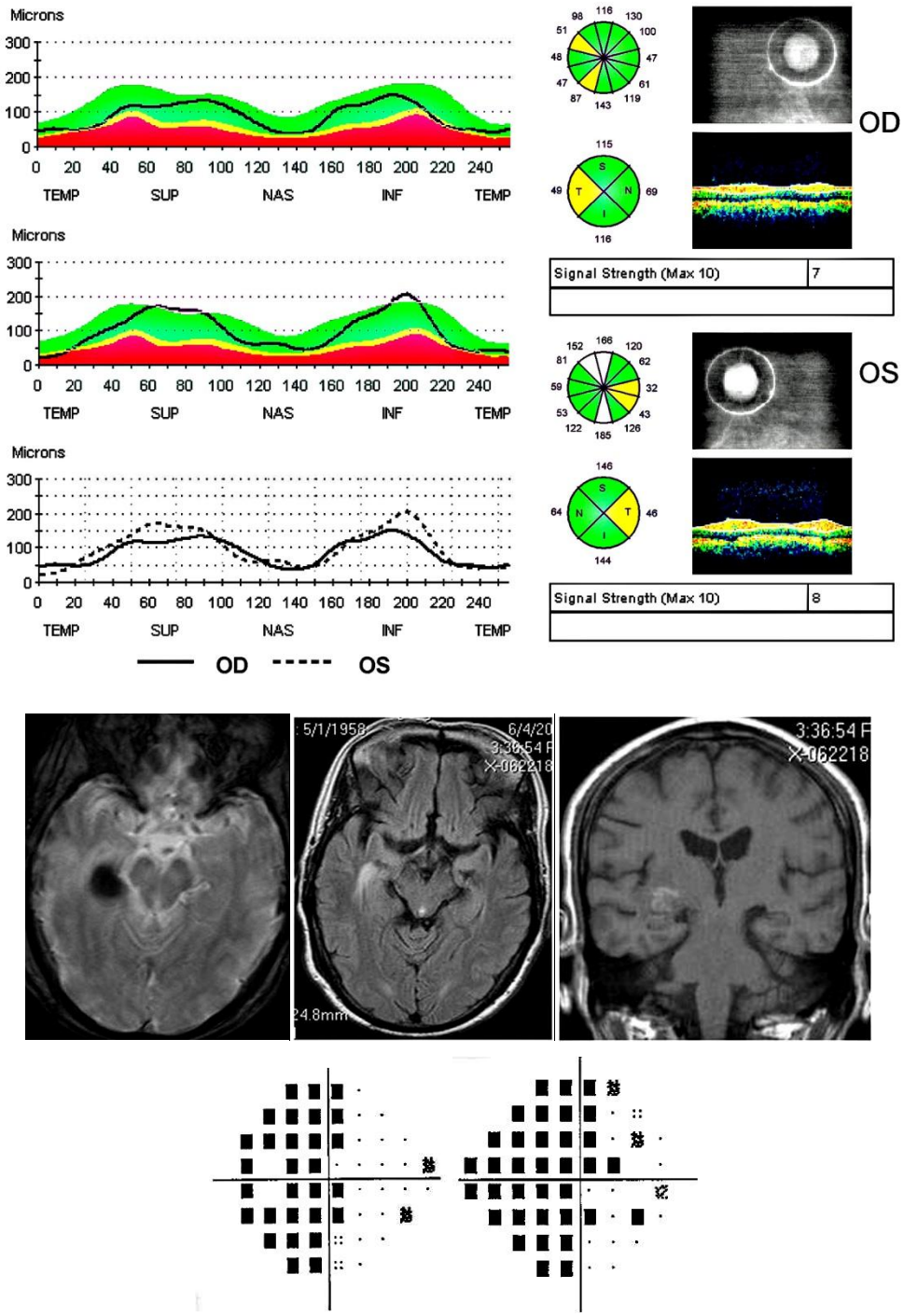

Figure 31 GIH: Humphrey perimetry, OCT, and MRI scans.

6 A comparison of the RNFL thickness between optic tract, optic chiasm, and post-geniculate lesions

6.1 Aims

To compare the magnitude of retrograde trans-synaptic degeneration following post-geniculate lesion and retrograde degeneration from optic tract and chiasmal lesion.

6.2 Methods

Twenty patients were recruited and were divided into three groups. The first group had 10 patients with dense homonymous hemianopia due to post-geniculate lesions. Age ranged from 46 to 73 years and duration was from 0.3 to 45 years. Causes of post-geniculate lesions included cerebral infarct (9 cases) and head injury (1). The second group had 5 patients with dense homonymous hemianopia due to unilateral optic tract lesions (Fig. 32). Causes of the tract lesions included tumour (1), aneurysm (2), and head injury (2). Age ranged from 30 to 70 years and duration was from 1.4 to 9 years. The third group had 5 patients with bitemporal hemianopia due to chiasmal lesions (Fig. 33). Age ranged from 33 to 71 years and duration was from 5 to 18 years. Causes of the chiasmal lesions included pituitary adenoma (4) and tuberculosis (TB) meningitis (1). Some details of the last group were presented in Table 6. Patients who had a combination of optic tract and chiasmal lesions were excluded except for one patient. MRI brain scans and Humphrey perimetry 24-2 were carried out in all subjects. The peripillary RNFL thickness measurement was performed by using OCT as in the previous chapter. The mean RNFL thickness of the crossing fibre defect eyes or the eyes with temporal hemianopia was used for a comparison. The result from the non-crossing fibre defect eyes or the eyes with nasal hemianopia was not used in this chapter. In patients with lesions in the chiasm and unilateral optic nerve, the RNFL thickness of the eye without optic neuropathy was chosen.

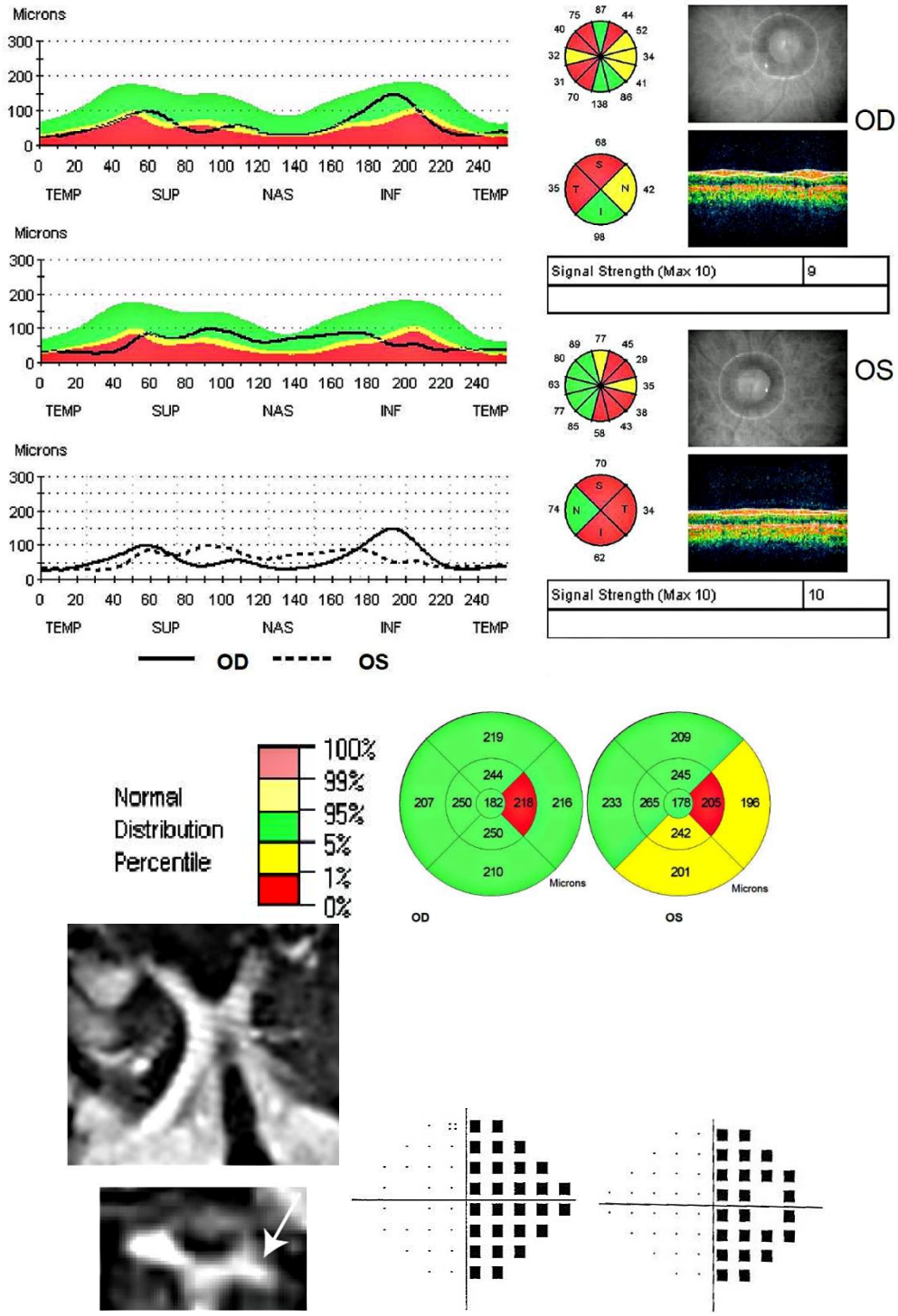

Figure 32 RID: Diagram showed evidence of retrograde degeneration in a patient who presented with dense right homonymous heminanopia from a left optic tract lesion following head injury 4 years ago. T1 weighted MRI scans on the bottom left revealed a thin left optic tract (white arrow) (Bridge, Jindahra, Barbur, & Plant, 2011). Other intracranial appearances were unremarkable. The pattern of RNFL

thinning on the top panel appeared similar to that found in post-geniculate lesion or RTSD in that the nasal part was thinner in the right eye (the eye with crossing fibre defect) than the left and the vertical areas, the inferior part in particular, appeared thinner in the left (the eye with non-crossing fibre defect) than the right. OCT measurement over the macular areas on the bottom right revealed reduced volume on the left half of both foveae (red). Reprinted MRI scans of the optic tracts from Invest Ophthalmol Vis Sci, vol 52, H Bridge, P Jindahra, J Barbur, & GT Plant, page 382-8, ©2011. Permission to reproduce the figures has been granted by Investigative ophthalmology and visual science.

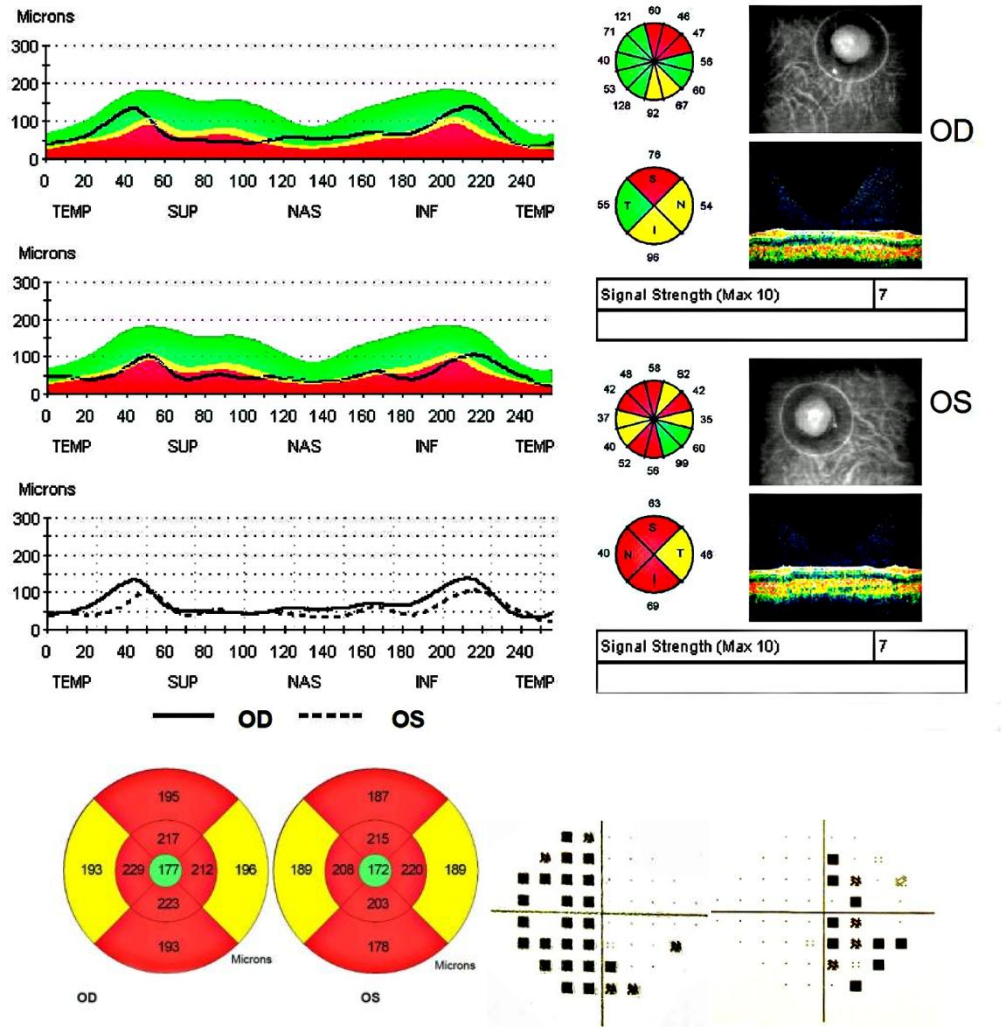

Figure 33 JET: A 39-year-old white male had bitemporal hemianopia from pituitary adenoma compressing the optic chiasm. The RNFL thickness and the macular volume were presented. The average right RNFL thickness was 70 microns and the left was 54.3 µm. The macular volume was diffusely affected with spared central region in both eyes.

Case	Cause	Acuity	Ishihara	Pupil	Disc	RNFL RE	RNFL LE	MD RE	MD LE
DaG(33)	TB meningitis 18 years ago	normal BE	normal BE	normal no RAPD	pale BE	55.2	55.5	-14.7	-16
SuW(62)	Pituitary adenoma Hypophysectomy 5 years ago Hematoma at the chiasm	normal BE	normal BE	normal no RAPD	pale BE	66.4	71.75	-12	-10.6
JeT(39)	Pituitary adenoma	6/12RE,6/6LE	1/17,2/17	left RAPD	pale BE	70	54.3	-11.3	-5.5
BrR (49)	pituitary adenoma Hypophysectomy 12 years ago Radiation 11 years ago	6/24RE,6/60LE	15/17,2/17	left RAPD	pale BE	36.1	33.3	-17.9	-23.2

Table 6 Data from patients with bitemporal hemianopia due to chiasmal lesions. Number in the parentheses represented age at the time of examination. Abbreviation: BE = both eyes, RE = right eye, LE = left eye, MD = median deviation.

6.3 Results

The range of the RNFL thickness was 57.4 to 70.2 microns in the patients with optic tract lesions; 36.1 to 70 microns in patients with chiasmal lesions; and 57.6 to 83.5 microns in patients with post-geniculate lesions (Fig. 34). The overlapped range for all groups was from 57 to 70 microns. The least value in the post-geniculate was comparable to that of the optic tract group but was less than the chiasmal group. The patient with the thinnest RNFL had a combination of chiasmal and optic nerve lesions.

6.4 Discussion

The extent of RNFL loss in the patients with chiasmal compression and optic neuropathy was greater than the loss from isolated chiasmal lesion. The magnitude of RNFL loss in severe retrograde trans-synaptic degeneration is comparable to that of severe retrograde degeneration in isolated optic tract or isolated chiasmal lesions. Notably the severe degeneration found in all groups developed in adulthood and diverse duration of diseases.

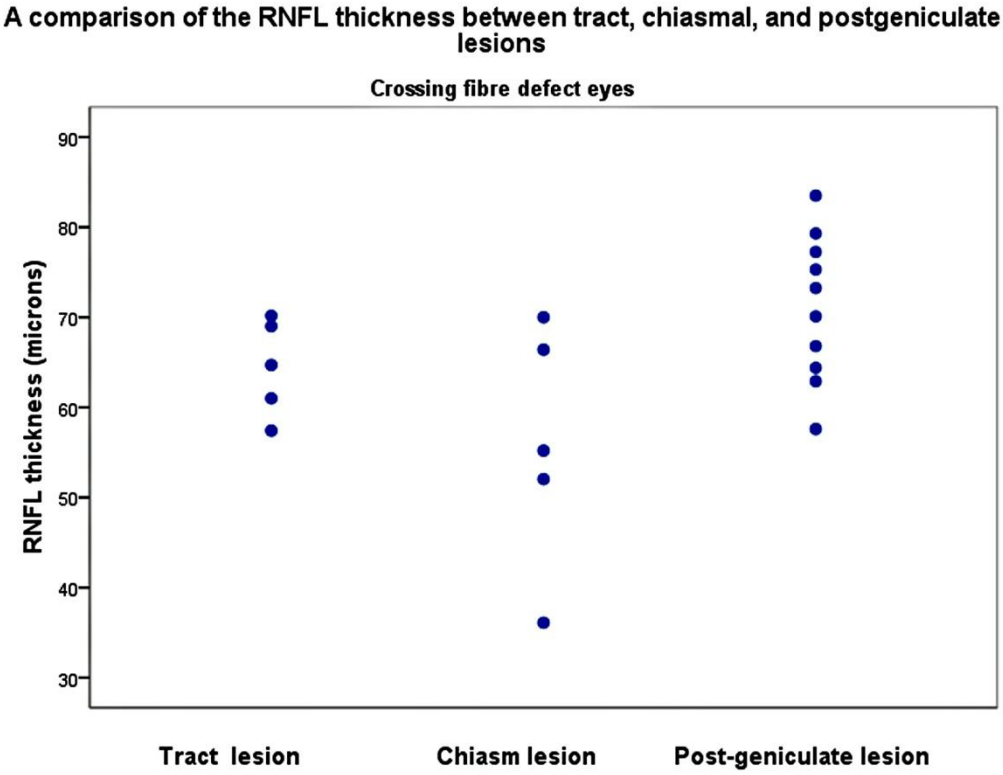

Figure 34 Diagram comparing the retinal nerve fibre layer thickness in the crossing fibre defect eyes or the eyes with temporal hemianopia between patients with optic tract, optic chiasm, and post-geniculate lesion.

7 A retrograde trans-synaptic degeneration study in patients with homonymous quadrantanopia from retrogeniculate lesion identified by optical coherence tomography

7.1 Aims

The retrograde trans-synaptic degeneration was demonstrated in the homonymous hemianopia patients who had large lesions. However we did not know whether the size of the lesion mattered and how it affected the retinal ganglion cell loss in human. The aim in this chapter was to study the retrograde trans-synaptic degeneration in patients with homonymous quadrantanopia.

7.2 Methods

Fourty-four cases were recruited to the present study. There were three groups. The first pathological group, comprising 14 cases, had acquired homonymous quadrantanopia (Fig. 35); the mean duration of disease was 9.6 years (range 1.8-25 years) and the mean age was 50.9 years (range 75-23 years). The second pathological group, comprising seven cases, had congenital homonymous quadrantanopia; the mean age was 40.6 years (range 55-23 years). The control group consisted of 23 volunteers, 11 females and 12 males, with normal vision and no ophthalmic disorder. The mean age of this group was 43 years (range 23-61 years). Visual field analysis was carried out using the Humphrey 24-2 perimetry. All patients had either MRI or CT scans performed. The peripapillary RNFL thickness was measured in each eye and in each of 12 sectors around the optic nerve head. The StratusTM Optical Coherence Tomography version 4 (Carl Zeiss Meditec, Inc.) was used in every case. The fast RNFL program was employed with a circle of 3.4mm diameter centred on the optic disc. All cases had no ophthalmologic condition and had normal intraocular pressure. Refractive error ranged from +4 to -4.

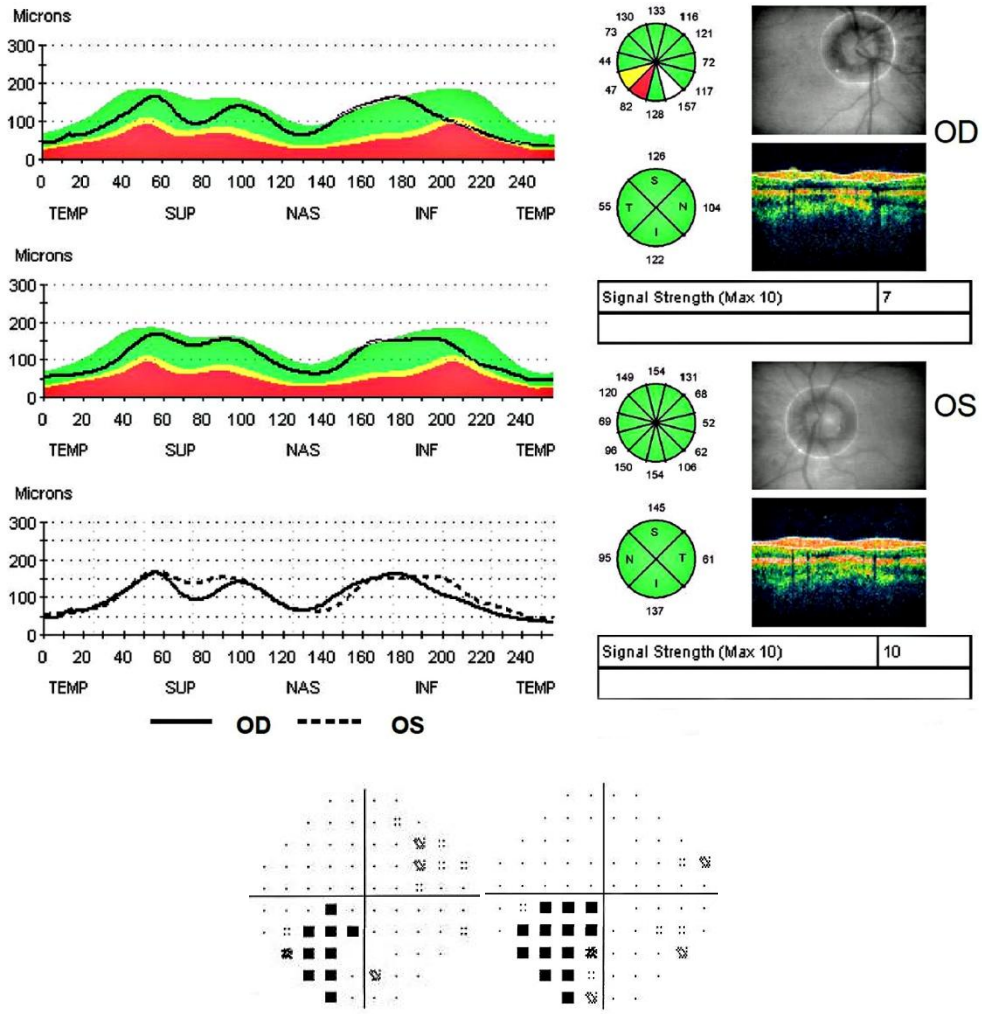

Figure 35 ROW: Diagram showed results from OCT and Humphrey perimetry 24-2 in a patient with left inferior homonymous quadrantanopia from right occipital tumour. The superior region of the right peripapillary RNFL was thinner than that on the left. The result corresponded to the retinotopic organization.

7.3 Statistical analysis

The right eye of each member of the control group was taken as equivalent to the crossing fibre defect eye. The estimated overall mean (over 12 sectors) RNFL thickness of each crossing fibre defect and each non-crossing fibre defect eye for the two quadrantanopia groups and for the right and left eyes in the control group were reported. We performed hierarchical repeated measures analysis of variance (ANOVA), with cases nested in groups, and sectors and eyes representing the two repeated measures. Since there was a significant interaction between groups and sectors, the data were split by sectors. ANOVA and Bonferroni *post hoc* comparisons were made among the groups in each sector separately thereafter.

Ratios of the thickness of crossing- to non-crossing fibre defect eyes were calculated for each sector. We compared the means of the ratios in the 3 groups, i.e. superior field defect, inferior field defect, and normal subjects. It was notable that each field defect group consisted of both acquired and congenital cases. We performed hierarchical repeated measures ANOVA on the ratios, with cases nested in groups and sectors as repeated measures. Since there was a significant interaction between groups and sectors, group means were compared for each sector separately using one-way ANOVA. The assumptions underlying every analysis were verified by a study of the residuals. A significance level of 0.025 was used throughout.

7.4 Results

The mean and the standard deviation of the RNFL thickness were calculated in each eye separately and both eyes together (Table 7). In crossing-fibre eyes the estimated mean RNFL was 88.3 microns (SD 36.4 microns) in the acquired group; 91.4 microns (SD 35 microns) in the congenital group; and 101.4 microns (SD 35.4 microns) in the right eyes of the control group. In non-crossing-fibre eyes the estimated mean RNFL was 88.14 microns (SD 32.8 microns) in the acquired group; 94.3 microns (SD 29.6 microns) in the congenital group; and 101.3 microns (SD 36.6 microns) in the left eyes of the control group. The estimated mean RNFL of both eyes was 88.2 microns (SD 34.6 microns) in the acquired group; 92.8 microns (SD 32.3 microns) in the congenital group; and 101.2 microns (SD 36 microns) in the left eyes of the control group. There were significant interactions between groups and sectors ($p<0.001$) but no significant interactions between groups and eyes ($p=0.7$). There was no significant difference between the mean RNFL thickness in the two eyes ($p=0.46$) (Fig. 36 & 37).

Figure 36 Means RNFL thickness for each sector in homonymous quadrantanopia patients' crossing fibre defect eyes and normal subjects' right eyes.

Figure 37 Means RNFL thickness for each sector in homonymous quadrantanopia patients' non-crossing fibre defect eyes and normal subjects' left eyes.

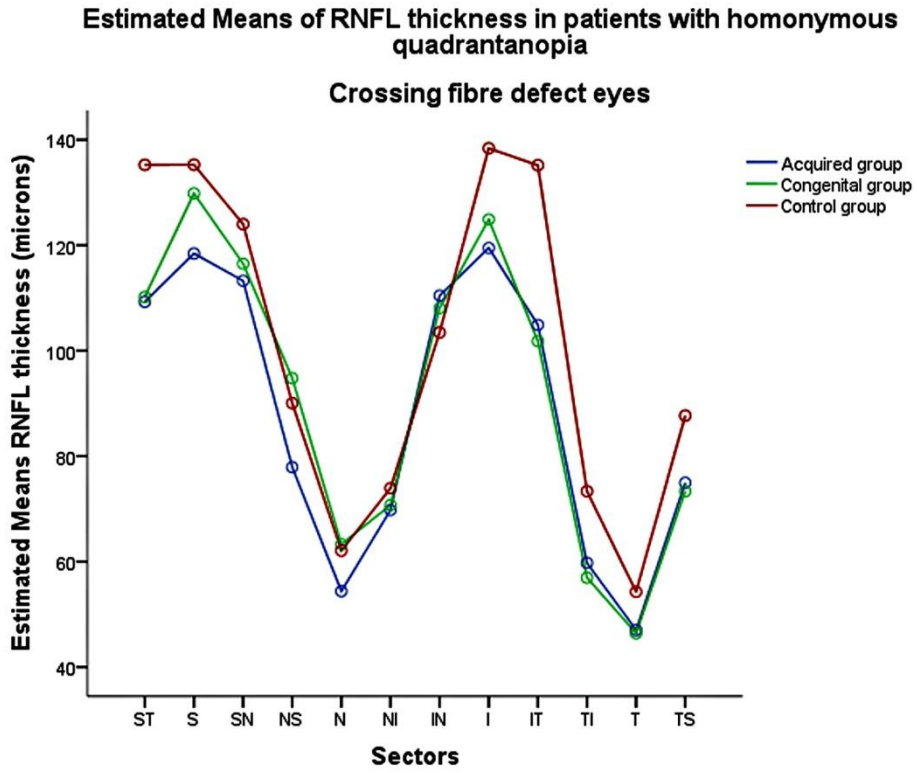

Figure 36

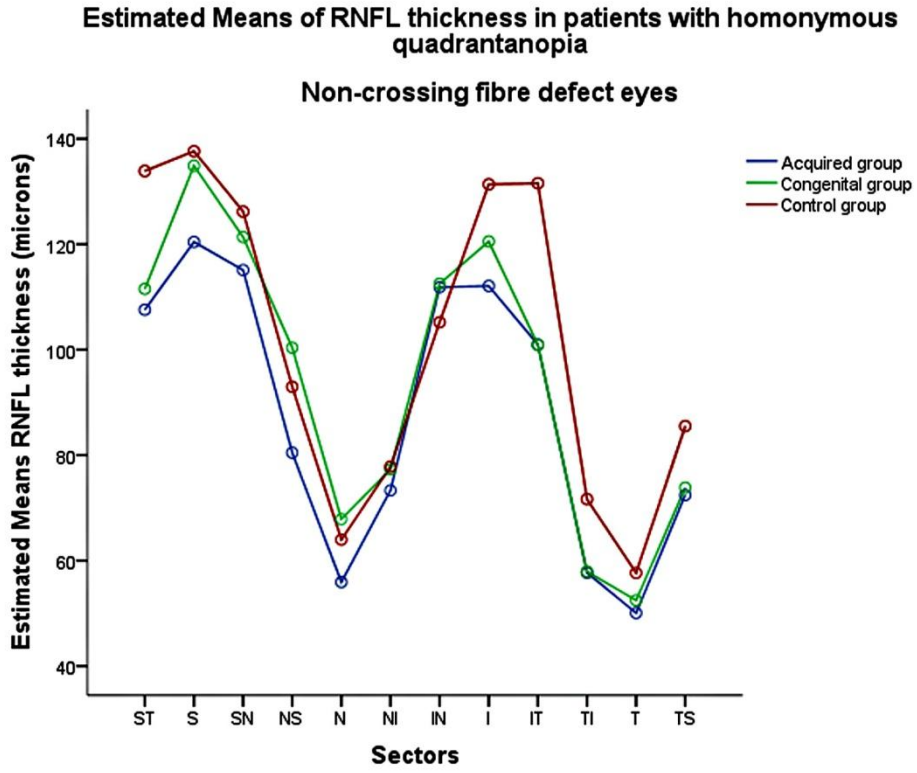

Figure 37

	Acquired group	Congenital group	Control group
Number of cases	14	7	22
Crossing fibre defect eyes	88.3 (36.4)	91.4 (35)	101.1 (35.4)
Non-crossing fibre defect eyes	88.14 (32.8)	94.3 (29.6)	101.3 (36.6)
Both eyes	88.2 (34.6)	92.8 (32.3)	101.2 (36)

Table 7 Table demonstrated the mean and standard deviation (in the parentheses) of peripapillary RNFL thickness in each eye and both eyes in all groups.

		Control-acquired	Control-congenital	Congenital-acquired
Sector ST	Mean	26.1	23.7	2.4
	95% CI	16 to 36	11 to 36	-10 to 15.7
	p-value	<0.001	<0.001	0.99
Sector IT	Mean	30.4	32	-1.5
	95% CI	19 to 42	17.5 to 46.5	-17 to 14
	p-value	<0.001	<0.001	0.99
Sector T	Mean	14	15	-1
	95% CI	7 to 20	7 to 23	-10 to 7.5
	p-value	<0.001	<0.001	0.99
Sector TS	Mean	13	13	-0.1
	95% CI	5.5 to 20	3.6 to 22	-10 to 10
	p-value	<0.001	0.004	0.99

Table 8 Mean difference of the RNFL thickness (microns) of Sector ST, IT, T, and TS among the three groups. Abbreviation: ST = superior-temporal sector, IT = inferior-temporal sector, T = temporal sector, TS =temporal-superior sector.

When comparing the mean RNFL thickness among the 3 groups for each separate sector, the ANOVA indicated that there were significant differences in group means in Sectors ST ($p=0.006$), IT ($p<0.001$), T ($p=0.003$), and TS ($p=0.046$). Differences in the group means in the remaining sectors did not reach statistical significance. *Post hoc* comparisons indicated that there were significant differences in the group means, using the data from both eyes, as shown in Table 8.

The ratio of the RNFL thickness of crossing fibre defect eyes to non-crossing fibre defect eyes was plotted for acquired and congenital groups and the ratio of the right eye to the left eye was plotted for the control group (Fig. 38). Three different groups were subdivided, namely, superior field defect, inferior field defect, and normal subjects so that the demonstration of the nerve fibre layer thinning would be better clarified than that of mixed superior and inferior filed defect groups. Since there was a significant interaction between groups and sectors ($p=0.006$), the groups were compared in each sector separately. The ANOVA indicated that there were significant differences in the mean ratio in sectors S ($p<0.001$) and I ($p<0.001$). Differences between the mean ratios in other sectors did not reach statistical significance. *Post hoc* comparison indicated that there were significant differences in the mean ratios as shown in Table 9.

Using the 24 sectors from both eyes, the mean RNFL thickness of both eyes and the mean median deviation (MD) of both eyes exhibited a linear relationship, MD= -18.64 + 0.14(RNFL thickness), Pearson correlation coefficient $r=0.41$, $p=0.016$ (Fig.39).

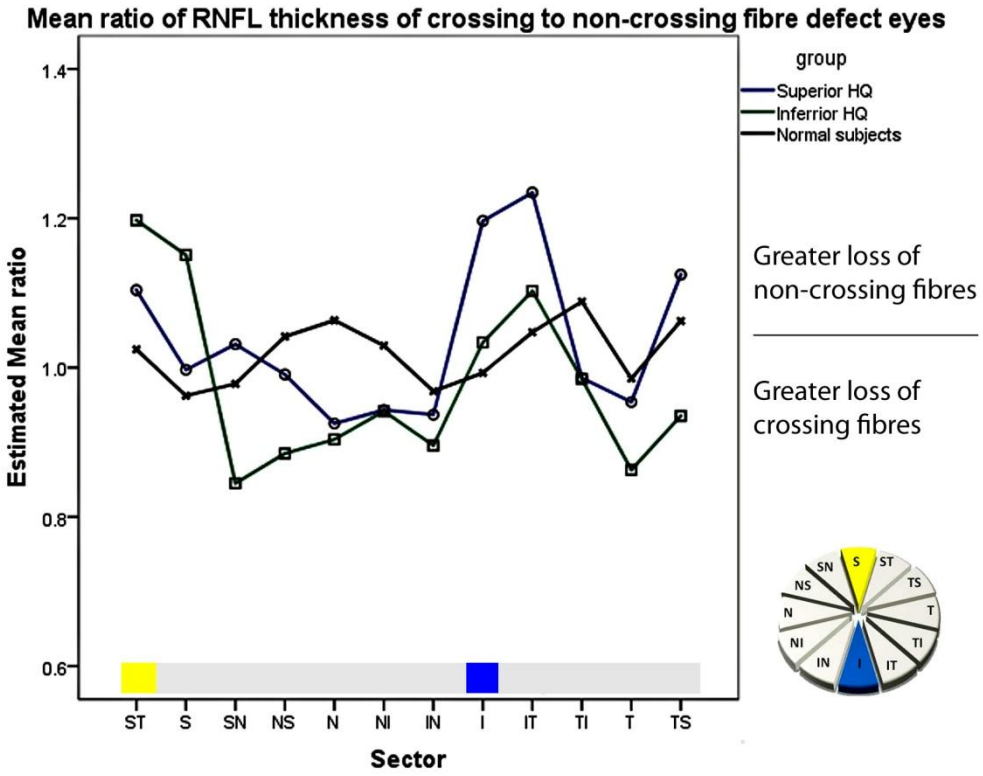

Figure 38 Mean ratio of the RNFL thickness of crossing fibre defect eyes: non-crossing fibre defect eyes in the quadrantanopia groups and right: left eyes in the control group.

	Mean ratio	Control-superior HQ	Control-inferior HQ	Superior HQ-Inferior HQ
Sector S	Mean difference	-0.03	-0.19	-0.15
	95% CI	-0.2 to -0.1	-0.4 to -.02	-0.3 to -0.04
	p-value	0.99	0.02	0.1
Sector I	Mean difference	-0.2	-0.04	0.16
	95% CI	-0.4 to -0.05	-0.2 to -0.1	-0.02 to -0.3
	p-value	0.005	0.99	0.09

Table 9 Mean ratio of the RNFL thickness of crossing fibre defect eyes: non-crossing fibre defect eyes in the quadrantanopia groups and right: left eyes in the control group.

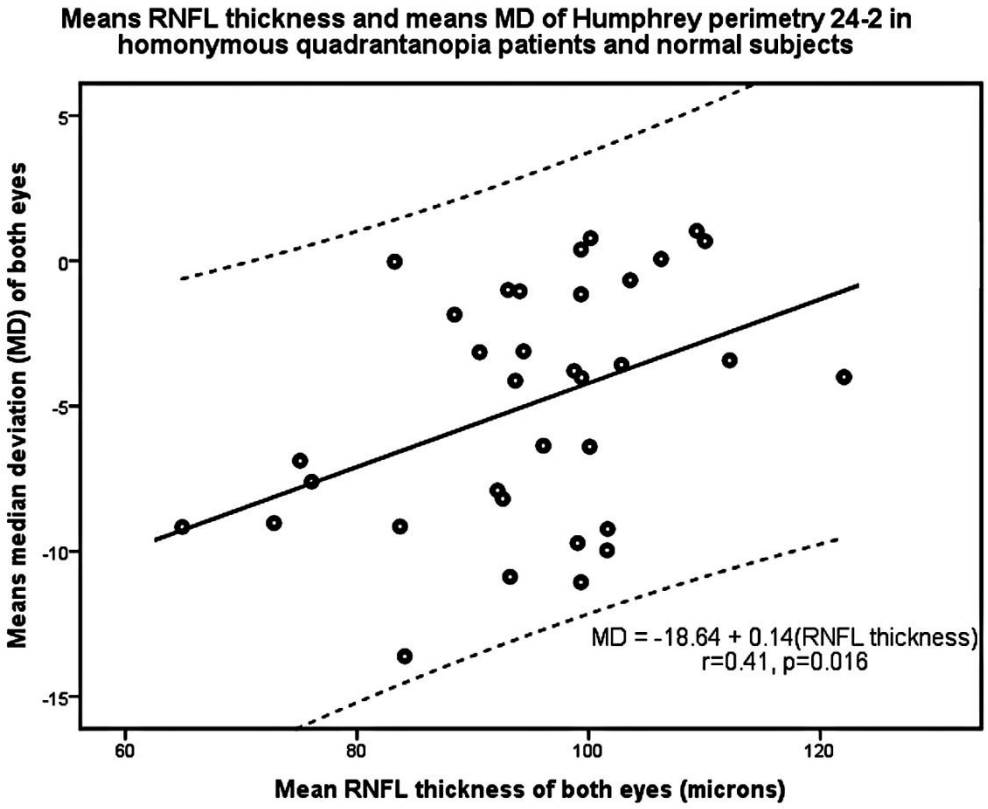

Figure 39 Linear relationship (black line) between mean RNFL thickness and mean of the median deviation (MD) of Humphrey perimetry 24-2 from both eyes in patients with homonymous quadrantanopia and normal subjects. The dashed lines represented the 95% confidence interval for the points.

7.5 Discussion

The results of the homonymous quadrantanopia cases appeared similar to that found in the homonymous hemianopia groups but in a lesser degree. As expected, the ratios in both homonymous quadrantanopia groups were less than one in the nasal and temporal areas, indicating the degeneration was greater in the crossing fibre defect eyes in these particular regions. The ratios in both homonymous quadrantanopia groups were higher than one in the remaining areas, indicating the thinning in these parts was greater in the non-crossing fibre defect eyes. The changes were most pronounced in the superior and inferior sectors for the inferior homonymous quadrantanopia and superior homonymous quadrantanopia groups respectively. Hence the retrograde trans-synaptic degeneration was also evident in the patients with small post-geniculate lesions. The RNFL thickness correlated well with the median deviation (MD) in Humphrey perimetry in the HQ data. It had been reported that MD reflected the spatial distribution of the retinal ganglion cells quite well (Lagrèze & Kordon, 1998).

Sizes of cortical lesions might influence the magnitude of retrograde trans-synaptic degeneration in primate studies. The greater the cortical or subcortical damage is, the greater the retina degenerates but this relationship did not reach statistical significance in a study (Cowey, Stoerig, & Williams, 1999). In another study, a cortical lesion was enlarged after the first operation but no further retinal ganglion cell loss was detected a few years afterwards (Ptito, Herbin, Boire, & Ptito, 1996). This result could be interpreted into 2 ways. Firstly the size of the lesion had no effect on thedegeneration or secondly the RTSD was not complete within 2-3 years after an occipital injury (Ptito, Herbin, Boire, & Ptito, 1996).

A large cortical lesion might include optic tract involvement and hence created an additional non-trans-neuronal degeneration (Cowey, Stoerig, & Williams, 1999; Kupersmith, Vargas, Hoyt, & Berenstein, 1994). Considering the optic tract involvement as a confounding factor in the retrograde trans-synaptic degeneration, Cowey et al performed operations on 3 young adult monkeys and studied their brain 8 to 9 years afterwards (Johnson & Cowey, 2000). The lesions were in both striate cortices that corresponded to the macular area in the retina. They were small and did not extend to the thalamus or the optic tract. The degeneration developed along the vertical midline of both dLGN and the number of RGCs diminished about

65-80% in the central retina. The results confirmed the retrograde trans-synaptic degeneration in small cortical lesions. However the absolute number of the neuronal loss varied among the 3 subjects. Their postoperative survival time was similar. The authors pointed out that the diversity might have been due to individual susceptibility to the retrograde trans-synaptic degeneration. The number of the retinal ganglion cells and optic nerve fibres in macaque monkeys were variable. It was difficult to evaluate the proportional loss precisely without knowing the baseline ganglion cell numbers for each individual. Moreover, the size of the striate cortex in macaque monkey (Van Essen, Newsome, & Maunsell, 1984) and humans (Andrews, Halpern, & Purves, 1997) varied. The same size of the lesion could produce different degree of the retinal degeneration (Johnson & Cowey, 2000). Interestingly the proportional RGC loss in smaller central cortical lesions was comparable to that in larger cortical lesions mentioned in the previous chapter. Perhaps it was due to cortical magnification that enhanced the central retinal representation area in the striate cortex. Thus the central retinal representation area in the cortex would be mostly damaged following a large occipital lobectomy, like the smaller lesions.

Further the size of a cortical lesion was correlated poorly to the volume of degenerated dLGN (Cowey, Stoerig, & Williams, 1999). A small projection from the dLGN towards extrastriate cortex, especially in the ventral occipito-temporal areas, might contribute to the outcome and blindsight (Cowey & Stoerig, The neurobiology of blindsight., 1991; Cowey, Stoerig, & Bannister , 1994; Stoerig & Cowey, Blindsight in man and monkey, 1997).

8 Rate of retrograde trans-synaptic degeneration study

8.1 Introduction

Retrograde trans-synaptic degeneration of neurons occurs following damage to the central nervous system (CNS). Evidence from clinical observation had suggested that RTSD of the retinal ganglion cells (RGCs) and their axons in the optic nerve and the optic tract occurred only following pre-natal, not post-natal acquired, damage to the visual pathway posterior to the lateral geniculate nucleus. Recent studies, however, have demonstrated thinning of the retinal nerve fibre layer (RNFL) using optical coherence tomography (OCT) (Jindahra, Petrie, & Plant, 2009) and of the optic tract using magnetic resonance imaging (MRI) following acquired damage to the occipital lobes in humans (Bridge, Jindahra, Barbur, & Plant, 2011; Cowey, Alexander, & Stoerig, 2011). These findings confirm the occurrence of RTSD in the human visual pathway.

Degeneration of an axon in the direction of its terminal following direct injury is classified as anterograde degeneration, whereas retrograde degeneration proceeds toward the cell body (Saxena & Caroni, 2007; Coleman, 2005). Anterograde degeneration was first described by Augustus Waller in 1850 and is also termed Wallerian degeneration. The pathological process has been the subject of extensive investigation (Fitzek, Fitzek, & Stoeter, 2004; Savoiardo, Pareyson, Grisoli, Forester, D'Incerti, & Farina, 1992; Danek, Bauer, & Fries, 1990). The time course of both Wallerian and of retrograde degeneration has been studied, using for example, microglial responses after axotomy in the spinal cord of the rat. Wallerian and retrograde degeneration have been shown to occur simultaneously within days (Koshinaga & Whittemore, 1995). In humans MRI studies have demonstrated both retrograde and Wallerian degeneration at 4 months after an internal capsule infarction as a short band of increased T2 weighted signal ascending to the precentral gyrus and another longer band descending to the brainstem (Danek, Bauer, & Fries, 1990) but no imaging studies of earlier changes have been published.

RTSD has been identified histopathologically in the immature human CNS following hypoxic damage (Sakai, Matsuda, Watanabe, Kamei, & Takashima, 1994). Post mortem histopathological studies of the brains of premature infants have revealed

RTSD in the olivocellebellar pathway: a cerebellar lesion leading to inferior olivary neuronal loss in the inferior olive as evidenced by decreased neurofilament staining of axonal fibres, axonal swelling and astrogliosis (Sakai, Matsuda, Watanabe, Kamei, & Takashima, 1994). Axonal swelling, a feature of RTSD shown in human brain, is associated with axonal transport interruption, which occurs prior to axonal separation (Sakai, Matsuda, Watanabe, Kamei, & Takashima, 1994; Povlishock, Becker, Cheng, & Vaughan, 1983).

In the visual pathway, a retrogeniculate lesion may be expected to give rise to retrograde degeneration of the geniculo-cortical neurones damaged directly which will be followed by RTSD of RGC axons. This has been identified post mortem in primate retina following occipital lobectomy: the number of RGCs in the region of the retina corresponding to the visual field representation of the damaged cortex was found to be reduced (Cowey, 1974; Johnson & Cowey, 2000). In addition, anterograde degeneration may be expected of the cortical-geniculate fibres. In humans, RTSD of the visual pathway has now been identified by post mortem examination in one case of occipital damage occurring early in life (Beatty, Sadun, Smith, Vonsattel , & Richardson Jr, 1982), clinical examination in congenital cases (Hoyt, Rios-Montenegro, Behrens, & Eckelhoff, 1972), MRI scan (Bridge, Jindahra, Barbur, & Plant, 2011), electroretinography (Porrello & Falsini, 1999), and OCT (Jindahra, Petrie, & Plant, 2009). OCT has been especially valuable because the thinning of the nerve fibre layer has been shown to correspond to the known trajectories of the crossed and uncrossed projections arising in the nasal and temporal hemiretinae respectively (Jindahra, Petrie, & Plant, 2009). The study in previous chapter has shown that retinal changes can be detected as early as 3.6 months following damage to the occipital lobe (Jindahra, Petrie, & Plant, 2009). However the precise time course of the process is unknown. The present study has been carried out to address this issue which is of fundamental importance to the understanding of the pathological process in humans; of how it might relate to animal studies of RTSD; and for the design of treatment strategies to prevent this class of neurodegeneration occurring following damage to the visual pathway and other regions of the brain.

8.2 Aims

The aim in the first part of the study was to ascertain the relationship between RNFL thickness and the time elapsed since the occipital damage. The aim of the second part of the study was to determine the time course of RNFL thinning in individual cases.

8.3 Methods

This study is divided into two parts. In the first part (the cross-sectional study), we investigated the relationship between duration of the disease and the peripapillary RNFL thickness. Thirty-eight patients with acquired homonymous hemianopia were recruited. All subjects had thorough neurological and ophthalmic examinations including intraocular pressure measurement. In each case it was confirmed that the hemianopia was the consequence of a single retrogeniculate lesion which was identified by appropriate neuro-imaging. Duration of the visual field defect ranged from 6 days to 67 years (mean 7.71 years). Age in the hemianopic group ranged from 17 to 83 years (mean 59.92 years). Twenty three control subjects were recruited. Age in the control group ranged from 23-61 years (mean 43 years). Exclusion criteria included evidence of more than one occipital lesion and evidence of any ophthalmic disorder such as retinopathy, glaucoma and high myopia (-6.00 diopters or more). The peripapillary RNFL thickness was measured by OCT (Stratus OCT, software version 4.0.1; Carl Zeiss Meditec, Inc., Dublin, CA) on a single occasion. A 3.4 mm diameter circular fast RNFL thickness protocol was employed. The strength of signal was at least 7. We evaluated the RNFL thickness in both eyes of each subject and took the mean for further statistical analysis.

In the second part (the longitudinal study), eleven patients were recruited, 7 with homonymous hemianopia and 4 with smaller homonymous visual field defects. All cases had occipital cerebral infarction as the cause of the post-geniculate damage except for case 4 (GIH; optic radiation haemorrhage) and case 7 (Trl; LGN infarction). All subjects had thorough neurological and ophthalmic examinations including intraocular pressure measurement. Exclusion criteria were as for the first part. Peripapillary RNFL thickness was measured by OCT in each case as soon as possible after the onset of stroke and on several occasions thereafter. We evaluated the RNFL thickness in both eyes of each subject and took the mean for further statistical analysis. A minimum of 3 measurements was made in each visit. The initial measurement was taken at a time interval ranging from 5 to 112 days post-stroke

and the last at an interval ranging from 170 to 917 days post-stroke. The RNFL measurements were carried out by a single operator (PJ) who has been shown to have a high reproducibility of measurements (Fig. 40). All participants gave their informed consent and the study was approved by the ethics committee of the National Hospital for Neurology and Neurosurgery.

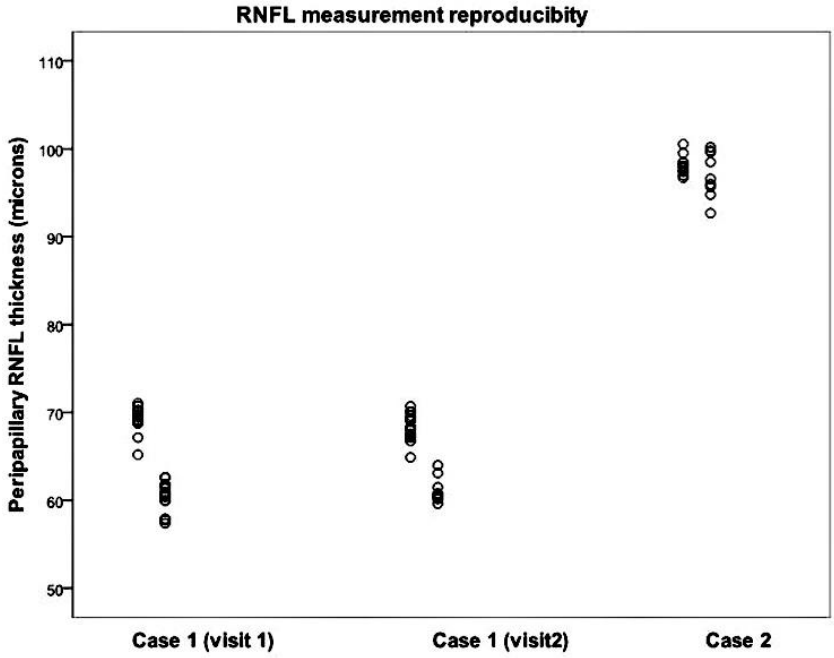

Figure 40 PJ's reproducibility of OCT measurement. Case 1 was measured on two occasions and case 2 was measured once. The RNFL thickness between the two visits was similar. The repeated measurements within one visit for the three groups showed a good reproducible result.

8.4 Statistical analysis

In the first part, multivariable linear regression analysis was performed to evaluate the relationship between the mean peripapillary RNFL thickness (in microns or μm) of both eyes and log elapsed time in years, with linear age in years as a covariate as it is known that the RNFL thickness declines with age. In the second part, univariable linear regression analysis was used to investigate the relationship between RNFL thickness (μm) and time elapsed in days after the onset of the stroke: this was carried out separately for each individual in each of the two groups, those with large and those with small visual field defects. A multi-level random effects analysis was used to estimate the overall slope for each group. The assumptions

underlying the univariable and multivariable regression analyses were checked by a study of the residuals and found to be satisfied. A Mann Whitney U test was used to compare the distribution of the slopes in the two groups of cases. A significance level of 0.05 was used throughout. IBM SPSS v 18.0 (www/spss.com) and Stata version 11 (StataCorp LP, www.Stata.com/product) were used to analyse the data.

8.5 Results

8.5.1 Cross sectional analysis

To investigate the effect of elapsed time since the injury on the thickness after adjusting for the age of the patient, a multivariable linear regression analysis was performed with linear age and log elapsed time as covariates. This showed that, after adjusting for the effect of age, elapsed time in log years had a significant effect on mean thickness with the mean thickness decreasing on average by -9.08 (95% CI -13.16 to -5) µm per log year ($p < 0.001$): chronological age also had a significant effect on mean thickness, after adjusting for elapsed time since the stroke, with mean RNFL thickness decreasing on average by -0.40 (95% CI -0.68 to -0.12) µm as the age increased by one year ($p = 0.006$) (Fig. 41; Table 10). For the control group, a linear regression was calculated with age as an independent factor and the RNFL thickness of both eyes as a dependent variable. The mean RNFL thickness declined by -0.11 µm (95% CI -0.2 to -0.45) as age increased by one year in the control group ($p = 0.5$) (Fig. 42). Our control group has an insufficient sample size to reach statistical significance but the trend is of a similar order to results obtained in other studies of the relationship between age and RNFL thickness which has been shown to decrease with age in healthy adults by -0.2 to -0.3 µm with each year of age (Barboni, et al., 2011; Budenz, et al., 2007).

Covariates	n	Slope (95% CI)	r	p value
Duration in log year	38	-9.0 (-13.2 to -5)	0.54	<0.001
Age in year	38	-0.4 (-0.7 to -0.1)	0.66	0.006

Table 10 Model summary of multivariable linear regression analysis on the RNFL thickness (µm) in homonymous hemianopia patients.

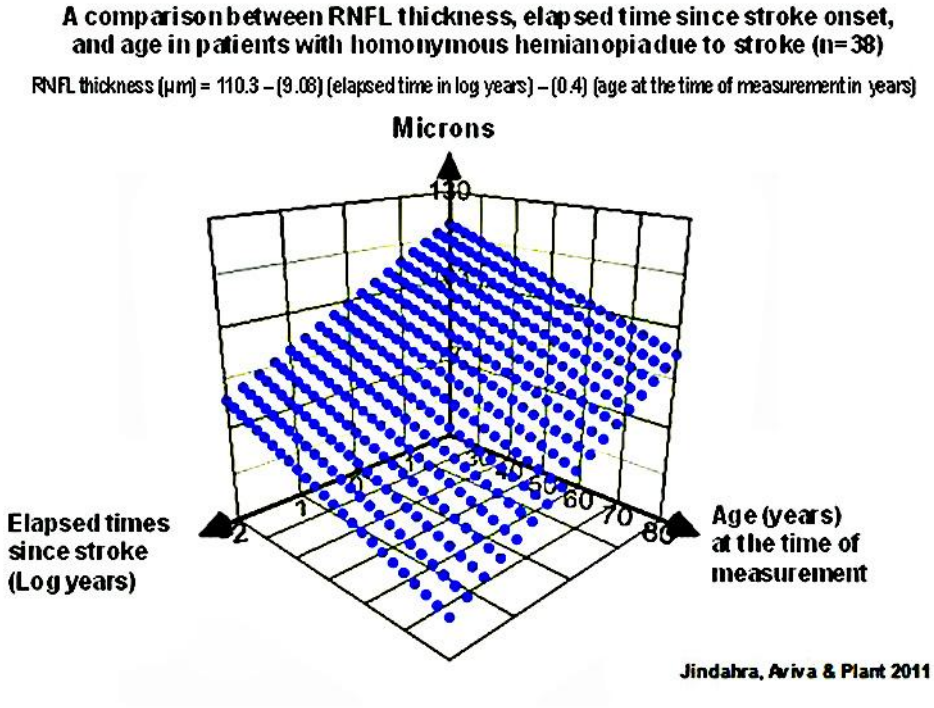

Figure 41 The 3-dimentional plot shows the negative linear relationships between RNFL thickness (µm; mean of both eyes; Z axis) and both elapsed time since the stroke (log years; X axis), and chronological age at the time the measurement was taken (years; Y axis) in homonymous hemianopia patients. There is a straight line relationship with the log of the number of years since the stroke and with a linear plot of chronological age. The relationship is described by: RNFL thickness (µm) = 110.3 – (9.08) (elapsed time in log years) – (0.4) (age at the time of measurement in years) (Equation 1).

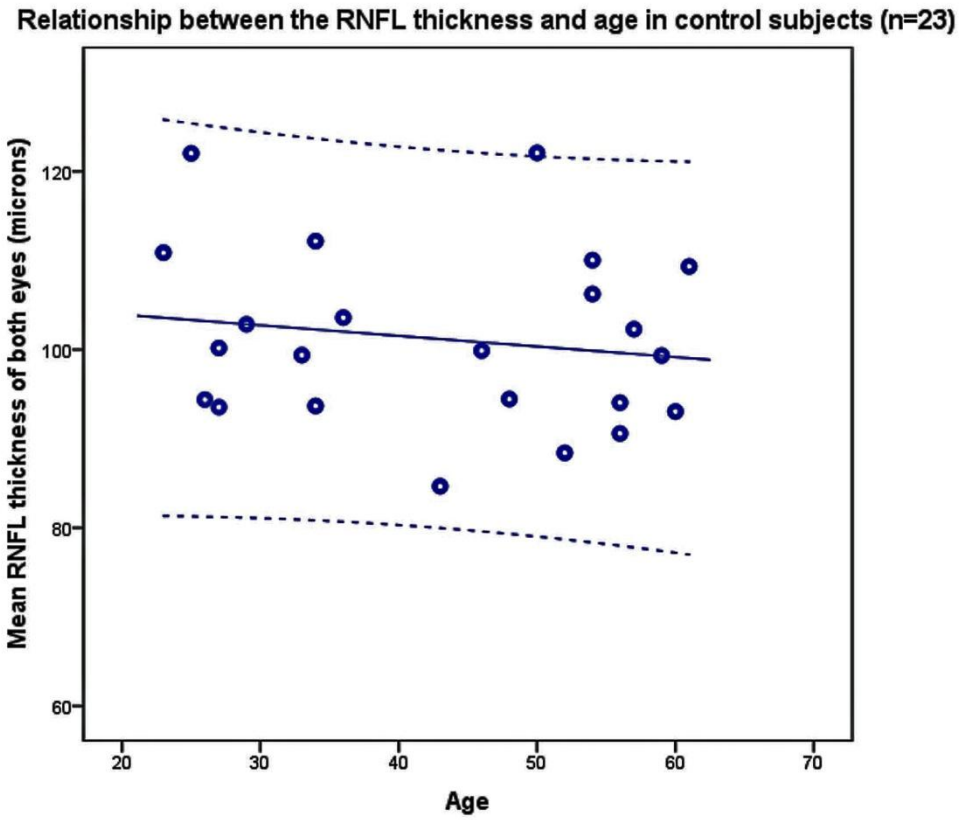

Figure 42 A relationship between the RNFL thickness of both eyes and age in normal subjects. The mean RNFL thickness declined by -0.11 µm (95% CI -0.2 to -0.45) as age increased by one year in the control group (p = 0.5). Blue line = mean of all data. Dash lines = 95% CI of each individual plot.

8.5.2 Longitudinal analysis

The total of 82 measurements for 11 patients have been analysed by using a univariable linear regression analysis for each patient, with mean RNFL thickness of both eyes (µm) as the outcome variable and elapsed time (days after stroke) as the explanatory variable. The results are shown for two groups, those with large visual field defects (Fig.43 & 44; Table 11) and those with small visual field defects (Fig. 45-47; Table 12). All hemianopia cases had a decreasing trend during the period of measurement (Fig. 44). All cases with larger visual field defects had a negative slope, although only 4 out of the 7 cases had slopes that were statistically significantly different from zero. In all 4 cases with significant regression coefficients the initial measurement was made within a month of stroke onset and none showed macular sparing. The third case who did not exhibit a significant linear relationship had macular sparing and an improving visual field. The attrition rate of the mean of

RNFL thickness from both eyes ranged from 0.9 to 6.3 μm for every 100 days in the first few years after stroke onset.

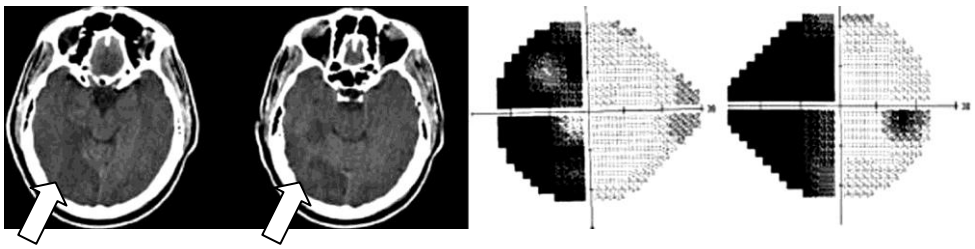

Figure 43 FRO: left homonymous hemianopia from the right occipital infarct.

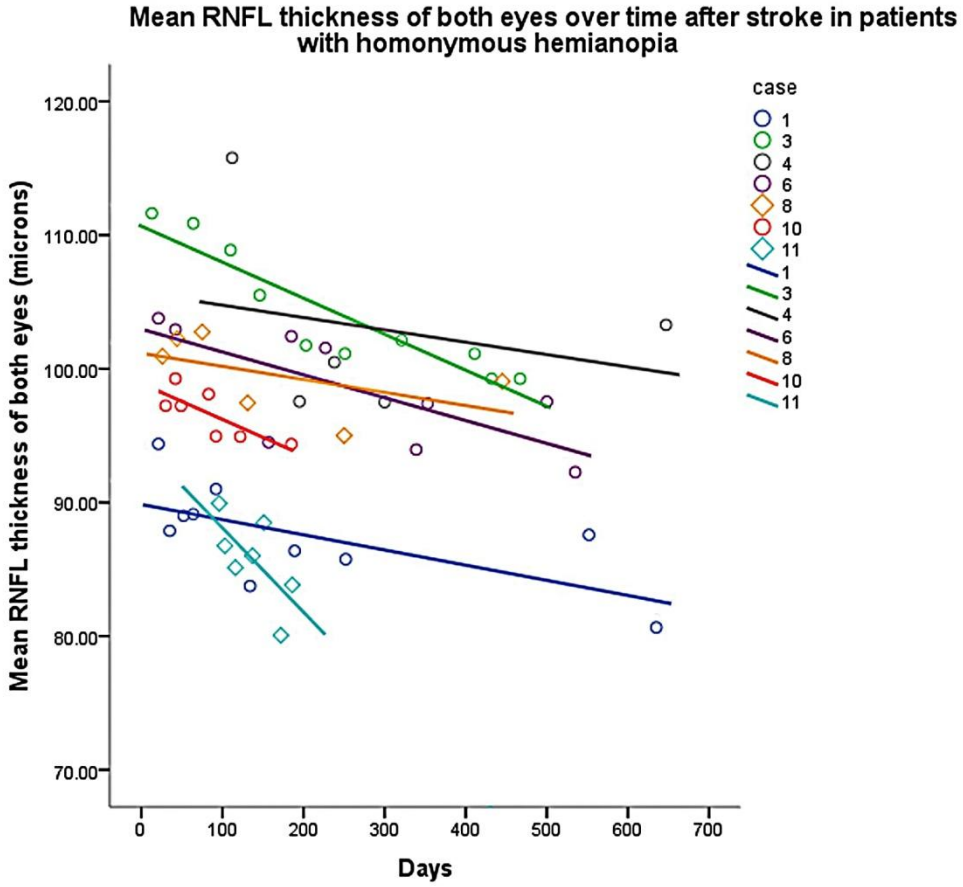

Figure 44 Relationships between the RNFL thickness and duration in each patient with homonymous hemianopia.

Case	r	p	Micron changes /100 days	95%CI of the changes /100 days	Number of visits	1st visit (days)	Macular sparing	Lesion	Followed up VF
1	0.7	0.04	-1.1	(-2.2 to-0.1)	10	21	no	occipital lobe	improved
3	0.9	<0.001	-2.7	(-3.6 to-1.7)	10	13	no	occipital lobe	stable
4	0.5	0.2	-0.9	(-2 to 0.4)	10	112	no	optic radiation	stable
6	0.7	0.03	-1.7	(-3.2 to-0.3)	9	21	no	occipital lobe	improved
8	0.5	0.3	-1	(-3.2 to 1.2)	6	26	yes	occipital lobe	improved
10	0.8	0.04	-2.7	(-5.1 to-0.2)	7	30	yes	occipital lobe	stable
11	0.7	0.1	-6.3	(-14.3 to 1.7)	7	96	no	occipital lobe	stable

Table 11 Table showed RNFL thickness and days after stroke onset in homonymous hemianopia group.

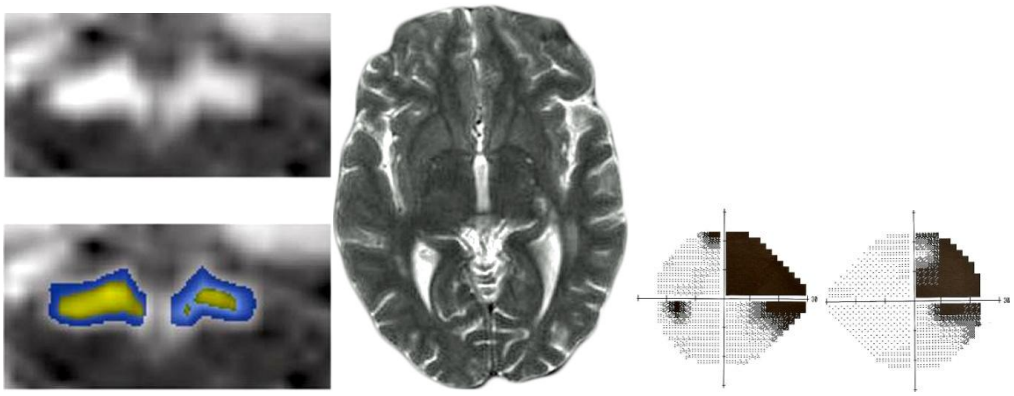

Figure 45 TRL: A case with right homonymous superior quadrantanopia from an infarct in the left LGN. A T2 weighted MRI scan on the axial section revealed hypersignal intensity over the left LGN. The two images on the top panel were her optic tract. The left optic tract was thinner than the right (Bridge, Jindahra, Barbur, & Plant, 2011). Reprinted MRI scans of the optic tracts from Invest Ophthalmol Vis Sci, vol 52, H Bridge, P Jindahra, J Barbur, & GT Plant, page 382-8, ©2011. Permission to reproduce the figures has been granted by Investigative ophthalmology and visual science.

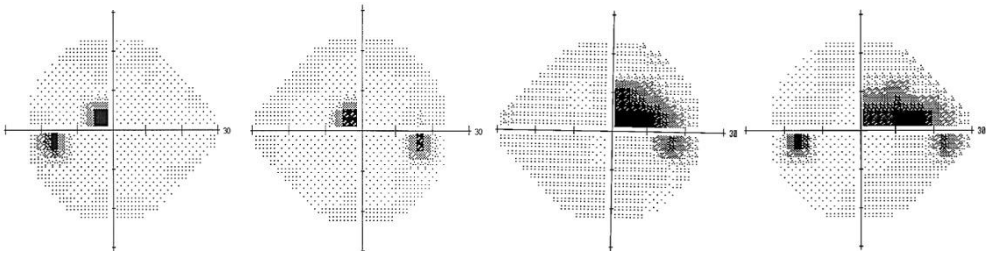

Figure 46 Humphrey perimetries. Two cases with left homonymous paracentral scotoma from right ligual infarct and with right homonymous superior quardrantanopia from left occipital infarct.

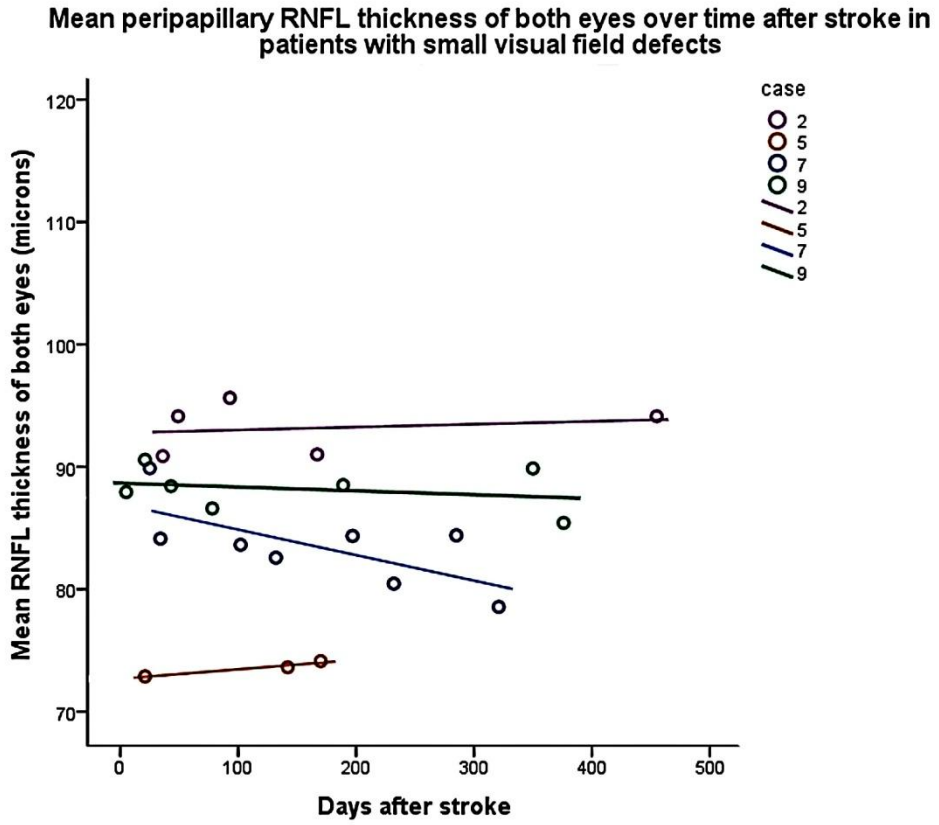

Figure 47 Relationships between the RNFL thickness and duration in patients with smaller field defects.

Case	r	p	Micron changes /100 days	95% CI of the changes /100 days	Number of visits	1st visit (days)	Lesion	Followed up VF
2	0.2	0.8	0.2	(-2 to 2.4)	5	36	lingual gyrus	stable
5	0.97	0.15	0.8	(-1.5 to 3.1)	3	21	occipital lobe	stable
7	0.7	0.06	-2.1	(-4.2 to 0.1)	8	25	LGN	stable
9	0.3	0.6	-0.3	(-1.6 to 0.9)	7	5	occipital lobe	improved

Table 12 Relationship between the mean of RNFL thickness of both eyes and duration after the stroke onset (days) in patients with smaller field defect.

None of the cases with small visual field defects exhibited a relationship between RNFL thickness and time elapsed that reached statistical significance with two cases having positive associations and two having negative associations. One case in this group did exhibit a greater rate of change than the other cases (-2.1 μm per 100 days). This case had a lesion involving the lateral geniculate nucleus (LGN) (Fig. 45) whereas the others had their lesions in the occipital lobe (Table 12) and it is impossible to exclude damage to the optic tract which would give rise to direct retrograde degeneration. However this was a trend which did not reach statistical significance.

A multi-level random effects linear regression analysis of RNFL thickness on elapsed time (days) estimated the mean slope as -0.012 (95% CI -0.016 to -0.008) for the homonymous hemianopia group and -0.004 (95% CI -0.126 to 0.003) for the small visual field defect group. The mean slope of the homonymous hemianopia group was significantly different from zero ($p < 0.001$) whereas the mean slope of the small visual field defect group was not significantly different from zero ($p = 0.2$). Furthermore, a Mann Whitney U test indicated that there was a significant difference of the slopes (μm per day post-stroke) between large and small post-geniculate lesions (p value = 0.016). The patient with LGN infarction was excluded in this last analysis.

8.5 Discussion

A negative linear relationship between the RNFL thickness and elapsed time since the stroke in log year was established in the cross-sectional study for patients with complete or near-complete homonymous hemianopia. Thinning of the retinal nerve fibre layer of all homonymous hemianopia cases can be seen to have developed in the first few months following injury to the post-geniculate visual pathway. The degeneration was progressive in the first few years, becoming relatively stable or evolving slowly in later years. An effect of age on the RNFL thickness is well established in the normal population, a multivariate linear regression was then performed for two factors, namely, elapsed time in log years and age at the time of measurement. An equation was derived from the relationship.

Mean RNFL thickness (μm) = 110.3 – (9.08) (elapsed time in log years) – (0.4) (age at the time of measurement) (Equation 1)

After adjusting for age, the RNFL change was 9.08 µm for each log year. For instance, the mean RNFL thickness of the two eyes would be 110.3 – (9.08) (1) – (0.4) (60) = 77.2 µm at the end of 10 years in a patient whose stroke occurred at age 50. After a further 10 years the mean RNFL thickness would be 110.3 - (9.08) (1.3) – (0.4) (70) = 70.5 µm. See Table 13 for further examples.

Elapsed time (log year)	Elapsed time (years)	Mean RNFL thickness of both eyes (µm)
-2.5	0.0027 (1 day)	113
-1	0.1 (36.5 days)	99.4
0	1	89.9
0.30103	2	86.8
0.47712	3	84.8
0.69897	5	81.9
1	10	77.2
1.3	20	70.5

Table 13 A prediction of the mean RNFL thickness of both eyes in a patient aged 50 with homonymous hemianopia acquired at time zero and a starting RNFL thickness of 113.9 µm at the onset of stroke.

It is notable that the baseline RNFL thickness is diverse in the normal population. There are confounding factors apart from age such as refractive error and ethnicity (Budenz, et al., 2007). However the equation gave an overall picture of the degeneration and showed in this example that the rate of RNFL thinning was strikingly high in the first few years after the stroke before becoming relatively slow (Fig. 48). The change in the second decade after the stroke was 0.67 µm per year which was slightly higher than the effect of increasing age alone.

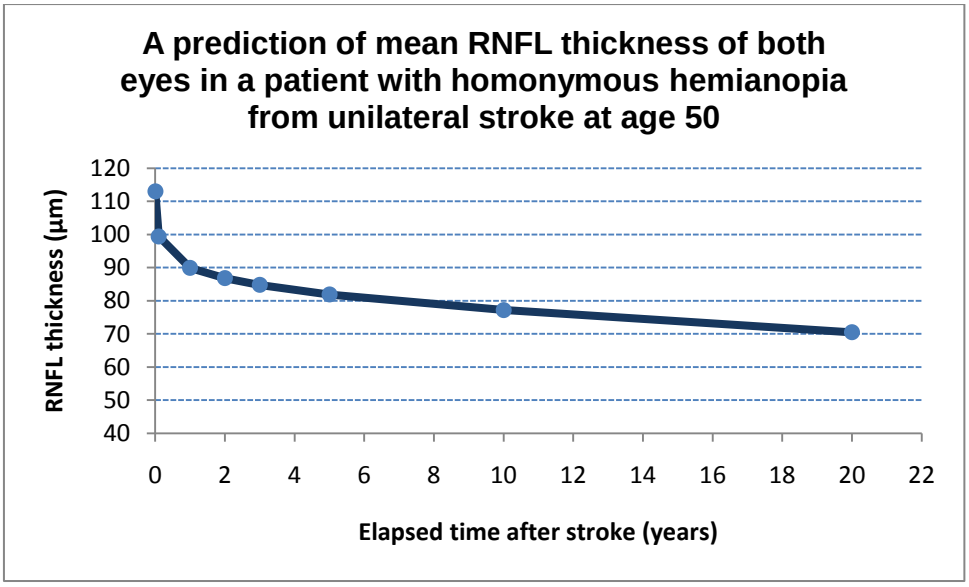

Figure 48 Diagram shows a prediction of mean RNFL thickness of both eyes in a patient with homonymous hemianopia from unilateral occipital stroke at age 50. The graph was derived from equation 1.

When measuring the RNFL on several occasions after the stroke over time in the longitudinal study, the rate of degeneration is seem to be high in the first 1-2 years. The findings were compatible with the results obtained in the cross-sectional study. The rate of degeneration for each homonymous hemianopia patient appeared linear with varying slope and the mean slope would indicate a loss of 4.4 µm in the first year which was ten times attrition rate resulting from ageing and within the confidence limits of equation 1. In the homonymous hemianopia group, most patients with smaller changes in the first few years after the stroke tended to have a better visual outcome. The rate of RTSD in our study had a trend that is more or less similar to results from adult old world monkeys (Fig. 49) and is comparable to findings from a patient with unilateral optic tract injury also (Fig. 50). Cowey et al recently demonstrated that the rate of RTSD developed robustly within the first few years after unilateral striatal decortication in macaque monkeys followed by a slight change from 3 to 14 years (Cowey, Alexander, & Stoerig, 2011).

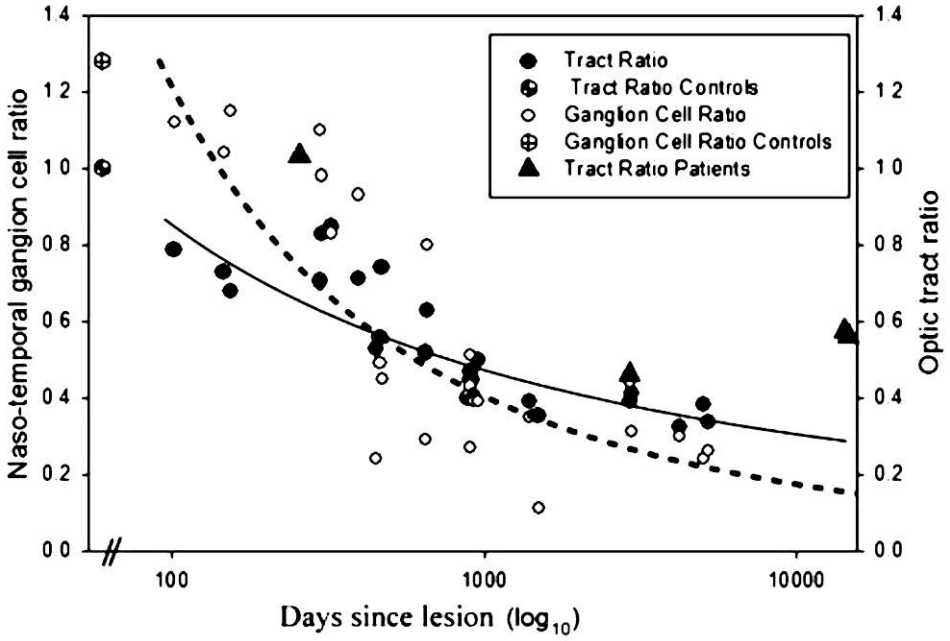

Figure 49 Diagram from a monkey study, the ratio of RGCs in the nasal (degenerated) and temporal (normal) hemiretinae of the eye contralateral to the lesion of striate cortex and the ratio of the cross-sectional area of the optic tract on the damaged and normal side were plotted against postoperative time (logarithmic scale shown in days). Reprinted from Brain, vol 134, A Cowey, I Alexander, & P Stoerig, Transneuronal retrograde degeneration of retinal ganglion cells and optic tract in hemianopic monkeys and humans, page 2149-57, ©2011. Permission to reproduce this figure has been granted by Oxford university press.

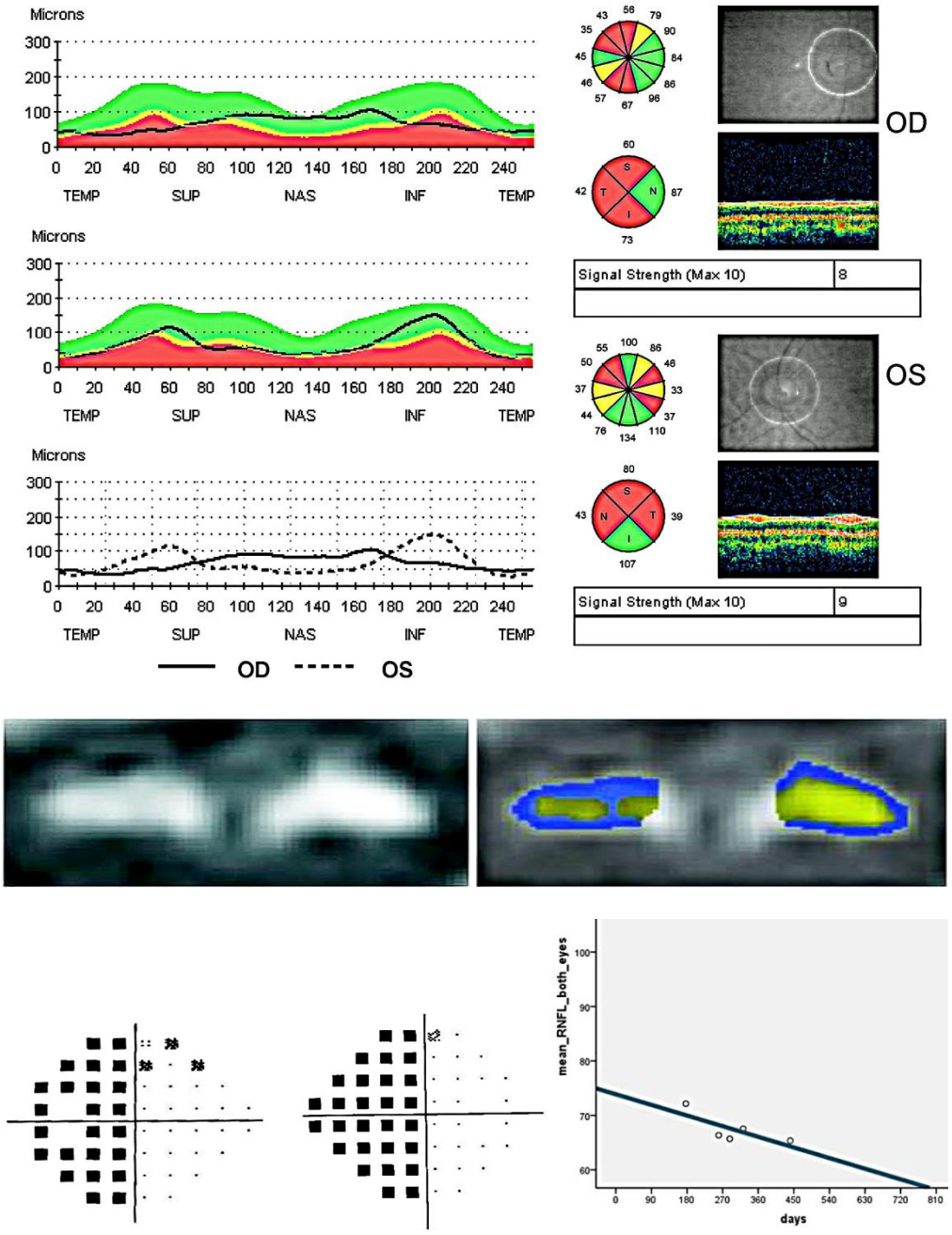

Figure 50 DAB: A 37-year-old male presented with left homonymous hemianopia from right optic tract injury following a car accident. Humphrey perimetry 24-2 and the peripapillary RNFL were demonstrated. A serial measurement of RNFL in the first two years after the injury was shown on the bottom right, a negative linear pattern with r=0.75, p= 0.1. MRI scans revealed slender right optic tract. Reprinted MRI scans of the optic tracts from Invest Ophthalmol Vis Sci, vol 52, H Bridge, P Jindahra, J Barbur, & GT Plant, page 382-8, ©2011. Permission to reproduce the figures has been granted by Investigative ophthalmology and visual science.

Patients with small field defects from the occipital lesions had stable results. The reason for the stable results in the small defect group was that the OCT might not be sensitive enough to detect a small change or alternatively there may be a protective mechanism from the healthy neurons subserving surviving regions of the visual field. It also indicates that the size of the lesion plays an important role in determining the magnitude of the RTSD. However the patient, who had a small field defect from a LGN lesion, showed the most RNFL regression among patients in the small defect group. The slope of the regression line was comparable to that in the HH group but did not reach the level of statistical significance. This implies that a strategic lesion can have an important influence on the RTSD outcome independently of the lesion size. A lesion in the LGN has large impact on RTSD.

To understand more about the time course of human RTSD, it is well worth to reviewing histological studies in a series of time in animals here. In a study performing unilateral occipital lobectomy in young adult squirrel monkeys (Wong-Riley, 1972), changes in the ipsilateral dLGN were very minimal in the first three days postoperatively and became more progressive afterwards whereas contralateral dLGN was normal throughout the course. In the early phase or around the fourth day after the operation, cortico-geniculate terminals in the dLGN started to degenerate. In the intermediate phase or during the fifth to tenth postoperative day, cortico-fugal endings changed: swelling, irregularity of the synaptic vesicles, electron dense disintegration, mitochondria disruption, and the engulfment of the glia cells. Some postsynaptic dendrites showed internal disintegrated structure but the synaptic morphology was still intact. The large neurons or retino-geniculate fibres in the dLGN began to degenerate retrogradely. The glia cells activities and numbers increased. In the late phase or after eleven days, the cortico-geniculate fibres in the ipsilateral dLGN gradually diminished in number. By 42 days postoperation, 90% of the cortico-geniculate fibres were lost and the relay cells in the dLGN disappeared. Many retino-geniculate fibres in the dLGN were undergoing retrograde degeneration, which was characterized by eccentric indented nuclei and densely packed mitochondria. There were significant synaptic reorganizations in the dLGN by day 42. The normal synaptic contacts, one axon terminal of the retinogeniculate fibres: ≥ 2 postsynaptic dendrites) became rare and new types of synapses were formed. Additionally non-synaptic junctions were developed

between the two retinogeniculate terminals and synapses between two postsynaptic dendrites were developed also. These synapses were not found in healthy subjects.

In a study on rhesus monkeys (Mihailović , Cupić, & Dekleva, 1971), the number of neurons in the ipsilateral dLGN reduced progressively over time. One week after unilateral radical occipital lobectomy, the number of neurons in the dLGN reduced by 80%. The survived cells had swollen nuclei that were shifted toward the periphery and surrounded by integrated granules. By the end of the third postoperative week, neurons became atrophied with large nuclei, thin cytoplasm, and occasional vacuoles and over 30% of neurons died. By 12 weeks, only a few neurons survived. By 25 weeks, the dLGN was deprived of neurones. The reactions of astrocyte, oligodendrocytes and microglia were observed. At 6 month postoperation, there was neither nerve cell nor their processes in the dLGN but normal number of astrocytes and double the number of oligodendrocytes and microglia. The dLGN on the contralateral side of the occipital lesion was intact.

A small population of dLGN projection neurons might have been spared in the degenerative processes by their collateral projections to the extrastriate cortex (Cowey & Stoerig, 1989; Yukie & Iwai, 1981).

In a rhesus monkey study, optic nerve fibres were evaluated at day 5, 14, 49, 79, and 180 days after unilateral striate cortex ablations (Horoupian, Ghetti, & Wiśniewski, 1973). The retinal ganglion cell terminals degenerated as early as 14 days after the operations (Horoupian, Ghetti, & Wiśniewski, 1973).

After a complete unilateral optic nerve transaction at the orbital apex in squirrel monkeys, retrograde and anterograde axonal degeneration was identified (Quigley, Davis, & Anderson, 1977). Regarding retrograde degeneration, RGCs appeared intact in the second week after the operation. The only abnormality found was focal aggregations of the intra-axonal organelles throughout the length of the fibres. In the third week post-operation, RGCs in the parafoveal region began to decrease in number and had abnormal appearances, namely, condensed nuclei, vacuolated cytoplasm, organelle accumulation, and myelin sheath disruption. By week 4 the RNFL loss was apparent on a clinical examination. The RGC degeneration was progressive until the 6^{th} week when only few ganglion cells or axons remained.

Retrograde degeneration in cats developed early in the first 2 to 3 weeks and independent of the distance of the lesion; the optic nerve, the optic tract, or the lateral geniculate nucleus (Lin & Ingram, 1973; Lin & Ingram, 1974). In human, the RNFL estimated by red free photographs began to disappear 4 weeks after a gunshot injury to the pre-chiasmatic optic nerve (Lundström & Frisén, 1975). In a human histology study, the retinal loss developed 5 weeks after unilateral optic tract transaction (Kupfer C. , 1963).

8.7 Conclusion

It is now well established that retrograde trans-synaptic degeneration occurs in the human visual system following damage to the occipital lobe. In this study the time course of the degeneration has been demonstrated using optical coherence tomographic measurements of the retinal nerve fibre layer thickness. In cases of homonymous hemianopia the thinning of the nerve fibre layer occurs at a rate that is maximal in the first few years following the occipital injury, and then slowing to a rate that is slightly higher than the rate that occurs as a result of ageing. This time course is similar to the pattern that has been demonstrated in primates following occipital lobectomy. In cases of smaller visual field defects no thinning of the retinal nerve fibre layer could be demonstrated except in a case in which damage to the optic tract (and therefore direct retrograde degeneration) is likely to have occurred. Whether the failure to detect thinning in such cases is due to lack of sensitivity of the technique or to a protective effect of the surviving regions of the visual field is not known.

9 Mechanisms of trans-synaptic degeneration

Retrograde trans-synaptic degeneration has been identified in the visual pathway and elsewhere in the central nervous system. Anterograde trans-synaptic degeneration was also clarified in the visual pathway in histological and imagings studies (Gupta, Ang, De Tilly, Bidaisee, & Yücel, 2006; Qing, Zhang, Wang, & Wang, 2010). A clinico-pathological study in a glaucoma patient showed significant changes in the optic tract, the dLGN, and the visual cortex (Gupta, Ang, De Tilly, Bidaisee, & Yücel, 2006). The changes respected the retinotopic organization. LGN atrophy could be demonstrated in glaucoma patients by studying a MRI brain (Gupta, Greenberg, De Tilly, Gray, Polemidiotis, & Yücel, 2009). The neuronal loss in the dLGN occurred in the magnocellular and parvocellular layers in experimental monkey models of glaucoma (Yücel, Zhang, Gupta, Kaufman, & Weinreb, 2000). Glaucomatous neuropathy from primary open angle glaucoma might lead to reduced cortical activity in the striate cortex, which corresponded to the visual field analysis (Qing, Zhang, Wang, & Wang, 2010). The anterograde trans-synaptic degeneration had also been studied in patients with early visual deprivation (Shu, Li, Li, Yu, & Jiang, 2009). By employing diffusion tensor imaging techniques, significant changes in the white matter of the geniculo-calcarine tract and its surrounding areas were detected (Shu, Li, Li, Yu, & Jiang, 2009).

A significant loss of neuronal synaptic target, dLGN degeneration in this instance, could account for retrograde or anterograde axonal degeneration. The synaptic targets are critical for neuron survival especially in early life (Cowan, Fawcett, O'Leary, & Stanfield, 1984; Weller, Kaas, & Wetzel, 1979). A sustaining neuron theory has been introduced (Dineen, Hendrickson, & Keating, 1982; Payne, Pearson, & Cornwell, 1984).

During CNS development, neuronal cells are over produced and a neurodegeneration process of cell death developed later at some stage between cell aggregration and maturation (Cowan, Fawcett, O'Leary, & Stanfield, 1984). The target fields determine the size of projecting neuronal population (Cowan, Fawcett, O'Leary, & Stanfield, 1984). When the entire projection field was ablated, the whole neuronal population disappeared (Cowan, Fawcett, O'Leary, & Stanfield, 1984). When the target field was partially removed, the amount of cell death rose among

the innervated neuronal population (Cowan, Fawcett, O'Leary, & Stanfield, 1984). When the target fields were extended, the amount of cell death declined (Cowan, Fawcett, O'Leary, & Stanfield, 1984). Interestingly ciliary ganglion in vitro were able to survive indefinitely in the presence of a proper medium and muscle cells on which they could form end plates (Cowan, Fawcett, O'Leary, & Stanfield, 1984) The trophic factor in this case was unknown (Cowan, Fawcett, O'Leary, & Stanfield, 1984).

What are the trophic factors that are critical for life? Why can the death of one nerve cell induce the death of its neighbour? Cell death happened inevitably without lack of blood supply or oxygen and the surrounding areas are still intact. There might be some kinds of energy transferring through the synaptic cleft from neuron to neuron and that energy must be essential for life. It might be a tentative source of energy separated from that created intracellularly.

Mitochondria are the essential energy generator of the cells and the synaptic function (Tong, 2007). Energy requirement around the synaptic cleft is high and there is evidence that mitochondria have been recruited to the nerve terminal near the synapse after nerve stimulations (Tong, 2007). The synaptic potentiation can be promoted or suppressed by manipulating the function of the mitochondria (Tong, 2007). The energy in the cell is produced by the mitochondria in the form of adenosine triphosphate or ATP, neucleotides. ATP consists of one molecular unit of adenosine coupled to a chain of 3 phosphate groups which were attached together with high energy chemical bonds. The amount of ATP in the brain is high, ranging from 2 to 4 mM in different areas (Verkhratsky & Krishtal, 2009). ATP is stored in synaptic vesicles together with or without other neurotransmitters and is released when nerve endings are depolarized (Cunha & Ribeiro, 2000). Since the cellular membrane is not permeable to ATP (Verkhratsky & Krishtal, 2009), it is released from nerves by specific mechanisms such as exocytotic vesicular mechanism (widespread throughout the CNS and PNS), voltage-dependent anion channels, connexin hemichannels, ATP-binding cassette transporters, and P2X7 receptors (Burnstock, 2006).

ATP acts as a neurotransmitter, co-transmitter and neuromodulator in the PNS and CNS on presynaptic and postsynaptic sites (Cunha & Ribeiro, 2000). P2 purinergic receptors act as ATP receptors and are demonstrated on presynaptic dendrites and

postsynaptic axons in animal central nervous systems (Fig. 51) (Loesch & Burnstock, 1998; Loesch, Miah, & Burnstock, 1999; Rubio & Soto, 2001)

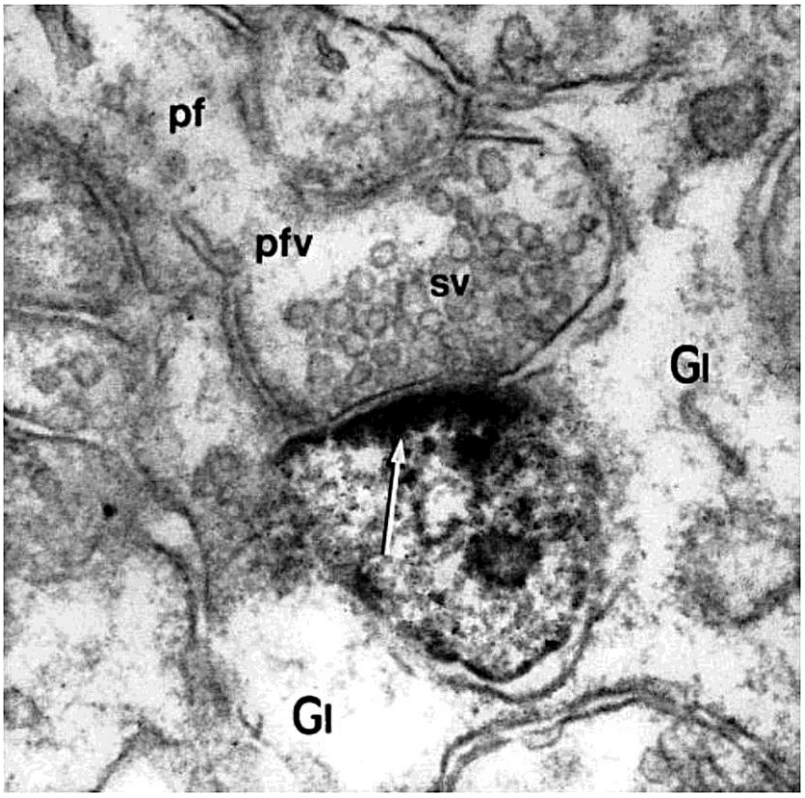

Figure 51 Diagram shows a molecular layer in rat cerebellum (Loesch & Burnstock, 1998). A P2X1 post-synaptic dendrite spine is displayed in white arrow. sv = spherical synaptic vesicles, pfv/pf = parallel fibre, Gl = neuroglia processes. Reprinted from Cell Tissue Res, vol 294, A Loesch & G Burnstock, Electron-immunocytochemical localization of P2X1 receptors in the rat cerebellum, page 253-60, ©1998. Permission to reproduce this figure has been granted by Springer.

P2 purinergic receptors are divided into P2X and P2Y classes (Burnstock & Kennedy, 1985). P2X receptors are trimeric ligand-gated ion channels and there are seven subtypes (P2X1-7) identified so far (Jarvis & Khakh, 2009; Khakh & North, 2006; Roberts, et al., 2006). All P2X receptor subtypes are permeable to sodium, potassium and calcium (Roberts, et al., 2006; Edwards & Gibb, ATP--a fast neurotransmitter., 1993) and mostly have inward current flows (Edwards & Gibb, 1993). Some subtypes are permeable to chloride (Roberts, et al., 2006). Influx of calcium through P2X receptors might occur in the absence of cell depolarization (Edwards & Gibb, 1993). Extracellular ATP enhances long-term potentiation (LTP) by increasing calcium influx into postsynaptic neurones via P2X receptor (Wang,

Haughey, Mattson, & Furukawa, 2004; Watano, Calvert, Vial, Forsythe, & Evans, 2004). Some P2X receptors undergo pore dilatation, allowing large molecules such as glutamate, NMDG, or ATP to pass through (Roberts, et al., 2006). P2X2 and P2X3 receptors are expressed in the retinal ganglion cells (Wheeler-Schilling, Marquordt, Kohler, Guenther, & Jabs, 2001). P2Y receptors are 7-transmembrane domain, G-protein-coupled receptors, and consist of eight subtypes. They are activated by purines ATP, ADP and pyrimidines (Abbracchio, et al., 2006). P2Y receptors at the presynaptic areas produce smaller LTPs than presynaptic P2X receptors (Wang, Haughey, Mattson, & Furukawa, 2004; Watano, Calvert, Vial, Forsythe, & Evans, 2004).

ATP was first identified by Holton as a neurotransmitter (Holton & Holton, 1953) and more specifically it acts as a fast excitatory neurotransmitter by activating postsynaptic P2-purinergic receptors at nerve-nerve synapses in the CNS and PNS (Evans, Derkach, & Surprenant, 1992; Edwards, Gibb, & Colquhoun, 1992; Burnstock, 2006). Evidence of neurotransmitter role of ATP in the CNS includes medial habenula (Edwards, Gibb, & Colquhoun, 1992), dorsal horn (Jo & Schlichter, 1999; Bardoni, Goldstein, Lee, Gu, & MacDermott , 1997), locus ceruleus (Nieber, Poelchen, & Illes, 1997), and CA1&3 pyramidal cells of the hippocampus (Pankratov, Castro, Miras-Portugal, & Krishtal, 1998; Wieraszko, Goldsmith, & Seyfried, 1989).

Postsynaptic neurons release ATP to elicit depolarization (Abood, Koketsu, & Miyamoto, 1962; Meunier, Israël, & Lesbats, 1975; Boyd & Forrester, 1968). ATP in the neuromuscular junction might be derived from depolarized muscle fibres and serves as a retrograde synaptic messenger as ATP release could be inhibited by alpha-bungarotoxin which is a selective postsynaptic nicotic acetylcholine receptor antagonist (Israël, Lesbats, Manaranche, Meunier, & Frachon, 1980; Santos, Salgado, & Cunha, 2003). Both ATP and its metabolite, adenosine, suppress the release of acetylcholine at the neuromuscular junction and are reabsorbed by muscle cells, becoming another valuable source of energy (Israël, Lesbats, Manaranche, Meunier, & Frachon, 1980). Although P2 receptors have been identified on the presynaptic areas in the CNS, the evidence of ATP action on the presynaptic sites in the CNS is slight.

ATP is a co-transmitter in sympathetic, parasympathetic, sensory, and non-adrenergic non-cholinergic nerves (Burnstock & Wood, 1996). ATP joins the

signaling with most neurotransmitters such as glutamate, acetylcholine, GABA, noradrenaline, and serotonin. These neurotransmitters have pre- and post-synaptic receptors (Starke, Göthert, & Kilbinger, 1989).

ATP acts as a transmitter between pre-, post-synaptic neurons and glia cells or tripatite synapses (Fig.52) (Halassa, Fellin, & Haydon, 2007; Burnstock, 2006). Astrocytes express P2X and P2Y receptors (Neary & Zimmermann, 2009). Outcomes of ATP trophic effects on astrocytes include proliferation, stellation, migration, and apoptosis (Neary & Zimmermann, 2009).

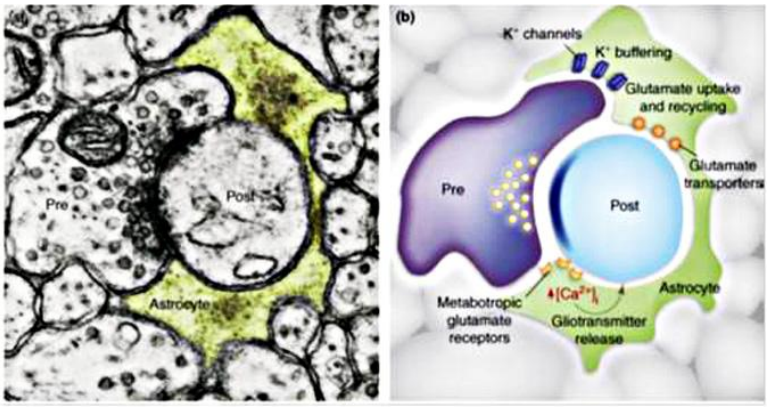

Figure 52 Tripartite synapse. (a) Electron micrograph showing a presynaptic terminal (Pre) and postsynaptic dendrite (Post) enwrapped by the astrocytic process (green) forming the tripartite synapse. (b) The astrocytic process, the presynaptic and postsynaptic terminals cleared potassium ions that accumulated following neuronal activity, and are involved in the glutamate uptake. Reprinted from Trends Mol Med, vol 13, MM Halassa, T Fellin, & PG Haydon, The tripartite synapse: roles for gliotransmission in health and disease, page 54-63, ©2007. Permission to reproduce this figure has been granted by Elsevier.

ATP controlled resting membrane potential (Abood, Koketsu, & Miyamoto, 1962; Abood, Koketsu, & Noda, 1961). With the use of P32 as a tracer, Abood et al (Abood, Koketsu, & Miyamoto, 1962) detected outflux of various phosphates such as ATP from muscle and spinal root of the frog as a consequence of electrical stimulation and exposure to calcium-free or potassium-rich media. In this study the electrical stimulation was performed through electrodes dipped in the solution containing the muscles. In the case of nerve fibres, the nerve roots were isolated together with the sciatic nerve, and stimulating and recording electrodes were positioned on the sciatic nerve. The outflux of P32 was measured in the solution

containing muscle and nerve roots. Hence this study measured phosphate release from postsynaptic muscle and presynaptic nerve root. The rise in P32 outflux was correlated to the external potassium concentration and membrane depolarization even there was no muscle contraction. It was noteworthy that phosphates diffused out from muscle and presynaptic nerve with or without membrane depolarization. Extracellular ATP and other phosphates were very much greater than those in the nerves or muscles after depolarization. This indicated that the loss of phosphates from pre and post synaptic terminals was high at one moment in time after depolarization. When adding 2,3 dinitrophenol (DNP), phosphorylation inhibitor, the resting membrane and intracellular potassium of the muscle and nerve declined without any alteration of action potential (Abood, Koketsu, & Noda, 1961). Abood proposed that ATP might be crucial for the maintenance of resting membrane potential. Without ATP, Na-K-ATPase pump cannot function, leading to sodium entry, cell swelling and destruction subsequently. Perhaps ATP, that passes from extracellular to intracellular spaces in the synaptic cleft without creating any action potentials, play an important part in stabilizing resting membrane potential and hence the survival of the neurons.

ATP is broken down in the extracellular spaces by ATPases and 5-nucleotidase to adenosine. Adenosine acts on P1 purinoreceptor and is taken up by varicosities presynaptically. Adenosine in the synaptic area is also broken down by adenosine deaminase to inosine which is removed by the circulation (Burnstock, 2006; Burnstock, 2009). Adenosine is a nucleoside, consisting of sugar ribose and purine base (adenine) (Polosa & Zeng, 2006). The metabolite of adenosine is inosine which is formed by adenosine deaminase (Pearson, et al., 2003). ATP is degraded to adenosine rapidly in less than one second (Dunwiddie, Diao, & Proctor, 1997; Harden & Lazarowski, 1999), with a half-life of 200 msecs (Dunwiddie, Diao, & Proctor, 1997). Extracellular cAMP converts to adenosine as well but in a slower rate (Dunwiddie, Diao, & Proctor, 1997). Adenosine is present in every cell and is released from all cells including neurons and glial cells (Ribeiro, Sebastião, & de Mendonça, 2002). A study on nucleoside map including adenosine of the human CNS revealed an uneven distribution throughout the brain, with the greatest concentrations in the cerebral cortex and basal ganglion, and the lowest in the locus ceruleus, the zona incerta, the substantia nigra, and the inferior colliculus (Kovács,

Dobolyi, Juhász, & Kékesi, 2010). Unlike ATP, adenosine is not stored in synaptic vesicles and does not act as a neurotransmitter. Extracellular adenosine originates from dephosphorylation of the extracellular adenine nucleotides and adenosine efflux via nucleoside transporters (Ribeiro, Sebastião, & de Mendonça, 2002; Gu, Foga, Parkinson, & Geiger, 1995; Dunwiddie, Diao, & Proctor, 1997). The nucleoside transporters are passive and do not depend on ATP or ion gradients (Masino & Dunwiddie, 1999). In the CNS adenosine can pass through the nucleoside transporters in bidirection depending on its concentration gradient across the cellular membrane (Gu, Foga, Parkinson, & Geiger, 1995; Dunwiddie & Masino, 2001). Normally intracellular adenosine level is relatively low and hence inducing adenosine influx to the cell or reuptake through the transporters (Dunwiddie & Masino, 2001). When intracellular adenosine increases, adenosine moves out from the cells through the transporters. Additionally, there is an active transport of adenosine using sodium gradient but its mechanism remains unclear (Dunwiddie & Masino, 2001). The increase of extracellular adenosine and its uptake and metabolism is in equilibrium that the basal concentrations of adenosine in the synaptic cleft ranges widely from 25 to 250 nm (Dunwiddie & Masino, 2001). A1 receptor modulates extracellular adenosine level as its inhibition lead to a rise in adenosine in the extracellular space (Andresen, Gillespie, Mi, Dubey, & Jackson, 1999). Intracellular adenosine is phosphorylated and transformed back to adenine nucleotide (Pearson, et al., 2003)(Fig 53). Adenosine receptors are seven transmembrane protein and G-protein-coupled receptors (A1, A2A, A2B, and A3) (Dunwiddie & Masino, 2001). Adenosine is a neuromodulator that modulates neuronal communications via pre- and post-synaptic transmissions (Ribeiro, Sebastião, & de Mendonça, 2002). Adenosine can exert inhibitory influences through A1 receptor pre-synaptically and post-synaptically in the same synapse by suppressing the release of glutamate and controlling gamma-aminobutyric acid (GABA) function (Dunwiddie & Masino, 2001). A2A receptor facilitates the release of GABA from hippocampal nerve terminals by activating adenylate cyclase/cAMP protein kinase A pathway and protein kinase C (Cunha & Ribeiro, 2000).

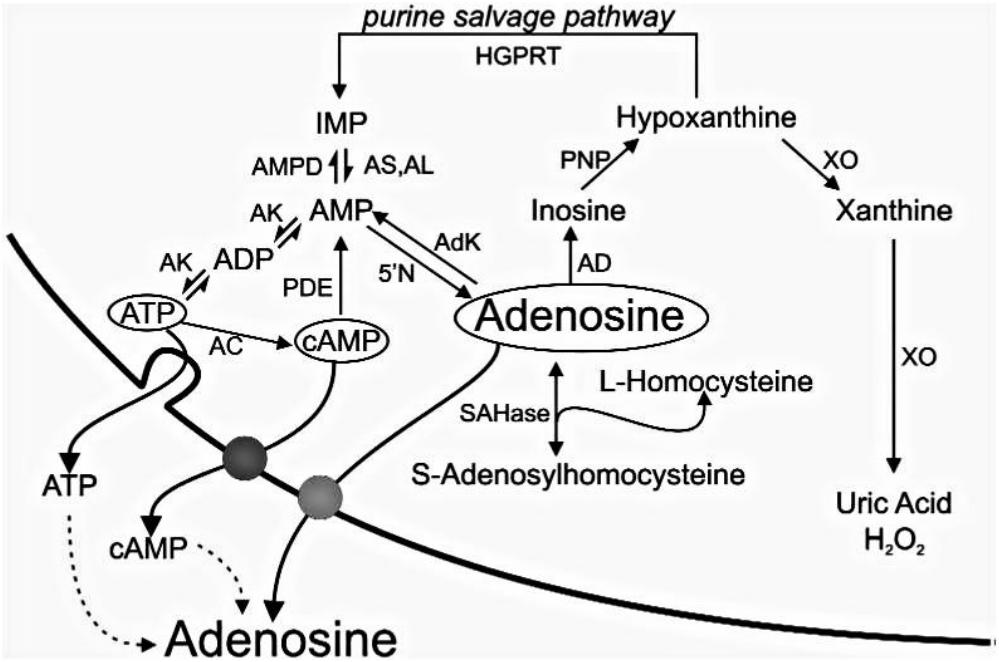

Figure 53 Diagram representation production, metabolism, and release of adenosine and ATP. Abbreviations: 5'N = cytosolic 5'-nucleotidase, AC = adenylate cyclase, AD = adenosine deaminase, AdK = adenylate kinase, ADK = adenosine kinase, AL = adenylosuccinate lyase, AS = adenylosuccinate synthase, e5'N = ecto 5'-nucleotidase, eAP = ectoalkalinephosphatase, ePD = ecto-phosphodiesterase, HGPRT = hypoxanthine phospho-ribosyl-transferase, NP = nucleoside phosphorylase, NPP = nucleotide pyrophosphatase/phosphodiesterase, NTPD = nucleoside triphosphate diphosphohydrolase, SAHase = S-adenosyl-Lhomocysteine hydrolase, XO = xanthine oxidase. Reprinted from J Cell Mol Med, vol 7, T Pearson et al, Plasticity of purine release during cerebral ischemia: clinical implications?, page 362-75, ©2003. Permission to reproduce this figure has been granted by John Wiley and Sons.

In summary, these studies demonstrated the overall traffic of adenine nucleotides and adenosine through the neuronal synapses in both directions. Extracellular ATP and its metabolites are possibly another source of energy supply to pre- and post-synaptic neurons especially in the high energy consumption area like synaptic cleft. Extracellular ATP and its metabolites are reabsorbed by pre- and post- synaptic neurons and are reused intracellularly. It has been shown that intracellular organic phosphates depleted significantly after their release and depolarization of the cells. Without the reuptake process, intracellular phosphate concentration would be constantly low, leading to unstable resting membrane potential. An absence of

either pre- or post-synaptic neurons limits the number of extracellular ATP and adenosine so there is not sufficient ATP for intracellular metabolism.

Furthermore, ATP and its metabolites play an important role in type I and II programmed cell death. Type I apoptotic cell death is characterized by DNA degradation, chromosome condensation, cell shrinkage and caspase activation (Gozuacik & Kimchi, 2004; Tait & Green, 2010). There are 2 main pathways namely, intrinsic and extrinsic pathways which converge on executioner caspases 3 and 7 (Tait & Green, 2010). In the intrinsic pathway, stimuli such as DNA damage or endoplasmic reticulum stress facilitate mitochondria outer membrane permeabilization (Tait & Green, 2010). As a consequence, mitochondria release cytochrome c, which then bind to apoptotic protease-activating factor 1 (APAF1) to form an apoptosome (Tait & Green, 2010; Miller, 2009). The apoptosome activates caspase enzymes to cleave both nuclear and cytoskeletal proteins (Tait & Green, 2010; Miller, 2009). Physiologic level of ATP suppresses apoptosis by preventing cytochrome c and APAF1 binding (Tait & Green, 2010).

Type II programmed cell death or autophagy proceeds by multiple membrane cytoplasmic vesicles that engulf proteins, organelles and cytoplasms and the vesicles are later destroyed by lysosomes (Gozuacik & Kimchi, 2004). It is not involved in caspase signalling (Gozuacik & Kimchi, 2004). Autophagy is ATP dependent (Gozuacik & Kimchi, 2004) and is inhibited by Mammalian target of rapamycin complex I (mTORC1) when there are sufficient nutrients (amino acids), growth factors such as insulin, and energy (Zoncu, Efeyan, & Sabatini, 2011). MTORC1 plays an important role in cell growth, proliferation and consumes high energy along its pathway (Fig. 54) (Zoncu, Efeyan, & Sabatini, 2011). During stress such as hypoxia, mitochondria dysfunction, and starvation, low ATP triggers energy signal AMP-activated kinase, which leads to mTORC1 suppression and autophagy upregulation subsequently. Autophagy of mitochondria provides energy supply to cells. It has been shown in animals that if autophagy could not overcome the energy deficiency, they would die (Zoncu, Efeyan, & Sabatini, 2011). There is evidence that mTOR signal enhancement promotes benign tumour formation in several organs (Nie, et al., 2010; Steck, et al., 1997). The activity of mTOR is much greater in embryonic mouse neurons than that in adult neurons (Park, et al., 2008).

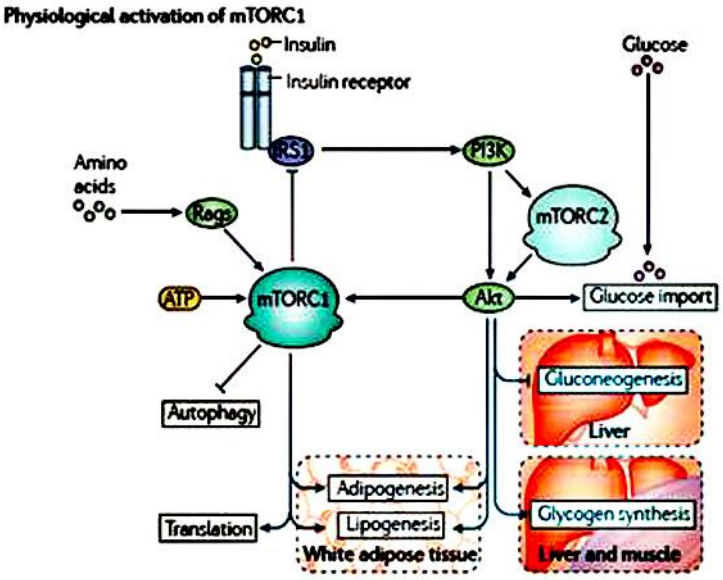

Figure 54 mTOR regulation. Reprinted by permission from Macmillian Publishers Ltd: Nature Reviews Molecular Cell Biology, vol 12, R Zoncu, A Efeyan, & DM Sabatini, mTOR: from growth signal integration to cancer, diabetes and ageing, page 21-35, ©2011. www.nature.com/nrm/

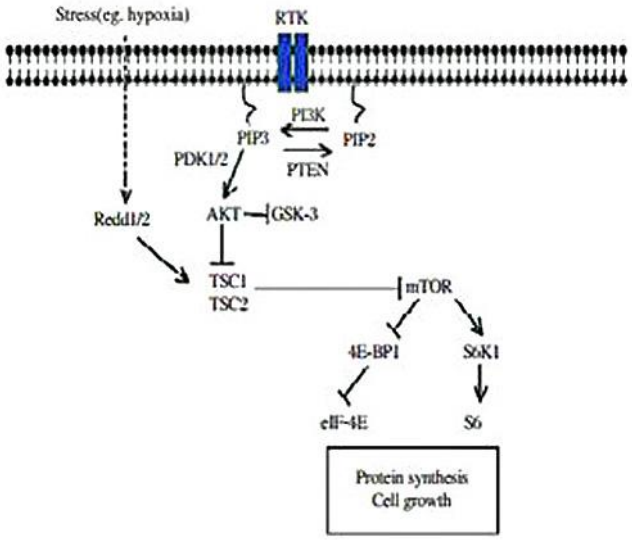

Figure 55 PTEN/ mTOR pathway (He, 2010). Receptor tyrosine kinase activates PI3K, which phosphorylates PIP2 to PIP3. PIP3 recruits PIDK1/2, which activates AKT. PTEN converts PIP3 to PIP2. AKT inhibits TSC1 and 2, which inhibits mTOR subsequently. Inactivation PTEN results in activation of AKT and mTOR respectively. mTOR controls protein translation, cell growth and other processes. The ribosomal protein S6 kinase (RP-S6) and the eukaryotic initiation factor 4E (eIF-4E) binding

protein 1 (4E-BP1) are the effectors of mTOR. Reprinted from J Biomed Res, 24, Z He, Intrinsic control of axon regeneration, page 2-5, ©2010. Permission to reproduce this figure has been granted by Elsevier.

PTEN (phosphate and tensin homolog) is a negative regulator of mTOR pathway as shown in Fig. 55. It converts phosphatidylinositol (3,4,5) trisphosphate (PIP3) to phosphatidylinositol (4,5) bisphosphate (PIP2) and antagonizes the effects of PI3K (He, 2010). PTEN/mTOR pathway is exhibited in adult neurons and is a key determinant of the intrinsic axon growth in adult CNS neurons (He, 2010). Inactivation of PTEN enhances mTOR activity (He, 2010). An experiment using optic nerve crush model in adult mice revealed that axotomy of the retinal ganglion cells induced a rapid down regulation of mTOR in all neurons (Park, et al., 2008). Deleted PTEN in axotomized retinal ganglion cells promoted cell survival and axonal regeneration soon after optic nerve injury (Park, et al., 2008). TSC, mTOR, and ephrin-Eph receptor system regulate axon guidance in the visual pathways (Nie, et al., 2010).

Binding of extracellular ATP to P2 purinergic receptors promote cell survival by mediating several enzymatic cascades through changes in intracellular calcium, cyclic AMP, and protein kinase C (PKC) concentrations, Akt, GSK-3beta, and mitogen activated extracellular signal regulating protein kinase (ERK), c-Jun –terminal kinases (JNK), and p38. ERK and Akt promote cell proliferation by activating mTOR whereas JNK and p38 promote growth arrest and apoptosis (Neary & Zimmermann, 2009) (Fig. 56). A study on pheochromocytoma cells and dorsal root ganglion neurons revealed that extracellular nucleotides such as ATP and UTP, signaling through P2Y2 receptors, modulate neuronal apoptosis. (Arthur, Georgi, Akassoglou, & Insel, 2006). Arthur et al have hypothesized that the release of nucleotides from glia, neurons, or perhaps other cell types such as vascular elements may serve as autocrine–paracrine sources of extracellular nucleotides that promote survival, either acting alone or through potentiation of neurotrophin signalling (Arthur, Georgi, Akassoglou, & Insel, 2006). Extracellular ATP serves as a neurotrophic factor on axonal growth in the CNS development via P2 receptors (Heine, Heimrich, Vogt, Wegner, Illes, & Franke, 2006). In a study using entorhinal-hippocampus slice co-culture model, P2 receptor (P2X1, P2X2, P2X4, P2Y1, and P2Y2) activation promoted nerve fibre growth which could be abolished by its antagonist (Heine, Heimrich, Vogt, Wegner, Illes, & Franke,

2006). In the presence of nerve growth factor, ATP and other P2 receptor agonists increased neuronal growth robustly while, in the absence of nerve growth factor, they promoted the neuronal regeneration (D'Ambrosi, Cavaliere, Merlo, Milazzo, Mercanti, & Volonté, 2000; D'Ambrosi, et al., 2001).

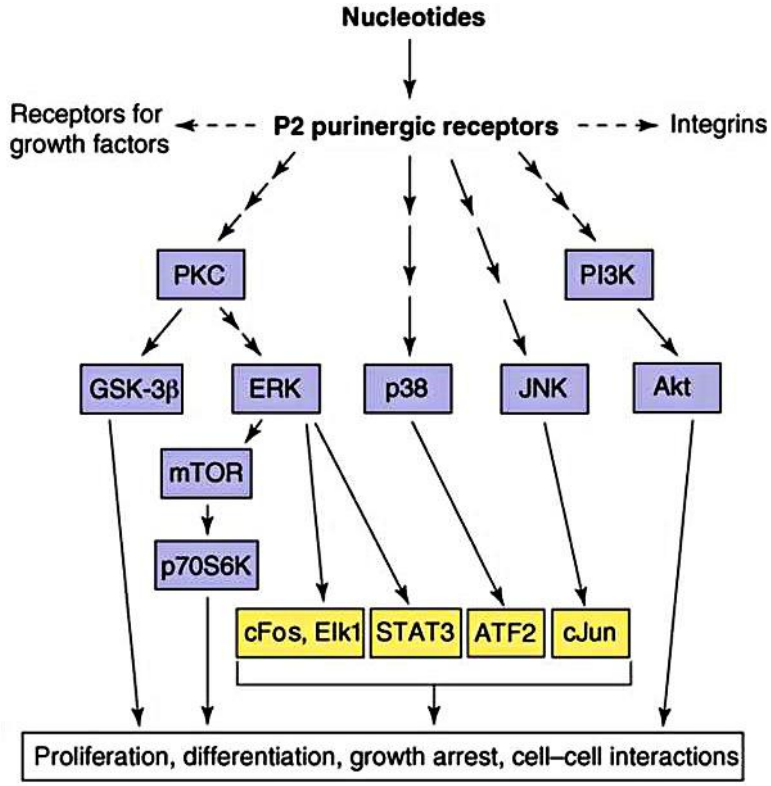

Figure 56 P2 purinergic receptor and protein kinase signalling pathway in astrocytes. Binding of extracellular nucleotides to P2 receptor led to MARK, AKt, and GSK-3beta stimulation and induced growth factor receptor pathway. Abbreviations: ATF = activating transcription factor; ERK = extracellular signal regulated protein kinase; GSK = glycogen synthase kinase; mTOR = mammalian target of rapamycin; PI3K = phosphoinositide 3-kinase; PKC = protein kinase C; JNK = c Jun N-terminal kinase; STAT = signal transducer and activator of transcription. Reprinted from Trends Neurosci, vol 32, JT Neary & H Zimmermann, Trophic functions of nucleotides in the central nervous system, page 189-98, ©2009. Permission to reproduce this figure has been granted by Elsevier.

Binding of adenosine to A2A receptors inhibit apoptosis by transactivating Trk receptor in the absence of neurotrophic factors (Lee, Rajagopal, & Chao, 2002; Lee & Chao, 2001; Wakade, Przywara, & Wakade, 2001) and by blocking glutamate-induced excitotoxicity (Ferreira & Paes-de-Carvalho, 2001). Stimulating A2A

receptor facilitates synaptic activity of brain derived neurotrophic factor (BNDF) (Sebastião & Ribeiro, 2009). BNDF is a neurotrophin, binding specifically to TrkB receptors (Sebastião & Ribeiro, 2009). Endogenous adenosine released during acute hypoxia and ischemia exerts a neuroprotective effect on neural tissues via A1 receptor activation (Dunwiddie & Masino, 2001). CNS excitatory synaptic transmission declines under hypoxic condition (Latini, Bordoni, Corradetti, Pepeu, & Pedata, 1998) or high temperature as a result of raised extracellular adenosine (Masino, Latini, Bordoni, Pedata, & Dunwiddie, 2001).

ATP at low concentration promotes proliferation; nonetheless ATP at high concentrations induces apoptosis (Coutinho-Silva, et al., 2005). In stress situations like spinal cord injury or cerebral ischemia, ATP is excessively released and P2X7 receptors are upregulated, causing an irreversible rise in cytosolic calcium and cell death eventually (Wang, et al., 2004; Franke, et al., 2004; Di Virgilio, et al., 1998). Other members of P2X receptor family (P2X1, P2X2, P2X3, P2X4, and P2X5) have a minimal role in ATP-induced apoptosis in a spinal cord model (Wang, et al., 2004). P2Y1 receptor activation is not associated with significant injury (Wang, et al., 2004).

Elegant studies in this review demonstrated that extracellular ATP and adenosine suppress programmed cell death by directly activating P2Y receptors or controlling several intracellular reactions such as apoptosome suppression and mTOR enhancement. We propose that trans-synaptic anterograde/retrograde degeneration might be a consequence of programmed cell death triggered by insufficient extracellular adenine nucleotides and their metabolites. Additionally, the dLGN or the synaptic site acts like an energy station, conveying energy or energy-carrier from neurons to neurons. It would be beneficial to create a synapse in regenerating nerve models. The hypothesis can explain the sustaining collateral hypothesis well.

As presented previously, P cells are more vulnerable to retrograde trans-synaptic degeneration than other retinal ganglion cell types. The sustaining collaterals theory has been proposed to explain the processes (Weller & Kaas, 1989). P cells project to the parvocellular layer of the dLGN and have no collateral branches to other areas. M cells project not only to the magnocellular layer of the dLGN but also the superior colliculus. Gamma cells mainly project to the superior colliculus. When neurons in the dLGN die as a consequence of cortical injury, P cells receive insufficient trophic

substances from their synaptic targets anymore and could not maintain life. In contrast to M cells which still receive trophic substances from their sustaining collaterals enough to survive. The trophic substances in this theory are most likely to be ATP and its metabolite.

The hypothesis can be account for the survival of all retinal ganglion cells after decortication in rabbits (Wilkes, Zingaro, & Murphy, 1985) and rats (Perry & Cowey, 1979a) for all or nearly all retinal ganglion fibres travelling to the dLGN give their branches to the superior colliculus in these animals (Linden & Perry, 1983; Vaney, Peichl, Wässle, & Illing, 1981). Another study using tectal transaction model in rats showed that the retinal ganglion cells were lost in infant (0-3 days) with aberrant reinnervations but did not significantly degenerate in older rats (30 days) because they were old enough to form sufficient collaterals (Perry & Cowey, 1982). Moreover the developmental period in higher primates is relatively slow and their developing neurons that highly depend on the synaptic targets still maintained to some degree in adulthood in macaques and humans (Weller & Kaas, 1989). The different RTSD found in different species could be a consequence of different developmental rate among species.

10 Pupillometry in homonymous hemianopia patients

10.1 Introduction

We have shown previously the RGC loss in retrograde trans-synaptic degeneration. It is still unknown whether pupillomotor RGCs would be involved in the process.

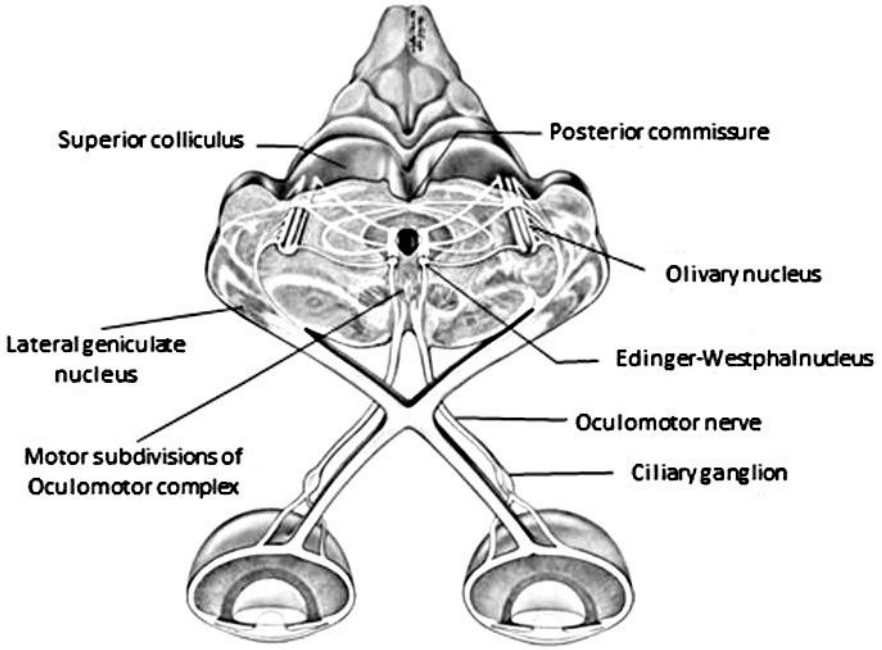

Figure 57 Pupil pathway (Kourouyan & Horton, 1997). Reprinted from J Comp Neurol, vol 381, HD Kourouyan & JC Horton, Transneuronal retinal input to the primate Edinger- Westphal nucleus, page 68-80, ©1997. Permission to reproduce this figure has been granted by John Wiley and Sons.

Afferent pupillary fibres (Fig. 57) run along from the optic nerve, the optic chiasm, the optic tract, and the brachium of superior colliculus (SC), then make a synapse at the pretectal olivary nuclei which project fibres to bilateral Edinger-Westphal nucleus (EW). Some fibres from the brachium of SC cross to the opposite side at the posterior commissure. Note that the brachium of SC is located on another plane and not shown in Fig. 57. Efferent pupillary fibres (parasympathetic system) originate from EW to join oculomotor nerve (CN III) and follow the course on the dorsomedial surface of the nerve. They pass the cavernous sinus and then follow the inferior oblique branch of the CN III to enter the orbit. The fibres then make a synapse at the ciliary ganglion. The postganglionic fibres from the ciliary ganglion

form short ciliary nerves that innervate the pupilloconstrictor muscle. They enter the eye via short ciliary nerve and terminate at the choroid, iris, and ciliary body. An activation of the parasympathetic pathway produces pupil constriction. (Loewenfeld, 1999; Barbur, 2004). Another type of efferent pupillary fibre is sympathetic nervous system (Loewenfeld, 1999; Barbur, 2004). There are three major classes of neurons in the sympathetic pathway. The first order neurons derive from the hypothalamus and terminate in the cervical cord. The second neurons or preganglionic neurons descend from the cervical cord to make a synapse at the superior cervical ganglion. The third neurons or postganglionic neurons give off two branches. One branch travels along the external carotid artery to innervate the facial vasomotor system and the other branch travel along the internal carotid artery to innervate pupillodilator muscle.

Pupil tests such as relative afferent pupillary defect (RAPD) have been used to evaluate retinal ganglion cell losses in optic neuropathy. RAPD is an asymmetrical pupil light response and a measurement of the loss of neuronal function in optic nerve disease (Thompson, Corbett, & Cox, 1981). The degree of the RAPD in unilateral optic neuropathy is highly correlated with the estimated RGC loss from Humphrey perimetry 30-2 but not very well correlated with the estimation from I4e Goldmann perimetry (Lagrèze & Kordon, 1998). RAPD developed when at least 25% of all RGCs, assessed by OCT, were lost and the relationship between RAPD and the ratio of the affected to unaffected mean RNFL thickness was a negative linear regression, R^2= 0.48 p = 0.0007 (Nakanishi, Nakamura, Tatsumi, Nagai-Kusuhara, & Negi, 2006). By using OCT 3000, the mean RNFL thickness of the affected eye was 50.7 ± 19.3 µm and the unaffected eye was 95.6 ± 17.3 µm. In quadrant analysis, there was no significant correlation between RNFL thickness ratio and RAPD. Hence a spatial relationship between pupillomotor RGCs and P/M cells could not be established in this study. The spatial distribution of pupillomotor RGCs might be comparable to that of the visual RGCs in another study (Lagrèze & Kordon, 1998). However pupils function relatively well out of proportion with the degree of visual loss in Leber hereditary optic neuropathy. A unilateral lesion at the superior collicular brachium can cause pupillary hemihypokinesia without visual field defect as the pupillary afferent fibres in the brachium are a continuation of the pupil fibres

in the optic tract (Loewenfeld, 1999; Papageorgiou, Wermund, & Wilhelm, 2009) (Fig. 58).

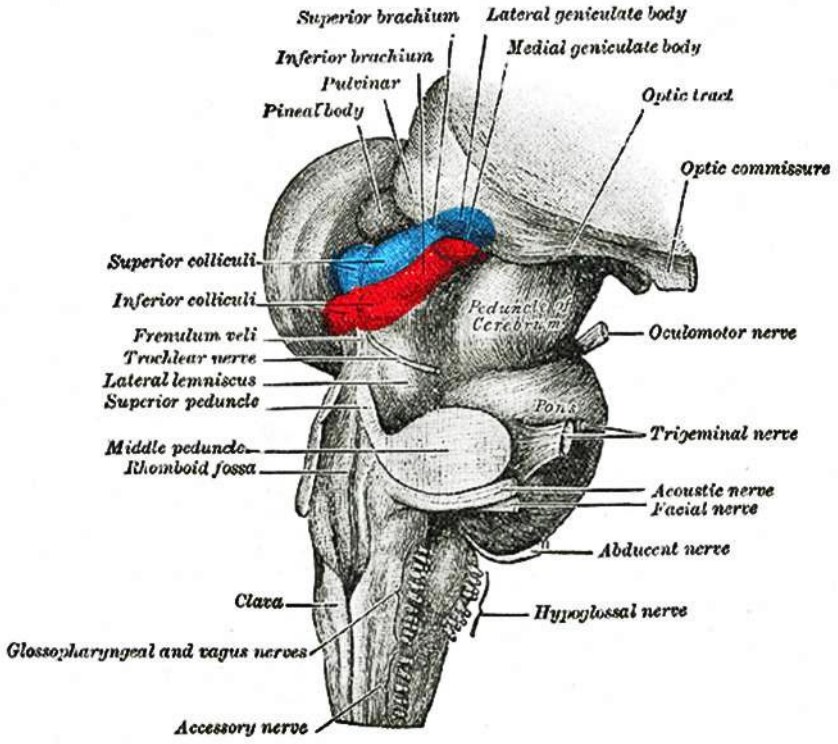

Figure 58 Midbrain postero-lateral view. This picture is a reproduction from Gray's Anatomy of the Human Body. This image is in the public domain because its copyright has expired. This applies worldwide.

Changes in the chromatic, spatial structure and movement of visual stimuli can bring constriction of the pupils without increasing light flux (Barbur, Harlow , & Sahraie, 1992; Barbur J. L., 2004). Pupil latencies and reactions times of the grating and colour stimuli are longer than those of the light flux increment in normal subjects. This result might reflect a processing delay along the cortical pathways (Barbur, Wolf , & Lennie , 1998). It is known that pupil light reactions change slightly after V1 damage. The impairment cannot be detected in a normal clinical settings or using a standard torch but only by using pupillometry. The responses to luminance contrast, grating, colour, and movement are absent or greatly reduced in a blind hemifield in a homonymous hemianopia patient due to occipital injury (Barbur, Watson, Frackowiak, & Zeki, 1993; Barbur, Sahraie, Simmons, Weiskrantz, & Williams, 1998). The responses from the sighted hemifield are better (Barbur, Watson, Frackowiak, & Zeki, 1993; Barbur, Sahraie, Simmons, Weiskrantz, &

Williams, 1998). These findings suggest that the striate or extrastriate cortex might have a role in pupillary control (Barbur J. L., 2004) (Fig. 59). Moreover, it has been shown that pupil grating/colour responses are preserved while pupil light responses are abolished in patients with dorsal midbrain syndrome (Wilhelm, Wilhelm, Moro, & Barbur, 2002). The findings suggest that the cortical control might be independent of the pretectal region (Wilhelm, Wilhelm, Moro, & Barbur, 2002).

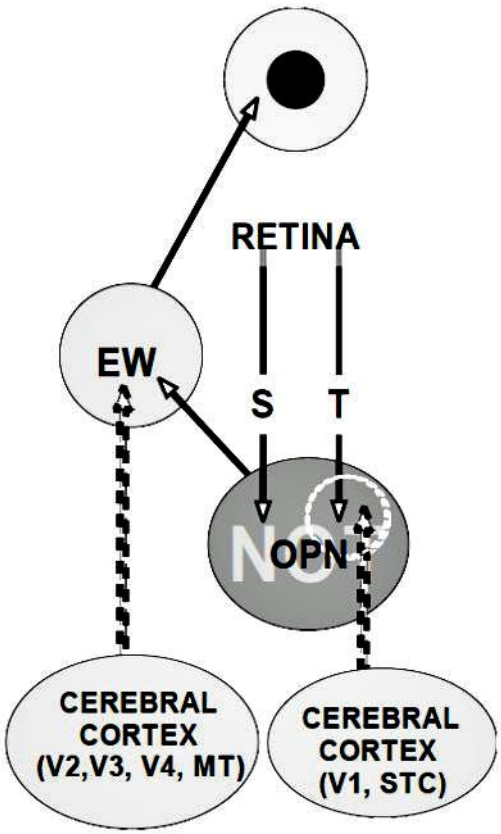

Figure 59 Diagram shows pupil pathway according to Barbur's theory. EW acts as a single generator which is controlled by cortical and subcortical inputs. The cortical inputs (V2, V3, V4, and MT) inhibit EW nucleus and the signals to the sphincter muscle of the iris decrease subsequently. This is called steady state inhibitory signals. In the absence of the cortical inputs, the size of pupils would be small or meiosis. When a healthy subject look at a colour/ grating/ or moving stimulus, the pupils constrict because the stimuli weaken the steady state inhibitory signals from the extrastriate cortex. The top image represents pupil. Abbreviation EW = Edinger-Westphal nucleus in the midbrain, OPN = olivary pretectal nucleus. Reprinted from Learning from the pupil: studies of basic mechanisms and clinical applications,

Barbur JL, from The VISUAL NEUROSCIENCES, edited by LM Chalupa & JS Werner, ©2004 MIT. Permission to reproduce this figure has been granted by The MIT Press.

10.2 Aims

The aim of this investigation was to study the retrograde trans-synaptic degeneration process in the pupil pathway.

There were five parts in this chapter.

1 Pupillometry in acquired homonymous hemianopia from post-geniculate lesions

2 Pupillometry in congenital homonymous hemianopia from post-geniculate lesions

3 Pupillometry in a patient with unilateral optic tract lesion

4 Comparisons of the RNFL thickness and the pupil responses in patients with acquired post-geniculate lesions, congenital post-geniculate lesions, optic tract lesion, and normal subjects.

5 Sympathetic denervation following occipital injury: an incidental finding

10.3 Pupillometry in acquired homonymous hemianopia from post-geniculate lesions

10.3 Pupillometry in acquired homonymous hemianopia from post-geniculate lesions

10.3.1 Methods

Twenty-one cases were recruited in the study and were divided into 2 groups. There were 11 patients in the acquired homonymous hemianopia group from post-geniculate lesions, age range from 44 to 72 years with a median of 53 years. There were 10 subjects in the control group, age range from 28 to 55 years with a median of 32 years. The age distribution in each group was skewed. The Mann-Whitney U test revealed a significant difference between the distribution of the ages in the two groups ($p=0.012$) (Fig. 60). Patient demographic data were presented in Table 14.

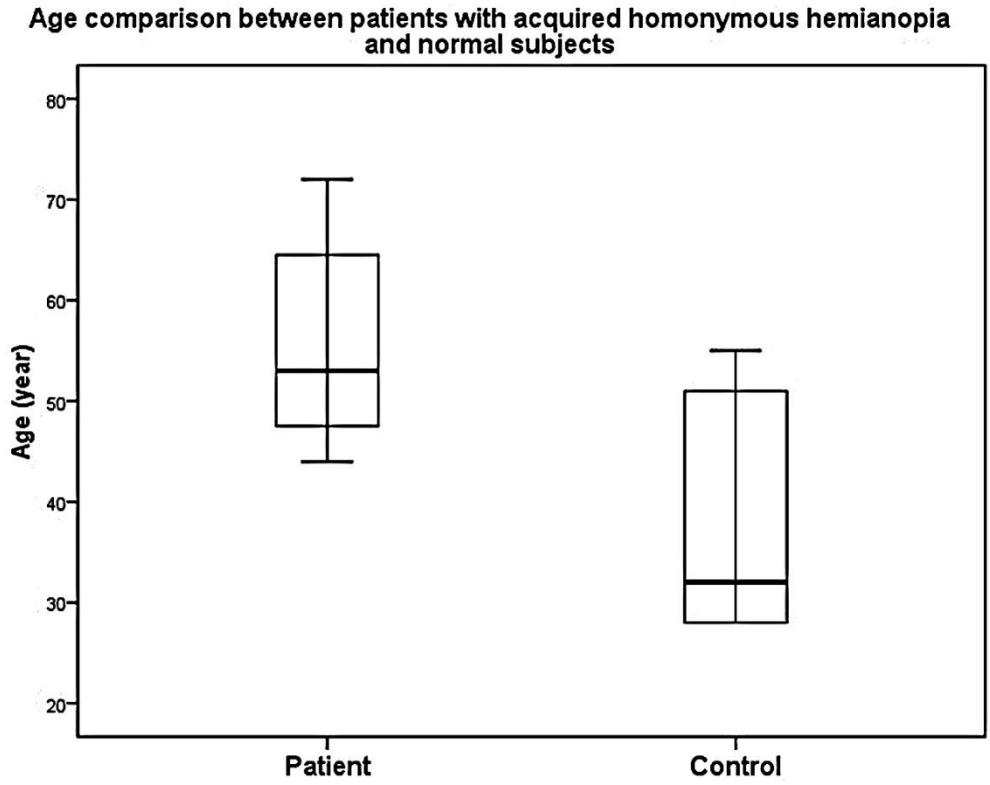

Figure 60 Age distribution between the two groups.

Case	Age	Sex	Disease	Duration (years)
BAM	66	male	occipital infarct	1
POV	72	male	occipital lesion, meningioma removal	18
GY	53	male	occpital lesion, head injury	40
JAS	67	male	occipital infarct (PCA territory)	3
LIL	44	female	occipital, temporal, parietal infarct	1
MAJ	46	male	occipital infarct (PCA territory)	5
ROWO	44	male	occipital lesion, head injury	34
SEM	62	male	occipital infarct (PCA territory)	1
WAR	50	male	occipital haemorrhage	1
ROWI	63	male	occipital, parietal, temporal infarct	2
GIH	49	male	optic radiation haemorrhage	2

Table 14 Patients' demographic data

The P_SCAN 100 system was employed to generate appropriate visual stimuli and to measure the corresponding pupil responses in each eye. The stimuli were presented randomly in the sighted and blind hemifields of the visual field, one side at a time, and the patients viewed a fixation point on a display binocularly. In control subjects, the stimuli were presented in a similar fashion in the right and left visual hemifields. Two types of stimuli were employed to stimulate selectively either chromatic or luminance contrast. The chromatic stimuli were photopically isoluminant and were not detected by rod photoreceptors because their wavelengths were beyond the range of rhodopsin. This restriction limits the chromaticities that can be employed to two directions in the CIE (x,y) 1931 chromaticity diagram (see appendix). These directions correspond to greenish and reddish colours. Two chromatic signal strengths were employed for the red stimulus (that were 0.076 and 0.155) and only one colour signal strength was employed for the green stimulus (that were 0.1). Three luminance contrast or achromatic stimuli were employed. They had a constant size and three different luminance contrasts that were 20%, 100%, and 400%. The percent of contrast used in this experiment was derived from (delta luminance/luminance background) x 100%. Delta luminance = luminance of stimulus – luminance background. Both types of stimuli caused an increment in light flux on the retina. Each stimulus was presented on a background of dynamic luminance contrast noise (Barbur, Harlow, & Plant, 1994). Each stimulus was presented on the display 16 times on each hemifield and 64 trials in total. Both chromatic and luminance contrast stimuli had the same size and location on the display (Fig. 61 & 62, Table 15 & 16). A viewing distance was 700 mm. The display was viewed through a large infrared reflecting mirror that makes it possible to image pupils of the eye. A tunnel-like enclosure that was covered with black velvet absorber connected to the display to the infrared reflecting mirror. This arrangement minimized the surrounding light to reach a subject. The pupil measurements were performed continuously for accuracy and reliability, 1000 ms before a stimulus presentation, 480 ms during the stimulus, and 2000 ms after the stimulus. All records contaminated by blinks or eye movement were rejected. Each trial was started by the experimenters when pupil size and the fixation were seen to be stable on a monitor. A pupil response (millimetres or mm) was a result of the diameter of pupil at baseline minus the smallest diameter after presenting a

stimulus. The primary outcome was the amplitude of the pupil responses or pupil constriction averaged from both eyes (mm).

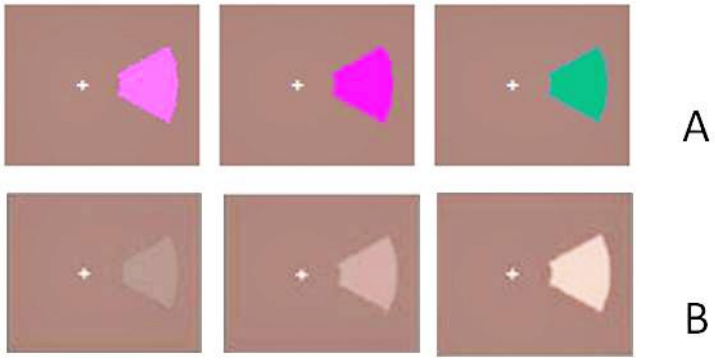

Figure 61 Diagrams showing the stimuli used in the study. A) Chromatic stimuli were shown from left to right: low wavelength low saturation (LWLS) CD= 0.076, Θ= 291, low wavelength high saturation (LWHS) CD= 0.155, Θ = 291, and medium wavelength (MW) CD= 0.1, Θ = 125. B) Luminance contrasts were shown from left to right 20% contrast, 100% contrast, and 400% contrast. Patients were asked to keep looking at the fixation point (+).

			Luminance	X	Y
Number of stimuli	3				
Luminance contrast	20, 100,400 %	Background	3	0.298	0.335
Shape	sector	Foreground	3	0.298	0.335
Sector extend	96°	Target	3	0.298	0.335
Position (degree)	640, 512°	Fixation	24	0.48	0.4

Table 15 Details of the luminance contrast stimuli.

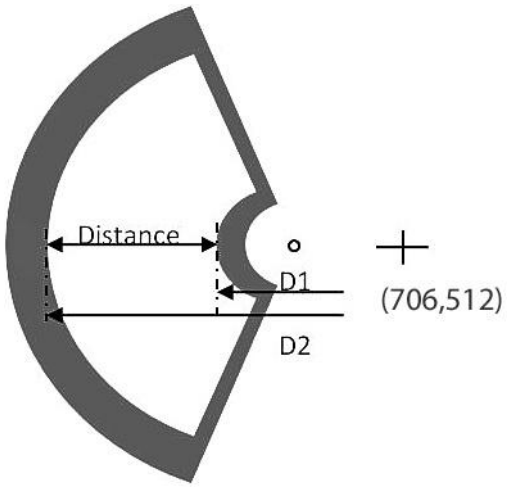

Figure 62 Diagram showing details of the colour and non-colour stimuli on the left side of the screen monitor. The grey annular was the best approximation for drawing. Its colour was the same as the background. The distance was 10.353 cm or 8.4^{o}. D1 was 5.133 cm or 4.2^{o}. D2 was 15.486 cm or 12.5^{o}. The area of the stimulus was 3.14 * (15.486^{2} - 5.133^{2})*96/360 = 178.744cm^{2} or 116.063deg^{2}. The subject viewed a uniform background of angular (background/screen size) subtense 33^{o} x 26^{o} and luminance 24 cd/m^{2}. The stimulus was a sector of an annulus that varied in luminance contrast for a fixed size of 92^{o}.

Number	3
CD	0.076, 0.155, 0.1
Θ	291, 291, 125
Shape	sector
Sector extend	96°
Position	640, 512°

	Luminance	X	Y
Background	3	0.298	0.335
Foreground	3	0.298	0.335
Target	3	0.298	0.335
Fixation	24	0.48	0.4

Table 16 Details of chromatic stimuli on the left side of the display.

10.3.2 Results

A few examples of the pupillary responses from control subjects and patients were demonstrated. Pupillary responses from presentation of the stimuli on either right or left hemifield were normal in control subjects. The responses from both hemifields paralleled to each other (Fig. 63). POV who had occipital meningioma removal 18 years ago showed no pupillary responses when the chromatic stimuli were presented on the blind hemifield as compared to the responses from the sighted hemifield (Fig. 64). There were little responses to the 20% and 100% luminance contrast but relatively good responses to 400% contrast from the blind hemifield (Fig. 65). The responses from the sighted hemifield were all intact. His results were comparable to GY's and GIH's results (Fig. 66 & 67). All acquired homonymous hemianopia patients could not perceive chromatic stimuli on their blind hemifield.

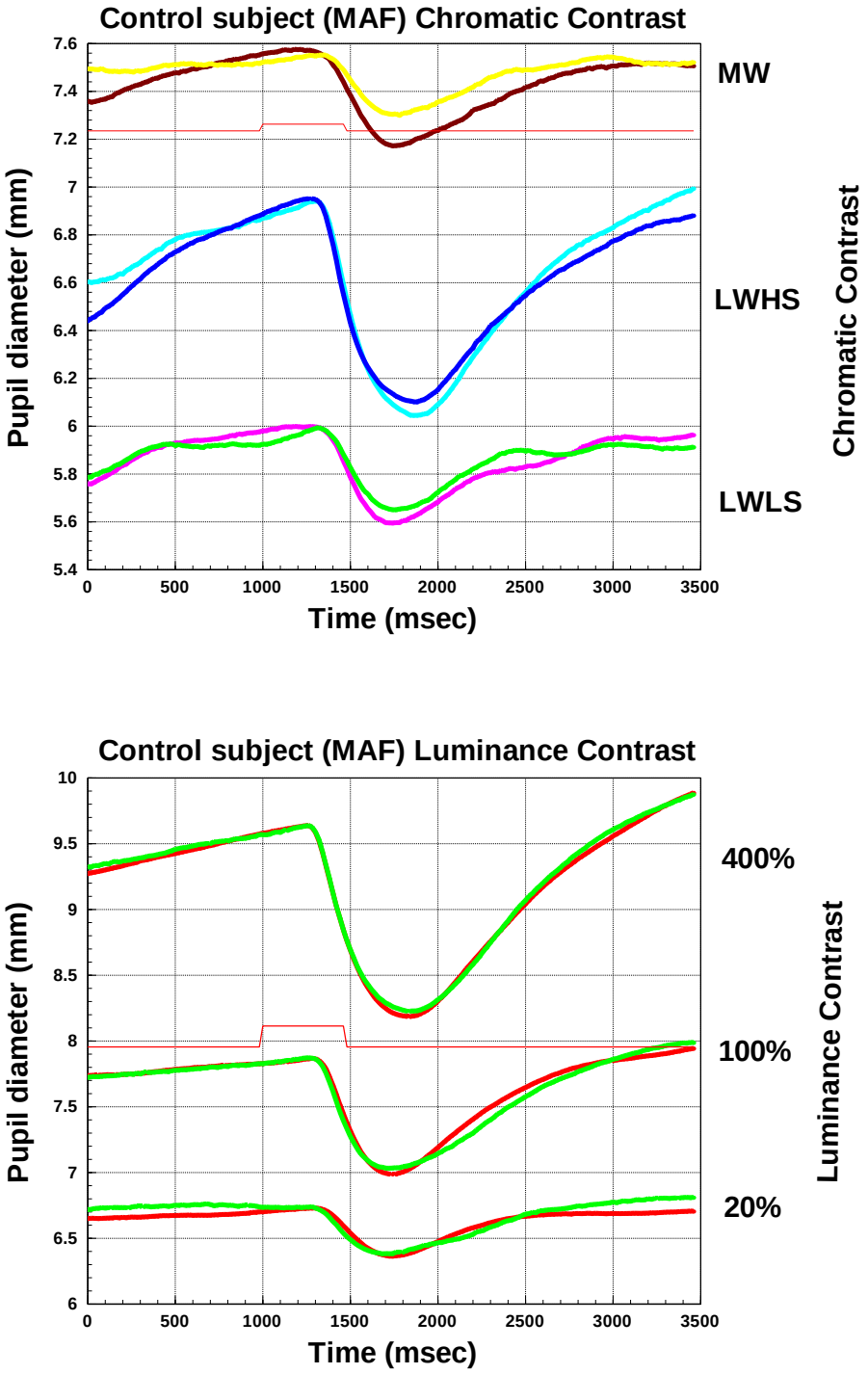

Figure 63 Pupillary responses to chromatic and luminance contrastc stimuli in normal subjects were presented in two diagrams. Responses from each hemifield were shown in different lines for each stimulus.

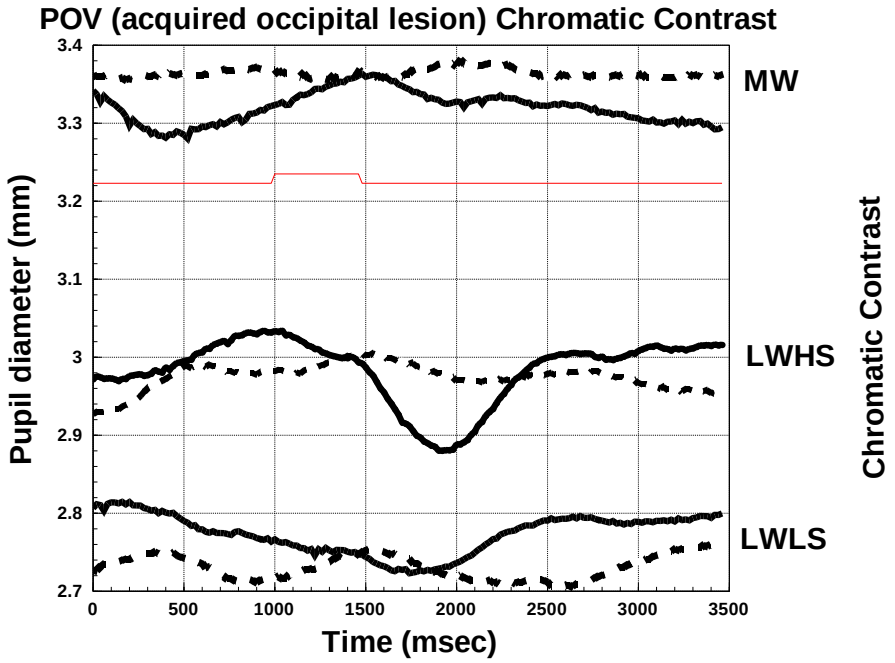

Figure 64 Pupil responses to chromatic stimuli from top to bottom graphs: medium wavelength (MW or green), low wavelength high saturation (LWHS or high red), and low wavelength low saturation or low red). Black lines represented pupil responses when the stimuli were presented in his sighted hemifield and dashed lines represented pupil responses in his blind hemifield. Each line was an average of the pupil reactions of all trials from both eyes. X axis represented time in milli-seconds (msec). Y axis represented pupil diameters in mm. A red line between 1000 and 1600 msec was an indicator that a stimulus was being presented. These parameters were similar to all diagrams in this chapter. This diagram was derived from an acquired homonymous hemianopia (POV) who was presented in the previous chapter. He had a meningioma removal at the occipital lobe 18 years ago. His pupil did not constrict when the stimuli were shown on the blind hemifield whereas the reactions were more detectable when the stimuli were shown on the good hemifield.

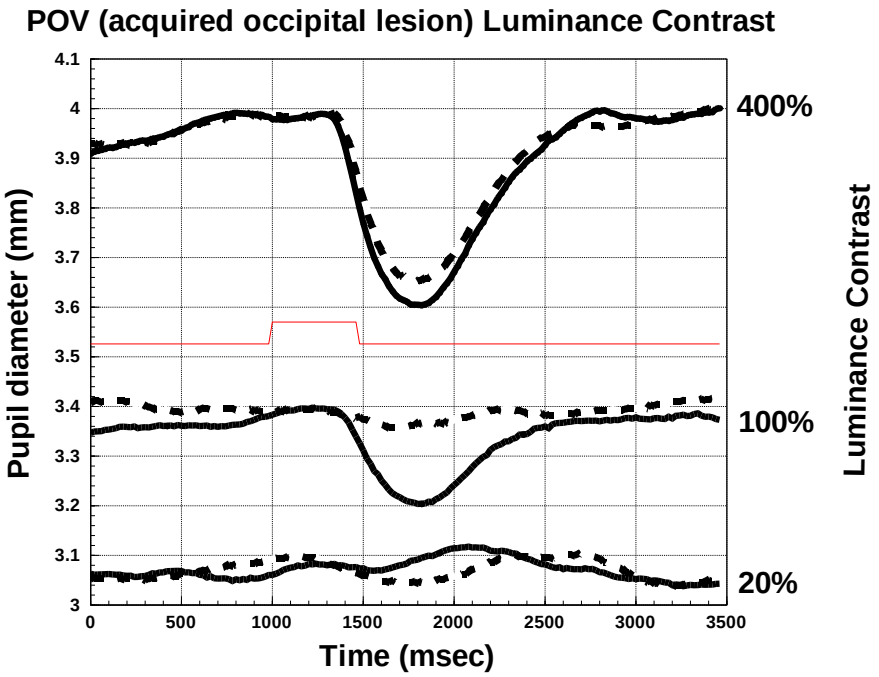

Figure 65 POV's pupil responses to luminance contrast 400%, 200%, and 20%. Black lines represented pupil responses when the stimuli presented in his sighted hemifield and dash lines represented pupil responses in his blind hemifield. Each line was an average of the pupil reactions of all trials from both eyes. X axis represented time in milli-seconds (msec). Y axis represented pupil responses in mm. A red line between 1000 and 1600 msec was an indicator that a stimulus was presenting. The pupillary responses to achromatic stimuli on the blind hemifield were better than the results from the chromatic tests. The pupil constriction was the greatest in 400% contrast.

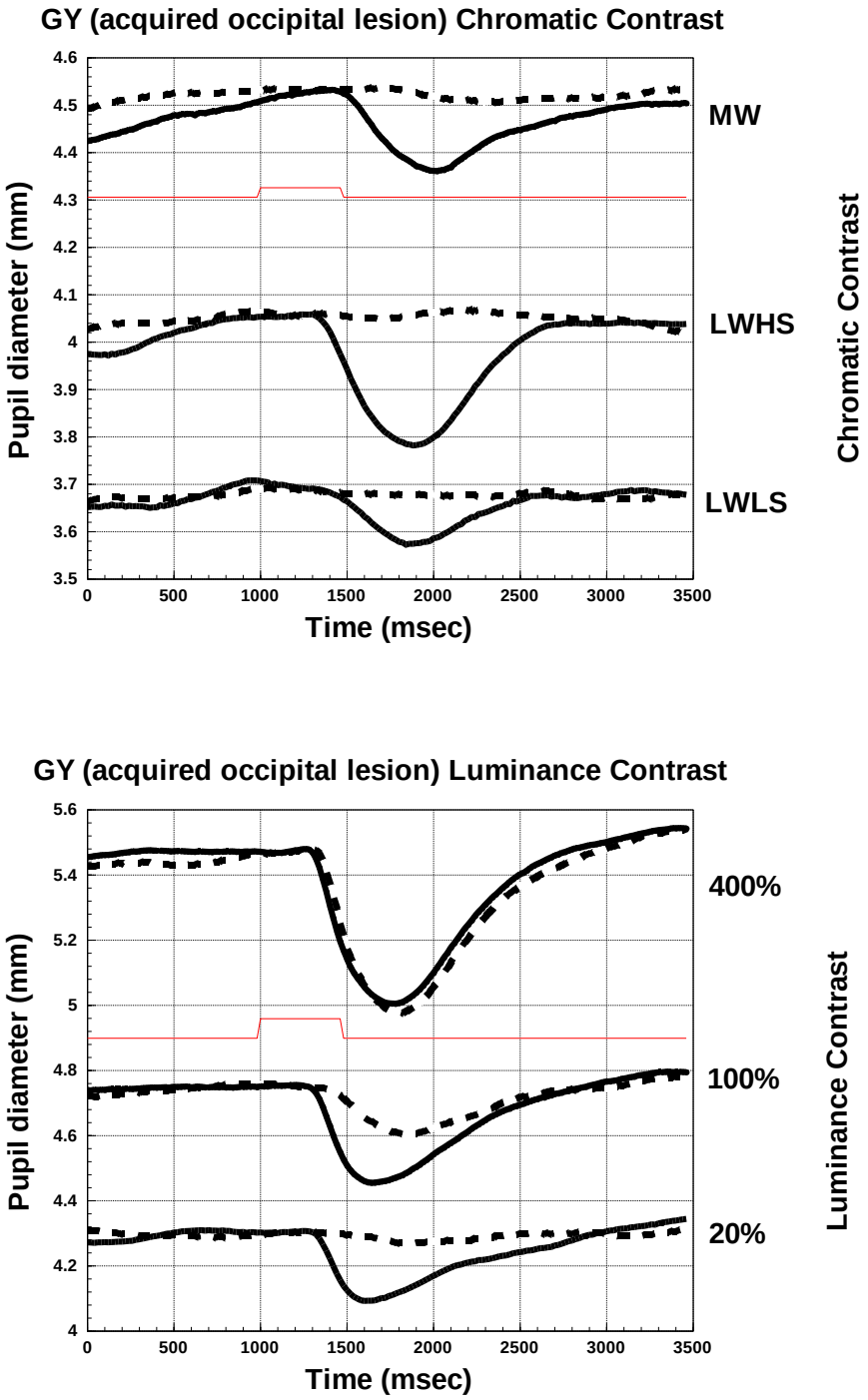

Figure 66 GY's pupil responses to chromatic and luminance contrast stimuli. Responses to chromatic stimuli in the blind hemifield were less than responses to luminance contrast in the blind hemifield. The pupil responses in the sighted hemifield appeared unremarkable.

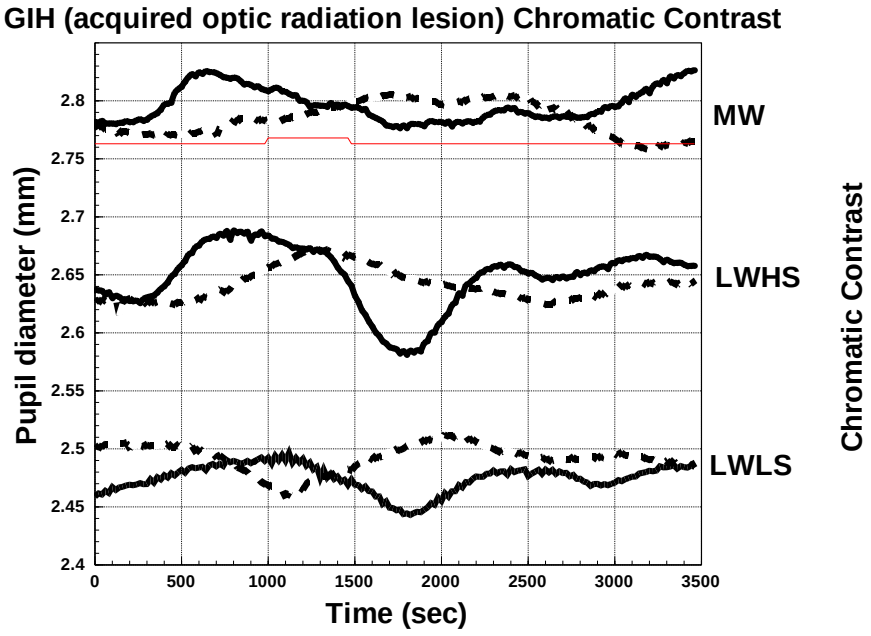

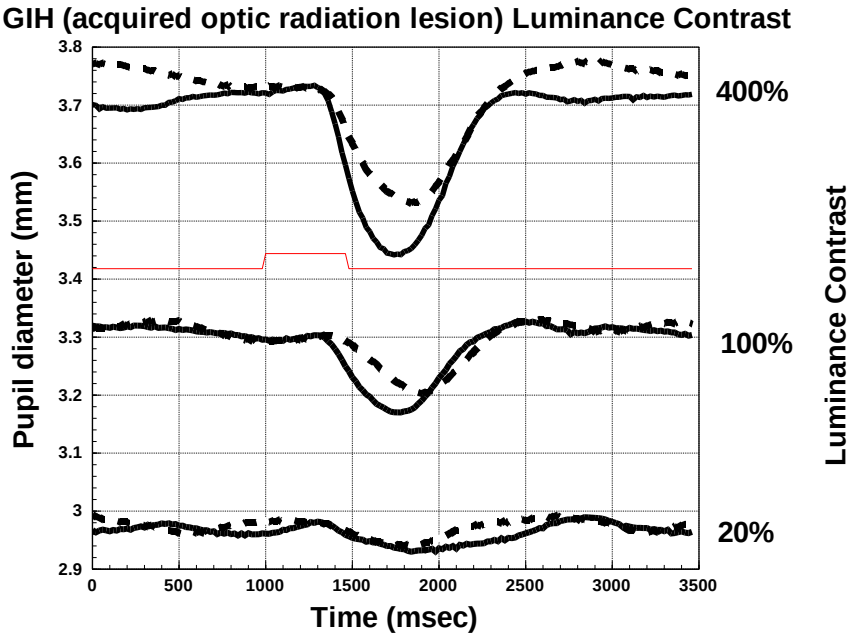

Figure 67 GIH's pupil responses. Responses to chromatic stimuli in the blind hemifield were less than responses to luminance contrast in the blind hemifield. The pupil responses in the sighted hemifield appeared unremarkable.

The distribution of data from both groups was right skewed (Fig. 68). Median, maximum and minimum were presented in Table 17. The Mann-Whitney U test revealed that the distribution of pupil responses in all stimuli and hemifields were significantly different between normal subjects and acquired patients ($p<0.001$). The pupil responses from the acquired homonymous hemianopia patient group were less than those from the control group in both chromatic and luminance contrast tests. Patients' pupil responses to chromatic stimuli were smaller than their responses to luminance contrast (Fig. 69 and Table 18).

However pupil responses were highly diverse among normal individuals. A comparison between individuals might have been confounded by this diversity. Hence we calculated ratios of the pupil responses from the stimuli on the blind hemifields to the responses from the stimuli on the sighted hemifields for the patients and ratios of the pupil responses from the stimuli on the right hemifields to the responses from the stimuli on the left hemifields for the normal subjects (Fig. 70, Table 19).

Considering two groups and two stimuli (chromatic and luminance contrast), Mann-Whitney U tests revealed that 1) the ratio of the overall pupil responses to stimuli on the blind hemifield to those on the sighted hemifield in the patient group were significantly less than the ratio of normal subjects, regardless of the types of stimuli ($p<0.001$). 2) There was a significant difference in the ratio between the patient and control groups in the chromatic test ($p<0.001$) and the luminance contrast test ($p<0.001$). 3) There was a significant difference between the chromatic and luminance contrast tests in the patient group ($p<0.001$) but no significant difference was found between the two tests in the controls ($p=0.6$).

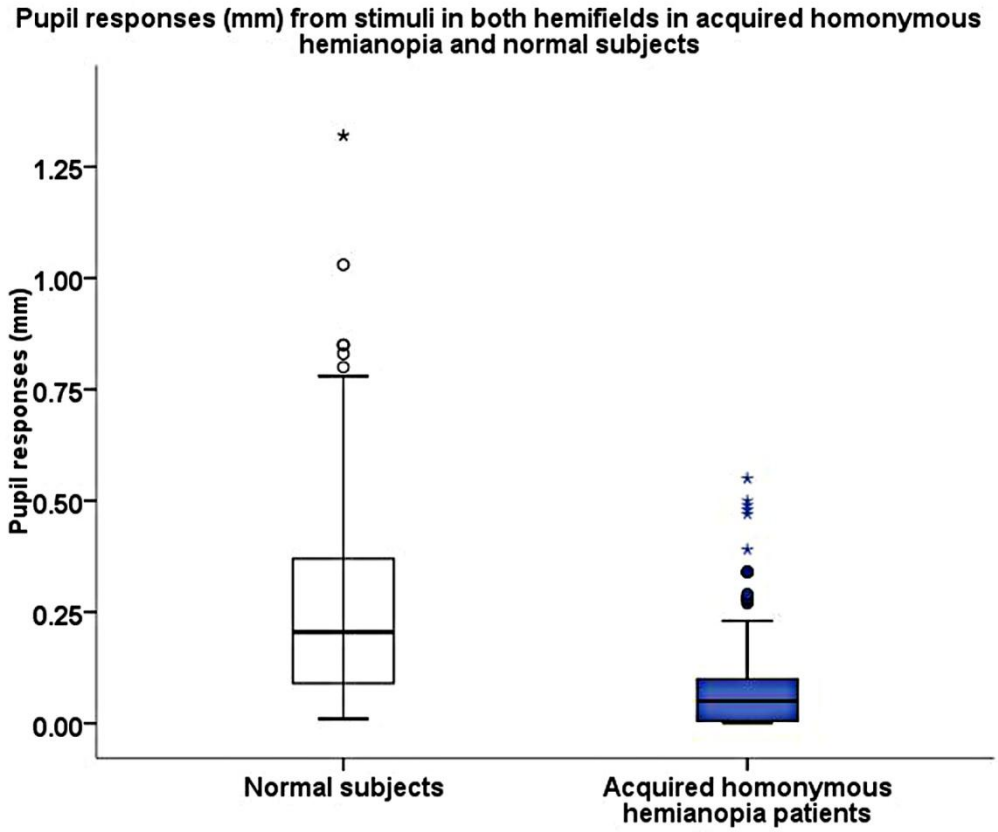

Figure 68 Boxplot of pupil responses in milimetres (mm) in control subjects and acquired homonymous hemianopia patients. The data from the patient group were shown in the blue box and the data from the normal subjects were shown in the white box. The pupil reactions in the patients appeared smaller than the controls.

	Median	Minimum	Maximum
Control (mm)	0.20	0.01	1.32
Acquired homonymous hemianopia patient (mm)	0.05	0.00	0.55

Table 17 Pupil responses in the acquired homonymous hemianopia patients and control groups.

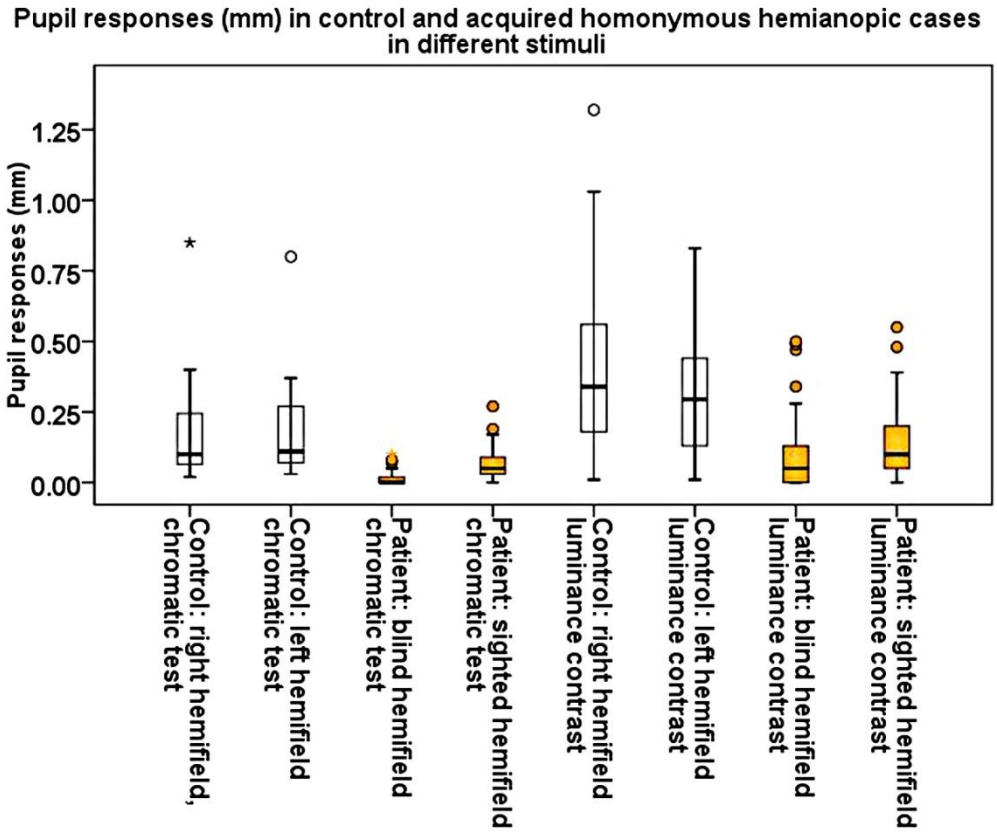

Figure 69 Diagram showing pupil responses in each stimulus and each hemifield in the acquired homonymous hemianopia patients (orange boxes) and the normal subjects (white boxes).

Group	Stimuli	hemifield	median	range
Control	colour	right	0.10	0.02-0.90
	colour	Left	0.10	0.03-0.80
	non-colour	right	0.30	0.01-1.30
	non-colour	left	0.30	0.01-0.80
Acquired HH	colour	blind	0.00	0.00-0.10
	colour	sighted	0.05	0.00-0.30
	non-colour	blind	0.05	0.00-0.50
	non-colour	sighted	0.10	0.00-0.55

Table 18 Pupil responses (mm) in various stimuli in the two groups

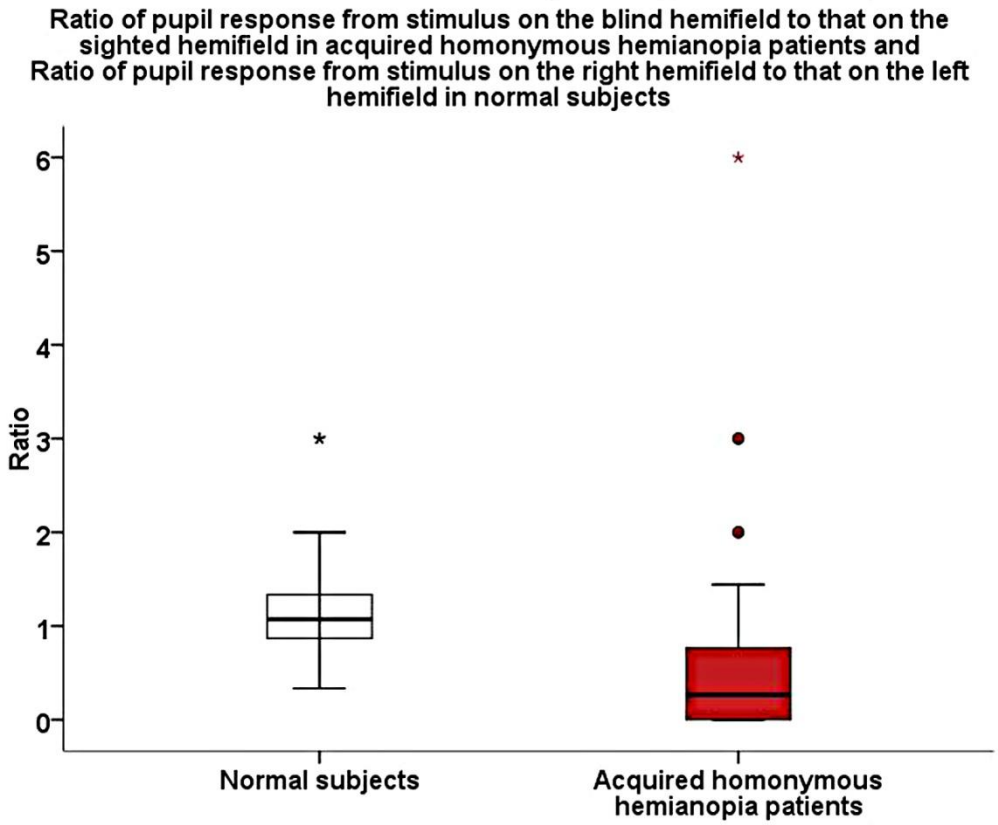

Figure 70 Boxplot of the ratio of pupil responses from stimulus on the blind to those on the sighted field in acquired homonymous hemianopia patients (red box), and ratios of pupil responses from stimulus on the right field to those on the left field in normal subjects (white box).

Group		Median	Minimum	Maximum
Control	Overall	1.07	0.3	3
	Chromatic test	1.06	0.3	3
	Luminance contrast	1.14	0.43	3
Acquired HH	Overall	0.27	0	6
	Chromatic test	0	0	1
	Luminance contrast	0.68	0	6

Table 19 Ratio of pupil responses from stimulus on the blind to those on the sighted field in acquired homonymous hemianopia patients, and ratio of pupil responses from stimulus on the right field to those on the left field in normal subjects.

A multiple regression analysis, using pupil response as the dependent variable and group (1=patient, 2=control) and age (years) as covariates, gave the results shown in Table 20, Fig. 71. After adjusting for age, a linear relationship between the group and the pupil responses was significant. After adjusting for group, a linear relationship between the age and the pupil responses were significant.

Pupil responses = 0.32 +0.089(group) -0.006(age)

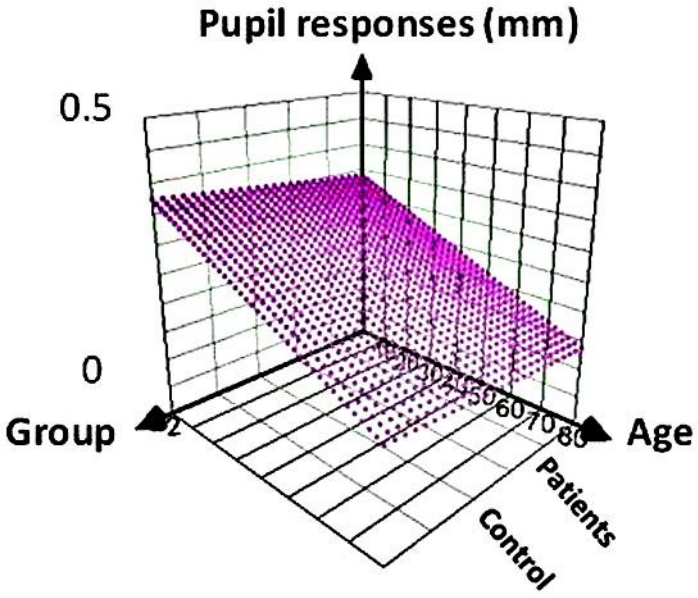

Figure 71 Multiple regression analysis for pupil responses (mm) in both groups (1= acquired homonymous hemianopia patient group, 2= normal subject group) adjusting for age.

	regression coefficient	p value
Constant	.320	.001
Group	.089	.005
Age	-.006	<0.001

Table 20 Multiple regression analysis for pupil responses (mm) in both groups adjusting for age

The results of a multiple regression analysis, using ratio as an outcome dependent variable and 2 covariates including group (1=patient, 2=control), and age are shown in Table 21. After adjusting for group, there was no significant linear relationship between ratio and age (p value = 0.17). After adjusting for age, there was a significant linear relationship between ratio and group (p value <0.001). The age had no effect on the ratio.

	regression coefficient	p value
Constant	-0.87	0.13
Group	0.83	<0.001
Age	0.01	0.17

Table 21 Multiple regression analysis for the ratio with group and age as covariates.

10.3.3 Discussion

There is no eveidence pupillary hypokinesia in patients with post-geniculate lesion if the light was shining to both blind and sighted hemifields at the same time (Loewenfeld, 1999). There was evidence of impaired pupil light reflex in patient suffering from severe diffuse brain edema and demyelination in hepatic encephalopathy grade 4 but the study did not show whether there was a brainstem involvement in MRI scans or not (Yan, et al., 2009). In this pupillary investigation, a stimulus was presented on either blind or sighted hemifield, one side at a time, in patients with post-geniculate lesions. Pupil responses from each hemifield appeared different. We used ratio of the pupil responses from blind to sighted hemifield for the statistical analysis since it provided more accurate interpretation. We demonstrated that the pupil response ratio had a significant linear relationship with the groups (acquired homonymous hemianopia and control) after adjusting for age. The ratio indicated how symmetrical the pupil constriction was when comparing the responses from stimulus presentation on the blind hemifield and the responses from stimulus presentation on the sighted hemifield. It also could tell us whether the pupils receiving stimuli from the blind hemifield responded well or not. However one must be careful when the ratio was one as it might indicate equally good or poor responses from both hemifield stimulus presentations. The ratio 0 strongly indicated no pupil reaction when the stimuli were shown on the blind hemifield. The ratio was used mainly in this analysis as the relationship between the ratio and age was not in a significant linear regression. The distribution of age among the

patient and control groups in our series was skewed. In pupil response analysis, there was a significant relationship between the patient and control group but age influences the pupil responses. The ratio could get rid of the age effect from the pupil response analysis as well as the variability of pupil responses in general population.

The median ratio of the patient group was significantly lower than that of the controls regarding all stimuli and both hemifields. This indicates that the pupil responses from the stimuli in the blind hemifield were affected by the post-geniculate lesions. The results were compatible with previous investigations (Loewenfeld, 1999; Barbur, 2004). We also revealed that patients' pupil responses to the chromatic stimuli were smaller than those to the luminance contrast or achromatic stimuli but there was no significant difference found among the normal subjects. It was not only that pupillary hemiakinesia on the blind hemifield was more prominent in the chromatic rather than achromatic luminance contrast stimuli. A study revealed pupillary hemiakinesia when achromatic grating stimuli was present on the blind hemifield (Trevethan, Sahraie, & Weiskrantz, 2002). In macaque monkeys, pupillomotor RGCs distribute throughout the entire retina and have a similar density gradient as visual RGCs (Roddeik 1993). Recently a study revealed projections of ipRGCs to the pretectal and also the dLGN in both parvocellular and magnocellular layers (Ecker, et al., 2010). The ipRGCs were also responsible to high contrast grating perception in mice (Ecker, et al., 2010). It has been not clarified yet whether they carry different wavelength signals or not. The ipRGCs might have been involved in the retrograde trans-synaptic degeneration. An alternative hypothesis to explain the findings is the absence of the central cortical control from anterograde degeneration following post-geniculate lesions.

Most patients' pupil responses to 400% contrast on the blind hemifield seemed to be preserved. This might be due to a leakage of light from the blind to the sighted hemifield or lack of orienting reaction or spared SBCs. It has been suggested that there are two types of pupil light reaction that are defensive and orienting reactions (Loewenfeld, 1999). The defensive pupil reaction is a reflex movement controlled by subcortical region and requires strong light intensity. The orienting pupil reaction is controlled by cortical region and requires low light intensity. The rise in the pupil

threshold following retrogeniculate lesion causes pupillary hypokinesia but never pupillary akinesia (Loewenfeld, 1999).

10.4 Pupillometry in congenital homonymous hemianopia from post-geniculate lesions

10.4.1 Methods

Three cases of congenital homonymous hemianopia from retrogeniculate lesions were recruited namely ANA , NAJ, and RIC (Fig. 72-74).

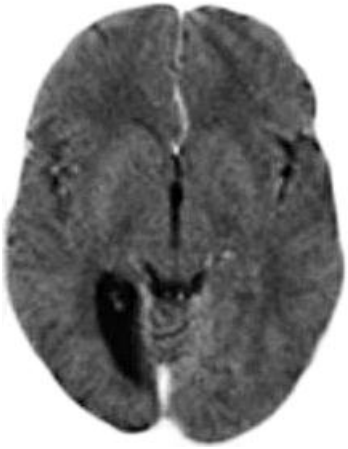

Figure 72 ANA: A computerized tomography revealed mature cystic damage in the right occipital lobe and enlarged right occipital horn of the right lateral ventricle. The findings were consistent with mature infarct.

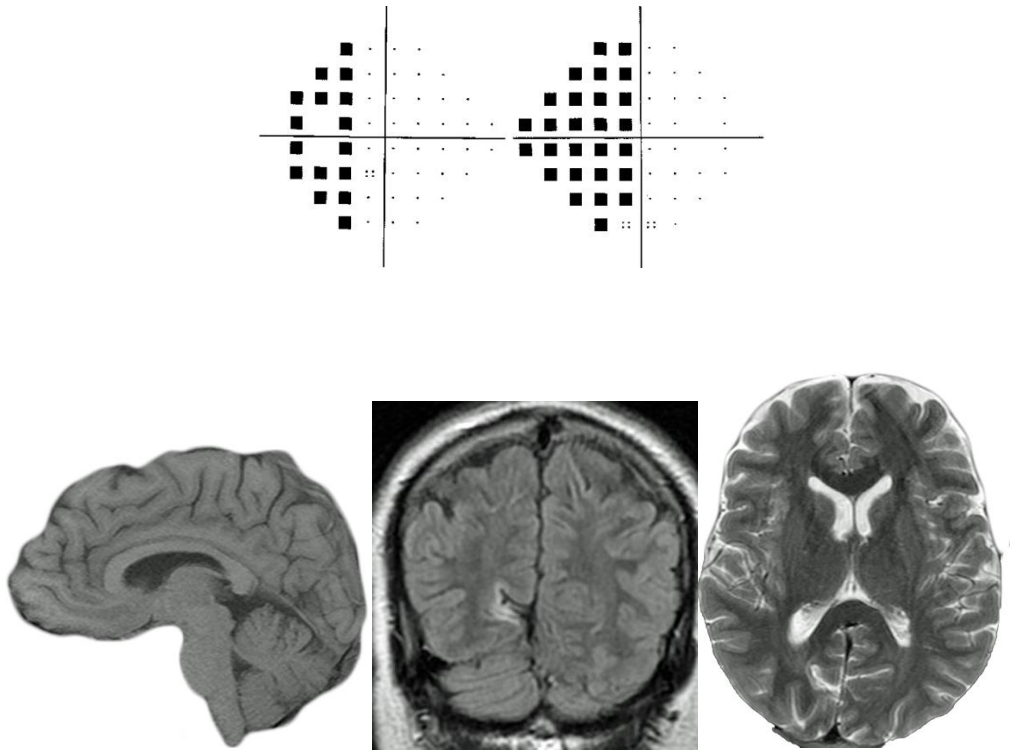

Figure 73 NAJ: Humphrey perimetry 24-2 and MRI scans revealed a mature parenchymal damage involving grey and white matter over the right medial occipital lobe with widening of the sulci and local right lateral ventricle enlargement, consistent with mature infarct.

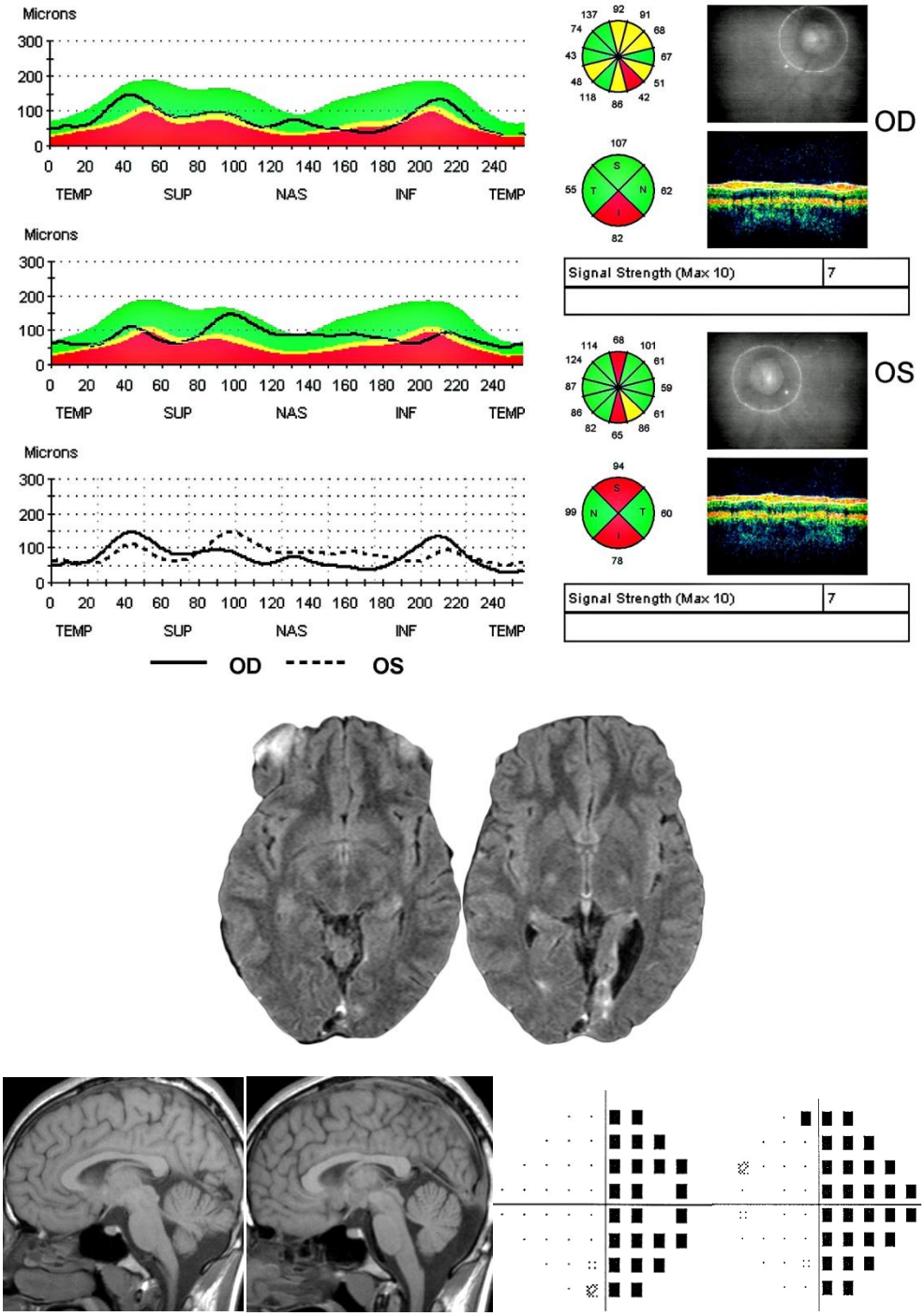

Figure 74 RIC: Humphrey perimetry 24-2, the RNFL thickness measurement, and MRI scans, reavealing a mature infarct in the left occipital lobe.

Six normal subjects were included in the study. Their age ranged from 28 to 32 years old with a median of 29.5 years. Pupillary tests were carried out in all cases. The program used in this part was exactly the same as in the previous part. A stimulus was shown on a screen while the patient looked at a fixation point. The location of the stimulus was either in the blind or sighted hemifields. Two types of

stimuli were employed that were chromatic and luminance contrast. Chromatic stimuli included MW, LWHS, and LWLS. Luminance contrast stimuli included 20%contrast, 100%contrast, and 400%contrast. Pupil diameter was measured throughout the trial.

10.4.2 Results

Pupil responses were presented in Fig. 75-80 for the three patients and a data summary was shown in Table 22.

Figure 75

NAJ: All pupil chromatic responses were good. In particular the reaction to LWHS in the blind hemifield was better than that in the sighted hemifield. The findings were surprisingly different from the acquired cases presented in the previous chapter. We performed the test twice on different occasions to check the reproducibility. The results from both trials were the same.

Figure 76

NAJ: Pupil reactions to three different luminance contrast stimuli were demonstrated. The pupil contrast responses were in the same way as his pupil chromatic responses in that the amplitude in the blind hemifield was larger than in the sighted hemifield.

Figure 77

ANA: Pupils reacted to all chromatic stimuli in the blind hemifield. The amplitudes were smaller when compared to the amplitude of the opposite side. The pupils responded better than the acquired case but less than NAJ.

Figure 78

ANA: The pupil contrast responses in the blind hemifields were comparable to the responses from the sighted hemifields particularly with 400% and 100% contrast.

Figure 79

RIC: The pupils constricted in the blind hemifield to LWLS and LWHS but not to MW. The amplitudes in the blind hemifield were slightly smaller than those in the sighted hemifield.

Figure 80

RIC: Pupil reactions from both hemifields were good to all luminance contrast stimuli.

Blind hemifield

Case	LWLS	LWHS	MW	LC 20%	LC 100%	LC 400%
NAJ	0.17	0.67	0.19	0.21	0.41	0.8
ANA	0.08	0.15	0.03	0.04	0.19	0.49
RIC	0.13	0.16	0.04	0.08	0.17	0.36

Sighted hemifield

Case	LWLS	LWHS	MW	LC 20%	LC 100%	LC 400%
NAJ	0.17	0.4	0.18	0.15	0.25	0.52
ANA	0.14	0.38	0.19	0.1	0.19	0.55
RIC	0.1	0.29	0.07	0.07	0.14	0.39

Table 22 Pupil responses (mm) in the three congenital homonymous hemianopia in 6 different stimuli presented in the blind and sighted hemifields. LC = Luminance contrast.

Among the normal subjects, the range of the pupil responses when the stimuli were presented on the right hemifield was as follows: 0.07 to 0.4 mm in LWLS, 0.22 to 0.85 mm in LWHS, 0.06 to 0.4 in MW, 0.04 to 0.22 mm in 20% contrast, 0.26 to 0.67 mm in 100% contrast, and 0.4 to 1.03 mm in 400% contrast. The range of the pupil responses when the stimuli were presented on the left hemifield was as follows: 0.07 to 0.3 mm in LWLS, 0.27 to 0.8 mm in LWHS, 0.11 to 0.3 mm in MW, 0.13 to 0.34 in 20% contrast, 0.29 to 0.83 in 100% contrast, and 0.4 to 0.78 in 400% contrast.

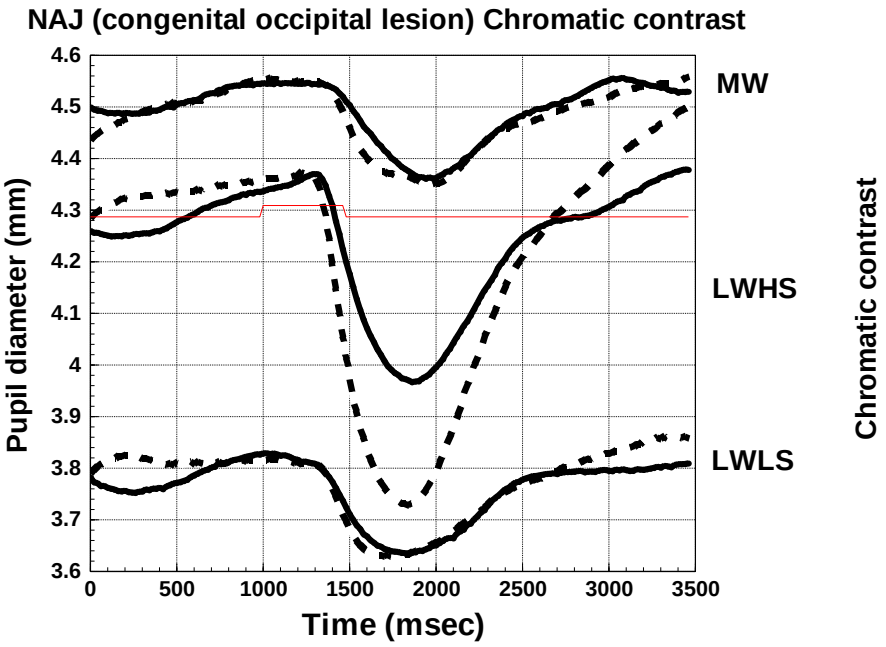

Figure 75

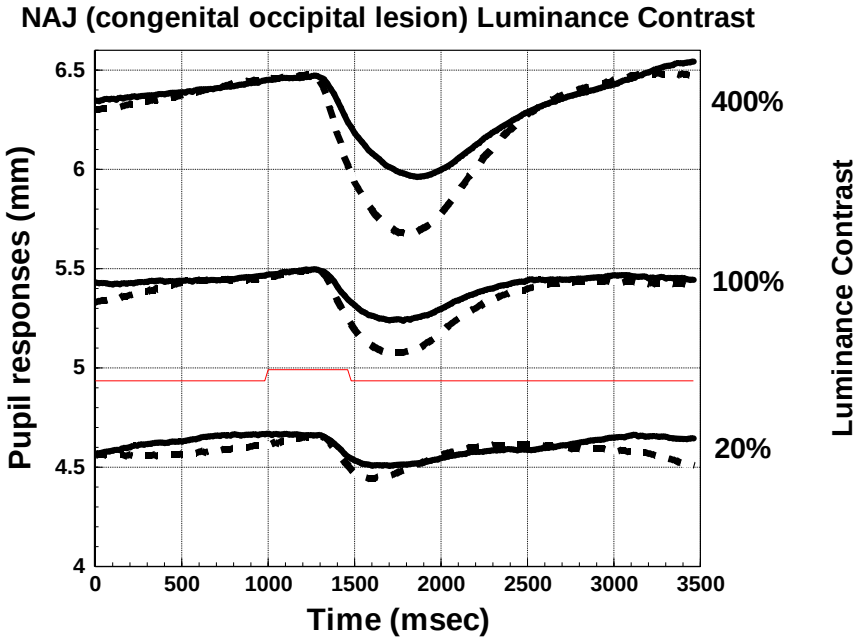

Figure 76

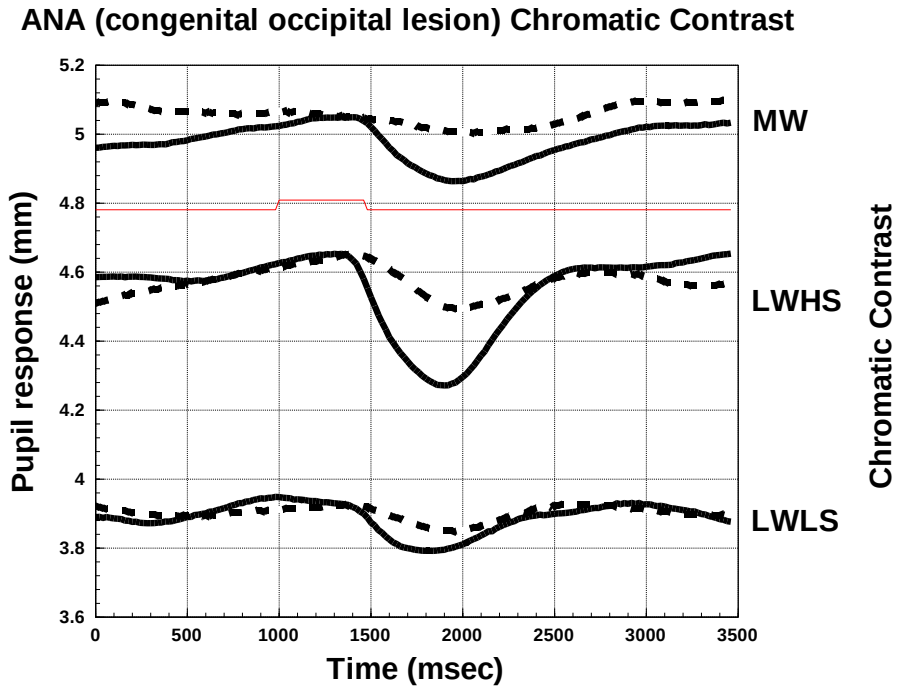

Figure 77

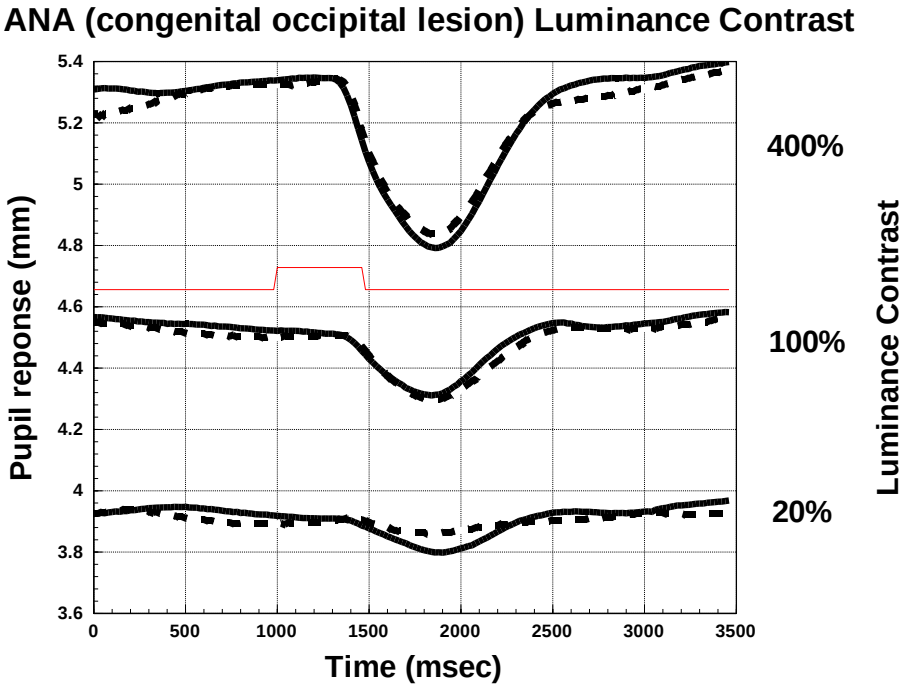

Figure 78

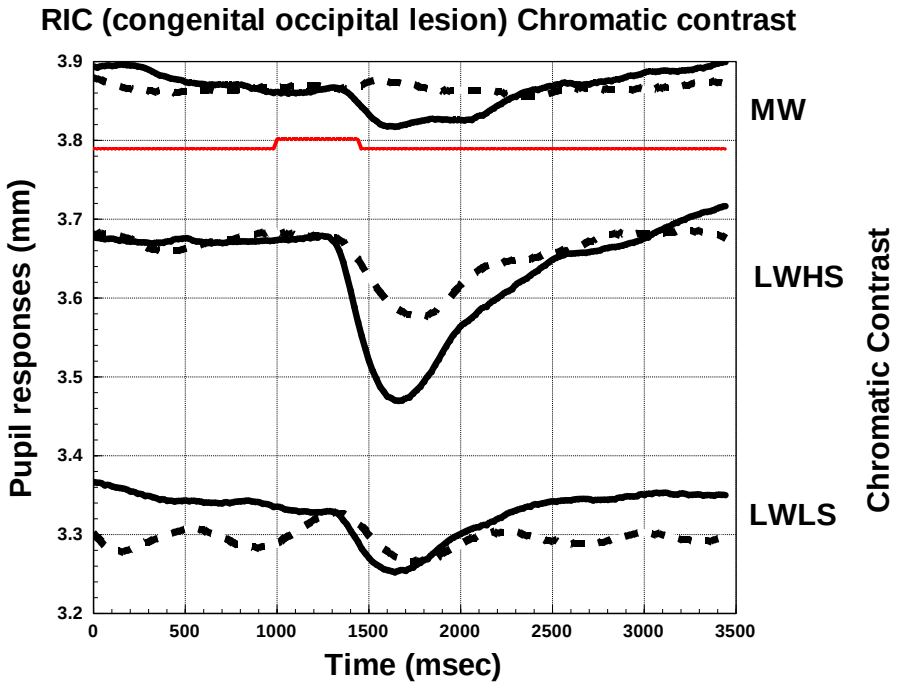

Figure 79

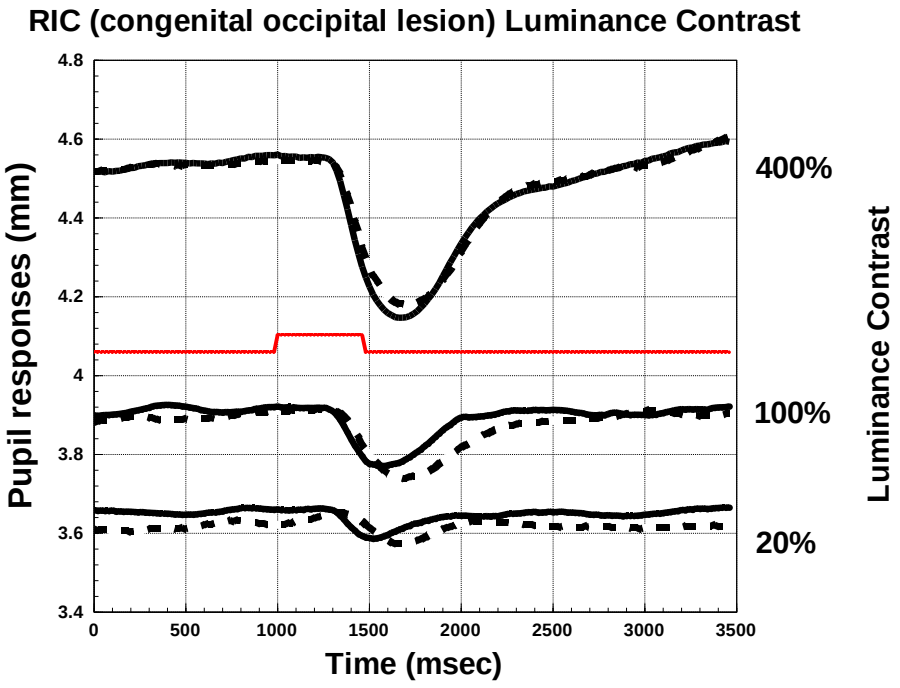

Figure 80

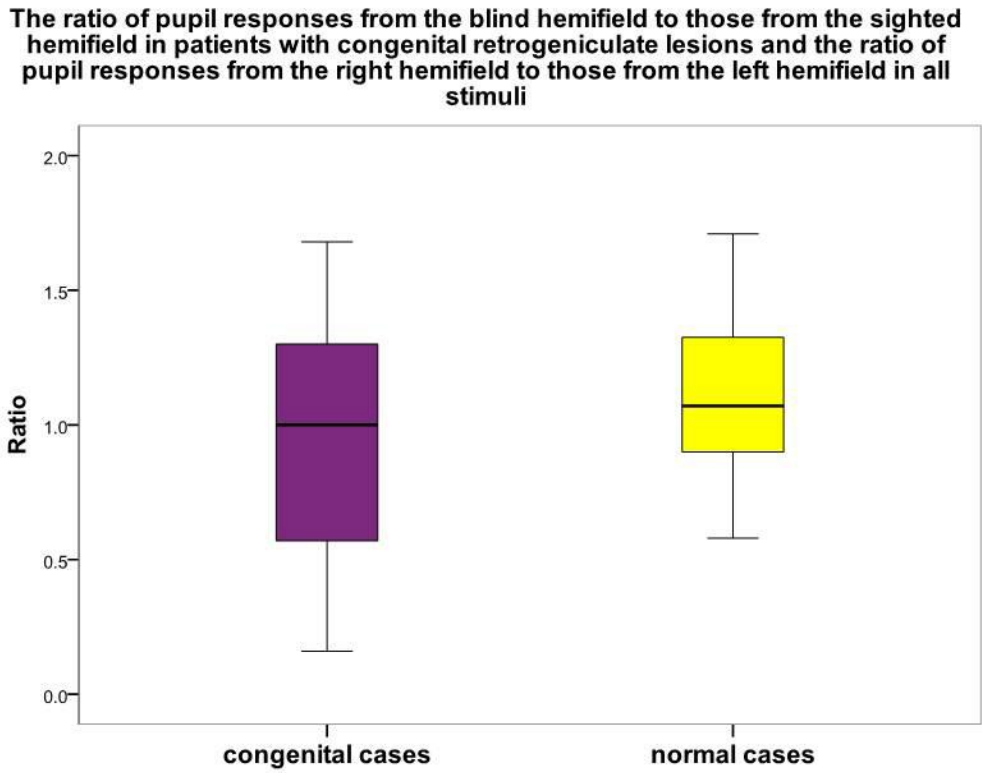

Figure 81 Boxplots revealed the distributions of the ratio in the congenital homonymous hemianopia group (purple box) and the control group (yellow box).

As in the first part, we used the ratio of pupil reaction when stimulus was presented on the blind hemifield to that in the sighted hemifield to analyze. Data distributions of both groups were shown in Fig. 81. The distribution in the congenital cases was symmetrical whereas that in the normal subjects was slightly skewed. The median ratio of the congenital homonymous hemianopia group was 1.00 with a range from 0.16 to 1.68. The median ratio of the control group was 1.07 µm with a range from 0.58 to 1.71. Mann-Whitney U test revealed that there was no significant difference between the median of the congenital homonymous hemianopia case and the normal subjects regarding all 6 stimuli (p value = 0.33). No significant difference between the median ratio of the congenital homonymous hemianopia group and the median ratio of the control group in the chromatic stimuli was found (p value =0.08). Moreover, no significant difference between the median ratio of the congenital homonymous hemianopia group and the median ratio of the control group in the luminance contrast stimuli was detected (p value = 0.8). In the congenital group, there was no significant difference between chromatic and luminance contrast tests (p value = 0.2). In the control group, there was no significant difference between chromatic and luminance contrast tests (p value = 1.0).

It was notable that NAJ could perceive all chromatic and fainted luminance contrast stimuli on the blind hemifield during the trials. ANA perceived aberrant colours on the blind hemifield. For instance: he saw blue instead of green; meshed red with blue on the top instead of bright red (LWHS). He could sense something colourless in the blind area when the LWLS was presenting. In the luminance contrast test, he could not see the 20% contrast but were able to see the higher contrasts on the blind area. RIC could not see any stimuli on his blind area.

10.4.3 Discussion

The three patients were all unaware of the dense visual field defect even after the homonymous hemianopia had been discovered. They could not identify the exact onset. They functioned well in normal daily life and hence we presumed that the visual field defect was congenital. The pupillary functions were relatively spared in our cases with congenital retrogeniculate lesions. The results were different from the acquired post-geniculate lesions. The results were also different from another

study that revealed an increase pupillary threshold in the blind hemifield in patients with congenital retrogeniculate lesion (Loewenfeld, 1999).

Two of the congenital cases could perceive chromatic stimuli in the blind hemifield which was in good agreement with another behavioural study (Stoerig, 1987). The residual colour perception and pupil reaction in the congenital post-geniculate lesion could be accounted by incomplete striate cortex destruction or a consequence of brain plasticity. It has been found in normal kittens that retinal ganglion cell axons have delicate processes and give rise to several collaterals during the developmental period which are gone by adulthood (Ramoa, Campbell, & Shatz, 1988). P retinal ganglion cells extend axons to the superior colliculus during embryo and disappear later when they are older (Ramoa, Campbell, & Shatz, 1989). The visual and pupillary functions in the congenital cases were relatively preserved because an injury might have occurred when P cell fibres were still in contact with the midbrain or areas that were not LGN. The collaterals to the midbrain or to other areas might be more pronounced when their synaptic targets at the dLGN die. There were fibre trajectories from the dLGN to V4 extrastriate cortex (colour perception area) identified in adults also (Cowey & Stoerig, 1991). Moreover it has been found that there was an incomplete separation of crossing and non-crossing RGCs (Kondo, Takada, Tokuno, & Mizuno, 1994); (Fukuda, Sawai, Watanabe, Wakakuwa, & Morigiwa, 1989) which might contribute to the preserved visual and pupillary functions.

10.5 Pupillometry in a patient with optic tract lesion

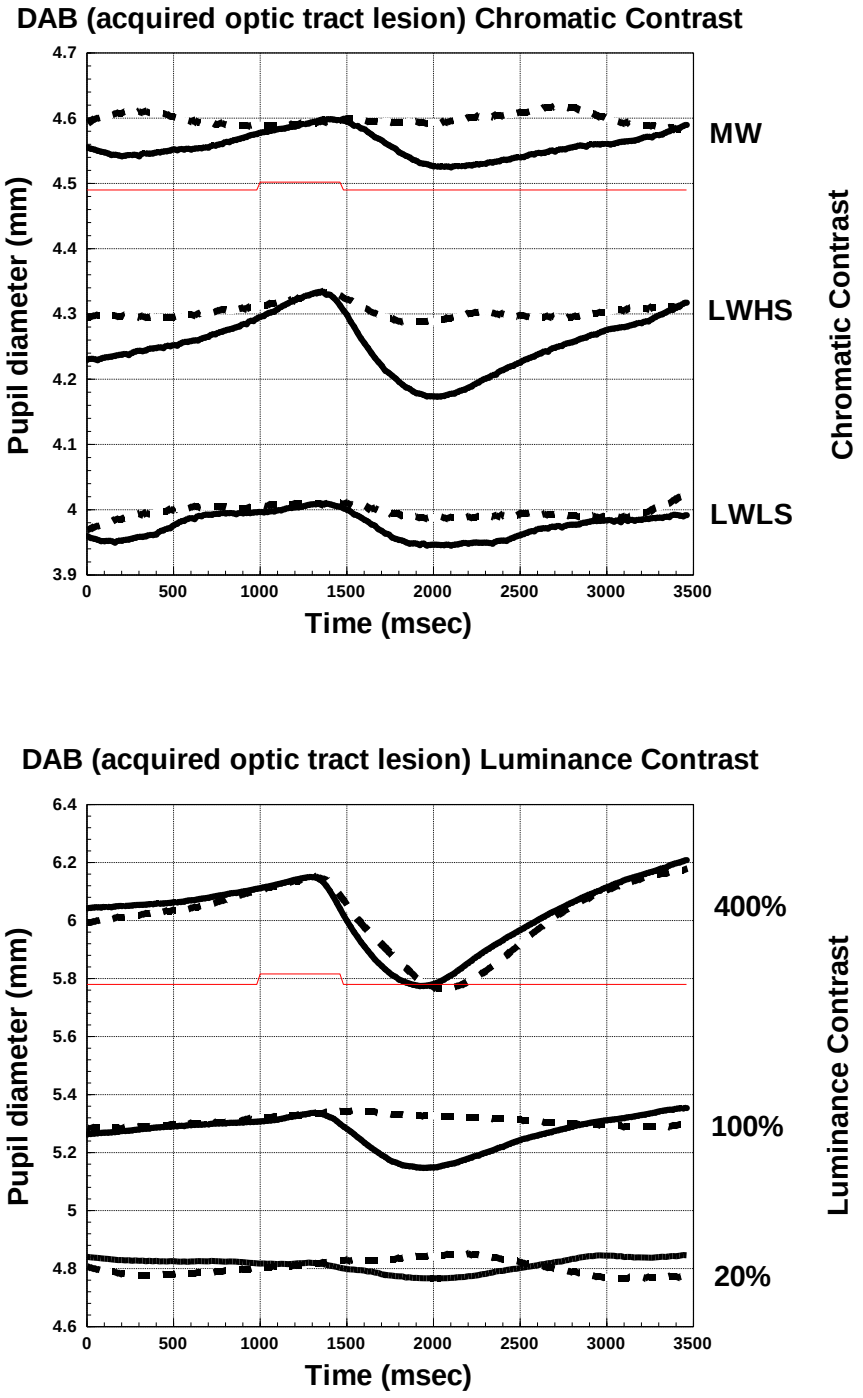

Figure 82 Pupillometry results in a patient with unilateral optic tract lesion (DAB) to the chromatic and luminance contrast stimuli were presented. There was no or nearly no pupil responses to all stimuli presented on the blind hemifield except for 400% contrast. The reactions from the sighted hemifield were spared. The findings are well known as Wernicke's sign or pupil hemiakinesia (Loewenfeld, 1999).

The result was compatible with a positive relative afferent pupillary defect following unilateral optic tract injury. The RAPD usually occurs in the eye with temporal hemianopia or crossing fibre defect eye because the number of the retinal ganglion cells in the nasal hemiretinae is greater than that in the temporal hemiretinae. The degree of his pupil function is also congruous with the degree of the retinal nerve fiber loss. This could be explained by a direct damage of the pupillomotor RGCs from retrograde degeneration (from optic tract towards retina). It occurs along the optic tract pathway, which contains fibres from P cells and pupillomotor RGCs, before leaving to the LGN and pretectal regions. As presented above, the pattern and severity of the RNFL degeneration in homonymous hemianopia patients from optic tract lesion is comparable with those in the homonymous hemianopia from acquired post-geniculate lesion. However the pupillometry results in part 1 acquired post-geniculate lesion were not as severe as in this case. Likewise the relative afferent pupillary defect is clinically observed in patients with optic tract injury but has not been reported in cases with occipital damage. This implies that the loss of the pupillomotor RGCs from a tract lesion is more extensive than that from a striate cortex lesion. The collaterals of the pupillomotor RGC axons around the LGN and the midbrain might have contributed to the different outcome from the two lesions.

10.6 Comparisons of the RNFL thickness and the pupil responses in patients with acquired post-geniculate lesions, congenital post-geniculate lesions, optic tract lesion, and normal subjects.

The number of the cases in this part was too small for a statistical analysis. However we could see an overview of the pupil reactions and the RNFL thickness in various causes of homonymous hemianopia. Eleven subjects were included in this study and were divided into 4 groups. The first group had dense homonymous hemianopia from acquired post-geniculate lesion, comprising of 7 cases. The second group had dense homonymous hemianopia from congenital post-geniculate lesion, comprising of 2 cases. The third group had dense homonymous hemianopia from unilateral optic tract lesion, comprising of one case. The last group had one normal subject. Every subject had been presented in the previous chapters and had the lesion for least about a year. They all had pupillometry evaluation with the same

model previously described. The peripapillary RNFL thickness was also performed by using the optical coherence tomography.

Figure 83

A comparison of ratios of pupil responses to the chromatic stimuli when the stimulus was presented on the blind hemifield to those on the sighted hemifield and the mean RNFL thickness of both eyes in homonymous hemianopia from acquired post-geniculate lesion, congenital post-geniculate lesion, optic tract lesion, and normal subjects.

Figure 84

A comparison between pupil chromatic responses when the stimuli were presented on the blind hemifield and the mean RNFL thickness of both eyes in homonymous hemianopia cases from acquired and congenital post-geniculate lesion, from optic tract lesion, and normal subject.

The normal subject had the highest RNFL thickness, good pupil responses and ratios. The optic tract case showed poor pupil colour responses and ratio; and very thin RNFL. The pupil chromatic responses and the ratio in the congenital group were good with a relatively thin RNFL. The ratio in the acquired group varied highly. It is difficult to establish a relationship between the RNFL thickness and the ratio or the pupil responses in the acquired post-geniculate group. The pupil chromatic responses or the ratio was zero in a wide range of the RNFL thickness from 60 to 100 microns. The performance in some cases became better in thin RNFL. Hence the pupillary function was incongruous with the retinal ganglion cell loss following the acquired retrograde trans-synaptic degeneration. It has been demonstrated that the pupillary abnormality is also less extensive than the degree of the visual field defect in the acquired homonymous hemianopia due to post-geniculate lesions (Loewenfeld, 1999).

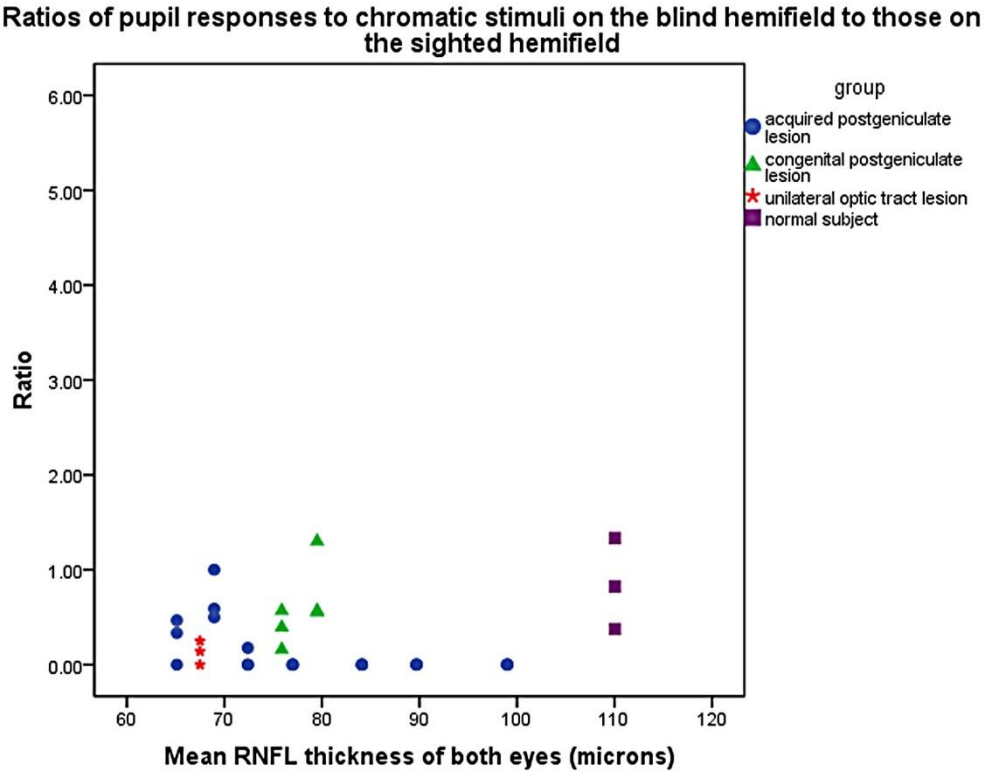

Figure 83

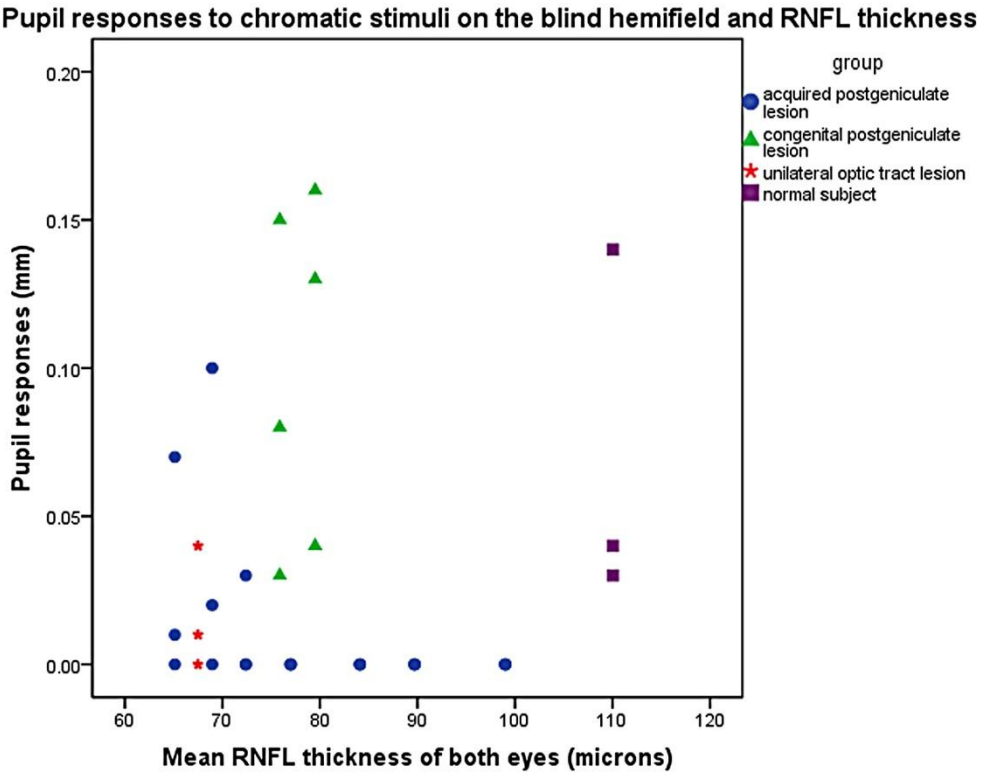

Figure 84

Figure 85

A comparison of ratios of pupil responses to the luminance contrast stimuli on the blind hemifield to those on the sighted hemifield and the mean RNFL thickness of both eyes in homonymous hemianopia from acquired post-geniculate lesion, congenital post-geniculate lesion, optic tract lesion, and normal subjects.

Figure 86

A comparison between pupil responses from luminance contrast stimuli on the blind hemifield and the mean RNFL thickness of both eyes in homonymous hemianopia patients from acquired and congenital post-geniculate lesions, optic tract lesion, and normal subject.

For the luminance contrast stimuli, the outcome of the congenital post-geniculate lesion, the optic tract lesion and the normal subjects was more or less the same as in the chromatic test except for the good pupil light reaction to the 400% contrast in the case with optic tract injury. The ratio and pupil light response from stimulus on the blind hemifield in the acquired post-geniculate lesion group were widely scattered. The degree of the pupil abnormality in the acquired post-geniculate lesion group was inconsistent with the degree of the retinal nerve fibre loss.

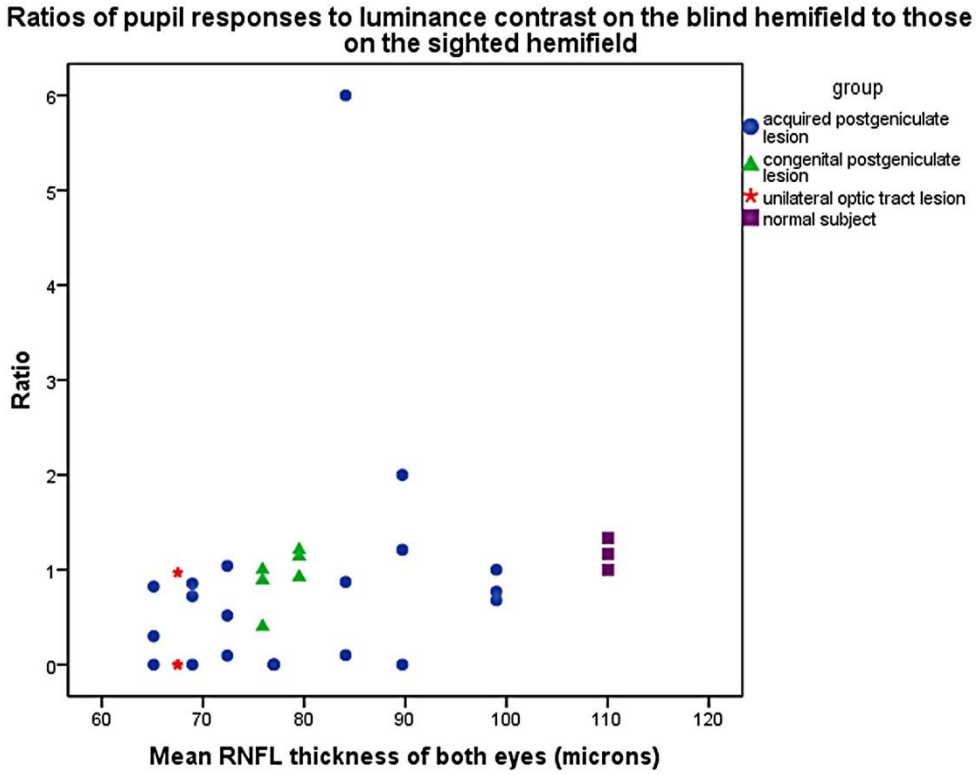

Figure 85

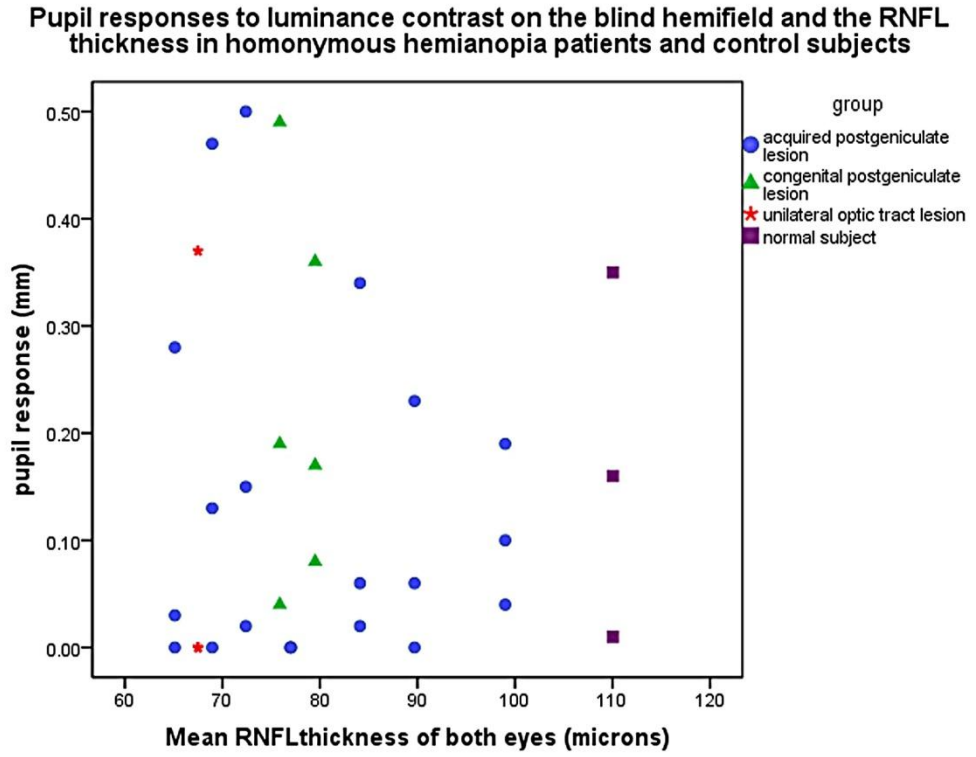

Figure 86

10.7 Sympathetic denervation after an injury to the post-geniculate lesion: an incidental finding

10.7.1 Introduction

A coincidental finding was discovered in the experiment in section 10.7.3 and was presented in this section. We found that some cases with acquired homonymous hemianopia from post-geniculate lesions had a pupillary dilatation lag (Fig.75, 76), a characteristic of Horner's syndrome (Loewenfeld, 1999). Common features in Horner's syndrome include miosis and slow pupil dilatation in the dark or so called dilation lag (Fig. 87). Dilation lag is specific for sympathetic denervation and can be tested by changing the light environment from bright to dark. In bright environment, normal and Horner's pupils in a patient constrict. In dark environment, the pupils dilate but the movement of the Horner's pupil is slower than the movement of the intact pupil. The difference of the pupil size becomes greater in the dark during the dilation lag (Loewenfeld, 1999). The pupil light reflex is normal in Horner's syndrome. Horner's syndrome is also associated with ipsilateral ptosis, enophthalmos, and pale iris colour in congenital cases (Loewenfeld, 1999). Notably these features have been documented in peripheral lesions of sympathetic nervous system but have never been reported in central lesions before.

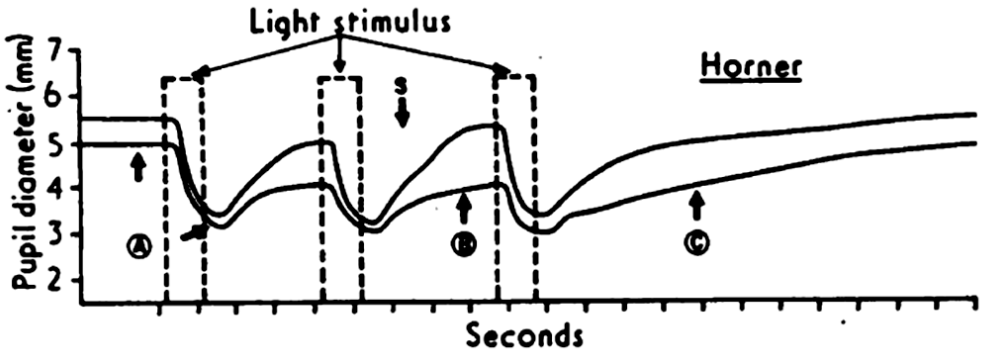

Figure 87 Diagram demonstrated dilatation lag in classic Horner's syndrome (Pilley & Thompson, 1975). A) more anisocora in the darkness than in light. B) sudden increase in anisocoria after psychosensory stimulus (S) due to sympathetic discharge to the dilator muscle. C) transient increase in anisocoria after the light is switched off due to dilatation lag of Horner's pupil. Reproduced from Pupillary "dilatation lag"

in Homer's syndrome, SF Pilley & HS Thompson, vol 59, page 731-5, ©1975 with permission form BMJ Publishing Group Ltd.

10.7.2 Aims

The aim of this part was to evaluate the difference in the pupillary redilation between acquired homonymous hemianopia and control group.

10.7.3 Methods

The patients with acquired homonymous hemianopia and the healthy subjects were similar to those in section 10.3 and the methods of experiments were exactly the same. Ten patients had unilateral lesion in the occipital lobe and only one subject (GIH) had a small lesion in the optic radiation. Pupillary amplitudes were plotted against time. An angle measured from x axis to the first dilatation part was evaluated in both hemifields of every case, identified as an orange star in Fig 90. A comparison of the angle between the results from two hemifields within the same individual was made. We did not compare the results between cases for the diversity of the pupil size in normal population is great.

10.7.4 Results

The angles between right and left hemifield were more or less the same in normal subject. Most pupillary responses of all stimuli except luminance contrast 400% were absent. Responses from the luminance contrast 400% were relatively well in most cases. Among ten patients who had unilateral occipital lesion, 6 of them or 60% showed evidence of dilatation lag at least in one stimulus. It was evidenced by the angles between the dilatation curve at the initial point and the x axis in the blind hemifield appeared smaller than those in the sighted hemifield (Table 23, Fig. 88 & 89). A patient with a lesion in the optic radiation did not show dilatation lag.

Case	Lesion	LC 20%	LC 100%	LC 400%	LWLS	LWHS	MW
BAM	Occipital lobe	0	0	40,50	0	30,30	0
POV	Occipital lobe	14,18	27,72	67,67	0	0	0
GY	Occipital lobe	0	34,55	45,45	0	0	0
JAS	Occipital lobe	0	0	26,26	0	0	0
LIL	Occipital lobe	24,24	24,24	54,54	0	0	0
MAJ	Occipital lobe	0	0	45,45	0	30,50	0
ROWO	Occipital lobe	0	55,55	65,65	38,38	61,71	0
SEM	Occipital lobe	0	0	70,70	0	0	0
WAR	Occipital lobe	0	0	0	0	40,59	17,17
ROWI	Occipital lobe	0	0	74,74	0	0	0
GIH	Optic radiation	20,20	42,42	52,52	0	0	0

Table 23 Table showed angles of the dilatation curve at the initial point and x axis. The first number represented an angle of the blind hemifield and the following number represented an angle of the sighted hemifield. Number 0 represented an absence of pupillary response in the blind hemifield. Blue highlight represented positive dilation lag in the blind hemifield since the angle in the blind hemifield appeared smaller than the sighted one. LC represented luminance contrast.

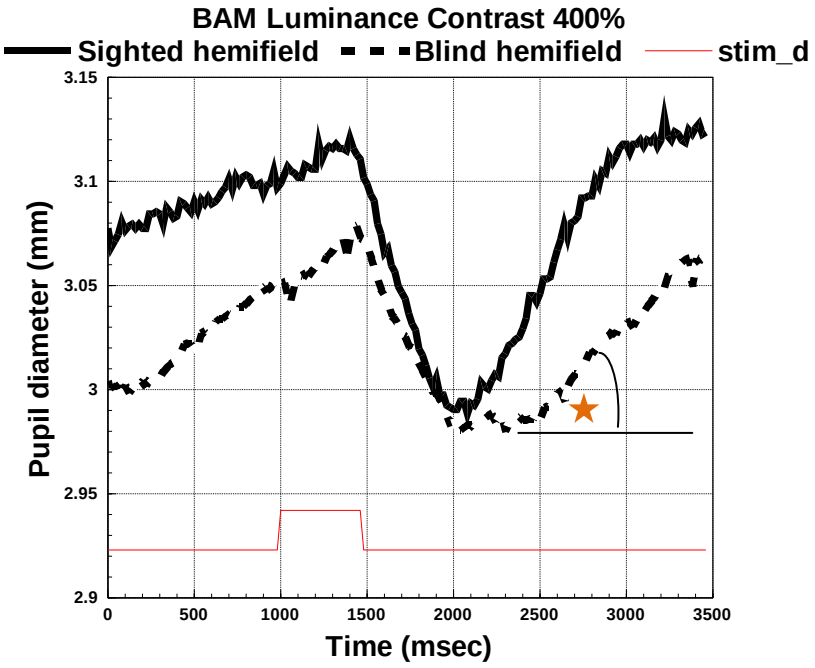

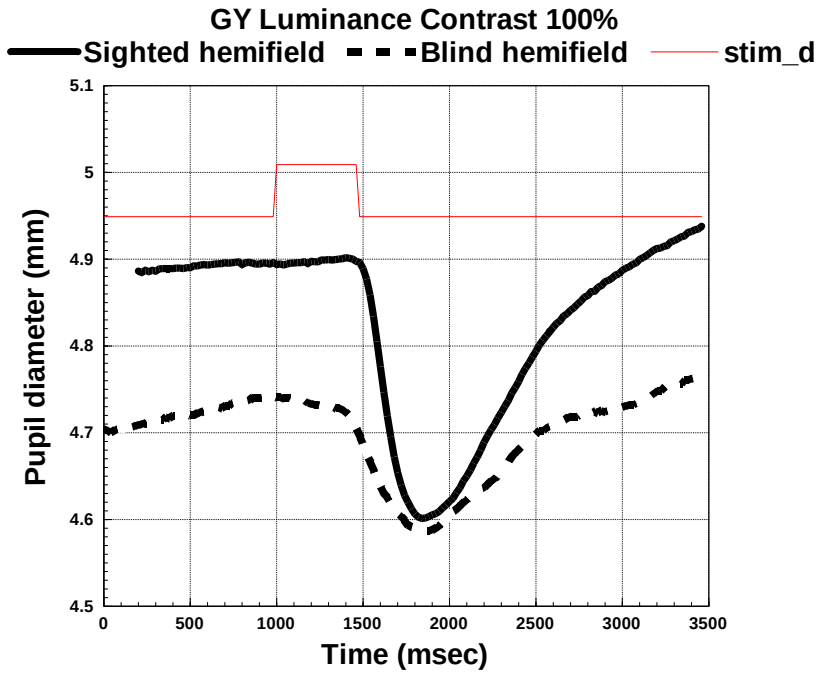

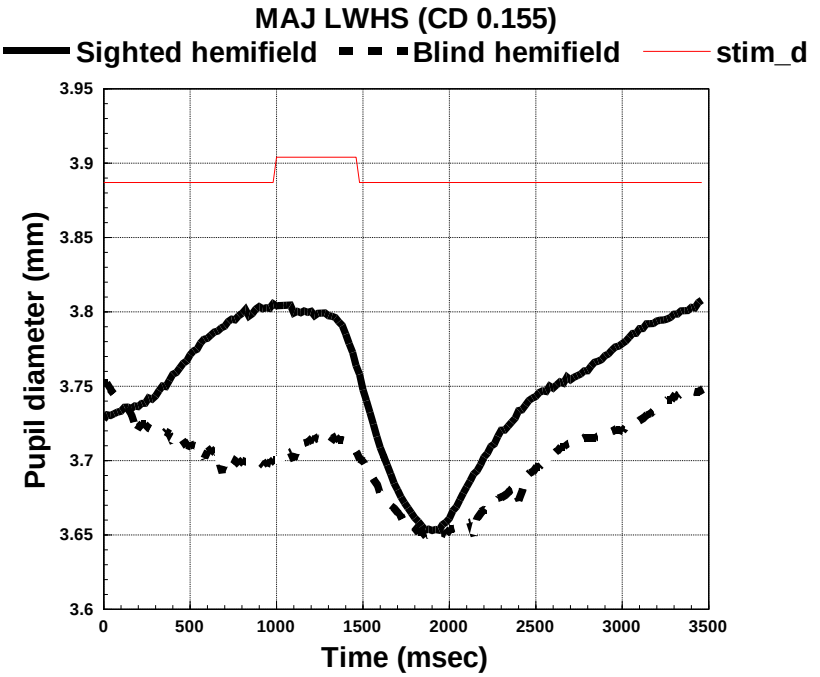

Figure 88 Three diagrams showed dilatation lag when a stimulus was presented on the blind hemifield in patients with acquired unilateral occipital lesion.

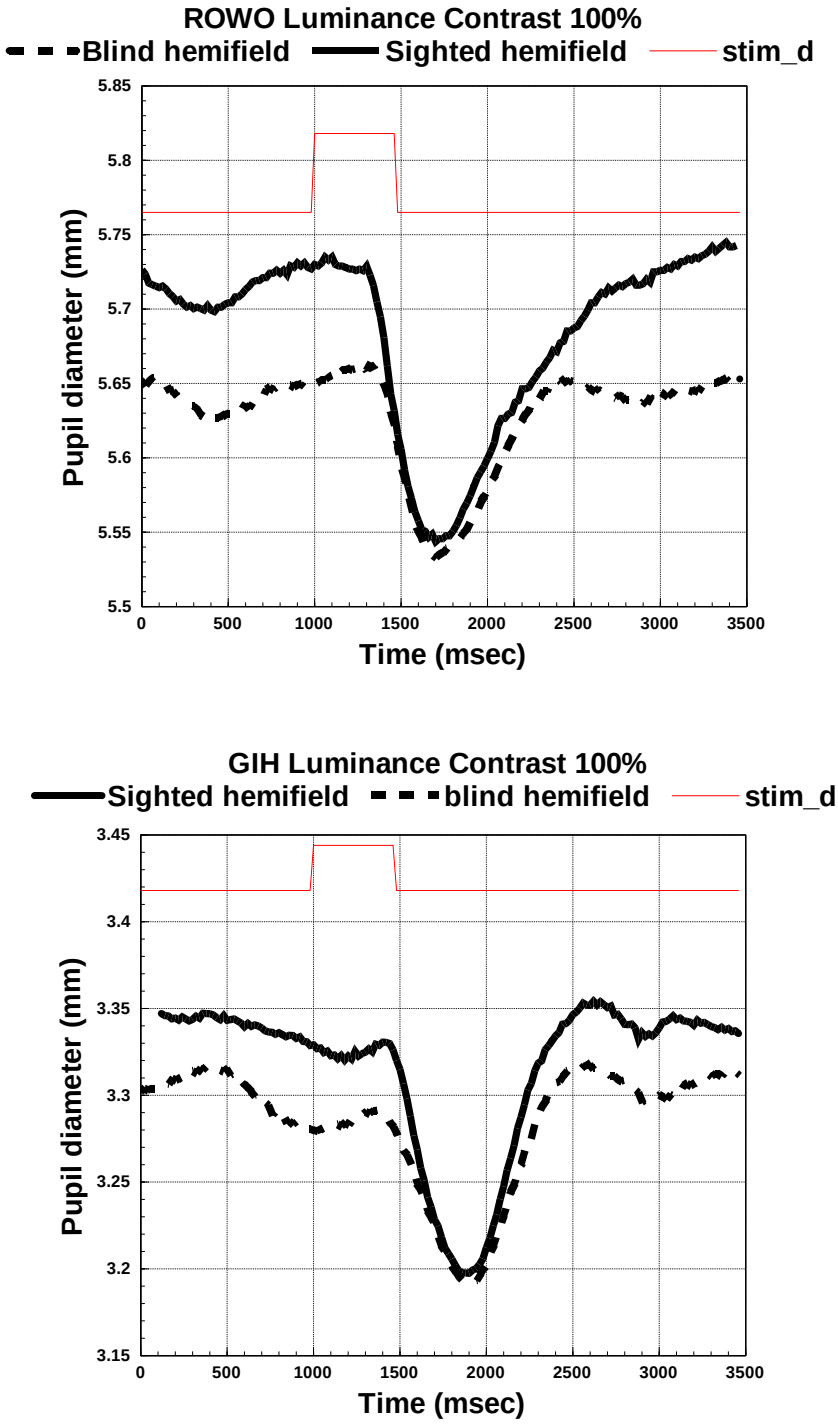

Figure 89 Two diagrams showed normal pupillary dilatation in both hemifields in a patient with occipital lesion (top) and a patient with optic radiation lesion (bottom).

10.7.5 Discussion

Dilatation lag, a characteristic of Horner's syndrome, was first identified in most patients with unilateral occipital lesion in this study. It was elicited when a stimulus was presented on the blind hemifield. The minority of patients did not show the

dilatation lag as the only responsive pupils were from 400% luminance contrast in some cases which might be due to a light leakage or spared nerve fibres. LIL who revealed negative results in other stimuli had a relatively incomplete small occipital lesion with short duration. The findings indicate that a part of sympathetic nervous system might originate from ipsilateral occipital lobe, perhaps extrastriate cortex and/or V1, before extending their fibres to subcortical areas or hypothalamus. Their fibre organization might be in a scattered pattern rather than a compact pathway since the dilatation lag was observed irregularly. The patient with a small lesion at the optic radiation did not show dilatation lag. A little review of sympathetic nervous system in the CNS was presented below.

The center of pupillary sympathetic control is the Edinger Westphal nucleus (EW). It receives peripheral and central innervations. The peripheral innervations originate from A1/A5 nuclei in the brainstem passing to the hypothalamus to the EW. The central inhibitory control in the EW receives afferents from the locus ceruleus directly (Loewenfeld, 1999). During sleep the central control is suppressed, leading to a rise in firing rate of parasympathetic tone in the EW (Sillito & Zbrozyna, 1970). The locus ceruleus is an essential source of norepinephrine (NE) projections to many areas in the brain except the hypothalamus (Bloom, 2010). NE is present in visual cortex of kitten (Gordon, Allen, & Trombley, 1988). NE fibres project from the locus ceruleus (LC) towards many areas in the visual cortex (Gordon, Allen, & Trombley, 1988). Electron microscopy reveals that terminals in the visual cortex contain dense core vesicles, possibly NE vesicles (Gordon, Allen, & Trombley, 1988). All four types of NE receptors have been demonstrated in rat visual cortex namely alpha 1, alpha 2, beta 1, and beta 2 (Gordon, Allen, & Trombley, 1988). Activation beta 2 receptor, coupling with adenylate cyclase, leads to inhibition of spontaneous firing of the cells through cyclic AMP synthesis (Gordon, Allen, & Trombley, 1988). Activation of alpha receptors leads to either excitation or inhibition (Gordon, Allen, & Trombley, 1988). It has been found that light increases the cathecholamine release in primate and cat visual cortices but not in the somatosensory cortices (mcclurkin1985). It is not certain technically if it is NE or dopamine (DA) or both. Cerebral NE and DA concentrations are low in new born kitten and high in adult cats (Jonsson & Kasamatsu, 1983). In the visual system, the LC-NE projections in primates are higher in the superior colliculus, the pulvina, and the extrastriate cortex than in the LGN

and the striate cortex (Bloom, 2010). The NE neurons in primates also project to the prefrontal cortex especially anterior cingulate cortex and dorso-medial prefrontal cortex (Bloom, 2010). Fibres from the prefrontal area project back to the LC (Aston-Jones & Cohen, 2005). This LC-NE system contributes to behavioural control (Aston-Jones & Cohen, 2005). Several studies were conducted to evaluate pupil functions during effort and attention. A study revealed that the more demanding a task was, the larger the pupil would be in a controlled light environment (Beatty J. , 1982). A recall memory to spoken digits and sentences also influence pupil size in that the more the memory load, the more pupils dilated (Piquado, 2010). In a visual feature and conjunction search task, pupil dilatation was indistinguishable between young (18-27 years) and older age (61-83) groups (Porter, Tales, Troscianko, Wilcock, Haworth, & Leonards, 2010).

Activating the hypothalamus leads to cardiovascular response (Sun, 1995). Sympathetic nerve related discharge pattern or baroreceptor reflex modulation have been recorded in the hypothalamus (Sun, 1995). The stimulation at the edge of the lateral hypothalamus by excitatory amino acids elicited depressive responses (Sun, 1995). When injecting a GABA-A agonist into the hypothalamus (same area as the excitatory amino acid injections), an opposite outcome develops (Wible Jr, Luft, & DiMicco, 1988). The increased heart rate triggered by stress can be block by injecting GABA-A agonist into the hypothalamus (Lisa, Marmo, Wible Jr, & DiMicco, 1989). As GABA-A receptor is not present in the axons; the hypothalamus is most likely to have sympathetic-excitatory neurones that control stress evoked cardiovascular responses (Sun, 1995). Fibres from the paraventricular nucleus of hypothalamus terminate at the preganglionic sympathetic neurones in the spinal cord (Luiten, ter Horst , Karst, & Steffens, 1985), the nucleus tractus solitarius (NTS), the parabrachial nuclei, the rostroventrolateral reticular nucleus (RVL), the midline PAG, the dorsal vagal nucleus, and the nucleus ambiguous (Swanson & Kuypers, 1980). The anteroventral region of the third ventricle contributes to blood pressure control (Sun, 1995). Electrical stimulation at the amygdala, a part of the limbic system, in lightly anesthetized animals increases the heart rate, blood pressure, and skeletal muscle vasodiation (Kapp, Gallagher, Underwood, McNall, & Whitehorn, 1982). The amygdala projects to the RVL and NTS directly (Takayama & Miura, 1991). The amygdala receives afferent fibres from the NTS (Saper & Loewy, 1980)

and the septal nuclei (Chiba & Masuko, 1987). Cerebral cortex controls the cardiovascular system (Hoff, Kell Jr, & Carroll Jr, 1963). Most investigations are performed with the insular cortex. Fibres from the insular cortex projects to the amygdala, the hypothalamus, the parabrachial nuclei, and the NTS; and the amydala receive inputs from other limbic systems (Sun, 1995).

11 General discussion

It has been controversial whether there is retrograde trans-synaptic degeneration (RTSD) following an acquired post-geniculate lesion in the human visual pathway. By measuring RNFL thickness with OCT, we demonstrated RTSD in patients with acquired and congenital homonymous hemianopia and quadrantanopia due to V1 or optic radiation lesions. The degree of RTSD seems to be smaller in homonymous quadrantanopia group. The magnitude of the retinal nerve fibre loss is comparable to that in patients with optic tract or optic chiasmal lesions. Furthermore RTSD has been first detected by using OCT within the first few months after unilateral post-geniculate stroke. The rate of degeneration is fastest in the first few years before becoming slower several years later. The changes are comparable to those in monkey studies. Patients who showed lower rate of RTSD within the first couple of years after stroke onset tend to have better visual outcomes. The RNFL measurement has a great potential to serve as a monitoring tool following visual pathway injury in the near future.

RTSD of the visual pathway exhibit intra-species differences since it occurs in primates and humans but not in rabbits and rats. This could be explained by sustaining collaterals theory. A nerve fibre that has several branches or collaterals could survive after axonal damage on one of its branches whereas a nerve fibre that extends no collaterals would die from an axonal injury. All retinal ganglion cells (RGCs) in rabbits and rats send all of their axons to the superior colliculus (SC) and some axons to the LGN, in contrast to humans and monkeys whose RGCs send more axons to the LGN and only 10% of axons to the SC. When LGN degenerates as a part of RTSD process, retino-geniculate fibres degenerate. The unaffected collaterals in the SC of rabbits and rats provide essential trophic factors to the RGCs; hence RGCs still maintain life. On the contrary, humans and monkeys possess insufficient SC collaterals to protect RGCs from RTSD process. We suggest that ATP and its metabolites are the crucial trophic factors that move across the synaptic site in bi-direction. Moreover there is evidence that ATP inhibits programmed cell death by interacting with P2 receptor at the cell membrane and controlling several intracellular reactions such as apoptosome suppression and mTOR enhancement. Following the death of post-synaptic neuron in RTSD, these nucleotides become

deficient at the synaptic site or LGN, leading to the death of the nearby pre-synaptic neuron inevitably. We propose that trans-synaptic anterograde/retrograde degeneration might be a consequence of programmed cell death triggered by insufficient extracellular adenine nucleotides and their metabolites

In the last pupillary chapter, two types of stimuli namely chromatic and luminance contrast were presented to homonymous hemianopia patients in either blind or sighted hemifield. We have shown pupillary hemiakinesia as a response to stimuli on the blind hemifield in patients from acquired unilateral post-geniculate lesion and also a case with unilateral tract lesion. The pupil responses to the chromatic stimuli in the acquired post-geniculate lesion seem to be smaller than those to the luminance contrast. The result is less striking in the congenital occipital lesion. It is difficult to establish a relationship between the RNFL thickness and the pupil responses in the acquired homonymous hemianopia from post-geniculate lesions. Additionally, most homonymous hemianopia patients from acquired unilateral occipital lesions have dilation lag which is a characteristic of Horner's syndrome. As far as we are aware, this is the first report of sympathetic denervation following unilateral occipital lesion. It is likely that sympathetic nervous system might originate in the cerebral hemisphere including occipital lobe before sending their fibres to the subcortical areas.

12 Appendix

12.1 Patient histories

POV: 72-year-old male presented with dense right homonymous hemianopia from left occipital meningioma removal 18 years ago. His vision has remained stable over these years and no other neurological deficit was found. His health in general is unremarkable. The average of median deviation (MD) in Humphrey perimetry 24-2 of both eyes was -13.87 dB (decibel) and the mean RNFL thickness of both eyes was 84.1 microns. Other ophthalmologic and neurological examinations were unremarkable.

GY: 53-year-old male presented with dense right homonymous hemianopia from head injury 45 years ago. The average of MD in Humphrey perimetry 24-2 of both eyes was -18 dB and the mean RNFL thickness of both eyes was 72.4 microns. His vision has not changed over these years. There were neither systemic diseases nor other neurological deficits. Other ophthalmologic and neurological examinations were unremarkable.

MAJ: 46-year-old male had a history of sudden onset of dense right homonymous hemianopia 5 years ago after renal angiogram. It was due to a cerebral infarction in the left occipito-temporal area. His vision did not change since the stroke. The average of MD in Humphrey perimetry 24-2 of both eyes was -16.83 db and the mean RNFL thickness of both eyes was 65.12 microns. Other ophthalmologic examinations were unremarkable.

JAS: 65-year-old male presented with an 18-month history of dense right homonymous hemianopia from left occipital infarction. Other ophthalmologic examinations were unremarkable. He also had another stroke from cerebellar infarction, resulting in mild gait ataxia. The average of MD in Humphrey perimetry 24-2 of both eyes was -17 dB and the mean RNFL thickness of both eyes was 89.7 microns.

GIH: 49-year-old male developed a sudden onset of left homonymous hemianopia from intracerebral haemorrhage at the right optic radiation. He had hypertension. Other ophthalmologic and neurological examinations were unremarkable. The average MD in Humphrey perimetry 24-2 of both eyes was -18.3

dB and the mean RNFL thickness of both eyes was 115.8 microns at 0.3 year post-stroke and 103.3 microns at 1.7 years post-stroke. His vision remained stable.

RID: A 56 year-old white male presented with dense right homonymous heminanopia from left optic tract lesion following head injury 4 years ago. The average RNFL thickness was 61 microns on the right and 60 microns on the left with signal strength at the level of 10 bilaterally. The signal strength of the macular measurement was 9 on both sides. The MD of Humphrey perimetry 24-2 was -17 dB. Other ophthalmologic and neurological examinations were unremarkable.

NAJ : 33-year-old Asian male, whose left homonymous hemianopia was detected in a routine eye check up. He was not aware of the defect. Past medical history included an illness since birth when he was admitted in a hospital and was treated with a respirator for several months. The exact cause of his illness was not known but he had recovered eventually. Other ophthalmologic and neurological examinations were unremarkable. The mean of both MD in Humphrey perimetry 24-2 was -13.2 dB.

ANA: 33-year-old Asian male whose left dense homonymous hemianopia had been detected in a routine eye check up. He was asymptomatic and no past medical history was noted. Other ophthalmologic and neurological examinations were unremarkable. The mean RNFL thickness of both eyes was 75.88 μm.

RIC: 22-year-old white male. He was asymptomatic and dense right homonymous hemianopia was detected in a routine eye check up. Other ophthalmologic and neurological examinations were unremarkable. The MD in Humphrey perimetry 24-2 was -19 dB. The mean RNFL thickness of both eyes was 79.51 microns (Fig.62).

DAB: 37-year-old male developed dense left homonymous hemianopia from right tract lesion after car accident. Other ophthalmologic examinations were unremarkable. The average MD in Humphrey perimetry 24-2 of both eyes was -31.7 dB and the mean RNFL thickness of both eyes was approximately 70 microns.

12.2 CIE (x,y) 1931 chromaticity diagram

(www.techmind.org, www.fho-demden.de/~hoffmann/ciegraph17052004.pdf) Colour is not an intrinsic property of objects but rather a sensation human see as a result from a given spectrum of light. There were three colour matching functions namely X, Y, and Z, which represent long, medium, and short wavelengths of light respectively and are perceived as red, green, and blue colour respectively. Each function has a wide band and overlaps with each other. CIE (x,y) 1931 chromaticity diagram identifies colour by using X and Y coordinates. The inverted U-shape represents monochromatic light or rainbow colours. Colours on the periphery are saturated and become more desaturated towards the centre. The point where X+Y+Z = 0.33 is white (Fig. 90).

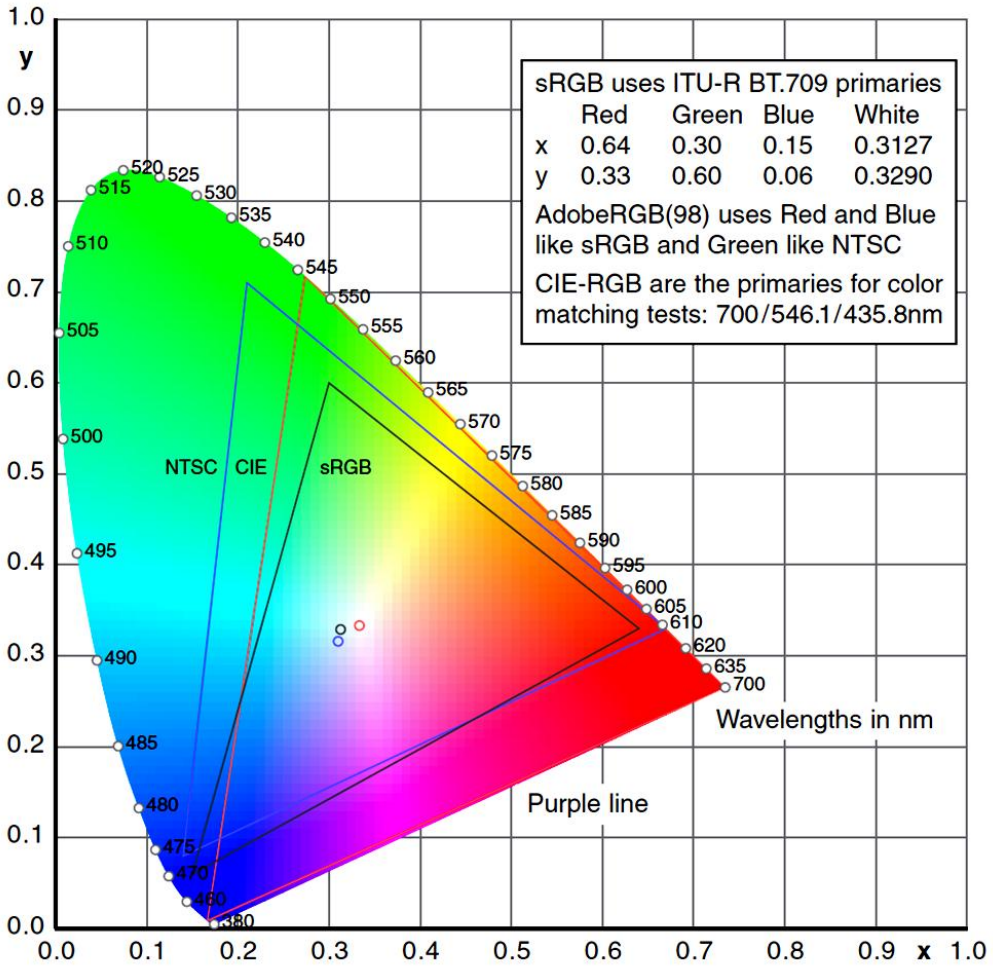

Figure 90 CIE (x,y) 1931 chromaticity diagram. Reprinted from www.fho-demden.de/~hoffmann/ciegraph17052004.pdf. Permission to reproduce this figure has been granted by Prof Gernot Hoffman.

Bibliography

Abbracchio, M. P., Burnstock, G., Boeynaems, J. M., Barnard, E. A., Boyer, J. L., Kennedy, C., et al. (2006). International Union of Pharmacology LVIII: update on the P2Y G protein-coupled nucleotide receptors: from molecular mechanisms and pathophysiology to therapy. *Pharmacol Rev, 58*, 281-341.

Abood, L. G., Koketsu, K., & Miyamoto, S. (1962). Outflux of various phosphates during membrane depolarization of excitable tissues. *Am J Physiol, 202*, 469-74.

Abood, L. G., Koketsu, K., & Noda, K. (1961). Effect of dinitrophenol on phosphorylation and bioelectric phenomena of excitable tissues. *Am J Physiol, 200*, 431-6.

Abramov, I., Gordon, J., Hendrickson, A., Hainline, L., Dobson, V., & LaBossiere, E. (1982). The retina of the newborn human infant. *Science, 217*, 265-7.

Adams, D. L., & Horton, J. C. (2003). Precise retinotopic map of primate striate cortex generated from the representation of angioscotomas. *J Neurosci, 23*, 3771-89.

Airaksinen, P. J., Drance, S. M., & Schulzer, M. (1985). Neuroretinal rim area in early glaucoma. *Am J Ophthalmol, 99*, 1-4.

Altintas, O., Iseri, P., Ozkan, B., & Cağlar, Y. (2008). Correlation between retinal morphological and functional findings and clinical severity in Parkinson's disease. *Doc Ophthalmol, 116*, 137–46.

Andresen, B. T., Gillespie, D. G., Mi, Z., Dubey, R. K., & Jackson, E. K. (1999). Role of adenosine A(1) receptors in modulating extracellular adenosine levels. *J Pharmacol Exp Ther, 291*, 76-80.

Andrews, T. J., Halpern, S. D., & Purves, D. (1997). Correlated size variations in human visual cortex, lateral geniculate nucleus, and optic tract. *J Neurosci, 17*, 2859-68.

Arthur, D. B., Georgi, S., Akassoglou, K., & Insel, P. A. (2006). Inhibition of apoptosis by P2Y2 receptor activation: novel pathways for neuronal survival. *J Neurosci, 26*, 3798 –804.

Aston-Jones, G., & Cohen, J. D. (2005). An integrative theory of locus coeruleus-norepinephrine function: adaptive gain and optimal performance. *Annu Rev Neurosci, 28*, 403–50.

Balazsi, A. G., Rootman , J., Drance , S. M., Schulzer, M., & Douglas, G. R. (1984). The effect of age on the nerve fiber population of the human optic nerve. *Am J Ophthalmol, 97*, 760-6.

Barboni, P., Savini, G., Parisi, V., Carbonelli, M., La Morgia, C., Maresca, A., et al. (2011, May 31). Retinal Nerve Fiber Layer Thickness in Dominant Optic Atrophy Measurements by Optical Coherence Tomography and Correlation with Age. *Ophthalmology*, in press.

Barbur, J. L. (2004). Learning from the pupil: studies of basic mechanisms and clinical applications. In *The visual neurosciences* (Vol. 1, pp. 641-56). Cambridge, MA: MIT press.

Barbur, J. L., Harlow , A. J., & Sahraie, A. (1992). Pupillary responses to stimulus structure, colour and movement. *Ophthalmic Physiol Opt, 12*, 137-41.

Barbur, J. L., Harlow, A. J., & Plant, G. T. (1994). Insights into the different exploits of colour in the visual cortex. *Proc Biol Sci, 258*, 327-34.

Barbur, J. L., Sahraie, A., Simmons, A., Weiskrantz, L., & Williams, S. C. (1998). Residual processing of chromatic signals in the absence of a geniculostriate projection. *Vision Res, 38*, 3447-53.

Barbur, J. L., Watson, J. D., Frackowiak, R. S., & Zeki, S. (1993). Conscious visual perception without V1. *Brain, 116*, 1293-302.

Barbur, J. L., Wolf , J., & Lennie , P. (1998). Visual processing levels revealed by response latencies to changes in different visual attributes. *Proc Biol Sci, 265*, 2321-5.

Bardoni, R., Goldstein, P. A., Lee, C. J., Gu, J. G., & MacDermott , A. B. (1997). ATP P2X receptors mediate fast synaptic transmission in the dorsal horn of the rat spinal cord. *J Neurosci, 17*, 5297-304.

Baver, S. B., Pickard, G. E., Sollars, P. J., & Pickard, G. E. (2008). Two types of melanopsin retinal ganglion cell differentially innervate the hypothalamic

suprachiasmatic nucleus and the olivary pretectal nucleus. *Eur J Neurosci, 27*, 1763–70.

Beatty, J. (1982). Task evoked pupillary responses, processing load, and the structure of processing resources. *Psychol Bull, 91*, 276-92.

Beatty, R. M., Sadun, A. A., Smith, L., Vonsattel , J. P., & Richardson Jr, E. P. (1982). Direct demonstration of transsynaptic degeneration in the human visual system: a comparison of retrograde and anterograde changes. *J Neurol Neurosurg Psychiatry, 45*, 143–6.

Beazley, L. D., & Dunlop, S. A. (1983). The evolution of an area centralis and visual streak in the marsupial Setonix brachyurus. *J Comp Neurol, 216*, 211-31.

Benevento, L. A., & Yoshida, K. (1981). The afferent and efferent organization of the lateral geniculo-prestriate pathways in the macaque monkey. *J Comp Neurol, 203*, 455-74.

Berisha, F., Feke, G. T., Trempe, C. L., McMeel, J. W., & Schepens, C. L. (2007). Retinal abnormalities in early Alzheimer's disease. *Invest Ophthalmol Vis Sci, 48*, 2285–9.

Berry, R. L., Nowicky, A., & Teyler , T. J. (1990). A slice preparation preserving the callosal projection to contralateral visual cortex. *J Neurosci Methods, 33*, 171-8.

Berson, D. M., Dunn, F. A., & Takao , M. (2002). Phototransduction by retinal ganglion cells that set the circadian clock. *Science, 295*, 1070–3.

Blakemore, C. (1969). Binocular depth discrimination and the nasotemnoral division. *J Physiol, 205*, 471-97.

Blanks, J. C., Hinton, D. R., Sadun, A. A., & Miller, C. A. (1989). Retinal ganglion cell degeneration in Alzheimer's disease. *Brain Res, 501*, 364–72.

Bleier, R. (1969). Retrograde transsynaptic cellular degeneration in mammillary and ventral tegmental nuclei following limbic decortication in rabbits of various ages. *Brain Res, 15*, 365-93.

Bloom, F. E. (2010). The catecholamine neuron: Historical and future perspectives. *Prog Neurobiol, 90*, 75-81.

Bons, N., & Petter, A. (1986). Retinal afferents of hypothalamic origin in a prosimian primate: Microcebus murinus. Study using retrograde fluorescent tracers. *C R Acad Sci III, 303*, 719–22.

Boyd, I. A., & Forrester, T. (1968). The release of adenosine triphosphate from frog skeletal muscle in vitro. *J Physiol, 199*, 115-35.

Bridge, H., Jindahra, P., Barbur, J., & Plant, G. T. (2011). Imaging reveals optic tract degeneration in hemianopia. *Invest Ophthalmol Vis Sci, 52*, 382-8.

Brouwer, B., & C Zeeman, W. P. (1926). The projection of the retina in the primary optic neuron in monkeys. *Brain, 49*, 1-35.

Bruesch, S. R., & Arey, L. B. (1942). The number of myelinated and unmyelinated fibers in the optic nerve of vertebrates. *J Comp Neurol, 77*, 631-65.

Budenz, D. L., Anderson, D. R., Varma, R., Schuman, J., Cantor, L., Savell, J., et al. (2007). Determinants of normal retinal nerve fiber layer thickness measured by Stratus OCT. *Ophthalmology, 114*, 1046-52.

Budenz, D. L., Chang, R. T., Huang, X., Knighton, R. W., & Tielsch, J. M. (2005). Reproducibility of retinal nerve fiber thickness measurements using the stratus OCT in normal and glaucomatous eyes. *Invest Ophthalmol Vis Sci, 46*, 2440-3.

Bullier, J., & Kennedy, H. (1983). Projection of the lateral geniculate nucleus onto cortical area V2 in the macaque monkey. *Exp Brain Res, 53*, 168-72.

Bunt, S. M. (1982). Retinotopic and temporal organization of the optic nerve and tracts in the adult goldfish. *J Comp Neurol, 206*, 209-26.

Burnstock, G. (2006). Historical review: ATP as a neurotransmitter. *Trends Pharmacol Sci, 27*, 166-76.

Burnstock, G. (2009). Adenosine Triphosphate (ATP). In *Encyclopedia of Neuroscience* (Vol. 1, pp. 105-13). Oxford: Academic Press.

Burnstock, G., & Kennedy, C. (1985). Is there a basis for distinguishing two types of P2-purinoceptor? *Gen Pharmacol, 16*, 433-40.

Burnstock, G., & Wood, J. N. (1996). Purinergic receptors: their role in nociception and primary afferent neurotransmission. *Curr Opin Neurobiol, 6*, 526-32.

Callaway, S., & Chatterjee, E. M. (2003). Parallel colour-opponent pathways to primary visual cortex. *Nature, 426*, 668–71.

Campbell, A. W. (1905). *Histological studies on the localisation of cerebral function.* Cambridge University Press.

Cao, D., Lee, B. B., & Sun, H. (2010). Combination of rod and cone inputs in parasol ganglion cells of the magnocellular pathway. *J Vis, 10*, 4.

Casagrande, V. A. (1994). A third parallel visual pathway to primate area V1. *Trends Neurosci, 17*, 305–10.

Chi, T., Ritch , R., Stickler , D., Pitman, B., Tsai, C., & Hsieh , F. Y. (1989). Racial differences in optic nerve head parameters. *Arch Ophthalmol, 107*, 836-9.

Chiba, T., & Masuko, S. (1987). Synaptic structure of the monoamine and peptide nerve terminals in the intermediolateral nucleus of the guinea pig thoracic spinal cord. *J comp Neurol, 262*, 242-55.

Chichilnisky, E. J. (1999). Retina. In *The MIT encyclopedia of the cognitive sciences.* MIT Press.

Coleman, M. (2005). Axon degeneration mechanisms: commonality amid diversity. *Nat Rev Neurosci, 6*, 889-98.

Compston, A., & Coles, A. (2008). Multiple sclerosis. *Lancet, 372*, 1502–17.

Conway, B. R. (2009). Color vision, cones, and color-coding in the cortex. *Neuroscientist, 15*, 274-90.

Cornwell, P., Overman, W., & Ross, C. (1978). Extent of recovery from neonatal damage to the cortical visual system in cats. *J Comp Physiol Psychol, 92*, 255-270.

Costa, R. A., Skaf, M., Melo Jr, L., Calucci, D., Cardillo, J. A., Castro, J. C., et al. (2006). Retinal assessment using optical coherence tomography. *Prog Retin Eye Res, 25*, 325–53.

Costello, F., Hodge, W., Pan, Y. I., Eggenberger, E., Coupland, S., & Kardon, R. H. (2008). Tracking retinal nerve fiber layer loss after optic neuritis: a prospective study using optical coherence tomography. *Mult Scler, 14*, 893–905.

Costello, F., Hodge, W., Pan, Y. I., Freedman, M., & DeMeulemeester, C. (2009). Differences in retinal nerve fiber layer atrophy between multiple sclerosis subtypes. *J Neurol Sci, 281*, 74-9.

Coutinho-Silva, R., Stahl, L., Cheung, K. K., de Campos, N. E., de Oliveira Souza, C., Ojcius, D. M., et al. (2005). P2X and P2Y purinergic receptors on human intestinal epithelial carcinoma cells: effects of extracellular nucleotides on apoptosis and cell proliferation. *Am J Physiol Gastrointest Liver Physiol, 288*, G1024-35.

Cowan, W. M., Fawcett, J. W., O'Leary, D. D., & Stanfield, B. B. (1984). Regressive events in neurogenesis. *Science, 225*, 1258-65.

Cowey, A. (1974). Atrophy of retinal ganglion cells after removal of striate cortex in a rhesus monkey. *Perception, 3*, 257–60.

Cowey, A. (2004). The 30th Sir Frederick Bartlett lecture. Fact, artefact, and myth about blindsight. *Q J Exp Psychol, 57*, 577–609.

Cowey, A., & Stoerig, P. (1989). Projection patterns of surviving neurones in the dorsal lateral geniculate nucleus following discrete lesions of striate cortex: Implications for residual vision. *Exp Brain Res, 75*, 631–8.

Cowey, A., & Stoerig, P. (1991). The neurobiology of blindsight. *Trends Neurosci, 14*, 140-5.

Cowey, A., Alexander, I., & Stoerig, P. (2011). Transneuronal retrograde degeneration of retinal ganglion cells and optic tract in hemianopic monkeys and humans. *Brain, 134*, 2149-57.

Cowey, A., Stoerig, P., & Bannister , M. (1994). Retinal ganglion cells labelled from the pulvinar nucleus in macaque monkeys. *Neuroscience, 61*, 691-705.

Cowey, A., Stoerig, P., & Perry, V. H. (1989). Transneuronal retrograde degeneration of retinal ganglion cells after damage to striate cortex in macaque monkeys: selective loss of P beta cells. *Neuroscience, 29*, 65–80.

Cowey, A., Stoerig, P., & Williams, C. (1999). Variance in transneuronal retrograde ganglion cell degeneration in monkeys after removal of striate cortex: effects of size of the cortical leisons. *Vision Res, 39*, 3642–52.

Crunelli, V., & Leresche, N. (1991). A role for GABAB receptors in excitation and inhibition of thalamocortical cells. *Trends Neurosci, 14*, 16-21.

Cunha, R. A., & Ribeiro, J. A. (2000). ATP as a presynaptic modulator. *Life Sci, 68*, 119-37.

Cunha, R. A., & Ribeiro, J. A. (2000). Purinergic modulation of [(3)H]GABA release from rat hippocampal nerve terminals. *Neuropharmacology, 39*, 1156-67.

Cunningham, T. J. (1982). Naturally occurring neuron death and its regulation by developing neural pathways. *Int Rev Cytol, 74*, 163-86.

Curcio, C. A., & Allen, K. A. (1990). Topography of ganglion cells in human retina. *J Comp Neurol, 300*, 5-25.

Curcio, C. A., & Drucker, D. N. (1993). Retinal ganglion cells in Alzheimer's disease and aging. *Ann Neurol, 33*, 248–57.

Dacey, D. (2004). Origins of perception: retinal ganglion cell diversity and the creation of parallel visual pathways. In M. Gazzaniga, *The Cognitive Neurosciences* (pp. 281-301). MIT Press.

Dacey, D. M., Peterson, B. B., Robinson, F. R., & Gamlin, P. D. (2003). Fireworks in the primate retina: in vitro photodynamics reveals diverse LGN-projecting ganglion cell types. *Neuron, 37*, 15-27.

Dacey, D., & Lee, B. (1994). The 'blue-on' opponent pathway in primate retina originates from a distinct bistratified ganglion cell type. *Nature, 367*, 731–5.

D'Ambrosi, N., Cavaliere, F., Merlo, D., Milazzo, L., Mercanti, D., & Volonté, C. (2000). Antagonists of P2 receptor prevent NGF-dependent neuritogenesis in PC12 cells. *Neuropharmacology, 39*, 1083–94.

D'Ambrosi, N., Murra, B., Cavaliere, F., Amadio, S., Bernardi, G., Burnstock, G., et al. (2001). Interaction between ATP and nerve growth factor signalling in the survival and neuritic outgrowth from PC12 cells. *Neuroscience, 108*, 527–34.

Danek, A., Bauer, M., & Fries, W. (1990). Tracing neuronal connections in the human brain by magnetic resonance imaging in vivo. *Eur J Neurosci, 2*, 112-5.

Danesh-Meyer, H. V., Birch, H., Ku, J. Y., Carroll, S., & Gamble, G. (2006). Reduction of optic nerve fibers in patients with Alzheimer disease identified by laser imaging. *Neurology, 67*, 1852–4.

Davis, J. N., & McKinnon, P. N. (1982). Anterograde and transcellular transport of a fluorescent dye, bisbenzimide, in the rat visual system. *Neurosci Lett, 29*, 207-12.

De Monasterio, F. M., & Gouras, P. (1975). Functional properties of ganglion cells of the rhesus monkey retina. *J Physiol, 251*, 167-95.

De Seze, J., Blanc, F., Jeanjean, L., Zéphir, H., Labauge, P., Bouyon, M., et al. (2008). Optical coherence tomography in neuromyelitis optica. *Arch Neurol, 65*, 920–3.

Dean, G., & Usher, C. H. (1903). Experimental research on the course of the optic fibres. *Brain, 26*, 524-42.

Di Virgilio, F., Chiozzi, P., Falzoni, S., Ferrari, D., Sanz, J. M., Venketaraman, V., et al. (1998). Cytolytic P2X purinoceptors. *Cell Death Differ, 5*, 191-9.

Dineen, J. T., & Hendrickson, A. E. (1981). Age correlated differences in the amount of retinal degeneration after striate cortex lesions in monkeys. *Invest Ophthalmol Vis Sci, 21*, 749-52.

Dineen, J., Hendrickson, A., & Keating, E. G. (1982). Alterations of retinal inputs following striate cortex removal in adult monkey. *Exp Brain Res, 47*, 446-56.

Djamgoz, M. B., Hankins, M. W., Hirano, J., & Archer, S. N. (1997). Neurobiology of retinal dopamine in relation to degenerative states of the tissue. *Vision Res, 37*, 3509–29.

Dodt, E. (1956). Centrifugal impulses in rabbit's retina. *J Neurophysiol, 19*, 301-7.

Dotty, R. W. (1961). Functional significance of the topographical aspects of the retinocortical projection. In R. J. Kronhuber (Ed.), *The visual system: Neurophysiology and psychophysics.* Heidelberg: Spring-Verlag.

Doty, R. W. (1971). Survival of pattern vision after removal of striate cortex in the adult cat. *J Comp Neurol, 143*, 341-69.

Duke-Elder, W. S. (1932). *Textbook of ophthalmology* (Vol. 1). St Louis: The CV Mosby company.

Dunwiddie, T. V., & Masino, S. A. (2001). The role and regulation of adenosine in the central nervous system. *Annu Rev Neurosci, 24*, 31-55.

Dunwiddie, T. V., Diao, L., & Proctor, W. R. (1997). Adenine nucleotides undergo rapid, quantitative conversion to adenosine in the extracellular space in rat hippocampus. *J Neurosci, 17*, 7673-82.

Ecker, J. L., Dumitrescu, O. N., Wong, K. Y., Alam, N. M., Chen, S. K., LeGates, T., et al. (2010). Melanopsin-Expressing Retinal Ganglion-Cell Photoreceptors: Cellular Diversity and Role in Pattern Vision. *Neuron, 67*, 49-60.

Edwards, F. A., & Gibb, A. J. (1993). ATP--a fast neurotransmitter. *FEBS Lett, 325*, 86-9.

Edwards, F. A., Gibb, A. J., & Colquhoun, D. (1992). ATP receptor-mediated synaptic currents in the central nervous system. *Nature, 359*, 144–7.

Evans, R. J., Derkach, V., & Surprenant, A. (1992). ATP mediates fast synaptic transmission in mammalian neurons. *Nature, 357*, 503-5.

Ferreira, J. M., & Paes-de-Carvalho, R. (2001). Long-term activation of adenosine A(2a) receptors blocks glutamate excitotoxicity in cultures of avian retinal neurons. *Brain Res, 900*, 169–76.

Field, G. D., Greschner, M., Gauthier, J. L., Rangel, C., Shlens, J., Sher, A., et al. (2009). High-sensitivity rod photoreceptor input to the blue-yellow color opponent pathway in macaque retina. *Nat Neurosci, 12*, 1159-64.

Field, G., & Chichilnisky, E. (2007). Information processing in the primate retina: circuitry and coding. *Annu Rev Neurosci, 30*, 1–30.

Fisher, J. B., Jacobs, D. A., Markowitz, C. E., Galetta, S. L., Volpe, N. J., Nano-Schiavi, M. L., et al. (2006). Relation of visual function to retinal nerve fiber layer thickness in multiple sclerosis. *Ophthalmology, 113*, 324–32.

Fitzek, C., Fitzek, S., & Stoeter, P. (2004). Bilateral Wallerian degeneration of the medial cerebellar peduncles after ponto-mesencepahalic infarction. *Eur J Radiol, 49*, 198-203.

Fitzgibbon, T., & Taylor, S. F. (1996). Retinotopy of the human retinal nerve fibre layer and optic nerve head. *J Comp Neurol, 375*, 238-51.

Fitzpatrick, D., Itoh, K., & Diamond, I. T. (1983). The laminar organization of the lateral geniculate body and the striate cortex in the squirrel monkey (Saimiri sciureus). *J Neurosci, 3*, 673-702.

Fletcher, W. A., Hoyt, W. F., & Narahara, M. H. (1988). Congenital quadrantanopia with occipital lobe ganglioglioma. *Neurology, 38*, 1892–4.

Franke, H., Günther, A., Grosche, J., Schmidt, R., Rossner, S., Reinhardt, R., et al. (2004). P2X7 receptor expression after ischemia in the cerebral cortex of rats. *J Neuropathol Exp Neurol, 63*, 686–99.

Fries, W. (1981). The projection from the lateral geniculate nucleus to the prestriate cortex of the macaque monkey. *Proc R Soc Lond B Biol Sci., 213*, 73-86.

Fugimoto, J. G., Brezinski, M. E., Tearney, G. J., Boppart, S. A., Bouma, B., Hee, M. R., et al. (1995). Optical biopsy and imaging using optical coherence tomography. *Nat Med, 1*, 970–2.

Fukuda, Y., Sawai, H., Watanabe, M., Wakakuwa, K., & Morigiwa, K. (1989). Nasotemporal Overlap of Crossed and Uncrossed Retinal Ganglion Cell Projections in the Japanese Monkey (Macaca fuscafa). *J Neurosci, 9*, 2353-73.

Gamlin, P. D., Peterson, B. B., & Dacey, D. M. (2001). Physiology and morphology of retinal ganglion cells projecting to the pretectal olivary nucleus of the rhesus monkey. *Invest Ophthalmol Vis Sci, (Suppl) 42*, 676.

Garey, L. J., Jones, E. G., & Powell, T. P. (1968). Interrelationships of striate and extrastriate cortex with the primary relay sites of the visual pathway. *J Neurol Neurosurg Psychiatry, 31*, 135-57.

Glovinsky, Y., Quigley, H. A., & Dunkelberger, G. R. (1991). Retinal Ganglion Cell Loss Is Size Dependent in Experimental Glaucoma. *Invest Ophthalmol Vis Sci, 32*, 484-91.

Goldberg, S., & Coulombre, A. J. (1972). Topographical development of the ganglion cell fibre layer in the chick retina. A whole mount study. *J Comp Neurol, 146*, 507-18.

Gordon, B., Allen, E. E., & Trombley, P. Q. (1988). The role of norepinephrine in plasticity of visual cortex. *Prog Neurobiol, 30*, 171-91.

Gordon-Lipkin, E., Chodkowski, B., Reich, D. S., Smith, S. A., Pulicken, M., Balcer, L. J., et al. (2007). Retinal nerve fiber layer is associated with brain atrophy in multiple sclerosis. *Neurology, 69*, 1603–9.

Gosavi, V. S., & Dubey, P. N. (1972). Projection of striate cortex to the dorsal lateral geniculate body in the rat. *J Anat, 113*, 75-82.

Gozuacik, D., & Kimchi, A. (2004). Autophagy as a cell death and tumor suppressor mechanism. *Oncogene, 23*, 2891-906.

Granit, R. (1955a). Centrifugal and antidromic effects on ganglion cells of retina. *J Neurophysiol, 18*, 388-411.

Granit, R. (1955b). *Receptors and sensory perception.* New Haven: Yale university press.

Grazioli, E., Zivadinov, R., Weinstock-Guttman, B., Lincoff, N., Baier, M., Wong, J. R., et al. (2008). Retinal nerve fiber layer thickness is associated with brain MRI outcomes in multiple sclerosis. *J Neurol Sci, 268*, 12-7.

Green, A. J., & Cree, B. A. (2009). Distinctive retinal nerve fiber layer and vascular changes in neuromyelitis optica. *J Neurol Neurosurg Psychiatry, 80*, 1002-5.

Gu, J. G., Foga, I. O., Parkinson, F. E., & Geiger, J. D. (1995). Involvement of bidirectional adenosine transporters in the release of L-[3H]adenosine from rat brain synaptosomal preparations. *J Neurochem, 64*, 2105– 10.

Guillery, R. W. (1967). Patterns of fiber degeneration in the dorsal lateral geniculate nucleus of the cat following lesions in the visual cortex. *J Comp Neurol, 130*, 197-221.

Güler, A. D., Ecker, J. L., Lall, G. S., Haq, S., Altimus, C. M., Liao, H. W., et al. (2008). Melanopsin cells are the principal conduits for rod-cone input to non-image-forming vision. *Nature, 453*, 102-5.

Gupta, N., Ang, L. C., De Tilly, L. N., Bidaisee, L., & Yücel, Y. H. (2006). Human glaucoma and neural degeneration in intracranial optic nerve, lateral geniculate nucleus, and visual cortex. *Br J Ophthalmol, 90*, 674-8.

Gupta, N., Greenberg, G., De Tilly, L. N., Gray, B., Polemidiotis, M., & Yücel, Y. H. (2009). Atrophy of the lateral geniculate nucleus in human glaucoma detected by magnetic resonance imaging. *Br J Ophthalmol, 93*, 56-60.

Hajee, M. E., March, W. F., Lazzaro, D. R., Wolintz, A. H., Shrier, E. M., Glazman, S., et al. (2009). Inner retinal layer thinning in Parkinson disease. *Arch Ophthalmol, 127*, 737–41.

Halassa, M. M., Fellin, T., & Haydon, P. G. (2007). The tripartite synapse: roles for gliotransmission in health and disease. *Trends Mol Med, 13*, 54-63.

Harden, T. K., & Lazarowski, E. R. (1999). Release of ATP and UTP from astrocytoma cells. *Prog Brain Res, 120*, 135-43.

Harman, A., Abrahams, B., Moore, S., & Hoskins, R. (2000). Neuronal density in the human retinal ganglion cell layer from 16-77 years. *Anat Rec, 260*, 124-31.

Harnois, C., & Di Paolo, T. (1990). Decreased dopamine in the retinas of patients with Parkinson's disease. *Invest Ophthalmol Vis Sci, 31*, 2473–5.

Harwerth, R. S., Carter-Dawson, L., Shen, F., Smith 3rd, E. L., & Crawford, M. L. (1999). Ganglion cell losses underlying visual field defects form experimental glaucoma. *Invest Ophthalmol Vis Sci, 40*, 2242-50.

He, Z. (2010). Intrinsic control of axon regeneration. *J Biomed Res, 24*, 2-5.

Heimel, A. J., Van Hooser, S. D., & Nelson, S. B. (2005). Laminar Organization of Response Properties in Primary Visual Cortex of the Gray Squirrel (Sciurus carolinensis). *J Neurophysiol, 94*, 3538 –54.

Heine, C., Heimrich, B., Vogt, J., Wegner, A., Illes, P., & Franke, H. (2006). P2 receptor-stimulation influences axonal outgrowth in the developing hippocampus in vitro. *Neuroscience, 138*, 303-11.

Henderson, A. P., Trip, S. A., Schlottmann, P. G., Altmann, D. R., Garway-Heath, D. F., Plant, G. T., et al. (2008). An investigation of the retinal nerve fibre layer in progressive multiple sclerosis using optical coherence tomography. *Brain, 131*, 277–87.

Herbin, M., Boire, D., Théoret, H., & Ptito, M. (1999). Transneuronal degeneration of retinal ganglion cells in early hemispherectomized monkeys. *Neuroreport, 10*, 1447-52.

Hinds, J. W., & Hinds, P. L. (1978). Early development of amacrine cells in the mouse retina: an electron microscopic, serial section analysis. *J Comp Neurol, 179*, 277-300.

Hinton, D. R., Sadun, A. A., Blanks, J. C., & Miller, C. A. (1986). Optic-nerve degeneration in Alzheimer's disease. *N Engl J Med, 315*, 485–7.

Hoff, E. C., Kell Jr, J. F., & Carroll Jr, M. N. (1963). Effects of cortical stimulation and lesions on cardiovascular function. *Physiol Rev, 43*, 68-114.

Hollander, H. (1972). Autoradiographic evidence for a projection from the striate cortex to the dorsal part of the lateral geniculate nucleus in the cat. *Brain Res, 41*, 464-6.

Hollyfield, J. G. (1972). Histogenesis of the retina in the killfish, Fundulum heteroclitum. *J Comp Neurol, 144*, 373-80.

Holmes, G., & Stewart, T. G. (1908). On the connection of the inferior olives with the cerebellum in man. *Brain, 31*, 125–37.

Holton, F. A., & Holton, P. (1953). The possibility that ATP is a transmitter at sensory nerve endings. *J Physiol, 119*, 50P-51P.

Horoupian, D. S., Ghetti, B., & Wiśniewski, H. M. (1973). Retrograde transneuronal degeneration of optic fibers and their terminals in lateral geniculate nucleus of Rhesus monkey. *Brain Res, 49*, 257-75.

Horton, J. C., & Hoyt, W. F. (1991). Quadrantic visual field defects. A hallmark of lesions in extrastriate (V2/V3) cortex. *Brain, 114*, 1703-18.

Horton, J. C., Greenwood, M. M., & Hubel, D. H. (1979). Non-retinotopic arrangement of fibres in cat optic nerve. *Nature, 282*, 720-2.

Hoyt, W. F., & Kommerell, G. (1973). Fundus oculi in homonymous hemianopia. *Klin Monbl Augenheilkd, 162*, 456–64.

Hoyt, W. F., Rios-Montenegro, E. N., Behrens, M. M., & Eckelhoff, R. J. (1972). Homonymous hemioptic hypoplasia. Fundoscopic features in standard and

red-free illumination in three patients with congenital hemiplegia. *Br J Ophthalmol, 56*, 537-45.

Huang, D., Swanson, E. A., Lin, C. P., Schuman, J. S., Stinson, W. G., Chang, W., et al. (1991). Optical coherence tomography. *Science, 254*, 1178–81.

Hubel, D. H., & Wiesel, T. N. (1960). Receptive fields of optic nerve fibres in the spider monkey. *J Physiol, 154*, 572-80.

Hübener, M., & Bolz, J. (1988). Morphology of identified projection neurons in layer 5 of rat visual cortex. *Neurosci Lett, 94*, 76-81.

Humphrey, N. K. (1974). Vision in a monkey without striate cortex: a case study. *Perception, 3*, 241-55.

Inzelberg, R., Ramirez, J. A., Nisipeanu, P., & Ophir, A. (2004). Retinal nerve fiber layer thinning in Parkinson disease. *Vision Res, 44*, 2793–7.

Ionuye, T. (1909). *Die Sehsto¨rungen bei Schussverletzungen der kortikalen Sehspha¨re nach Beobachtungen an Verwundeten der letzten japanischen Kriege.* Leipzig: Engelmann.

Iseri, P. K., Altinas, O., Tokay, T., & Yüksel, N. (2006). Relationship between cognitive impairment and retinal morphological and visual functional abnormalities in Alzheimer disease. *J Neuroophthalmol, 26*, 18–24.

Israël, M., Lesbats, B., Manaranche, R., Meunier, F. M., & Frachon, P. (1980). Retrograde inhibition of transmitter release by ATP. *J Neurochem, 34*, 923-32.

Jacobson, L., Hård, A. L., Svensson, E., Flodmark, O., & Hellström, A. (2003). Optic disc morphology may reveal timing of insult in children with periventricular leucomalacia and/or periventricular haemorrhage. *Br J Ophthalmol, 87*, 1345–9.

Jarvis, M. F., & Khakh, B. S. (2009). ATP-gated P2X cation-channels. *Neuropharmacology, 56*, 208-15.

Jindahra, P., Petrie, A., & Plant, G. T. (2009). Retrograde trans-synaptic retinal ganglion cell loss identified by optical coherence tomography. *brain, 132*, 628-34.

Jo, Y. H., & Schlichter, R. (1999). Synaptic corelease of ATP and GABA in cultured spinal neurons. *Nat Neurosci, 2*, 241-5.

Johnson, B. M., Miao, M., & Sadun, A. A. (1987). Age-related decline of human optic nerve axon populations. *Age, 10*, 5-9.

Johnson, E. N., Hawken, M. J., & Shapley, R. (2001). The spatial transformation of color in the primary visual cortex of the macaque monkey. *Nat Neurosci, 4*, 409-16.

Johnson, E. N., Van Hooser, S. D., & Fitzpatrick, D. (2010). The representation of S-cone signals in primary visual cortex. *J Neurosci, 30*, 10337–50.

Johnson, H., & Cowey, A. (2000). Transneuronal retrograde degeneration of retinal ganglion cells following restricted lesions of striate cortex in the monkey. *Exp Brain Res, 132*, 269-75.

Jonas, J. B., Gusek, G. C., & Naumann, G. O. (1988). Optic Disc, cup and neurorefinal rim size, configuration and correlations in normal eyes. . *Invest Ophthalmol Vis Sci, 29*, 1151-8.

Jonas, J. B., Müller-Bergh, J. A., Schlötzer-Schrehardt, U. M., & Naumann, G. O. (1990). Histomorphometry of the human optic nerve. *Invest Ophthalmol Vis Sci, 31*, 736-44.

Jonas, J. B., Nguyen, N. X., & Naumann, G. O. (1989). Optic disc morphometry in simple optic nerve atrophy. *Acta Ophthalmol (Copenh), 67*, 199-203.

Jonas, J. B., Schmidt, A. M., Müller-Bergh, J. A., Schlötzer-Schrehard, U. M., & Naumann, G. O. (1992). Human optic nerve fiber count and optic disc size. *Invest Ophthalmol Vis Sci, 33*, 2012-8.

Jonsson, G., & Kasamatsu, T. (1983). Maturation of monoamine neurotransmitters and receptors in cat occipital cortex during postnatal critical period. *Exp Brain Res, 50*, 449-58.

Kaas, J. H., Huerta, M. F., Weber, J. T., & Harting, J. K. (1978). Patterns of retinal terminations and laminar organization of the lateral geniculate nucleus of primates. *J Comp Neurol, 182*, 517-53.

Kanamori, A., Nakamura, M., Matsui, N., Nagai, A., Nakanishi, Y., Kusuhara, S., et al. (2004). Optical coherence tomography detects characteristic retinal nerve fiber layer thickness corresponding to band atrophy of the optic discs. *Ophthalmology, 111*, 2278-83.

Kaplan, E., Lee, B. B., & Shapley, R. M. (1990). New views of primate retinal function. *Prog Retinal Res, 9*, 273–336 .

Kapp, B. S., Gallagher, M., Underwood, M. D., McNall, C. L., & Whitehorn, D. (1982). Cardiovascular responses elicited by electrical stimulation of the amygdala central nucleus in the rabbit. *Brain Res, 234*, 251-62.

Kaushik, S., Pandav, S. S., Ichhpujani, P., & Gupta, A. (2009). Fixed diameter scan protocol preferable for retinal nerve fiber layer measurement by Optical Coherence Tomography in all sizes of optic discs. *Br J Ophthalmol, 93*, 895-900.

Khakh, B. S., & North, R. A. (2006). P2X receptors as cell-surface ATP sensors in health and disease. *Nature, 442*, 527-32.

Klistorner, A., Arvind, H., Nguyen, T., Garrick, R., Paine, M., Graham, S., et al. (2008). Axonal loss and myelin in early ON loss in postacute optic neuritis. *Ann Neurol, 64*, 325–31.

Knighton, R. W., Huang, X. R., & Greenfield, D. S. (2002). Analytical model of scanning laser polarimetry for retinal nerve fiber layer assessment. *Invest Ophthalmol Vis Sci, 43*, 383–92.

Koch, C. (1987). The action of the corticofugal pathway on sensory thalamic nuclei: a hypothesis. *Neuroscience, 23*, 399-406.

Kondo, Y., Takada, M., Tokuno, H., & Mizuno, N. (1994). Single retinal ganglion cells projecting bilaterally to the lateral geniculate nuclei or superior colliculi by way of axon collaterals in the cat. *J Comp Neurol, 346*, 119-26.

Koshinaga, M., & Whittemore, S. R. (1995). The temporal and spatial activation of microglia in fibre tracts undergoing anterograde and retrograde degeneration following spinal cord lesion. *J Neurotrauma, 12*, 209-22.

Kourouyan, H. D., & Horton, J. C. (1997). Transneuronal retinal input to the primate Edinger- Westphal nucleus. *J Comp Neurol, 381*, 68-80.

Kovács, Z., Dobolyi, A., Juhász, G., & Kékesi, K. A. (2010). Nucleoside map of the human central nervous system. *Neurochem Res, 35*, 452-64.

Krist, R., Hoffmann, E. M., & Schwenn, O. (2005). Reproducibility of measurements of the peripapillary retinal nerve fibre layer thickness. Optical coherence tomography versus retinal thickness analyzer. *Ophthalmologe, 102*, 1175-8.

Kupersmith, M. J., Vargas, M., Hoyt, W. F., & Berenstein, A. (1994). Optic tract atrophy with cerebral arteriovenous malformations: direct and transsynaptic degeneration. *Neurology, 44*, 80-3.

Kupfer, C. (1963). Retinal ganglion cell degeneration following chiasmal lesions in man. *Arch Ophthalmol, 70*, 256-60.

Labandeira-Garcia, J. L., Guerra-Seijas, M. J., Gonzalez, F., Perez, R., & Acuña, C. (1990). Location of neurons projecting to the retina in mamals. *Neurosci Res, 8*, 291–302.

Labar, D. R., Berman, N. E., & Murphy, E. H. (1981). Short- and long-term effects of neonatal and adult visual cortex lesions on the retinal projection to the pulvinar in cats. *J Comp Neurol, 197*, 639-59.

Lagrèze, W. D., & Kordon, R. H. (1998). Correlation of relative afferent pupillary defect and estimated retinal ganglion cell loss. *Graefes Arch Clin Exp Ophthalmol, 236*, 401–4.

Latini, S., Bordoni, F., Corradetti, R., Pepeu, G., & Pedata, F. (1998). Temporal correlation between adenosine outflow and synaptic potential inhibition in rat hippocampal slices during ischemia-like conditions. *Brain Res, 794*, 325-8.

Lee, B. B., Smith, V. C., Pokorny, J., & Kremers, J. (1997). Rod inputs to macaque ganglion cells. *Vision Res, 37*, 2813–28.

Lee, F. S., & Chao, M. V. (2001). Activation of Trk neurotrophin receptors in the absence of neurotrophins. *Proc Natl Acad Sci U S A, 98*, 3555–60.

Lee, F. S., Rajagopal, R., & Chao, M. V. (2002). Distinctive features of Trk neurotrophin receptor transactivation by G protein-coupled receptors. *Cytokine Growth Factor Rev, 13*, 11-7.

Leventhal, A. G., Thompson, K. G., Liu, D., Zhou, Y., & Ault, S. J. (1995). Concomitant sensitivity to orientation, direction, and color of cells in layers 2, 3, and 4 of monkey striate cortex. *J Neurosci, 15*, 1808-18.

Lin, H., & Ingram, W. R. (1973). Axonal degeneration in the peripheral optic pathway of the cat. *Exp Neurol, 39*, 234-48.

Lin, H., & Ingram, W. R. (1974). Retrograde degeneration of primary optic fibers in the cat. *Exp Neurol, 44*, 21-34.

Linden, R., & Perry, V. H. (1983). Massive retinotectal projection in rats. *Brain Res, 272*, 145-9.

Lisa, M., Marmo, E., Wible Jr, J. H., & DiMicco, J. A. (1989). Injection of muscimol into posterior hypothalamus blocks stress-induced tachycardia. *Am J Physiol, 257*, R246-51.

Liu, J., & Wandell, B. A. (2005). Specializations for chromatic and temporal signals in human visual cortex. *J Neurosci, 30*, 3459-68.

Loesch, A., & Burnstock, G. (1998). Electron-immunocytochemical localization of P2X1 receptors in the rat cerebellum. *Cell Tissue Res, 294*, 253 - 60.

Loesch, A., Miah, S., & Burnstock, G. (1999). Ultrastructural localisation of ATP-gated P2X2 receptor immunoreactivity in the rat hypothalamo-neurohypophysial system. *J Neurocytol, 28*, 495–504.

Loewenfeld, I. E. (1999). *The pupil: anatomy, physiology and clinical applications.* Boston: Butterworth Heinemann.

Luiten, P. G., ter Horst , G. J., Karst, H., & Steffens, A. B. (1985). The course of paraventricular hypothalamic efferents to autonomic structures in medulla and spinal cord. *Brain Res, 329*, 374-8.

Lundström, M., & Frisén, L. (1975). Evolution of descending optic atrophy. A case report. *Acta Ophthalmol (Copenh), 53*, 738-46.

Malmo, R. B. (1966). Effects of striate cortex ablation on intensity discrimination and spectral intensity distribution in the rhesus monkey. *Neuropsychologia, 4*, 9-26.

Marshak, D. W. (2009). Retinal ganglion cells: Anatomy. In *Encyclopedia of Neuroscience* (pp. 211-218). Elsevier Ltd.

Martin, P. R., White, A. J., Goodchild, A. K., Wilder, H. D., & Sefton, A. E. (1997). Evidence that Blue-on Cells are Part of the Third Geniculocortical Pathway in Primates. *Eur J Neurosci, 9*, 1536-41.

Masino, S. A., & Dunwiddie, T. V. (1999). Temperature-dependent modulation of excitatory transmission in hippocampal slices is mediated by extracellular adenosine. *J Neurosci, 19*, 1932-9.

Masino, S. A., Latini, S., Bordoni, F., Pedata, F., & Dunwiddie, T. V. (2001). Changes in hippocampal adenosine efflux, ATP levels, and synaptic transmission induced by increased temperature. *Synapse, 41*, 58–64.

Masland, R. (2001). The fundamental plan of the retina. *Nat Neurosci, 4*, 877–86.

Mastronarde, D. N., Thibeault, M. A., & Dubin, M. W. (1984). Non-uniform postnatal growth of the cat retina. *J Comp Neurol, 228*, 598-608.

McDonald, W. I. (1984). Multiple sclerosis: epidemiology and HLA associations. *Ann N Y Acad Sci, 436*, 109–17.

Mehta, J. S., & Plant, G. T. (2005a). OCT and band atrophy correlation. *Ophthalmology, 112*, 2055–6.

Mehta, J. S., & Plant, G. T. (2005b). Optical coherence tomography findings in congenital/longstanding homonymous hemianopia. *Am J Ophthalmol, 140*, 727–9.

Merigan, W. H., & Eskin, T. A. (1986). Spatio-temporal vision of macaques with severe loss of P beta retinal ganglion cells. *Vision Res, 26*, 1751-61.

Merle, H., Olindo, S., Donnio, A., Richer, R., Smadja, D., & Cabre, P. (2008). Retinal peripapillary nerve fiber layer thickness in neuromyelitis optica. *Invest Ophthalmol Vis Sci, 49*, 4412–7.

Meunier, F., Israël, M., & Lesbats, B. (1975). Release of ATP from stimulated nerve electroplaque junctions. *Nature, 257*, 407-8.

Meyer, P. M. (1963). Analysis of visual behavior in cats with extensive neocortical ablations. *J Comp Physiol Psychol, 56*, 397-401.

Mihailović , L. T., Cupić, D., & Dekleva, N. (1971). Changes in the numbers of neurons and glial cells in the lateral geniculate nucleus of the monkey during retrograde cell degeneration. *J Comp Neurol, 142*, 223-9.

Miller. (2009). *Encyclopedia of neuroscience*, 523-529.

Miller, N. R., & Newman, S. A. (1981). Transsynaptic degeneration. *Arch Ophthalmol, 99*, 1654.

Murphy, E. H., Mize, R. R., & Schechter, P. B. (1975). Visual discrimination following infant and adult ablation of cortical areas 17, 18, and 19 in the cat. *Exp Neurol, 49*, 386-405.

Naismith, R., Tutlam, N., Xu, J., Klawiter, E. C., Shepherd, J., Trinkaus, K., et al. (2009a). Optical coherence tomography differs in neuromyelitis optica compared with multiple sclerosis. *Neurology, 72*, 1077–82.

Naismith, R., Tutlam, N., Xu, J., Shepherd, J. B., Klawiter, E. C., Song, S. K., et al. (2009b). Optical coherence tomography is less sensitive than visual evoked potentials in optic neuritis. *Neurology, 73*, 46–52.

Naito, J. (1986). Course of retinogeniculate projection fibres in the cat optic nerve. *J Comp Neurol, 251*, 376-87.

Naito, J. (1989). Retinogeniculate projection fibers in the monkey optic nerve:a demonstration of the fiber pathways by retrograde axonal transport of WGA-HRP. *J Comp Neurol, 284*, 174–86.

Nakanishi, Y., Nakamura, M., Tatsumi, Y., Nagai-Kusuhara, A., & Negi, A. (2006). Quantification of retinal nerve fiber layer thickness reduction associated with a relative afferent pupillary defect. *Graefes Arch Clin Exp Ophthalmol, 244*, 1480-4.

Nealey, T. A., & Maunsell, J. H. (1994). Magnocellular and parvocellular contributions to the responses of neurons in macaque striate cortex. *J Neurosci, 14*, 2069-79.

Neary, J. T., & Zimmermann, H. (2009). Trophic functions of nucleotides in the central nervous system. *Trends Neurosci, 32*, 189-98.

Nettleship, E. (1896). Experimental research on the course of the optic nerve fibres. *Br Med J, 2*, 71-2.

Nie, D., Di Nardo, A., Han, J. M., Baharanyi, H., Kramvis, I., Huynh, T., et al. (2010). Tsc2-Rheb signaling regulates EphA-mediated axon guidance. *Nat Neurosci, 13*, 163-72.

Nieber, K., Poelchen, W., & Illes, P. (1997). Role of ATP in fast excitatory synaptic potentials in locus coeruleus neurones of the rat. *Br J Pharmacol, 122*, 423-30.

Ogden, T. E. (1983). Nerve fibre layer of the macaque retina: retinotopic organization. *Invest Ophthalmol Vis Sci, 24*, 85-98.

Olmsted, D. D. (2006). *Frog and toad eyes.* Simple brain stimulation resources (http://neurocomputing.org/FrogEye.aspx).

Oppel, O. (1963). Microscopic investigations of the number and caliber of the medullated nerve fibers of the optic fasciculus in man. *Graefes Arch Clin Exp Ophthalmol, 166*, 19-27.

Pankratov, Y., Castro, E., Miras-Portugal, M. T., & Krishtal, O. (1998). A purinergic component of the excitatory postsynaptic current mediated by P2X receptors in the CA1 neurons of the rat hippocampus. *Eur J Neurosci, 10*, 3898-902.

Papageorgiou, E., Wermund, T., & Wilhelm, H. (2009). Pupil perimetry demonstrates hemifield pupillary hypokinesia in a patient with a pretectal lesion causing a relative afferent pupil defect but no visual field loss. *J Neuroophthalmol, 29*, 33-6.

Paquet, C., Boissonnot, M., Roger, F., Dighiero, P., Gil, R., & Hugon, J. (2007). Abnormal retinal thickness in patients with mild cognitive impairment and Alzheimer's disease. *Neurosci Lett, 420*, 97–9.

Parisi, V. (2003). Correlation between morphological and functional retinal impairment in patients affected by ocular hypertension, glaucoma, demyelinating optic neuritis and Alzheimer's disease. *Semin Ophthalmol, 18*, 50–7.

Parisi, V., Manni, G., Spadaro, M., Colacino, G., Restuccia, R., Marchi, S., et al. (1999). Correlation between morphological and functional retinal impairment in multiple sclerosis patients. *Invest Ophthalmol Vis Sci, 40*, 2520–7.

Park, K. K., Liu, K., Hu, Y., Smith, P. D., Wang, C., Cai, B., et al. (2008). Promoting axon regeneration in the adult CNS by modulation of the PTEN/mTOR pathway. *Science, 322*, 963–6.

Parsons, J. H. (1902). Degenerations following lesions of the retina in monkeys. *Brain, 25*, 257-69.

Payne, B. R., Pearson, H. E., & Cornwell, P. (1984). Transneuronal degeneration of beta retinal ganglion cells in the cat. *Proc R Soc Lond B Biol Sci, 222*, 15-32.

Pearson, T., Currie, A. J., Etherington, L. A., Gadalla, A. E., Damian, K., Llaudet, E., et al. (2003). Plasticity of purine release during cerebral ischemia: clinical implications? *J Cell Mol Med, 7*, 362-75.

Perry, V. H., & Cowey, A. (1979a). The effects of unilateral cortical and tectal lesions on retinal ganglion cells in rats. *Exp Brain Res, 35*, 85-95.

Perry, V. H., & Cowey, A. (1979b). Changes in the retino-fugal pathways following cortical and tectal lesions in neonatal and adult rats. *Exp Brain Res, 35*, 97-108.

Perry, V. H., & Cowey, A. (1982). A sensitive period for ganglion cell degeneration and the formation of aberrant retino-fugal connections following tectal lesions in rats. *Neuroscience, 7*, 583-94.

Perry, V. H., & Cowey, A. (1984). Retinal ganglion cells that project to the superior colliculus and pretectum in the macaque monkey. *Neurosci, 12*, 1125-37.

Perry, V. H., Oehler, R., & Cowey, A. (1984). Retinal ganglion cells that project to the dorsal lateral geniculate nucleus in the macaque monkey. *Neuroscience, 12*, 1101-23.

Pilley, S. F., & Thompson, H. S. (1975). Pupillary "dilatation lag" in Homer's syndrome. *Brit J Ophthal, 59*, 731-5.

Piquado. (2010). Pupillometry as a measure of cognitive effort in younger and older adults. *Psychophysiology, 47*, 560-9.

Plant, G. T. (2008). Optic neuritis and multiple sclerosis. *Curr Opin Neurol, 21*, 16-21.

Plant, G. T., & Perry, V. H. (1990). The anatomical basis of the caecocentral scotoma. New observation and a review. *Brain, 113*, 1441-57.

Polosa, R., & Zeng, D. (2006). Adenosine and adenine nucleotide. In G. F. Laurent, *Encyclopedia of Respiratory Medicine* (pp. 24-29). Elsevier Ltd.

Polyak, S. (1957). Structure of the vertebral retina. In *The vertebrate visual system.* (pp. 238 -246). Chicago: University of Chicago Press.

Porrello, G., & Falsini, B. (1999). Retinal ganglion cell dysfunction in humans following post-geniculate lesions: specific spatio-temporal losses revealed by pattern ERG. *Vision Res, 39*, 1739-45.

Porter, G., Tales, A., Troscianko, T., Wilcock, G., Haworth, J., & Leonards, U. (2010). New insights into feature and conjunction search: I. Evidence from pupil size, eye movements and ageing. *Cortex, 46*, 621-36.

Potts, A. M., Hodges, D., Shelman , C. B., Fritz , K. J., Levy, N. S., & Mangnall , Y. (1972). Morphology of the Primate Optic Nerve: I. Method and Total Fiber Count. *Invest ophthalmol vis sci, 11*, 980-8.

Povlishock, J. T., Becker, D. P., Cheng, C. L., & Vaughan, G. W. (1983). Axonal change in minor head injury. *J Neuropathol Exp Neurol, 42*, 225-42.

Prichard, J. R., Stoffel , R. T., Quimby, D. L., Obermeyer, W. H., Benca, R. M., & Behan, M. (2002). Fos immunoreactivity in rat subcortical visual shell in response to illuminance changes. *Neuroscience, 114*, 781–93.

Provis, J. M. (1979). The distribution and size of ganglion cells in the regina of the pigmented rabbit: a quantitative analysis. *J Comp Neurol, 185*, 121-37.

Provis, J. M. (1987). Patterns of cell death in the ganglion cell layer of the human fetal retina. *J Comp Neurol, 259*, 237-46.

Provis, J. M., Driel, D. V., Bilson, F. A., & Russell, P. (1985). Human fetal optic nerve: overproduction and elimination of retinal axons during development. *J Comp Neurol, 238*, 92-100.

Ptito, M., Herbin, M., Boire, D., & Ptito, A. (1996). Neural bases of residual vision in hemicorticectomized monkeys. *Prog Brain Res, 112*, 385-404.

Pueyo, V., Ara, J. R., Almarcegui, C., Martin, J., Güerri, N., García, E., et al. (2010). Sub-clinical atrophy of the retinal nerve fibre layer in multiple sclerosis. *Acta Ophthalmol, 88*, 1–5.

Pueyo, V., Martin, J., Fernandez, J., Almarcegui, C., Ara, J., Egea, C., et al. (2008). Axonal loss in the retinal nerve fiber layer in patients with multiple sclerosis. *Mult Scler, 14*, 609–14.

Pulicken, M., Gordon-Lipkin, E., Balcer, L. J., Frohman, E., Cutter, G., & Calabresi, P. A. (2007). Optical coherence tomography and disease subtype in multiple sclerosis. *Neurology, 69*, 2085–92.

Qing, G., Zhang, S., Wang, B., & Wang, N. (2010). Functional MRI signal changes in primary visual cortex corresponding to the central normal visual field of patients with primary open-angle glaucoma. *Invest Ophthalmol Vis Sci, 51*, 4627–34.

Quigley, H. A., & Addicks, E. M. (1982). Quantitative studies of retinal nerve ifber layer defects. *Arch Ophthalmol, 100*, 807-14.

Quigley, H. A., Addicks, E. M., & Green, W. R. (1982). Optic nerve damage in human glaucoma: III Quantitative correlation of nerve fiber loss and viual field defect in glaucoma, ischemic neuropathy, papilledema and toxic neuropathy. *Arch Ophthalmology, 100*, 135-46.

Quigley, H. A., Coleman, A. L., & Dorman-Pease, M. E. (1991). Larger optic nerve heads have more nerve fibers in normal monkey eyes. *Arch Ophthalmol, 109*, 1441-3.

Quigley, H. A., Davis, E. B., & Anderson, D. R. (1977). Descending optic nerve degeneration in primates. *Invest Ophthalmol Vis Sci, 16*, 841-9.

Ragge, N. K., Barkovich, A. J., Hoyt, W. F., & Lambert, S. R. (1991). Isolated congenital hemianopia caused by prenatal injury to the optic radiation. *Arch neuro, 48*, 1088–91.

Ramoa, A. S., Campbell, G., & Shatz, C. J. (1988). Dendritic growth and remodeling of cat retinal ganglion cells during fetal and postnatal development. *J Neurosci, 8*, 4239-61.

Ramoa, A. S., Campbell, G., & Shatz, C. J. (1989). Retinal ganglion cells project transiently to the superior colliculus during development. *Proc Natl Acad Sci U S A, 86*, 2061-5.

Rapaport, D. H., & Stone, J. (1982). The site of commencement of maturation of mammalian retina: Observations in the cat. *Brain Res, 281*, 273-9.

Ratchford, J. N., Quigg, M. E., Conger, A., Frohman, T., Frohman, E., Balcer, L. J., et al. (2009). Optical coherence tomography helps differentiate neuromyelitis optica and MS optic neuropathies. *Neurology, 73*, 302–8.

Repka, M. X., & Quigley, H. A. (1989). The effect of age on normal human optic nerve fiber number and diameter. *Ophthalmology, 96*, 26-32.

Ribeiro, J. A., Sebastião, A. M., & de Mendonça, A. (2002). Adenosine receptors in the nervous system: pathophysiological implications. *Prog Neurobiol, 68*, 377-92.

Roberts, J. A., Vial, C., Digby, H. R., Agboh, K. C., Wen, H., Atterbury-Thomas, A., et al. (2006). Molecular properties of P2X receptors. *Pflugers Arch, 452*, 486-500.

Rodieck, R. W. (1988). The primate retina. *Comparative primate biology, 4*, 203-78.

Rosner, B. S. (1974). Recovery of function and localization of function in historical perspective. In D. Stein, J. J. Rosen, & N. Butters (Eds.), *Plasticity and recovery of function in the central nervous system.* New York: Academic press.

Roth, R. L. (1979). Decussation geometries in the goldfish nervous system: Correlation with probability of survival. *Proc Natl Acad Sci U S A, 76*, 4131-5.

Rubio, M. E., & Soto, F. (2001). Distinct Localization of P2X Receptors at Excitatory Postsynaptic Specializations. *J Neurosci, 21*, 641–53.

Sabel, B. A., Kenkel, S., & Kasten, E. (2005). Vision restoration therapy. *Br J Ophthalmol, 89*, 522–4.

Sahraie, A., Trevethan, C. T., MacLeod, M. J., Murray, A. D., Olson, J. A., & Weiskrantz, L. (2006). Increased sensitivity after repeated stimulation of

residual spatial channels in blindsight. *Proc Natl Acad Sci U S A, 103*, 14971–6.

Sakai, T., Matsuda, H., Watanabe, N., Kamei, A., & Takashima, S. (1994). Olivocerebellar retrograde trans-synaptic degeneration from the lateral cerebellar hemisphere to the medial inferior olivary nucleus in an infant. *Brain Dev, 16*, 229-32.

Santos, D. A., Salgado, A. I., & Cunha, R. A. (2003). ATP is released from nerve terminals and from activated muscle fibres on stimulation of the rat phrenic nerve. *Neurosci Lett, 338*, 225-8.

Saper, C. B., & Loewy, A. D. (1980). Efferent connections of the parabrachial nucleus in the rat. *Brain Res, 197*, 291-317.

Savini, G., Zanini, M., Carelli, V., Sadun, A. A., Ross-Cisneros, F. N., & Barboni, P. (2005). Correlation between retinal nerve fibre layer thickness and optic nerve head size: an optical coherence tomography study. *Br J Ophthalmol, 89*, 489-92.

Savoiardo, M., Pareyson, D., Grisoli, M., Forester, M., D'Incerti, L., & Farina, L. (1992). The effects of Wallerian degeneration of the optic radiations demonstrated by MRI. *Neuroradiology, 34*, 323-5.

Saxena, S., & Caroni, P. (2007). Mechanisms of axon degeneration: from development to disease. *Prog Neurobiol, 83*, 174-91.

Schiller, P. H., & Malpeli, J. G. (1977). Properties and tectal projections of monkey retinal ganglion cells. *J Neurophysiol, 40*, 428-45.

Schmidt, T. M., & Kofuji, P. (2009). Functional and morphological differences among intrinsically photosensitive retinal ganglion cells. *J Neurosci, 29*, 476–82.

Sebastião, A. M., & Ribeiro, J. A. (2009). Triggering neurotrophic factor actions through adenosine A2A receptor activation: implications for neuroprotection. *Br J Pharmacol, 158*, 15–22.

Sepulcre, J., Murie-Fernandez, M., Salinas-Alaman, A., García-Layana, A., Bejarano, B., & Villoslada, P. (2007). Diagnostic accuracy of retinal abnormalities in predicting disease activity in MS. *Neurology, 68*, 1488–94.

Shapley, R., & Perry, V. H. (1986). Cat and monkey retinal ganglion cells and their visual functional roles. *Trends Neurosci, 9*, 229-35.

Shatz, C. J. (1992). How are specific connections formed between thalamus and cortex? *Curr Opin Neurobiol, 2*, 78-82.

Sherman, S. M. (2007). The thalamus is more than just a relay. *Curr Opin Neurobiol, 17*, 417–22.

Shu, N., Li, J., Li, K., Yu, C., & Jiang, T. (2009). Abnormal diffusion of cerebral white matter in early blindness. *Hum Brain Mapp, 30*, 220-7.

Siger, M., Dziegielewski, K., Jasek, L., Bieniek, M., Nicpan, A., Nawrocki, J., et al. (2008). Optical coherence tomography in multiple sclerosis: thickness of the retinal nerve fiber layer as a potential measure of axonal loss and brain atrophy. *J Neurol, 255*, 1555–60.

Sillito, A. M., & Zbrozyna, A. W. (1970). The activity characteristics of preganglionic pupilloconstrictor neurones. *J Physiol, 211*, 769-79.

Spear. (1969). pattern discrimination following removal of visual neocortex in the cat. *Exp neuro, 25*, 331-348.

Starke, K., Göthert, M., & Kilbinger, H. (1989). Modulation of neurotransmitter release by presynaptic autoreceptors. *Physiol Rev., 69*, 864-989.

Steck, P. A., Pershouse, M. A., Jasser, S. A., Yung, W. K., Lin, H., Ligon, A. H., et al. (1997). Identification of a candidate tumour suppressor gene, MMAC1, at chromosome 10q23.3 that is mutated in multiple advanced cancers. *Nat Genet, 15*, 356–62.

Stoerig, P. (1987). Chromaticity and achromaticity. Evidence for a functional differentiation in visual field. *Brain, 110*, 869-86.

Stoerig, P., & Cowey, A. (1997). Blindsight in man and monkey. *Brain, 120*, 535-559.

Stone, J., & Johnston, E. (1981). The topography of primate retina: A study of the human, bushbaby, and new- and old- world monkeys. *J Comp Neurol*, 205-223.

Sumner, P., Anderson, E. J., Sylvester, R., Haynes, J. D., & Rees, G. (2008). Combined orientation and colour information in human V1 for both L-M and S-cone chromatic axes. *Neuroimage, 39*, 814–24.

Sun, M. (1995). Central neural organization and control of sympathetic nervous system in mammals . *Progress in Neurobiology, 47*, 157-233.

Swanson, L., & Kuypers, G. (1980). The paraventricular nucleus of the hypothalamus: Cytoarchitectonic subdivisions and organization of projections to the pituitary, dorsal vagal complex,and spinal cord as demonstrated by retrograde fluorescence double-labelling methods. *J. comp. Neurol., 194*, 555-570.

Szmajda, B. A., Buzás, P., Fitzgibbon, T., & Martin, P. R. (2006). Geniculocortical relay of blue-off signals in the primate visual system. *Proc Natl Acad Sci U S A, 103*, 19512-7.

Szmajda, B., Grunert, U., & Martin, P. (2008). Retinal ganglion cell inputs to the koniocellular pathway. *J Comp Neurol, 510*, 251–68.

Tailby, C., Szmajda, B. A., Buzás, P., Lee, B. B., & Martin, P. R. (2008). Transmission of blue (S) cone signals through the primate lateral geniculate nucleus. *J Physiol, 586*, 5947–67.

Tait, S. W., & Green, D. R. (2010). Mitochondria and cell death: outer membrane permeabilization and beyond. *Nat Rev Mol Cell Biol, 11*, 621-32.

Takayama, K., & Miura, M. (1991). Glutamate-immunoreactive neurons of the central amygdaloid nucleus projecting to the subretrofacial nucleus of SHR and WKY rats: a double-labeling study. *Neurosci Lett, 134*, 62-6.

Talbot, S. A., & Marshall, W. H. (1941). Physiological studies on neural mechanisms of visual localization and discrimination. *Am J Ophthalmol, 24*, 1255–64.

Taylor, J. S. (1987). Fibre organization and reorganization in the retinotectal projection of Xenopus. *Development, 99*, 393-410.

Terris, J., Ecelbarger, C. A., Marples, D., Knepper, M. A., & Nielsen, S. (1995). Distribution of aquaporin-4 water channel expression within rat kidney. *Am J Physiol, 269*, F775-85.

Thompson, H. S., Corbett, J. J., & Cox, T. A. (1981). How to measure the relative afferent pupillary defect. *Surv Ophthalmol, 26*, 39-42.

Thorell, L. G., De Valois, R. L., & Albrecht, D. G. (1984). Spatial mapping of monkey V1 cells with pure color and luminance stimuli. *Vision Res, 24*, 751–69.

Tong, J. J. (2007). Mitochondrial delivery is essential for synaptic potentiation. *Biol Bull, 212*, 169-75.

Tootell, R. B., Hamilton, S. L., & Switkes, E. (1988). Functional anatomy of macaque striate cortex. IV. Contrast and magno-parvo streams. *J Neurosci, 8*, 1594-609.

Torrealba, F. R., Guillery, R. W., Eysel, U., Polley, E. H., & Mason, C. A. (1982). Studies of retinal representations within the cat's optic tract. *J Comp Neurol, 211*, 377-96.

Torrealba, F., Partlow, G. D., & Guillery, R. W. (1981). Organization of the projection from the superior colliculus to the dorsal lateral geniculate nucleus of the cat. *Neuroscience, 6*, 1341-60.

Trapp, B. D., Peterson, J., Ransohoff, R. M., Rudick, R., Mörk, S., & Bö, L. (1998). Axonal transection in the lesions of multiple sclerosis. *N Engl J Med, 338*, 278–85.

Trevethan, C. T., Sahraie, A., & Weiskrantz, L. (2002). Spatial vision in cortical blindness: a pupillometric investigation. *Perception, 31*, ECVP Abstract Supplement .

Trip, S. A., Schlottmann, P. G., Jones, S. J., Altmann, D. R., Garway-Heath, D. F., Thompson, A. J., et al. (2005). Retinal nerve fiber layer axonal loss and visual dysfunction in optic neuritis. *Ann Neurol, 58*, 383–91.

Tsumoto, T., Masui, H., & Sato, H. (1986). Excitatory amino acid transmitters in neuronal circuits of the cat visual cortex. *J Neurophysiol, 55*, 469-83.

Turner, J. P., & Salt, T. E. (1998). Characterization of sensory and corticothalamic excitatory inputs to rat thalamocortical neurones in vitro. *J Physiol*(510), 829-43.

Turner, J. P., Leresche, N., Guyon, A., Soltesz, I., & Crunelli, V. (1994). Sensory input and burst firing output of rat and cat thalamocortical cells: the role of NMDA and non-NMDA receptors. *J physiol, 480*, 281-95.

Uggetti, C., Egitto, M. G., Fazzi, E., Bianchi, P. E., Zappoli, F., Martelli, A., et al. (1997). Transsynaptic degeneration of lateral geniculate bodies in blind children: in vivo MR demonstration. *Am J Neuroradiol, 18*, 233–8.

Updyke, B. V. (1977). Topographic organization of the projections from cortical areas 17, 18 and 19 onto the thalamus, pretectum and superior colliculus in the cat. *J Comp Neurol, 173*, 81-122.

Usrey, W. M., & Reid, R. C. (2000). Visual physiology of the lateral geniculate nucleus in two species of new world monkey: Saimiri sciureus and Aotus trivirgatis. *J Physiol, 523*, 755-69.

Van Buren, A. (1963). *The retinal ganglion cell layer.* Springfield.

Van Buren, J. M. (1963). Trans-synaptic retrograde degeneration in the visual system of primates. *J Neurol Neurosurg Psychiatry, 26*, 402–9.

Van Essen, D. C., Newsome, W. T., & Maunsell, J. H. (1984). The visual field representation in striate cortex of the macaque monkey: asymmetries, anisotropies, and individual variability. *Vision Res, 24*, 429-48.

Van Velthoven, M. E., Faber, D. J., Verbraak, F. D., van Leeuwen, T. G., & de Smet, M. D. (2007). Recent developments in optical coherence tomography for imaging the retina. *Prog Retin Eye Res, 26*, 57–77.

Vaney, D. I., Peichl, L., Wässle, H., & Illing, R. B. (1981). Almost all ganglion cells in the rabbit retina project to the superior colliculus. *Brain Res, 212*, 447-53.

Verkhratsky, A., & Krishtal, O. (2009). Adenosine Triphosphate (ATP) as a Neurotransmitter. In L. R. Squire, *Encyclopedia of Neuroscience* (pp. 115-23). Elsevier.

von Krosigk, M., Monckton, J. E., Reiner, P. B., & McCormick, D. A. (1999). Dynamic properties of corticothalamic excitatory postsynaptic potentials and thalamic reticular inhibitory postsynaptic potentials in thalamocortical neurons of the guinea-pig dorsal lateral geniculate nucleus. *Neuroscience, 91*, 7-20.

Wakade, A. R., Przywara, D. A., & Wakade, T. D. (2001). Intracellular, nonreceptor-mediated signaling by adenosine: induction and prevention of neuronal apoptosis. *Mol Neurobiol, 23*, 137–53.

Walsh, C., & Polley, E. H. (1985). The topography of ganglion cell production in the cat's retina. *J neurosci, 5*, 741-50.

Walsh, C., Polley, E. H., Hickey, T. L., & Guillery, R. W. (1983). Generation of cat retinal ganglion cells in relation to central pathways. *Nature, 302*, 611-4.

Walsh, F. B., & Hoyt, W. F. (1969). *Clinical neuro-ophthalmology* (Vol. 1). Baltimore: Williams & Wilkins .

Walsh, T. J. (1996). *Visual fields: examination and interpretation* (2 ed.). San Francisco: American academyof ophthalmology.

Wang, X., Arcuino, G., Takano, T., Lin, J., Peng, W. G., Wan, P., et al. (2004). P2X7 receptor inhibition improves recovery after spinal cord injury. *Nat Med, 10*, 821– 7.

Wang, Y., Haughey, N. J., Mattson, M. P., & Furukawa, K. (2004). Dual effects of ATP on rat hippocampal synaptic plasticity. *Neuroreport, 15*, 633-6.

Wässle, H., & Illing, R. B. (1980). The retinal projection to the superior colliculus in the cat: a quantitative study with HRP. *J Comp Neurol, 190*, 333-56.

Watano, T., Calvert, J. A., Vial, C., Forsythe, I. D., & Evans, R. J. (2004). P2X receptor subtype-specific modulation of excitatory and inhibitory synaptic inputs in the rat brainstem. *J Physiol, 558*, 745–57.

Weiskrantz, L. (1972). Behavioural analysis of the monkey's visual nervous system. *Proc R Soc Lond B Biol Sci, 182*, 427-55.

Weller, R. E., & Kaas, J. H. (1989). Parameters affecting the loss of ganglion cells of the retina following ablations of striate cortex in primates. *Vis Neurosci, 3*, 327-349.

Weller, R. E., Kaas, J. H., & Wetzel, A. B. (1979). Evidence for the loss of X-cells of the retina after long-term ablation of visual cortex in monkeys. *Brain Res, 160*, 134-8.

Wetzel, A. B., Thompson, V. E., Horel, J. A., & Meyer, P. M. (1965). Some consequences of perinatal lesions of the visual cortex in the cat. *Psychonom Sci, 3*, 381-2.

Wheeler-Schilling, T. H., Marquordt, K., Kohler, K., Guenther, E., & Jabs, R. (2001). Identification of purinergic receptors in retinal ganglion cells. *Brain Res Mol Brain Res, 92*, 177–80.

White, A. J., Solomon, S. G., & Martin, P. R. (2001). Spatial properties of koniocellular cells in the lateral geniculate nucleus of the marmoset Callithrix jacchus. *J Physiol, 533*, 519-35.

Wible Jr, J. H., Luft, F. C., & DiMicco, J. A. (1988). Hypothalamic GABA suppresses sympathetic outflow to the cardiovascular system. *Am J Physiol, 254*, R680-7.

Wieraszko, A., Goldsmith, G., & Seyfried, T. N. (1989). Stimulation-dependent release of adenosine triphosphate from hippocampal slices. *Brain Res, 485*, 244-50.

Wilhelm, B. J., Wilhelm, H., Moro, S., & Barbur, J. L. (2002). Pupil response components: studies in patient with parinaud's syndrome. *Brain, 125*, 2296-307.

Wilkes, M., Zingaro, G., & Murphy, E. H. (1985). Survival of the ganglion cell population in the rabbit retina following neonatal visual cortex ablation. *Brain Res, 353*, 293-7.

Williams, C., Azzopardi, P., & Cowey, A. (1995). Nasal and temporal retinal ganglion cells projecting to the midbrain: implications for 'blindsight'. *Neuroscience, 65*, 577-86.

Williams, S. R., Turner, J. P., Anderson, C. M., & Crunelli, V. (1996). Electrophysiological and morphological properties of interneurones in the rat dorsal lateral geniculate nucleus in vitro. *J Physiol, 490*, 129-47.

Wolter, J. R. (1965). The centrifugal nerves in human optic tract,chiasm, optic nerve and retina. *Trans Am Ophthalmol Soc, 63*, 678–707.

Wong-Riley, M. T. (1972). Changes in the dorsal lateral geniculate nucleus of the squirrel monkey after unilateral ablation of the visual cortex. *J Comp Neurol, 146*, 519-48.

Woodward, W. R., & Coull, B. M. (1984). Localization and organization of geniculocortical and corticofugal fiber tracts within the subcortical white matter. *Neuroscience, 12*, 1089-99.

Wu, Z., Huang, J., Dustin, L., & Sadda, S. R. (2009). Signal strength is an important determinant of accuracy of nerve fiber layer thickness measurement by optical coherence tomography. *J Glaucoma, 18*, 213-6.

Yan, S., Tu, Z., Lu, W., Zhang, Q., He, J., Li, Z., et al. (2009). Clinical utility of an automated pupillometer for assessing and monitoring recipients of liver transplantation. *Liver Transpl, 15*, 1718-27.

Yeh, E., Weinstock-Guttman, B., Lincoff, N., Reynolds, J., Weinstock, A., Madurai, N., et al. (2009). Retinal nerve fiber thickness in inflammatory demyelinating diseases of childhood onset. *Mult Scler, 15*, 802–10.

Yücel, Y. H., Zhang, Q., Gupta, N., Kaufman, P. L., & Weinreb, R. N. (2000). Loss of neurons in magnocellular and parvocellular layers of the lateral geniculate nucleus in glaucoma. *Arch Ophthalmol, 118*, 378-84.

Yukie, M., & Iwai, E. (1981). Direct projection from the dorsal lateral geniculate nucleus to the prestriate cortex in macaque monkeys. *J Comp Neurol, 201*, 81-97.

Zaveri, M. S., Conger, A., Salter, A., Frohman, T. C., Galetta, S. L., Markowitz, C. E., et al. (2008). Retinal imaging by laser polarimetry and optical coherence tomography evidence of axonal degeneration in multiple sclerosis. *Arch Neurol, 65*, 924–8.

Zoncu, R., Efeyan, A., & Sabatini, D. M. (2011). mTOR: from growth signal integration to cancer, diabetes and ageing. *Nat Rev Mol Cell Biol, 12*, 21-35.